



Zhdanov, Oleksandr (2021) *Wind influence on plants: ecophysiological, biomechanical, and aerodynamic aspects*. PhD thesis.

<http://theses.gla.ac.uk/82171/>

Copyright and moral rights for this work are retained by the author

A copy can be downloaded for personal non-commercial research or study, without prior permission or charge

This work cannot be reproduced or quoted extensively from without first obtaining permission in writing from the author

The content must not be changed in any way or sold commercially in any format or medium without the formal permission of the author

When referring to this work, full bibliographic details including the author, title, awarding institution and date of the thesis must be given

Enlighten: Theses
<https://theses.gla.ac.uk/>
research-enlighten@glasgow.ac.uk



Wind influence on plants: ecophysiological, biomechanical, and aerodynamic aspects

Oleksandr Zhdanov

Submitted in fulfilment of the requirements for the
Degree of Doctor of Philosophy

Aerospace Sciences Research Division
James Watt School of Engineering
College of Science and Engineering
University of Glasgow

January 2021

Declaration

I certify that the thesis presented here for examination for PhD degree of the University of Glasgow is solely my own work other than where I have clearly indicated that it is the work of others (in which case the extent of any work carried out jointly by me and any other person is clearly identified in it) and that the thesis has not been edited by a third party beyond what is permitted by the University's PGR Code of Practice.

The copyright of this thesis rests with the author. No quotation from it is permitted without full acknowledgement.

I declare that the thesis does not include work forming part of a thesis presented successfully for another degree.

I declare that this thesis has been produced in accordance with the University of Glasgow's Code of Good Practice in Research.

I acknowledge that if any issues are raised regarding good research practice based on review of the thesis, the examination may be postponed pending the outcome of any investigation of the issues.

Signature: Oleksandr Zhdanov

Date: January 2021

Abstract

Wind has a wide range of effects on plants: from wind-induced damage in the form of lodging to an increased rate of photosynthesis. Climate models predict that plants will be exposed to elevated wind conditions in many regions around the world due to global warming. To be able to attenuate the negative impact of changing wind patterns on plants, it is necessary to expand our understanding of wind-plant interaction. In this thesis two different aspects of wind-plant interaction are investigated.

In the first part, the acclimation response of a model plant, *Arabidopsis thaliana*, to mechanical stress in the form of continuous wind of a constant speed is explored. A bespoke wind tunnel, suitable for continuous growth of plants, was developed. For the mechanical characterisation of *Arabidopsis* stems a new multiple resonant frequency method was devised and validated. As a result of the wind treatment, the plants exhibited a positive anemotropic response. This response was documented for the first time in any plant system. Overall, the wind-induced thigmomorphogenetic changes and alterations in the mechanical properties of the primary inflorescence stem were considered to be adaptive to this type of mechanical stress. The mechanical properties can be related to modification in the anatomical tissue organisation and ion content, providing possible sources of the observed changes. In many experiments reported in the literature, wind is mimicked by brushing treatments. In this project, the validity of this approach was investigated by conducting a comparison of the response of *Arabidopsis* to uni- and bidirectional brushing treatments with the wind-induced changes. While some of the changes to *Arabidopsis* morphology can be reproduced by matching the vectorial influence of wind and brushing treatments, the changes in the mechanical properties occurred in opposite directions. The unidirectional brushing treatment also evoked a positive tropic response, which can be considered thigmotropic and has been demonstrated for the first time in *Arabidopsis* shoot.

The second part of this thesis explores the aerodynamics of succulent-inspired cylinders using numerical and experimental techniques. Succulents and cacti are,

probably, the most well-known examples of convergent evolution in plants, where two different species have independently developed similar traits and features in similar environments but in different parts of the Earth. Investigations inspired by the Saguaro cactus reported in the literature, showed that the presence of ribs on its trunk, among other functions, helps to reduce the aerodynamic forces and decreases unsteady force fluctuations. In contrast to Saguaro, which can have up to 30 ribs, succulents tend to have a considerably lower number of ribs, with only three and four ribs found in many species. This work investigates whether succulent-inspired bluff bodies with a low number of ribs show similar aerodynamic benefits as cactus-shaped cylinders with many ribs. 2D URANS simulations were carried out for two cylinders with three and four ribs, which resemble the succulents *Euphorbia trigona* and *Euphorbia abyssinica*, respectively, at Reynolds number 20,000. The succulent-inspired cylinder with four ribs was also investigated using wind tunnel tests with Reynolds numbers ranging from 50,000 to 150,000. For both studied cylinders, a strong angle of attack dependence of all aerodynamic properties was found. For the four-ribbed cylinder no Reynolds number dependence of these properties was observed within the tested range. Overall, succulent-inspired cylinders with a low number of ribs show some aerodynamic advantages in terms of reduction of the mean drag coefficient and the Strouhal number, albeit over a limited range of angles of attack.

Acknowledgements

First of all, I would like to thank my supervisors, Dr Angela Busse, Dr Hossein Zare-Behtash, and Prof Mike Blatt, for their invaluable guidance, expertise, encouragement, feedback, and time to discuss any of my questions. Working in a multidisciplinary team was the most interesting part of this project, which helped me to develop professional skills and motivation for research.

I would like to express my gratitude to Dr Richard Green for his support and guidance during the wind tunnel tests and access to the National Wind Tunnel Facility and its equipment, and to Dr Andrea Cammarano for help and guidance with the development of vibration tests procedure and access to the Space lab.

Moreover, I gratefully acknowledge the funding of this multidisciplinary project through the University of Glasgow's Lord Kelvin/Adam Smith (LKAS) PhD scholarship scheme.

Also, I would like to thank my friends who encouraged and distracted me when it has been required. In particular, I would like to thank Thomas Jelly for support and discussions on scientific and other topics.

I would like to thank Naomi Donald and Amparo Ruiz-Prado for their help with growing *Arabidopsis*, looking after plants, and assistance in plant related experiments. I extend my thanks to technical staff of James Watt School of Engineering, especially to Stevie Monaghan for his help with assembling the wind tunnel.

Finally, I would like to express my thanks to my parents, Oleksandr and Valentyna, and my sister Mariya who always supported me in my endeavours. And of course, to Connie for her understanding, patience, and encouragement during this journey.

List of publications

Journal publications

- Zhdanov, O., Blatt, M.R., Zare-Behtash, H. and Busse, A., 2021. Wind-evoked anemotropism affects the morphology and mechanical properties of Arabidopsis. *Journal of Experimental Botany*, 72(5), pp.1906-1918. doi: 10.1093/jxb/eraa541
- Zhdanov, O., Green, R. and Busse, A., 2021. Experimental investigation of the angle of attack dependence of the flow past a cactus-shaped cylinder with four ribs. *Journal of Wind Engineering and Industrial Aerodynamics*, 208, p.104400. doi: 10.1016/j.jweia.2020.104400
- Zhdanov, O., Blatt, M.R., Cammarano, A., Zare-Behtash, H. and Busse, A., 2020. A new perspective on mechanical characterisation of Arabidopsis stems through vibration tests. *Journal of the Mechanical Behavior of Biomedical Materials*, 112, p.104041. doi: 10.1016/j.jmbbm.2020.104041
- Zhdanov, O. and Busse, A., 2019. Angle of attack dependence of flow past cactus-inspired cylinders with a low number of ribs. *European Journal of Mechanics-B/Fluids*, 75, pp.244-257. doi: 10.1016/j.euromechflu.2018.09.008

Conference presentations

- Zhdanov, O., Green R. and Busse, A. (2020) Aerodynamic properties of a succulent inspired cylinder. *33rd Scottish Fluid Mechanics Meeting*, Edinburgh, UK, 28 May 2020.
- Zhdanov, O. and Busse, A. (2019) Do ribs help succulents to cope with aerodynamic loads in their natural environment? *72nd Annual Meeting of the APS Division of Fluid Dynamics*, Seattle, WA, USA, 23-26 November 2019.

- Zhdanov, O., Busse, A., Cammarano, A., Zare-Behtash, H. and Blatt, M. (2019) Effect of wind on morphology and mechanical properties of *Arabidopsis thaliana*. *SES 2019 – Society of Engineering Science, 56th Annual Technical Meeting*, Washington University, St. Louis, MO, USA, 13-15 October 2019.
- Zhdanov, O. and Busse, A. (2019) LES-based investigation of the angle of attack dependence of flow past a cactus-shaped cylinder with four ribs. *UK Fluids Conference 2019*, Cambridge, UK, 27-29 August 2019
- Zhdanov, O., Busse, A., Zare-Behtash, H., Cammarano, A. and Blatt, M. (2018) Influence of wind on structural, aerodynamic and mechanical properties of *Arabidopsis thaliana*. *9th International Plant Biomechanics Conference*, Montreal, Canada, 9-14 August 2018.
- Zhdanov, O., Busse, A., Blatt, M. and Zare-Behtash, H. (2017) A wind tunnel for the investigation of the response of plants to a turbulent boundary layer. *Summer School at Imperial College London 2017: Turbulent Flows*, London, UK, 24-27 July 2017.

Poster presentations

- Zhdanov, O. and Busse, A. (2019) Large-eddy simulations of flow past a cactus-shaped cylinder with a low number of ribs. *32nd Scottish Fluid Mechanics meeting*, Dundee, UK, 30 May 2019.
- Zhdanov, O. and Busse, A. (2018), Scale-resolved simulations of the flow past cactus shaped cylinders. *International HPC Summer School 2018*, Ostrava, Czech Republic, 8-13 July 2018.
- Zhdanov, O., Busse, A., Blatt, M. and Zare-Behtash, H. (2018) A specialised wind tunnel for investigation of ecophysiological response of plants to wind. *31st Scottish Fluid Mechanics Meeting*, Aberdeen, UK, 29 May 2018.
- Zhdanov, O. and Busse, A. (2017) Flow past cactus-shaped cylinders with a low number of ribs. *30th Scottish Fluid Mechanics meeting*. Glasgow, UK, 19 May 2017.

Contents

Declaration	i
Abstract	iii
Acknowledgements	v
List of publications	vii
Contents	ix
Nomenclature	xv
List of Figures	xvii
List of Tables	xxvii
1 Introduction	1
1.1 Structure of the thesis	4
2 Background	7
2.1 Preliminary concepts of fluid mechanics	7
2.2 Plant adaptation strategies to wind	10
2.2.1 Streamlining and reconfiguration	10
2.2.2 Damping	12
2.2.3 Wind-induced pruning	13
2.2.4 Cacti and succulents	13
2.3 Thigmomorphogenesis	15
2.4 Tropic responses in plants	16
2.5 Research objectives	19

I	Response of Arabidopsis to wind and other types of mechanical stress	21
3	Methodology for experiments with Arabidopsis	23
3.1	Model plant <i>Arabidopsis thaliana</i>	23
3.2	Growth and development of Arabidopsis	25
3.3	Cultivation of Arabidopsis	26
3.3.1	Seed stratification	27
3.3.2	Photoperiodism and growth cycles	27
3.3.3	Light intensity	28
3.4	Phenotyping	28
3.5	Anatomical structure and histochemical staining	30
3.6	Cuticle disruption using carborundum powder	31
3.7	Flame photometry	33
4	Bespoke wind tunnel	35
4.1	Overview of wind environments for studies on plants	35
4.2	Bespoke wind tunnel	42
4.2.1	Wind tunnel design	42
4.2.2	Characterisation of the test section	46
4.2.3	Plant growth environment	48
4.2.4	Summary	50
5	A new perspective on mechanical characterisation of Arabidopsis stems through vibration tests	51
5.1	Introduction	52
5.2	Materials and methods	55
5.2.1	Plants	55
5.2.2	Sample preparation	55
5.2.3	Three-point bending tests	56
5.2.4	Vibration tests	57
5.2.5	Examining the influence of stem clamping in the vibration test holder	60
5.2.6	Investigation of influence of turgor pressure on the mechanical properties	60
5.2.7	Statistical analysis	61
5.3	Results	61

5.3.1	Bottom part of the stem	61
5.3.2	Top part of the stem	62
5.3.3	Influence of stem clamping	65
5.3.4	Influence of turgor pressure on the mechanical properties of Arabidopsis stems	66
5.4	Discussion	68
5.4.1	Design of the holder for vibration tests	68
5.4.2	Clamped-clamped boundary conditions	68
5.4.3	Comparison with other recently developed dynamic methods .	69
5.4.4	Limitations	70
5.4.5	Considerations for future studies	71
5.5	Conclusions	71

6 Wind-evoked anemotropism affects the morphology and mechanical properties of Arabidopsis 75

6.1	Introduction	76
6.2	Materials and methods	79
6.2.1	Plants	79
6.2.2	Wind treatment	80
6.2.3	Wind tunnel	80
6.2.4	Phenotyping	82
6.2.5	Mechanical characterization	82
6.2.6	Anatomical measurements	84
6.2.7	Ca ²⁺ measurements	84
6.2.8	Statistical analysis	84
6.3	Results	85
6.3.1	Wind treatment induces changes in Arabidopsis phenotype . .	85
6.3.2	Wind changes mechanical properties of Arabidopsis stems . .	88
6.3.3	Wind changes anatomical structure of Arabidopsis stems . . .	88
6.3.4	Wind changes Ca ²⁺ content of Arabidopsis stems	89
6.4	Discussion	89
6.4.1	Morphological response of Arabidopsis	89
6.4.2	Anemotropic response of Arabidopsis to a constant unidirec- tional wind	93
6.4.3	Acclimation of Arabidopsis to a constant unidirectional wind .	95
6.4.4	Changes in the mechanical properties of Arabidopsis stems . .	96

6.4.5	Changes in the stem anatomy and ion content related to the changes in the mechanical properties	97
6.4.6	Wind and water stress in plants	98
6.5	Conclusions	99
7	Unidirectional versus bidirectional brushing: simulating wind influence on <i>Arabidopsis thaliana</i>	101
7.1	Introduction	102
7.2	Materials and methods	104
7.2.1	Plants	104
7.2.2	Mechanical perturbations	104
7.2.3	Phenotyping	106
7.2.4	Mechanical characterisation	106
7.2.5	Anatomical measurements	107
7.2.6	Statistical analysis	108
7.3	Results	108
7.3.1	<i>Arabidopsis</i> morphology	108
7.3.2	Mechanical properties of primary inflorescence stems	110
7.3.3	Anatomical tissue composition	111
7.4	Discussion	112
7.4.1	Morphological changes	112
7.4.2	Changes to mechanical properties and anatomical tissue organisation	114
7.4.3	Tropic response	116
7.5	Conclusions	118
II	Aerodynamics of succulent-inspired cylinders	121
8	Introduction	123
9	Angle of attack dependence of flow past cactus-inspired cylinders with a low number of ribs	127
9.1	Introduction	128
9.2	Investigated geometries	131
9.3	Numerical method	132
9.4	Results and discussion	135
9.4.1	Drag coefficient	137

9.4.2	Lift coefficient	139
9.4.3	Strouhal number	142
9.4.4	Influence of the projected frontal width	143
9.4.5	Flow visualisations	148
9.5	Conclusions	152
10	Experimental investigation of the angle of attack dependence of the flow past a cactus-shaped cylinder with four ribs	155
10.1	Introduction	156
10.2	Experimental setup	159
10.2.1	Force measurements	161
10.2.2	Pressure measurements	161
10.2.3	Hot-wire measurements	162
10.2.4	PIV measurements	162
10.3	Experimental results	164
10.3.1	Mean force coefficients	164
10.3.2	Unsteady lift force	165
10.3.3	Surface pressure distribution	167
10.3.4	Strouhal number	169
10.3.5	Quantitative flow visualisations	169
10.3.6	Critical angle of attack	171
10.3.7	Power spectra	172
10.3.8	Comparison with earlier 2D URANS results	174
10.4	Conclusions	176
11	Conclusions and future work	179
11.1	Conclusions	179
11.1.1	Response of Arabidopsis to wind-induced and other types of mechanical stress	180
11.1.2	Aerodynamics of succulent-inspired cylinders	181
11.2	Future work	182
11.2.1	Response of Arabidopsis to wind-induced and other types of mechanical stress	182
11.2.2	Succulent-inspired passive flow control	183
	Bibliography	185

Nomenclature

Roman Symbols

A Frontal area

C_D, C_d Drag coefficient

C'_d Fluctuating drag coefficient

C_L, C_l Lift coefficient

C_l^{amp} Amplitude of the lift force coefficient fluctuations

C'_L, C'_l Fluctuating lift coefficient

C_p Pressure coefficient

D Diameter / Drag

E Young's modulus of elasticity

EI Bending rigidity

I Second moment of area

L Length. For phenotyping – stem length; for mechanical characterisation – distance between supports in the holder; for fluid mechanics – characteristic linear dimension

Re Reynolds number

St Strouhal number

U_∞ Freestream flow velocity

V Vogel exponent

Greek Symbols

α	Angle of attack
f_i	Natural frequency
λ_i	Dimensionless parameter that is obtained from the characteristic equation corresponding to the applied boundary conditions and vibration mode
m	Mass per unit length
ν	Kinematic viscosity
μ	Dynamic viscosity of the fluid
ρ	Density of the fluid

Abbreviations

co	cortex
DAS	Days after sowing
ep	epidermis
if	interfascicular tissue
LES	Large-eddy simulation
ph	phloem
pi	pith
PIV	Particle image velocimetry
SD	Standard deviation
URANS	Unsteady Reynolds-Averaged Navier-Stokes
vb	vascular bundle
xy	xylem

List of Figures

2.1	Drag coefficients for different orientations of various two- and three-dimensional bodies with respect to the incoming flow in the range of Reynolds numbers between 10^4 and 10^6 . Flow direction is from left to right. Data is taken from Hoerner (1965).	9
2.2	Flagged tree a result of irreversible streamlining and reconfiguration that occurs over time due to regular and continuous exposure to strong prevailing winds in the natural environment. This photo was taken in Gourock on the windy west coast of Scotland.	12
2.3	Representatives of Cactaceae and Euphorbiaceae families that developed similar plant structure to adapt to dry desert conditions in the process of convergent evolution. (A) Saguaro cactus (<i>Carnegiea gigantea</i>) in Saguaro National Park, USA (Magnuson, 2018). (B) Candelabra tree (<i>Euphorbia ingens</i>) in the Royal Botanic Garden Edinburgh, Scotland.	14
2.4	Schematic example of gravitropic response in plants. When a plant is tilted from the vertical orientation both root and shoot exhibit gravitropism until they are realigned with the direction of gravity vector.	16
2.5	An example of tropic response in Arabidopsis. Roots of Arabidopsis Col-0 exhibit positive gravitropism and reorient their growth direction with respect to the new direction of the gravity vector. (A) Control group. (B) Plate with experimental group seedlings, that was turned 90° in the counterclockwise direction after the initial growth period. The length of the roots at the point in time, when the experimental plate was turned, is marked with the dot in both groups.	17
3.1	<i>Arabidopsis thaliana</i> a widely used model organism in plant science. (A) Columbia (Col-0) wildtype. (B) PIN-1 mutant.	24

3.2	Arabidopsis growth and development. (A) Seed germination stage. (B) Leaf development stage. (C) Rosette growth stage. (D) Inflorescence emergence stage. (E) Flower production stage.	26
3.3	Arabidopsis morphology.	29
3.4	A transverse cross-section of Arabidopsis inflorescence stem stained with toluidine blue. Anatomical features and main tissues are shown: epidermis (ep), cortex (co), vascular bundle (vb), xylem (xy), phloem (ph), interfascicular tissue (if), and pith (pi).	30
4.1	Schematic representation of the field setup for a periodic wind treatment at INRA Pierroton near Bordeaux, France. After the descriptions and drawings of this setup in Tamasi et al. (2005); Berthier and Stokes (2005, 2006).	36
4.2	Schematic representation of a simple wind environment created by a fan that was employed in numerous studies on wind-plant interaction.	37
4.3	Overview of the wind environments that are used for studies on wind influence on plants.	41
4.4	Bespoke wind tunnel for investigations on wind-plant interaction. (A) Wind tunnel CAD model showing its main components. (B) Actual wind tunnel inside the Bower building glasshouse.	43
4.5	(A) Wind tunnel test section floor. (B) CAD model of the bespoke traverse system for the wind tunnel. The x-axis spans in the stream-wise, y-axis in the wall normal, and z-axis in the spanwise direction.	44
4.6	Mean flow speed at the centre of the wind tunnel test section over four independent measurements as a function of the variac output. Error bars represent standard deviations.	47
4.7	Representative examples of the mean velocity contours at several location along the test section length for three settings of the variable transformer. The flow direction is into the page. (A) Variac setting 70, $x/h = 0.875$. (B) Variac setting 70, $x/h = 2.775$. (C) Variac setting 70, $x/h = 3.975$. (D) Variac setting 130, $x/h = 0.875$. (E) Variac setting 130, $x/h = 2.775$. (F) Variac setting 130, $x/h = 3.975$. (G) Variac setting 230, $x/h = 0.875$. (H) Variac setting 230, $x/h = 2.775$. (I) Variac setting 230, $x/h = 3.975$. Velocity is normalised by the mean flow velocity in the test section, and where h - is the test section half height.	49

5.1	Experimental setups used for the mechanical tests. (a) Three-point bending test; (b) Vibration test.	57
5.2	Schematic diagram of the experimental setup used for multiple resonant frequency dynamic tests.	58
5.3	Representative example of a transfer function. This transfer function was obtained from one of the vibration tests performed on the bottom part of the stem. Peaks on the transfer function correspond to the natural frequencies of a tested stem.	59
5.4	Scatter diagrams showing bending rigidity vs stem diameter raised to the fourth power for the bottom parts of the Arabidopsis stems. (a) Scatter diagram based on the results of the three-point bending tests; (b) Scatter diagram based on the results of the vibration tests.	62
5.5	Modulus of elasticity determined for the bottom parts of the Arabidopsis stems. (a) Mean values of the modulus of elasticity, E , determined using the vibration method, errorbars represent standard deviations; (b) Box plots presenting E , determined from vibration (n=40) and three-point bending tests (n=31).	63
5.6	Scatter diagrams showing bending rigidity vs stem diameter raised to the fourth power for the top parts of the Arabidopsis stems. (a) Scatter diagram based on the results of the three-point bending tests; (b) Scatter diagram based on the results of the vibration tests.	64
5.7	Modulus of elasticity determined for the top parts of the Arabidopsis stems. (a) Mean values of the modulus of elasticity, E , tested using the vibration method, errorbars represent standard deviations; (b) Box plots presenting E , determined from vibration (n=40) and three-point bending tests (n=17).	65
5.8	Examination of the effect of clamping in the holder on the measured natural frequencies of Arabidopsis stems. (a) Stem ends are squeezed by the clamps; (b) Spacers are inserted to prevent squeezing of stem ends; (c) Box plots representing the effect of squeezing of stem ends on the natural frequencies of the tested stems (n=25).	66

5.9	Influence of turgor pressure on the modulus of elasticity of Arabidopsis stems. (a) Mean values of the modulus of elasticity determined for the baseline case (×) and after hyperosmotic treatment (○), errorbars represent standard deviations; (b) Box plot representing E , determined for the baseline tests (n=20) and after hyperosmotic treatment (n=20).	67
6.1	Changes to the morphological parameters as a result of unidirectional wind treatment with a constant flow speed of 5 m s^{-1} in both conducted experiments. (A) Length of the primary inflorescence stem. (B) Number of stems. (C) Number of branches. Error bars represent the SD. Statistically significant difference ($P \leq 0.05$) from the two-sided Wilcoxon rank sum tests comparing medians of the corresponding parameters in the control (n=19 and n=21 for the first and second experiments, respectively) and experimental (n=21 for both experiments) groups is marked with (*).	86
6.2	Changes to the Arabidopsis stem segments diameter as a result of the unidirectional wind treatment with a constant flow speed of 5 m s^{-1} measured in the first experiment. Error bars represent the SD. A statistically significant difference ($P \leq 0.05$) from the two-sided Wilcoxon rank sum tests comparing medians of the corresponding parameters in the control (n=19) and experimental (n=21) groups is marked with (*).	87
6.3	Changes to the mechanical properties of Arabidopsis stem segments as a result of the unidirectional wind treatment with a constant flow speed of 5 m s^{-1} in the first experiment. (A) Bending rigidity. (B) Young's modulus of elasticity. Error bars represent the SD. Statistically significant difference ($P \leq 0.05$) from the two-sided Wilcoxon rank sum tests comparing medians of the corresponding parameters in the control (n=19) and experimental (n=21) groups is marked with (*).	89
6.4	Representative examples of the primary inflorescence stem cross-section showing anatomical tissue organisation of its bottom part: (A) plant from the control group. (B) plant from the experimental group. co, cortex; ph, phloem; xy, xylem; if, interfascicular tissue; pi, pith. . . .	90

6.5 Changes to the Ca^{2+} content of Arabidopsis stems as a result of the unidirectional wind treatment with a constant flow speed of 5 m s^{-1} in the second experiment. Error bars represent the SD. A statistically significant difference ($P \leq 0.05$) from the two-sided Wilcoxon rank sum tests comparing medians of the corresponding parameters in the control ($n=8$) and experimental ($n=8$) groups is marked with (*). 92

6.6 Arabidopsis ecotype Col-0 grown under the constant unidirectional wind exhibits positive anemotropic response. (A) Young Arabidopsis seedlings (30 DAS) from experimental and control groups. (B) Young Arabidopsis seedlings (30 DAS) inside the wind tunnel test section. (C) Arabidopsis plants (34 DAS) from experimental and control groups. (D) Arabidopsis plants (34 DAS) inside the wind tunnel test section. Note that in (A) and (C) plants from the experimental group were removed from the wind tunnel and the curvature of their stems is increased compared to plants in (B) and (D) where Arabidopsis is subjected to a constant unidirectional wind of 5 m s^{-1} . For reference in all parts of the figure the diameter of the pot is 76 mm. 94

7.1 Brushing machine and its operational modes used in the present study. (A) Schematic diagram of the brushing machine and its components. (B) Bidirectional brushing mode: the plants are brushed in both directions by moving brushing material back and forth (from position 1 to position 2). (C) Unidirectional brushing mode: the plants are brushed in a single direction by moving the brushing material from position 1 to position 2. Upon reaching the end of the horizontal axis (position 2), the brushing materials is lifted to position 3, moved back to the beginning of the axis (position 4) and returned to the initial position 1. The plants are placed under the brushing material on both sides of the brushing machine. The position of the beam with brushing material is adjusted in the vertical direction as the plants grow. 105

- 7.2 The effect of mechanical perturbations by different types of brushing treatment and brushing material on Arabidopsis morphology. (A) Primary inflorescence stem length. (B) Number of stems. (C) Number of branches. The legend in part (A) applies to all parts of this figure. Experimental group 1 was brushed with textured jute fabric while experimental group 2 with a smooth plastic in both experiments. Statistically significant differences ($P \leq 0.05$) were identified using the two-sided Wilcoxon rank sum test comparing medians of the corresponding parameters between groups. * marks statistically significant difference compared with the control group in the respective experiment. 109
- 7.3 The effect of mechanical perturbations by different types of brushing treatment and brushing material on the intensive mechanical properties of Arabidopsis primary inflorescence stem. (A) Modulus of elasticity of the bottom part of the stem. (B) Modulus of elasticity of the top part of the stem. The legend in part (B) applies to both parts of this figure. Experimental group 1 was brushed with textured jute fabric while experimental group 2 with smooth plastic in both experiments. Statistically significant differences ($P \leq 0.05$) were identified using the two-sided Wilcoxon rank sum test comparing medians of the corresponding parameters between groups. * marks a statistically significant difference compared with the control group in the respective experiment. 111
- 7.4 Depending on the direction of brushing treatment it is possible to evoke a tropic response in Arabidopsis similar to that observed as a result of constant unidirectional wind. (A and C) Arabidopsis does not exhibit any tropic response in the bidirectional brushing experiment. (B and D) Arabidopsis exhibits a positive tropic response in the unidirectional brushing experiment. Experimental group 1 was brushed with a smooth plastic while a textured jute fabric was used as brushing material for experimental group 2 in both experiments. The photos were taken on the fourth day after the start of the brushing treatment. 117

8.1	Reynolds number dependence of the mean drag coefficient of a circular cylinder and a square cylinder at $\alpha = 0^\circ$. The data is taken from Bai and Alam (2018). Flow regimes for the circular cylinder are marked: A - subcritical, B - critical, C - supercritical, and D - post-critical.	124
8.2	Schematics of the average flow patterns around a square cylinder at different angles of attack illustrating the classification by Igarashi (1984). (A) ‘Perfect separation type with symmetric flow’ ($0^\circ \leq \alpha \leq 5^\circ$). (B) ‘Perfect separation type with asymmetric flow’ ($5^\circ < \alpha < \alpha_{cr}$). (C) ‘Reattachment type’ ($\alpha_{cr} \leq \alpha < 35^\circ$). (D) ‘Wedge flow type’ ($35^\circ \leq \alpha \leq 45^\circ$). The critical angle of attack (α_{cr}) varies between 12° and 15° depending on experimental conditions.	125
9.1	<i>Euphorbia trigona</i> , a member of the Euphorbiaceae family, in Glasgow Botanic Gardens.	130
9.2	Succulents with low number of ribs: a - <i>Euphorbia trigona</i> , b - <i>Euphorbia Abyssinica</i>	132
9.3	Geometrical representation of the tested cactus shapes. Left: three-rib configuration approximating <i>Euphorbia trigona</i> ; right: four-rib configuration approximating <i>Euphorbia Abyssinica</i>	133
9.4	Computational domain with grid used for the simulations.	134
9.5	Mesh close to (a) circular cylinder and (b) three-rib cactus-shaped cylinder with enlarged prism layers.	135
9.6	Angle of attack definition for the cactus-shaped cylinder.	136
9.7	Mean drag coefficient versus angle of attack. The angle of attack has been normalised with the maximum angle of attack (three-rib case: $\alpha_{max} = 60^\circ$, four-rib case: $\alpha_{max} = 45^\circ$). The dashed line indicates the value for the smooth circular cylinder case. ¹	137
9.8	Rms drag coefficient versus angle of attack. The angle of attack has been normalised with the maximum angle of attack (three-rib case: $\alpha_{max} = 60^\circ$, four-rib case: $\alpha_{max} = 45^\circ$). The dashed line shows the value for the smooth cylinder case.	138
9.9	Mean lift coefficient versus angle of attack. The angle of attack has been normalised with the maximum angle of attack (three-rib case: $\alpha_{max} = 60^\circ$, four-rib case: $\alpha_{max} = 45^\circ$). The dashed line shows the value for the smooth cylinder case.	139

9.10	Rms lift coefficient versus angle of attack. The angle of attack has been normalised with the maximum angle of attack (three-rib case: $\alpha_{\max} = 60^\circ$, four-rib case: $\alpha_{\max} = 45^\circ$). The dashed line shows the value for the smooth cylinder case.	141
9.11	Time history of C_l for three- and four-rib cylinders at angles of attack normalised with maximum angle of attack: (a) - $\alpha/\alpha_{\max} = 0$, (b) - $\alpha/\alpha_{\max} = 0.5$, (c) - $\alpha/\alpha_{\max} = 1$	142
9.12	Strouhal number versus angle of attack. The angle of attack has been normalised with the maximum angle of attack (three-rib case: $\alpha_{\max} = 60^\circ$, four-rib case: $\alpha_{\max} = 45^\circ$). The dashed line shows the value for the smooth cylinder case.	143
9.13	Mean and fluctuating lift force coefficients and Strouhal number calculated using projected frontal width as characteristic linear dimension versus angle of attack for the three-rib case and triangular prism: a) C_d^* , b) $C_d'^*$, c) C_l^* , d) $C_l'^*$, e) St^* . The dashed line shows the value for the smooth cylinder case. Data from experimental studies for low-aspect ratio triangular cylinders Iungo and Buresti (2009) and high-aspect ratio cylinders Seyed-Aghazadeh et al. (2017) are shown for comparison where available.	145
9.14	Mean and fluctuating lift force coefficients and Strouhal number calculated using projected frontal width as characteristic linear dimension versus angle of attack for the four-rib case and square prism: a) C_d^* , b) $C_d'^*$, c) C_l^* , d) $C_l'^*$, e) St^* . The dashed line shows the value for the smooth cylinder case. Data from Huang et al. (2010) (standard square cylinder) and Carassale et al. (2014) (standard square cylinder and square cylinder with rounded corners; datasets for smooth flow conditions) are shown for comparison where available.	146
9.15	Mean streamlines variation with angle of attack for the three-rib cylinder case: a) $\alpha = 0^\circ$, b) $\alpha = 10^\circ$, c) $\alpha = 27.5^\circ$, d) $\alpha = 30^\circ$, e) $\alpha = 40^\circ$, f) $\alpha = 50^\circ$, g) $\alpha = 60^\circ$	149
9.16	Mean streamlines variation with angle of attack for the four-rib cylinder case: a) $\alpha = 45^\circ$, b) $\alpha = 40^\circ$, c) $\alpha = 30^\circ$, d) $\alpha = 22.5^\circ$, e) $\alpha = 15^\circ$, f) $\alpha = 7.5^\circ$, g) $\alpha = 0^\circ$	150
9.17	Vortex development around the four-rib cylinder at $\alpha = 45^\circ$ at different phases in the shedding cycle.	151

9.18	Vortex development around the four-rib cylinder at $\alpha = 22.5^\circ$ at different phases in the shedding cycle.	153
10.1	a) Geometrical representation of the studied geometry. b) Definitions of length scales, angle of attack, and location of the pressure taps on the model of the cactus-shaped cylinder with four ribs.	160
10.2	Schematic diagram of the experimental setup. a) Top view, showing 2D insert to the test section and location of pressure taps on the cactus-shaped cylinder model. b) Side view, showing force platform mounted beneath the wind tunnel test section.	161
10.3	Schematic diagram of the experimental setup used for PIV quantitative visualisations of the flow over the top part of the cactus-shaped cylinder with four ribs.	162
10.4	Mean aerodynamic force coefficients as a function of angle of attack. (a) mean drag coefficient; (b) mean lift coefficient. Data for the square cylinder from Tamura and Miyagi (1999) ($Re=30,000$) and from Carassale et al. (2014) ($Re=37,000$) was recalculated with projected frontal width for comparison purposes. (The legend in part b) applies to both parts of this figure.)	165
10.5	Unsteady lift force coefficient of the cactus-shaped cylinder as a function of angle of attack at $Re = 100,000$. Data for the square cylinder from Lee (1975) ($Re=176,000$) and from Carassale et al. (2014) ($Re=37,000$) was recalculated with projected frontal width for comparison purposes.	166
10.6	Distribution of the pressure coefficient on the surface of the cactus-shaped cylinder with four ribs at $Re=100,000$. a) angular orientations up to critical angle of attack ($\alpha = 0^\circ - 13^\circ$); b) angular orientations above critical angle of attack ($\alpha = 14^\circ - 45^\circ$).	168
10.7	Strouhal number of the cactus-shaped cylinder with four ribs as a function of angle of attack. Data for the square cylinder from Igarashi (1984) ($Re=37,000$) and Huang et al. (2010) ($46,000 \leq Re \leq 94,000$) is presented for comparison.	169
10.8	Contours of the mean vorticity fields and mean flow streamlines around the top part of the cactus-shaped cylinder with four ribs at $Re=50,000$. a) $\alpha = 0^\circ$; b) $\alpha = 5^\circ$; c) $\alpha = 10^\circ$; d) $\alpha = 13^\circ$; e) $\alpha = 15^\circ$; f) $\alpha = 30^\circ$. The freestream velocity is in the negative x-direction.	170

10.9	Mean flow streamlines around the back rib of the cactus-shaped cylinder with four ribs at $Re=50,000$. a) $\alpha = 10^\circ$; b) $\alpha = 13^\circ$. The freestream velocity is in the negative x-direction.	171
10.10	Power spectra of the u-component of the velocity determined for four angular orientations at two locations behind the cactus-shaped cylinder at $Re=100,000$. a) $x = 2.5D$, $y = 2.5D$ b) $x = 6.5D$, $y = 2.5D$. The scale on the vertical axis is arbitrary but the same scale is used for each spectrum. For clarity, the spectra have been shifted relative to each other along the vertical axis.	173
10.11	Aerodynamic force coefficients and Strouhal number as a function of an angle of attack obtained from the present experiments at representative Reynolds number of 100,000 compared to the URANS results (Zhdanov and Busse, 2019) for the same shape at Reynolds number of 20,000. (a) Force coefficients; (b) Strouhal number.	174

List of Tables

5.1	Values of λ_i for different vibration modes from Blevins (1979).	59
5.2	Modulus of elasticity determined from mechanical tests for the bottom part of Arabidopsis inflorescence stems. Data is presented as mean \pm standard deviation. \overline{E}_1 , \overline{E}_2 and \overline{E}_3 mean values of the modulus of elasticity determined from corresponding natural frequencies in the vibration tests. \overline{E} mean values of the elastic modulus.	63
5.3	Modulus of elasticity determined from mechanical tests for the top part of Arabidopsis inflorescence stems. Data is presented as mean \pm standard deviation. \overline{E}_1 , \overline{E}_2 , \overline{E}_3 and \overline{E}_4 mean values of the modulus of elasticity determined from corresponding natural frequencies in the vibration tests. \overline{E} mean values of the elastic modulus.	65
5.4	Comparison of the current method with other recent dynamic methods that can be applied on Arabidopsis inflorescence stems.	70
6.1	Overview of the changes to the Arabidopsis biomass (mean \pm SD) that were assessed after the end of the unidirectional wind treatment with a constant flow speed of 5 m s ⁻¹ in the second experiment.	88
6.2	Contribution of tissues to the total cross-sectional area of the Arabidopsis primary inflorescence stem segments (mean \pm SD) that was assessed after the end of the unidirectional wind treatment with a constant flow speed of 5 m s ⁻¹ in the second experiment.	91
7.1	The effect of mechanical perturbations by different types of brushing and brushing material on morphological and biomechanics parameters of Arabidopsis.	110
7.2	The effect of mechanical perturbations by different types of brushing and brushing material on the contribution of anatomical tissues to the total cross-sectional area of the the primary inflorescence stem of Arabidopsis.	112

9.1	Overview of the experimental and numerical values of the aerodynamic coefficients and Strouhal number for circular cylinder at $Re = 20,000$. Entries for the rms lift coefficient C'_l marked with * have been computed from the amplitude of the lift fluctuations C_l^{amp} assuming a sinusoidal signal.	136
10.1	Overview of the extreme values of aerodynamic coefficients and Strouhal number at critical angle of attack for cactus-shaped cylinder and previously reported data on the square cylinder.	172

Chapter 1

Introduction

*Who has seen the wind?
Neither I nor you:
But when the leaves hang
trembling,
The wind is passing through.*

*Who has seen the wind?
Neither you nor I:
But when the trees bow down
their heads,
The wind is passing by.*

Christina G. Rossetti
(1830–1894)

Wind-induced motion of plants has been observed over millennia and is reflected in poetry and prose of many cultures. The most basic observation of wind is often through its effects on plants, such as the motion of branches, forming a part of the empirical description of wind conditions on the Beaufort wind force scale. Wind-plant interaction is a universal human experience, since wind is ubiquitous on Earth and plants are present on all continents constituting more than 80% of the whole biomass on our planet (Bar-On et al., 2018). While wind is an important environmental and ecological factor that plays a significant role in the life cycle of plants and their evolution (Nobel, 1981), plants, in turn, are of great importance for humans and animals since they are the most important source of food on Earth. Therefore, it is essential to investigate how wind affects plants and how plants respond to these interactions. The importance of this research topic is reflected in the United Nations

Sustainable Development Goals (United Nations, 2011), where out of the 17 defined goals, wind-plant interaction studies can directly or indirectly contribute to at least four, namely: #2 Zero hunger, #7 Affordable and clean energy, #13 Climate action, and #15 Life on land.

One of the major motivations for studies on wind-plant interaction is global food security, where wind induced lodging¹ poses a serious challenge. A number of major crop plants, such as wheat, rice, barley, oats, maize, rice, oilseed rape, etc. are susceptible to this type of wind damage (Berry et al., 2004; Kashiwagi and Ishimaru, 2004; Berry and Spink, 2006). In cereals, lodging can account for over 80% of the total yield reduction (Shah et al., 2017a). Wind damage in the form of windthrow², caused by extreme and strong winds, is also one of the main abiotic threats to trees and is a primary concern in risk management in forestry (Gardiner and Quine, 2000; Gardiner et al., 2013). Schelhaas et al. (2003) estimated that storms caused over 50% of total damage from all natural sources to the forests in Europe between 1950 and 2000. Moreover, the amount of damage caused by strong winds is showing an increasing trend. Climate models predict that the frequency of extreme wind conditions in middle latitudes beyond tropics will increase due to global warming (Gastineau and Soden, 2009). In addition, various global climate models and meteorological records show significant increase in surface winds over the UK and Northern Europe (Hosking et al., 2018; Ruosteenoja et al., 2019), and China (Zhang et al., 2020). The detrimental impact of high winds on crops and trees is the subject of concern not only to scientists but also governments, as economic consequences are usually substantial. The estimated economic losses in the UK due to lodging of crop plants can be up to £105 million for wheat and up to £64 million for oilseed rape per annum (Baker et al., 2014). Although the economic impact of Hurricane Low Q in 1968, one of the worst windstorms in Scotland and Glasgow in particular, was not recorded, the affected area lost up to 30% of the forest stock (Quine et al., 1995). Gardiner et al. (2016) estimated the total cost of the storm ‘Klaus’ in 2009 to the forestry in south-west France to be over 3 billion Euros. Therefore, research of wind effects on plants is essential to reduce the negative impacts of extreme and elevated wind conditions on crops yield, food security, forestry, and economy through management practices that are based on the results of these studies and take into account wind induced changes to plants. In addition, wind-plant interaction studies

¹Wind induced lodging is permanent displacement of plants from their vertical orientation caused by wind.

²Windthrow is uprooting of trees by wind.

can be used to inform the direction of breeding of new traits to provide resistance against wind induced damage.

In addition to the negative effects in the form of irreversible damage from the aforementioned extreme wind conditions, wind-plant interaction studies are motivated by the need to understand the fundamental influence of low and moderate winds on plants. These wind conditions are more common and are regularly experienced by plants in their natural environment. Wind regulates the microclimate of plants and can alter heat and mass transfer in them (Jones, 2013). Also, it influences plants' reproduction through pollination (Niklas, 1985) and seed dispersal (Howe and Smallwood, 1982), and can modify photosynthesis (Burgess et al., 2016). Furthermore, wind exerts mechanical stress on plants that can affect their growth, morphology, and mechanical properties (de Langre, 2008; Gardiner et al., 2016). Thus, wind influences vital plant functions and can have either beneficial or detrimental effects on plant growth, development, and survival.

Overall, all the aforementioned studies contribute to achieving the UN sustainable development goals #2, #13, and #15. In addition, studies on wind effects on plants are also important in the context of increasing global demand for generation of renewable energy that forms the core of goal #7. Plants are used for production of contemporary biofuels such as bioethanol and biodiesel. While biofuels of the first generation are made of starch and sucrose of maize and sugarcane, respectively, the second generation is based of lignocellulosic biomass of various plants (Sims et al., 2010; Chum et al., 2014). Thus, in addition to the aforementioned wind induced lodging and other types of wind damage it is important to understand what impact wind has on the yield and quality of plant biomass. Wind-plant interaction also found practical application in the wind energy generation, where plant-inspired designs of wind energy harvesters have been developed (see e.g. Oh et al. 2010; McCloskey et al. 2017; Wang et al. 2018). The design of these synthetic plants may be more visually appealing and generate less noise, addressing common adverse environmental impacts of conventional wind turbines (Premalatha et al., 2014). Moreover, such harvesters can pose a lower hazard to birds and bats that suffer from collisions with wind-energy farms (Curry, 2009).

While biomimetic designs, especially in terms of flow control, drag reduction, and flight are dominated by the representatives of the animal kingdom (see e.g. Bushnell and Moore 1991; Fish and Lauder 2006), plants have been evolving in windy environments, and thus studying their adaptation strategies can make contributions to this field as well. For example, ribs and spines on the trunks of tall cacti have shown

potential for biologically inspired passive flow control over bluff bodies (Talley et al., 2001; Levy and Liu, 2013). Furthermore, wind dispersal of seeds inspired biomimetic designs of unmanned aerial vehicles (UAV), micro air vehicles (MAV), e.g. Samarai, a maple seed-inspired UAV (Lockheed Martin, 2011), and long range drones based on the recent finding on the flight mechanics of a dandelion fruit (Cummins et al., 2018), that can potentially be used for Mars exploration (Sherman et al., 2020).

Another, probably less obvious, motivation to study wind-plant interaction is for creation of realistic scenes of nature in the virtual environments of video games, films, virtual reality applications, etc. (Diener et al., 2009; Derzaph and Hamilton, 2013). To create a high-quality product with enhanced realism, not only static plant models, i.e. detailed modelling of plant geometry, are required, but also dynamic plant models, which allow to recreate plant motion in response to external forces such as wind. Dynamic models are created based on biological, physiological, and biomechanical principles and require corresponding studies to simulate valid and realistic behaviour. In addition, these principles are used for scientific simulations of plant development under predefined conditions.

Overall, studies of wind-plant interaction and wind effects on plants have significant economic, scientific, and practical importance. Driven by a diverse range of motivations from purely biological to practical engineering applications, these investigations often require a multidisciplinary approach. Thus, most of these studies lie in the domain of biomechanics – “a discipline that operates at the interface of engineering and biology” (Niklas, 1992), plant biomechanics to be precise. This PhD project is a plant biomechanics study that combines fluid mechanics, engineering, and plant sciences to investigate the effects of continuous mechanical stress imposed by wind on plants and how plants adapt to it. Two different aspects of wind-plant interaction, namely the response of *Arabidopsis* to wind and other types of mechanical stress and flow past succulent-inspired cylinders, are explored in the two distinct parts of this thesis. The detailed structure of the thesis is given in the following.

1.1 Structure of the thesis

Following this general introduction, the structure of this thesis is as follows:

Chapter 2 presents the detailed background to this PhD project. The detailed research objectives for both parts are also formulated.

Part I: Response of *Arabidopsis* to wind and other types of mechanical stress

Chapter 3 provides information on the widely used model organism *Arabidopsis thaliana* and methodology for experiments with it for readers who do not have a background in plant science.

Chapter 4 begins with a review of the existing and previously used facilities for research on wind-plant interaction, followed by the design and characterisation of the bespoke wind tunnel that was developed as part of this project.

Chapter 5 describes the multiple resonant frequency forced vibration method for mechanical characterisation of *Arabidopsis* stems, including its validation and comparison with other recent dynamic testing methods for plants. This method was developed as part of this PhD project. This chapter is given in the form of the paper titled “A new perspective on mechanical characterisation of *Arabidopsis* stems through vibration tests” published in the Journal of the Mechanical Behavior of Biomedical Materials in 2020.

Chapter 6 explores the influence of a constant unidirectional wind treatment on *Arabidopsis*. The wind induced anemotropic response and the effects on *Arabidopsis* morphology, mechanical properties, anatomical tissues organisation, and ion content are discussed. This chapter is given in the form of the paper titled “Wind-evoked anemotropism affects the morphology and mechanical properties of *Arabidopsis*” published in the Journal of Experimental Botany in 2021.

Chapter 7 investigates the possibility to mimic effects of wind on *Arabidopsis* by the widely used brushing method. Thigmomorphogenetic response of *Arabidopsis* as well as changes in its mechanical properties as a result of two different types of brushing treatment are explored, discussed, and compared with the previously reported wind-induced alterations. This chapter is given in the form of a manuscript in preparation.

Part II: Aerodynamics of succulent-inspired cylinders

Chapter 8 presents the specific background for the second part of the thesis.

Chapter 9 investigates the angle of attack dependence of the flow past two succulent-inspired cylinders with three and four ribs at a biologically relevant Reynolds number of 20,000 using 2D URANS simulations. This chapter is given in the form of the paper titled “Angle of attack dependence of flow past cactus-inspired cylinders with a low number of ribs” published in the European Journal of Mechanics-B/Fluids in 2019.

Chapter 10 presents a wind tunnel investigation of the angle of attack and Reynolds number dependence of the aerodynamic characteristics and flow around a succulent-inspired cylinder with four ribs identical in shape to the four rib cylinder previously investigated by URANS simulations. This chapter is given in the form of the paper titled “Experimental investigation of the angle of attack dependence of the flow past a cactus-shaped cylinder with four ribs” published in the Journal of Wind Engineering and Industrial Aerodynamics in 2021.

Chapter 11 provides the conclusions for both parts of this thesis. Suggestions for future work based on the obtained results are also given in this chapter.

Chapter 2

Background

In their natural environment plants experience various biotic and abiotic stresses that have impacts on their morphology, anatomy, physiology, and growth. Among abiotic stresses, wind is one of the most important types that imposes mechanical loading on plants. This in turn leads to wind-plant interaction – one of the major subjects of plant biomechanics that has been actively and widely studied (for reviews see Van Gardingen and Grace, 1991; de Langre, 2008; Gardiner et al., 2016; Gosselin, 2019).

This chapter describes the fundamental concepts of wind influence on plants with the intent to provide a common foundation for both engineers and plant scientists. The more specific aspects are expanded and completed in the context of the following chapters. The research objectives for this PhD project are formulated at the end of this chapter.

2.1 Preliminary concepts of fluid mechanics

Wind imposes an external force on any object, including plants, which is the sum of three orthogonal components, namely drag, lift, and side force. Drag is the component of the total force acting in the direction of the flow, whereas lift and side forces are the components of the total force acting in the directions normal to the flow. In the context of wind-plant interaction, drag is the most important force exerted on plants by wind, while the other components are normally excluded from consideration. The drag (D) of an object depends on its size, shape, flow speed, and properties of the fluid with which it is in the relative motion. It is defined as:

$$D = \frac{1}{2}\rho AC_D U_\infty^2, \quad (2.1)$$

where ρ is the density of the fluid, A is the frontal area of the object, C_D is the drag coefficient, and U_∞ is the flow velocity in the freestream. The drag coefficient is a dimensionless representation of drag that takes into account shape of the object and is also dependent on another dimensionless parameter – the Reynolds number (Re). This number is defined as a ratio of inertial and viscous forces

$$Re = \frac{\rho L U_\infty}{\mu}, \quad (2.2)$$

where L is the characteristic linear dimension and μ is the dynamic viscosity of the fluid. When Re is low, viscous forces dominate in the flow and it stays laminar. At high Reynolds numbers inertial forces prevail and the flow becomes turbulent.

Drag is comprised of two components, namely skin friction (frictional drag) and pressure drag. Both types of drag are essentially a result of the fluid viscosity, but frictional drag is caused by the friction of fluid against the surface of an object and is proportional to the surface area of an object exposed to the flow. Pressure drag is caused by the pressure difference between the front and rear sides of the body due to flow separation from the body and consequent wake formation. However, the relative contributions of these types of drag to the total drag differ depending on the shape of the body and the Reynolds number.

Based on the dominant type of drag component objects can be subdivided into streamlined and bluff bodies. Objects from the former group (e.g. airfoils, submarines, sharks) have a shape that minimises or eliminates flow separation and consequently the wake, or minimises them to a small region just behind the body. For streamlined bodies viscous drag is the dominant type of drag regardless of the Reynolds number. On the other hand, flow separates from the bluff bodies (e.g. chimneys, buildings, lamp posts) due to their shape and a large wake region is formed. Consequently, pressure drag makes the largest contribution to the total drag. However, since separation is in general Reynolds number dependent, skin friction can account for a significant part of the total drag of bluff bodies at low Re , where viscous effects are dominant. At the same time, at high Reynolds numbers most of the total drag of a bluff body arises from its pressure component. For example, for a circular cylinder at $Re = 10.5$ frictional drag contributes approximately 42% to the total drag (Thom, 1933), while at $Re = 100,000$ only approximately 0.75% (Achenbach, 1968).









2D bodies		C_D	3D bodies		C_D
	hollow semi-cylinder	2.30		solid hemisphere	1.17
	hollow semi-cylinder	1.20		solid hemisphere	0.42
	triangular cylinder	1.55		hollow hemisphere	1.42
	triangular cylinder	2.00		hollow hemisphere	0.38

Figure 2.1: Drag coefficients for different orientations of various two- and three-dimensional bodies with respect to the incoming flow in the range of Reynolds numbers between 10^4 and 10^6 . Flow direction is from left to right. Data is taken from Hoerner (1965).

It should be noted that depending on its orientation with respect to the flow, the same object can be either a streamlined or a bluff body. A widely used example to demonstrate this phenomenon is the infinitely thin flat plate. When it is placed parallel to the flow direction its surface is aligned with the flow, while frontal area is infinitely small, and no separation is observed. Thus, the drag experienced by the plate in this orientation is friction drag. On the other hand, when the same plate is placed with the surface normal to the flow direction, its frontal area is significantly higher compared to the previous case, the flow separation occurs from its edges, and a wake is formed behind. Consequently, its drag is mainly due to pressure drag which is a result of pressure difference between the front and rear surfaces of the plate. The same behaviour, but in the plant biomechanics context, was demonstrated for an artificial leaf of the broad bean (*Vicia faba*) in the wind tunnel experiments by Thom (1968). When an aluminium leaf model was mounted parallel to the flow, its drag coefficient was very close to the theoretical value for the skin friction coefficient of a flat plate of the same shape and surface area. At an orientation normal to the flow, the drag coefficient was mostly due to pressure drag.

The shape of an object significantly influences its drag reduction abilities that come from the change of orientation with respect to the incoming flow (see Figure 2.1). For example, C_D of a hollow hemisphere facing downstream is more than three times lower compared to the same hemisphere facing flow with its concave surface. On the other hand, reorientation of a right isosceles triangular cylinder from downstream to upstream position of its right angle reduces drag coefficient

only by 22.5%.

2.2 Plant adaptation strategies to wind

Plants must face and cope with the wind since, unlike humans or animals, they cannot shelter or hide themselves from it. To grow and survive in windy environments plants have developed a number of adaptation strategies. These strategies include streamlining and reconfiguration, damping and wind-induced pruning (brittle reconfiguration) (Gardiner et al., 2016).

2.2.1 Streamlining and reconfiguration

One approach plants use to lower the experienced drag force is to adjust their orientation with respect to the wind direction, taking advantage of the previously discussed dependence of drag on the orientation. For instance, the drag coefficient of a daffodil flower facing downwind (convex shape) is lower by approximately 30% compared to its upwind (concave shape) orientation (Etnier and Vogel, 2000). Moreover, it was observed that with an increase of the wind speed daffodils utilise this dependence and reorient themselves by twisting their stems, to achieve the flower position of minimum drag and thus reduce experienced wind loading.

Most of the plants and their parts (e.g. leaves, branches) deform under wind due to their relative flexibility. Vogel (1984) pointed out the term ‘deformation’ has some pathological meaning for plants and introduced term ‘reconfiguration’ to describe changes of plant shape under wind. Together with the streamlining of the plants shape with the increase of the flow speed, reconfiguration is an important adaptation strategy of plants to wind and wind gusts in their environment. In terms of this adaptation strategy, plants reduce their frontal area and aerodynamically optimise their shape to experience less force from the wind. The details of the physics and mechanics behind streamlining and reconfiguration can be found in Vogel (1994) or in the review by Gosselin (2019).

Harder et al. (2004) showed that streamlining by reconfiguration and reorientation is a common feature for plants regardless of their size and growth environment. Studying the reconfiguration mechanism in brown seaweed (*Durvillaea*) and the giant reed (*Arundo donax*) they discovered that these plants share the same streamlining concepts even though their growth environments and size are quite different. In addition, Vollsinger et al. (2005) showed in wind tunnel experiments with various

hardwood species that streamlining and decrease in tree crown frontal area is common for all of them. In general, the effects of reconfiguration on drag reduction are widely studied for trees at various wind speeds (Hedden et al., 1995; Speck, 2003; Rudnicki et al., 2004).

Reconfiguration was also studied separately for tree leaves. Vogel (1989) conducted wind tunnel experiments with various broad leaves and determined that pinnately compound leaves of black locust (*Robinia pseudoacacia* L.) form cylinders with increasing wind speed and have the lowest drag among the studied species. The general trend of decreasing drag coefficient with the increase of wind speed was found in all leaves except for individually tested white oak (*Quercus alba* L.).

For rigid objects, e.g. plants that cannot reconfigure under wind, the drag scales with the square of the wind speed (see equation 2.1). This relationship between drag and wind speed has been generalised by Vogel (1984, 1989) to account for the streamlining and reconfiguration that can be observed for most plants:

$$D \propto U^{2+V}, \quad (2.3)$$

where V is the Vogel exponent. The Vogel exponent of a plant or its part can be determined experimentally by conducting a series of drag measurements at various flow speeds and plotting speed specific drag (D/U^2) versus speed on a log-log scale. V is then evaluated as a slope of this curve (see Vogel (1994) for details). The values of the Vogel exponent were determined for many aquatic and terrestrial species and their parts (Harder et al., 2004; de Langre et al., 2012) in the range from -1.16 to 0.

When plants are subjected to strong prevailing winds, the streamlining and reconfiguration can become irreversible and result in so called flagged trees (Figure 2.2). The windswept shape of flagged trees is a result of plastic and viscoelastic deformations of branches due to wind loading and is an important acclimation response to windy environments that occurs over long periods of time (Telewski, 2012). Streamlined crowns of windswept trees experience less speed specific drag and decrease the probability of stem breakage or uprooting from wind loading (Telewski and Jaffe, 1986a). The degree of crown streamlining in trees depends on the wind strength and exposure time, i.e. it is dose specific (Griggs, 1946). Moreover, the ability to develop a windswept form appears to be plant specific as not all trees become flagged in a response to the same wind exposure in their natural environment (Noguchi, 1979).



Figure 2.2: Flagged tree a result of irreversible streamlining and reconfiguration that occurs over time due to regular and continuous exposure to strong prevailing winds in the natural environment. This photo was taken in Gourock on the windy west coast of Scotland.

2.2.2 Damping

Another method by which plants deal with wind loading is through damping of wind-induced oscillations. Wind energy is dissipated in plants from stem to bigger branches and further to small branches through structural damping as was shown by Spatz et al. (2007) for Douglas fir tree (*Pseudotsuga menziesii*). Spatz and Theckes (2013) classified the different types of oscillation damping in trees as viscous damping, aerodynamic damping, structural damping, damping by interaction with neighbouring trees, and damping by root soil interaction. A similar concept was discussed by James et al. (2006), who pointed out that the complex branch structure of trees decreases sway motion through mass interaction between branches and trunk. Moreover, James et al. (2006) described the detuning strategy of trees, i.e. the minimisation of occurrence of resonant and harmonic frequencies through dynamic mass damping. In addition to increasing tree stability, detuning helps in dealing with wind loading by minimising energy transfer from the wind to the trunk and root.

2.2.3 Wind-induced pruning

Wind-induced pruning is an extreme case of reconfiguration, during which a plant sheds leaves and/or branches in order to decrease wind loading on the whole structure. This strategy is a common mechanism for plants to reduce the negative impacts of high loadings. Mathematical modelling showed that wind-induced pruning of the crown area by 50% significantly reduced fatal damage to loblolly pine (*Pinus taeda* L.) during hurricane winds (Hedden et al., 1995). Similarly, fracture and subsequent loss of a number of tree branches during high winds decrease the impact of the wind-induced bending moment on the tree trunk and prevent its breakage (Niklas and Spatz, 2000). Wind-induced pruning also improves dynamic mass damping of trees in windy conditions through reduction of excessive sway motions of the trunks and thus contributes to their overall mechanical stability (James et al., 2006). In addition, prevention of trunk fracture or plant uprooting by brittle reconfiguration is of biological importance as a broken trunk in most cases will lead to the death of the tree, while branches can re-grow (Lopez et al., 2011).

2.2.4 Cacti and succulents

While streamlining and reconfiguration is a common way for most plants to deal with the wind loading, some plants cannot employ this strategy, even when subjected to high winds, due to their structure. Cacti and a number of other arborescent succulents (Figure 2.3) do not have leaves and their stems and branches lack flexibility, thus disabling reduction of the experienced drag force through reconfiguration. However, these plants are still able to cope with high wind loadings in their natural environment – usually deserts, without being broken or uprooted. This phenomenon has most widely been studied for the saguaro cactus (*Carnegiea gigantea*) (Figure 2.3A). These columnar cacti are typically 8 to 15 m tall, have up to 30 ribs on their stems of diameter ranging from 0.3 to 0.8 m, but their root system is too shallow to provide adequate anchorage during wind gusts (Pierson and Turner, 1998). Based on the Remote Automatic Weather Stations (RAWS) USA climate archive data, the maximum recorded wind speed in the region of natural habitat of saguaro cacti between 2002 and 2020 was 29.5 m/s (Western Regional Climate Center (2020), Selles, AZ RAWS). Moreover, wind gusts over 17 m/s occurred regularly in this area over the same time period. In the context of a saguaro cactus of 0.6 m in diameter this would correspond to Reynolds numbers of 1.1×10^6 and 6.5×10^5 , respectively, in dry air at 25 °C. Under the same wind conditions, a succulent with stem diameter

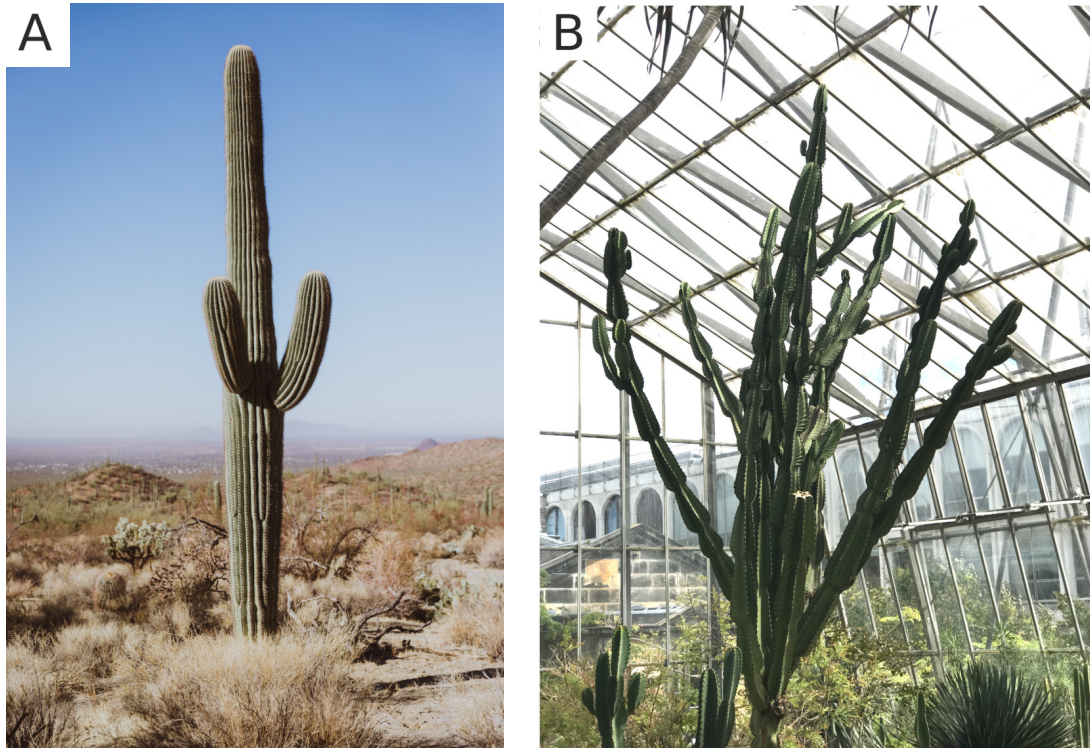


Figure 2.3: Representatives of Cactaceae and Euphorbiaceae families that developed similar plant structure to adapt to dry desert conditions in the process of convergent evolution. (A) Saguaro cactus (*Carnegiea gigantea*) in Saguaro National Park, USA (Magnuson, 2018). (B) Candelabra tree (*Euphorbia ingens*) in the Royal Botanic Garden Edinburgh, Scotland.

of 0.2 m would experience Reynolds numbers of 1.9×10^5 and 1×10^5 . A number of studies performed on cactus-like cylinders showed that ribs and spines modify the flow field around the cactus and minimise wind impact at low and high Reynolds number (Talley et al., 2001; Babu and Mahesh, 2008; Levy and Liu, 2013; Wang et al., 2014; Cheng et al., 2018).

It should be noted that enhancement of aerodynamics performance is not the only function of the ribs and spines that are present on trunks of cacti and succulents. Plants are complex organisms and their parts usually have multiple functions that complement each other. In the case of spines, they also protect from herbivores, provide shading (Nobel et al., 1986), collect moisture from fog (Ju et al., 2012), and guide movement of dew drops towards the stems (Malik et al., 2016). In turn, the ribs on the cactus trunk provide shading that reduces surface temperature of the plant (Nobel, 1978), facilitate in cactus swell and shrink during raining and dry seasons, respectively (Nobel, 1977), and contribute to mechanical stability (Niklas et al., 1999).

2.3 Thigmomorphogenesis

When subjected to external mechanical stimuli plants exhibit physiological response through changes in their growth and development. A similar observation was already made by Newcombe (1895) more than a century ago in a review of early works on the regulatory growth of plants. However, only in the late 20th century Jaffe (1973) coined the term ‘thigmomorphogenesis’ to describe these changes and more systematic research of this phenomena began (see also Biddington (1986); Braam (2005); Telewski (2016); Gardiner et al. (2016) for reviews). Thigmomorphogenesis occurs gradually and therefore is not noticeable right away but over time the changes can become significant and obvious (Braam, 2005). The common thigmomorphogenetic responses found in a large number of plants include (see e.g. Jaffe, 1973; Telewski and Jaffe, 1986a,b; Telewski and Pruyn, 1998; Paul-Victor and Rowe, 2011; Gladala-Kostarz et al., 2020):

- inhibition of the shoot elongation;
- increase in shoot radial growth (in case when cambium layer is present);
- decrease in aboveground and increase in below ground plant biomass.

On the other hand, no consistent thigmomorphogenetic effect was observed on mechanical properties of plants. For example, mechanical treatment resulted in both more flexible (Telewski and Jaffe, 1986b) and more rigid stems (Kern et al., 2005). Thigmomorphogenetic changes are likely to be adaptive and help plants to withstand stresses in their natural environment (Jaffe, 1973; Telewski and Jaffe, 1986a).

Initially, thigmomorphogenesis was observed as a result of mechanical bending of plants (Gardiner et al., 2016). On the other hand, it has been long known that plants subjected to wind, especially to high winds, demonstrate similar changes in their growth and development. For example, more than 200 years ago, Knight (1803) experimentally showed that young apple trees, which were free to sway in the wind, increased radial growth in the bottom parts of their trunks while their overall growth (extension) was inhibited compared to the staked apple trees that grew in the same field. Taking into account these similarities, a number of studies used various types of mechanical perturbations such as brushing (Paul-Victor and Rowe, 2011), bending (Niez et al., 2020), and vibration (Niklas, 1998) to simulate effects of wind on plants. However, results of factorial studies (Smith and Ennos, 2003; Anten et al., 2010), where effects of wind and mechanical stress were separated in the same

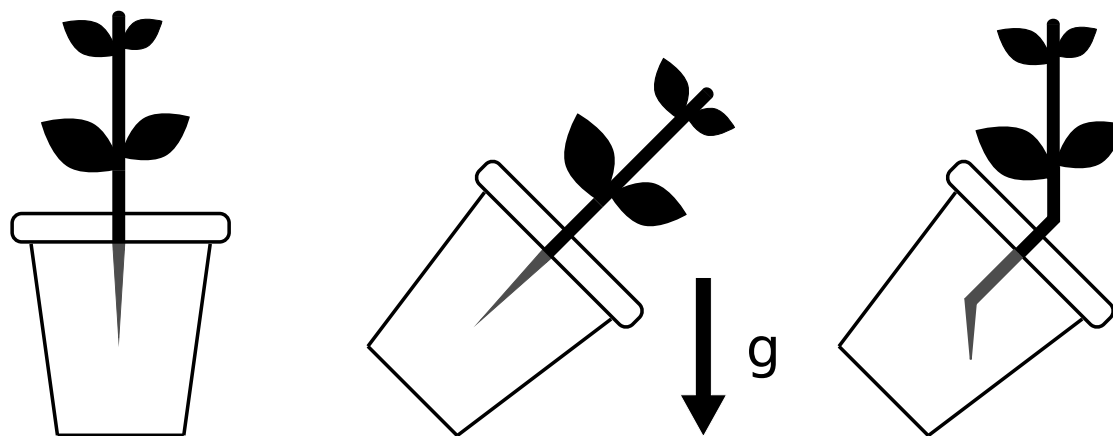


Figure 2.4: Schematic example of gravitropic response in plants. When a plant is tilted from the vertical orientation both root and shoot exhibit gravitropism until they are realigned with the direction of gravity vector.

experiment, cast doubt on whether this approach is entirely correct. Smith and Ennos (2003) found that wind and flexing have opposite effects on plant growth in sunflowers. Compared to the control plants, which were grown without any imposed stress, mechanical bending inhibited stem length while exposure to air flow alone resulted in taller plants. Anten et al. (2010) reported that while growth reduction was common for mechanically treated and wind exposed *Plantago major* plants the changes in their morphology and mechanical properties differed.

2.4 Tropic responses in plants

Despite the fact that plants are sessile organisms they still can move to cope with changes in their environment and to ensure optimum growth conditions. Probably, the most widely known examples of plant movements are catching of prey by the Venus fly trap (*Dionaea muscipula*) and the folding of leaves of the sensitive plant (*Mimosa pudica* L.) or carambola (*Averrhoa carambola*) after being touched. These movements are independent of the external stimulus direction and are known as nastic movements.

In addition, plants exhibit movements through tropism (tropic response), which is defined as a growth movement or reorientation induced in a direction related to the direction of external stimuli (Iino, 2006). Depending on the relative directions of tropism and stimulus the former can be either positive or negative. A tropic response is considered positive when the direction of growth is towards the stimulus. On the other hand, when growth direction is away from the stimulus a tropic response is

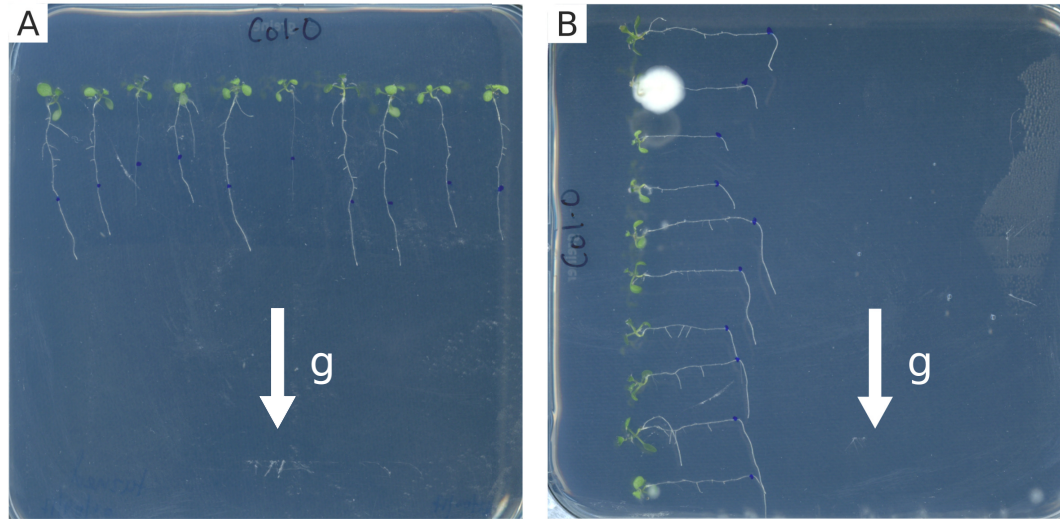


Figure 2.5: An example of tropic response in Arabidopsis. Roots of Arabidopsis Col-0 exhibit positive gravitropism and reorient their growth direction with respect to the new direction of the gravity vector. (A) Control group. (B) Plate with experimental group seedlings, that was turned 90° in the counterclockwise direction after the initial growth period. The length of the roots at the point in time, when the experimental plate was turned, is marked with the dot in both groups.

negative. Plants are known to respond to a number of environmental factors and consequently exhibit tropic responses to them. Depending on the type of the stimulus different tropisms are distinguished and studied, e.g. plants respond to light through phototropism (Sakai et al., 2001; Legris and Boccaccini, 2020), to gravity through gravitropism (Mouliia and Fournier, 2009; Chauvet et al., 2016), to touch through thigmotropism (Huberman and Jaffe, 1986; Takahashi and Jaffe, 1990).

An example of a typical gravitropic response is schematically shown in Figure 2.4. Under normal conditions a plant grows vertically in the pot, i.e. it is aligned with the direction of the gravity vector. When the pot is tilted, misalignment with the gravity vector is sensed by the plant and a gravitropic response is triggered. As a result, plant parts exhibit gravitropic bending until realignment with the gravity vector. It should be noted that the direction of the gravitropism in above (shoot) and below ground (root) parts of a plant is different. While the shoot demonstrates negative gravitropism, change in the direction of the root growth is an example of positive tropic response. A further example of positive gravitropism of roots is presented in Figure 2.5 for Arabidopsis Col-0. This shows results of a standard experiment that was conducted for training purpose during the first year of this PhD project:

seeds of *Arabidopsis* were sown on two plates, so the root development could be visually observed. The seed germination and development of the roots took place in a growth chamber where both plates were placed vertically on the rack. When the roots of all plants were around 10-15 mm long, one plate (experimental group) was turned by 90° in the counterclockwise direction. The orientation of the second plate (control group) remained unchanged. The length of the roots in every plant from both control and experimental groups was marked at this stage. After a few days, no change in the direction of root growth was observed in the control group (Figure 2.5A). In contrast, the roots of the experimental plants responded to their new orientation with respect to the gravity vector by reorienting their growth in the direction of gravity vector (Figure 2.5B).

While wind is widely considered as an external stimulus, the tropic response of plants to it has not been widely studied and it is not clear whether plants exhibit a directional response, i.e. anemotropism, to this environmental stimulus. Interestingly, an anemotropic response was clearly demonstrated in the representatives of another biological kingdom, namely fungi (e.g. Badham, 1982; Geer et al., 1990). However, there is only a limited number of studies that contain information regarding this tropic response in plants. In addition, the available insights for plants are indirect, since anemotropic response was not the main subject of these studies. Rees and Grace (1980) investigated growth of lodgepole pine (*Pinus contorta* Douglas) subjected to a constant unidirectional wind treatment inside the wind tunnel. It was observed that the new shoots developed a curvature towards the wind, thus suggesting that a positive anemotropic response may exist. Another indirect observation of positive anemotropism can be found in Berthier and Stokes (2006) who applied periodic unidirectional wind to artificially inclined maritime pines. Wind treated plants reduced the inclination of their basal and middle parts significantly faster compared to the control group. It should be noted that in both aforementioned studies the authors did not acknowledge the observed response as anemotropic. In a review of the tropic responses of trees to wind Telewski (2012) concludes that a tropic response of plants to a unidirectional wind has not been documented in any plant system so far. In the same review, the author, based on available evidence, rejects the hypothesis that a windswept form of trees is due to negative tropic response to wind. Consequently, it is an open question whether plants have a directional response to wind.

2.5 Research objectives

This PhD thesis consists of two parts that explore different aspects of plant adaptation to the wind. The first part investigates the acclimation of a living plant to a unidirectional wind of a constant speed. While there are a number of studies on wind influence on various plants, there is no systematic study of the effects of wind on a model plant *Arabidopsis thaliana* which is widely used as a model organism in plant science. Moreover, in many studies wind influence is mimicked by other types of mechanical perturbations, opening the question of reliability of this approach. Therefore, the first part aims to provide a comprehensive study of the influence of a unidirectional wind of a constant speed on the acclimation of *Arabidopsis* and explores the possibility to simulate wind influence through the widely used brushing approach.

The main objectives of this part are as follows:

- Create a controlled and well characterised wind environment suitable for continuous growth of *Arabidopsis* (Chapter 4).
- Develop and validate a method for mechanical characterisation of *Arabidopsis* stems to assess their mechanical properties and changes induced by various types of treatment (Chapter 5).
- Perform experiments in which *Arabidopsis* is subjected to a unidirectional wind treatment at a constant wind speed (Chapter 6):
 - Evaluate wind-induced changes in plant phenotype, mechanical properties, and anatomical tissue composition of *Arabidopsis* stems.
 - Investigate whether *Arabidopsis* exhibits anemotropic response to a constant unidirectional wind and, in case such response is present, establish its direction.
 - Study the acclimation strategy of *Arabidopsis* to this type of environmental stimulus.
- Investigate whether it is possible to simulate impacts of unidirectional wind of a constant speed on *Arabidopsis* through other types of mechanical perturbation. In this case the widely used brushing method is applied (Chapter 7).

The second part of this thesis focusses on the flow past succulent-inspired cylinders. Succulents (Figure 2.3B) are native to the Eastern Hemisphere and have independently developed a plant structure similar to cacti (Figure 2.3A) of the Western Hemisphere in the process of convergent evolution (McGhee, 2011). As discussed above, for a cactus-shaped cylinder with many ribs aerodynamic benefits have been confirmed in a number of experimental and numerical studies. On the other hand, succulents tend to have a lower number of ribs and it is unexplored whether their ribs also provide aerodynamic benefits.

From a biomechanical point of view, since these two plant families have evolved similar features in similar environments, ribs in succulents could be expected to perform aerodynamically similar functions as in cacti. However, the direct extrapolation of results obtained for cactus-inspired cylinders with many ribs to succulents is not possible, since the outer shape of succulents with low number of ribs does not resemble a circular cylinder and, for example, a significant dependence of the aerodynamic forces on the angle of attack is expected.

The main research objectives of the second part of this thesis are:

- Perform a preliminary 2D URANS investigation of an angle of attack dependence of aerodynamics coefficients and Strouhal number and assess drag reduction abilities of the succulent-inspired cylinders with three and four ribs (Chapter 9).
- Conduct wind tunnel experiments (force, pressure, hot-wire anemometry and PIV measurements) with the succulent-inspired cylinder with four ribs to explore further its aerodynamics over a range of Reynolds numbers (Chapter 10).

Part I

Response of Arabidopsis to wind and other types of mechanical stress

Chapter 3

Methodology for experiments with *Arabidopsis*

This chapter provides background information on the model plant *Arabidopsis*, which was used in the experiments studying how plants adapt to various mechanical stimuli in this PhD project. The chapter starts with general information on *Arabidopsis thaliana* and why it is a popular model organism in plant science. Next, the growth and developmental stages of *Arabidopsis* are presented followed by some basic concepts of the cultivation process of this plant, including optimal conditions for its growth. Background information on the experimental methods and techniques that were used in this project is also presented. This includes: plant phenotyping, histochemical staining, turgor pressure reduction, cuticle disruption, and flame photometry.

The present chapter is intended for readers without background in plant science or related areas and provides a foundation for the later chapters of this thesis related to experiments with *Arabidopsis*.

3.1 Model plant *Arabidopsis thaliana*

Arabidopsis thaliana (Figure 3.1A) is a small herbaceous annual plant from Brassicaceae family. In plant science, it plays the same role as the fruit fly (*Drosophila melanogaster*) in genetics and developmental biology or the house mouse (*Mus musculus*) in biology and medicine, i.e. it is a model organism. *Arabidopsis* has been known to scientists for more than four hundred years, has been used as a plant model system for more than seventy (Rédei, 1992), and holds the title of the most studied flowering plant (Koornneef and Meinke, 2010). An overview of the history of

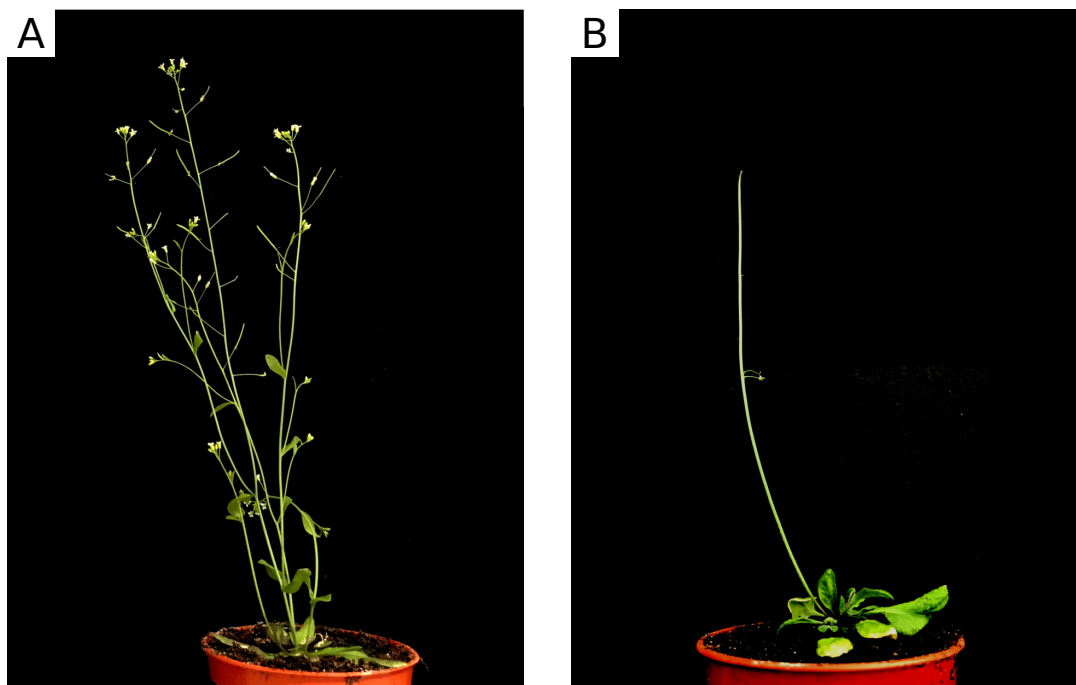


Figure 3.1: *Arabidopsis thaliana* a widely used model organism in plant science. (A) Columbia (Col-0) wildtype. (B) PIN-1 mutant.

Arabidopsis research can be found in the aforementioned references. The advantages of using *Arabidopsis* as a model organism were first outlined in 1943 by Friedrich Laibach, a scientist who laid the cornerstone of *Arabidopsis* experimental research. The key benefits, which are also relevant to the current PhD project, can be summarised as follows: (i) The plant's small size gives the possibility to grow a number of plants simultaneously within a limited space of a controlled environment, (ii) The fast development of approximately six weeks decreases the required time for experiments, (iii) The possibility to get a high number of seeds from a single plant (up to 10,000) is also beneficial in terms of using *Arabidopsis* for experimental research.

Arabidopsis has numerous natural accessions as well as thousands of mutant lines (Lamesch et al., 2012) with altered properties that are readily available, e.g. inflorescence stems of PIN-1 mutants (see Figure 3.1B) do not have lateral organs and produce no, or few flowers (Gälweiler et al., 1998). This makes *Arabidopsis thaliana* an object of a wide range of studies including plant development, physiology, and biochemistry. In addition, *Arabidopsis* is the primary choice for investigations of plant molecular genetics due to the small size of its genome (Koornneef and Meinke, 2010).

Studies on the model organism *Arabidopsis thaliana* have also contributed to

various aspects of plant biomechanics. For example, such investigations facilitated understanding of how growth forms respond to different environmental conditions (e.g. Xu et al., 1995; Bailey et al., 2001) and provided insights into wood formation (Chaffey et al., 2002). In addition, Brulé et al. (2016) discussed the possibility to use *Arabidopsis* in plant biomechanics studies as a model plant to investigate the influence of various parameters on plant stiffness.

Among all available variations of *Arabidopsis*, *Arabidopsis* genotype Columbia (Col-0) is usually considered as the reference genotype, i.e. wild type (Koornneef and Meinke, 2010). *Genotype* is a term used to describe the genetic constitution of the plant. Another term that is used throughout the following chapters is *ecotype*, which is a distinct genotype within a species that is a result of adaptation to local environmental conditions. In the scientific literature, natural accessions of *Arabidopsis* are usually referred to as ecotype, even though they do not meet its exact definition. This convention is followed in the present project, where *Arabidopsis thaliana* ecotype Col-0 was chosen as model organism to investigate the response and acclimation of plants to constant unidirectional wind and mechanical stress.

3.2 Growth and development of *Arabidopsis*

Boyes et al. (2001) classified the life cycle of *Arabidopsis* into principal growth stages. These stages cover growth and development of *Arabidopsis* from seed imbibition to maturation of the new seeds and include (in developmental order): seed germination, leaf development, rosette growth, inflorescence emergence, flower production, silique ripening, and senescence. Under normal growth conditions (discussed later) the growth stages, after completion of seed germination, overlap in time, e.g. the inflorescence stem starts to develop while the rosette growth stage is not yet complete.

In the first stage, cotyledon (embryonic leaves) and hypocotyl (part of the stem between cotyledon and roots) emerge as a result of seed germination (see Figure 3.2A). After the cotyledon is fully opened, the new leaves, which form the rosette, start to develop (Figure 3.2B). In the next stage, the rosette size increases as leaves grow bigger (Figure 3.2C) until the rosette growth is completed. The inflorescence emergence begins with the appearance of the first flower buds (see Figure 3.2D) and is accompanied by the development of the inflorescence stem. The opening of the first flower bud marks the start of the flower production stage of *Arabidopsis* development (see Figure 3.2E). With time, the flowers turn into seed holding siliques (seed pots), which start to shatter during the silique ripening stage. In the final stage of the

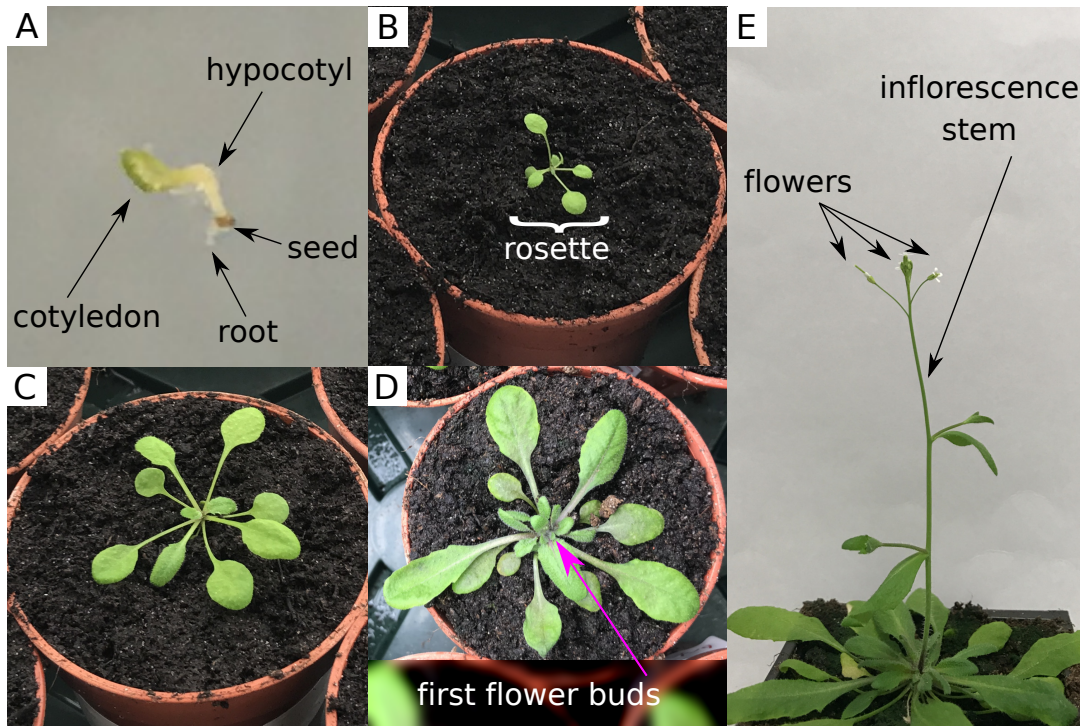


Figure 3.2: Arabidopsis growth and development. (A) Seed germination stage. (B) Leaf development stage. (C) Rosette growth stage. (D) Inflorescence emergence stage. (E) Flower production stage.

Arabidopsis growth and development cycle, the plant is going through senescence and seeds are ready to be harvested.

In the present project, wind and mechanical treatment of Arabidopsis started at the beginning of the inflorescence emergence stage and continued up to the end of the flower production stage, but before any signs of plant senescence appeared. The choice of the stage to finish treatment and proceed to destructive mechanical and anatomical characterisation of stems is motivated by the following reasons: first, close to the middle of the flower production stage, the elongation rate of the inflorescence stem starts to decrease, and its overall length remains almost constant towards the end of this stage (see Boyes et al., 2001). Second, the studied properties of plant stems are not yet affected by senescence.

3.3 Cultivation of Arabidopsis

The process of growing the model plant Arabidopsis and the required environmental conditions are well known and standard protocols exist (e.g. Sanchez-Serrano and Salinas, 2014). In this section some basic concepts of the Arabidopsis cultivation

process in soil and importance of growth conditions are explained. The following information is mainly related to ecotype Col-0 and some alterations may be required for growing other ecotypes and especially mutant lines.

3.3.1 Seed stratification

Seeds of many plants can show a period of dormancy, during which their germination does not occur even during favourable conditions. Dormancy is considered as an adaptation mechanism by which germination is avoided during unsuitable environmental conditions that can affect development and survival of the seedling (Finch-Savage and Leubner-Metzger, 2006). In order to induce seed germination, the dormancy needs to be broken. This is achieved by exposing them to a treatment that imitates natural conditions in a process called *stratification*.

For *Arabidopsis*, cold stratification (i.e. exposure to low temperature) is commonly used. In addition, subjecting *Arabidopsis* seeds to cold treatment improves germination rate and synchronises it between the seeds (Rivero et al., 2014). The latter is quite important for having plants of similar age and at the same developmental stage during the experiments. In the current project, stratification of freshly sown seeds of *Arabidopsis thaliana* ecotype Col-0 was carried out at 4°C for 48 hours, which is a standard practice for this ecotype in the Laboratory of Plant Physiology and Biophysics at the University of Glasgow.

3.3.2 Photoperiodism and growth cycles

Photoperiodism in plants includes non-directional developmental and physiological responses to non-directional but periodic light stimuli (Jones, 2013). In the natural environment, photoperiodism is related to the changes in the length of the day, which varies with season and plant growth location on Earth, and is an important adaptation mechanism. Plants respond to these changes in order to ensure favourable conditions for their growth and reproduction. In general, angiosperms can be subdivided into two types, namely short-day and long-day plants. The plants from the former group (e.g. rice, soybean and some varieties of tobacco) require a certain number of days with day duration below a certain threshold in order to start flowering. On the other hand, plants from the latter group (e.g. wheat, lettuce) begin to flower only after the duration of the daylight they are exposed to is above a certain threshold. In addition, some plants are day neutral (e.g. sunflower, tomato), i.e. their flowering response does not depend on the duration of the day. The threshold

amount of daylight duration is highly variable between species and many plants from the aforementioned groups can actually flower within the range of 12 to 14 hours of daylight even though it is not optimal for them (Garner, 1933).

Arabidopsis thaliana is a facultative long-day plant, i.e. *Arabidopsis* flowers earlier under long days than under short days. Ecotype Columbia (Col-0) used in the present study is known to flower within 3 weeks under long-day conditions, while under short-day conditions the time to flower will be extended to a minimum of 5 weeks (Pineiro and Coupland, 1998). The flowering threshold between short- and long-day photoperiods for *Arabidopsis* is 12 hours (Rivero et al., 2014). In plant science, 16h of light/8h of dark cycle is widely used for the long-day conditions, while 8h of dark/16 hours of light cycle is used for the short-day. For the experiments in the present project, a long-day growth cycle was adopted in order to achieve rapid development of the inflorescence stems, and thus reduce the total duration of the experiments.

3.3.3 Light intensity

For the growth and development of plants it is also important to ensure that they receive a sufficient amount of light. Radiation and hence amount of light are quantified in a number of different ways in plant science (see e.g. Bell and Rose, 1981). Commonly it is expressed in terms of photosynthetically active radiation and quantified using photosynthetic photon flux density (number of photons in the 400-700 nm wavelength range received by the surface over a period of time) and is referred to as light intensity.

Optimum light intensity for growing *Arabidopsis* is in the range of 120-150 $\mu\text{mol}/\text{m}^2\text{s}$ (Rivero et al., 2014). *Arabidopsis* plants grown under low light intensity will be weak and slow growing, while too high light intensity may result in the death of young *Arabidopsis* seedlings. In the present project, LED growth lights were set to provide light intensity at 150 $\mu\text{mol}/\text{m}^2\text{s}$ in all conducted experiments.

3.4 Phenotyping

There is no single definition of the term *phenotype* and its exact meaning largely depends on the context in which it is employed (Mahner and Kary, 1997). In this thesis, this term is used to describe a set of observable structural properties of a plant. A plant's phenotype can change, i.e. exhibit phenotypic plasticity, under

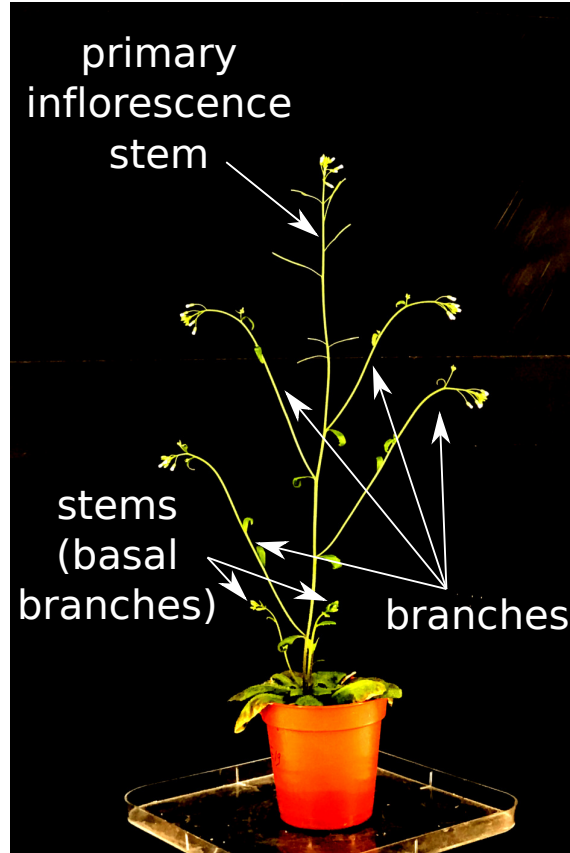


Figure 3.3: Arabidopsis morphology.

the influence of environmental conditions, allowing plants to survive and develop. Moreover, phenotypic plasticity is considered to be a more important factor for plant adaptation to the changing climate than genetic diversity (Vitasse et al., 2010; Gratani, 2014). Plant phenotyping, in the broad sense, covers protocols and methodologies for characterisation of plant growth, architecture, and composition (Fiorani and Schurr, 2013). In the context of this thesis, this term is used to describe the process of characterisation of Arabidopsis phenotype.

Arabidopsis exposed to wind environment or subjected to mechanical perturbations is expected to exhibit phenotypic plasticity. Evaluation of the changes to its phenotype can provide insights into the acclimation strategy of this model plant. In the experiments carried out in this project, plant phenotyping was performed several times throughout their duration. During each phenotyping the following parameters were measured and recorded: length of the primary inflorescence stem, number of stems, and number of branches. The length of the primary inflorescence stem is defined as the distance from its base to its tip. The number of stems includes all inflorescence stems, i.e. the primary inflorescence stem and other inflorescence stems

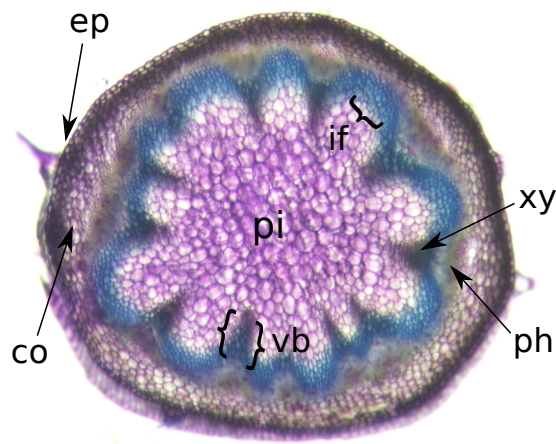


Figure 3.4: A transverse cross-section of *Arabidopsis* inflorescence stem stained with toluidine blue. Anatomical features and main tissues are shown: epidermis (ep), cortex (co), vascular bundle (vb), xylem (xy), phloem (ph), interfascicular tissue (if), and pith (pi).

that are also known as basal branches (see Figure 3.3). The number of branches refers to the total number of branches on the plant, excluding the basal branches (Figure 3.3).

3.5 Anatomical structure and histochemical staining

Arabidopsis stems consist of multiple tissues that perform specific functions (Figure 3.4). The epidermis is the outermost tissue of the *Arabidopsis* stem, which is formed by a single layer of cells. It provides a barrier between the inner part of the stem and the external environment. On the outer side of the epidermis cells is a waterproof cuticle that reduces water losses from plant organs. Vascular bundles are part of the transport system in plants and consist of two types of vascular tissues, namely xylem and phloem. Xylem cells are typically located adaxial in the stem and transport water and other nutrients from roots up to the top parts of the plant by the means of hydrostatic pressure. Another plant vascular tissue – the phloem, lies abaxial to xylem. Most of the organic compounds, including products of photosynthesis, are moved and distributed in the plant through this tissue. Interfascicular tissue occupies the space between two vascular bundles. The epidermis is separated from the interfascicular tissue and vascular bundles by the cortex (Figure 3.4). The innermost part of the stem is formed by the pith that is composed of soft cells that

store water.

In order to withstand negative hydrostatic pressure, without collapsing, xylem cell walls are lignified (Turner and Somerville, 1997). Thus, lignified xylem has superior mechanical properties and provides structural support for the plant stem. In addition, lignification is also present in interfascicular tissue (Barros et al., 2015) that also contributes to the structural support.

The distribution of tissue structures in Arabidopsis stem can be visualised and identified using histochemical staining. A simple and fast way to visualise multiple tissues in a single step is staining with toluidine blue. Toluidine blue O is a cationic dye that allows for polychromatic staining of plant cell wall, i.e. it stains cell walls in different colours depending on their composition (O'Brien et al., 1964). This dye stains lignified tissues in blue while non-lignified cell walls turn purple (see Figure 3.4). The procedure of histochemical staining using toluidine blue is a standard method in plant sciences. The detailed protocol together with video instructions for various types of histochemical staining, including toluidine blue, are available in Mitra and Loqué (2014). In general, the procedure can be briefly summarised as follows. First, an approximately 0.2 mm thick transverse section should be cut from the inflorescence stem either manually or using dedicated equipment, e.g. a vibratome or a microtome. Next, the section is placed into a microcentrifuge tube and 0.02% toluidine blue solution is added. After approximately two minutes, the section is rinsed a couple of times with distilled water until the solution inside the tube is clear. After this, the section is ready for examination under a microscope.

3.6 Cuticle disruption using carborundum powder

As was mentioned in the previous section, Arabidopsis stems have a cuticle on their outer surface that is the main barrier between the environment and the cells. The cuticle has low permeability that is required for normal growth and development of a plant but can be disadvantageous for certain experiments.

In the present project, as a part of the development and validation of the new, vibration based method for mechanical characterisation of Arabidopsis stems, it was necessary to alter the mechanical properties of the tested stem segments (see Chapter 5). This was achieved by reducing the turgor pressure, which is an internal hydrostatic pressure that acts uniformly on the cell walls through the plasma membrane.

Turgor pressure plays an important role in cell growth (e.g. Geitmann and Ortega, 2009) and also contributes to the overall stiffness of cells and tissues (Beauzamy et al., 2014).

To lower the turgor pressure, the tested stem segments were treated with carborundum powder before their submersion into a hyperosmotic solution. The primary purpose of this preliminary treatment was disruption of the stem cuticle by creating micro-scratches on its surface. This treatment made stems permeable for the hyperosmotic treatment and allowed for a reduction in turgor pressure. This method for abrading the cuticle is widely reported in the literature, see e.g. Jacobs and Ray (1976); Evans and Vesper (1980); Cosgrove and Steudle (1981); Brummell (1986), and is very effective for this purpose. As was shown in Cosgrove and Steudle (1981), segments of pea that were treated with carborundum powder had a fast response to the osmotic medium, while untreated segments showed very little changes.

Some of the basic concepts of osmotic treatment are briefly introduced here, the detailed explanations can be found in Nobel (2020). The water movement in plant cells is driven by the water potential, which can be defined through the sum of the pressure (Ψ_P), osmotic (Ψ_Π), and gravitational (Ψ_h) potentials. In many practical applications only the first two potentials are considered, thus

$$\Psi = \Psi_P + \Psi_\Pi \quad (3.1)$$

The pressure potential (Ψ_P) is usually given as the hydrostatic pressure (P), while the osmotic potential, which is caused by the presence of solutes, is given by the negative of the osmotic pressure (Π). Thus, the previous equation can be written as

$$\Psi = P - \Pi \quad (3.2)$$

The osmotic pressure of the hyperosmotic solution (Π^0) is higher compared to the osmotic pressure of the intracellular fluid (Π^i) in the plant part submerged in it, i.e. $\Pi^0 > \Pi^i$. $P^0 = 0$ since the hyperosmotic solution is at atmospheric pressure. In order to achieve equilibrium between water potentials,

$$\Pi^0 = P^i - \Pi^i \quad (3.3)$$

the hydrostatic pressure inside the plant cells (P^i) will drop, while Π^i normally is not affected much (Nobel, 2020) and cells will become less turgid. This in turn will

affect the mechanical properties of the treated plant part.

3.7 Flame photometry

In the experiments studying the influence of various types of mechanical stress on Arabidopsis the ion content of the stems was determined using flame photometry. This is a widely used method and standard protocols for the procedure are in place. In brief, when the solution that contains ions of metals is subjected to a flame test, the electrons of the ion emit light of certain colours. With the help of an optical filter the selected wavelength can be isolated. The number of ions in the solution can be determined by taking into account that the amount of emitted light is proportional to the number of ions in the flame. The test requires calibration against standards with known ion concentrations.

Chapter 4

Bespoke wind tunnel

4.1 Overview of wind environments for studies on plants

To study wind effects on plants and related aspects, first of all, it is necessary to subject plants to a wind environment. A number of ways to achieve this goal are reported in the literature and are reviewed here, excluding those where wind influence was simulated through other stimuli (e.g. bending, brushing). This section is intended to provide an overview of the main approaches to investigate wind-plant interaction and highlight related challenges. At the end of the section the choice of the wind environment for the present project is motivated based on this overview.

Probably the most straightforward way to study wind influence on plants is in the natural environment. Indeed, a number of studies were conducted in locations with elevated wind levels (e.g. coastal areas, hills) or at dedicated research field sites (see e.g. Richmond and Mueller-Dombois, 1972; Smith, 1972; Noguchi, 1979; Cordero, 1999). In addition, field studies are common for investigations of various aspects of wind influence on crop plants (see e.g. Boldes et al., 2002; Joseph et al., 2020). While this type of experiment ensures that experimental conditions are identical to those experienced by plants in their natural environment, the drawback is that none of these conditions is controlled and often a detailed characterisation of the wind environment is not possible. In addition, comparative experiments with control groups are challenging.

Another approach is to create an artificial wind environment at the site of the field test. Sterling et al. (2003) used a portable wind tunnel that was designed and built at the University of Birmingham for investigation of the lodging in wheat. The

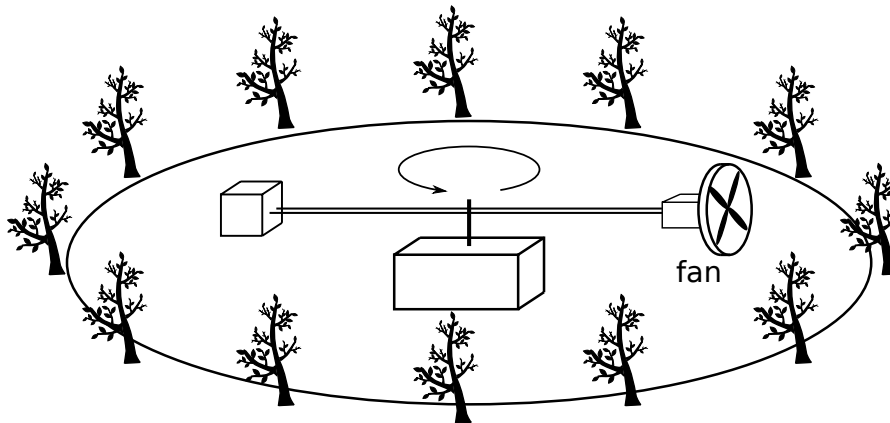


Figure 4.1: Schematic representation of the field setup for a periodic wind treatment at INRA Pierroton near Bordeaux, France. After the descriptions and drawings of this setup in Tamasi et al. (2005); Berthier and Stokes (2005, 2006).

wind tunnel is 10 m long with a cross-section of 2.7×2.7 m and can be moved from site to site. Six axial fans arranged in two rows of three can provide wind speed in the range from 1 to 6 m/s. In addition, it is possible to create wind gusts of a flow speed up to 8.5 m/s. The swirl of the flow is reduced by a grid and mesh installed before each fan. The detailed description of this wind tunnel is available in the aforementioned reference. In the experiments carried out by Sterling et al. (2003) the wind tunnel was placed over the treated plants only for a short duration of time to study the occurrence of different types of lodging, i.e. plants did not grow and develop under the wind. The use of a portable wind tunnel for field studies on winter wheat was also reported by Smika and Shawcroft (1980). Their 9 m long wind tunnel with a cross-section of 1×1 m was additionally equipped with a heater to increase the flow temperature in order to evaluate damage to the wheat from hot wind. The flow speed was not uniform along the wind tunnel with reported values ranging from 9.7 m/s to 19.4 m/s along its length. However, from the aforementioned publication it is not clear why such variation of the flow speed along the tunnel length was present.

A different way to generate wind in field experiments was applied by Tamasi et al. (2005), Berthier and Stokes (2005), and Berthier and Stokes (2006) who studied the influence of wind loading on trees at the forest nursery INRA Pierroton near Bordeaux, France. Their field setup (Figure 4.1) allowed for a periodic wind treatment with a constant flow speed. The wind was created by an electric fan that was mounted on an 8 m long arm. The arm was rotating at a constant speed around an axis which was located at the distance of 4 m from the fan. The plants from the

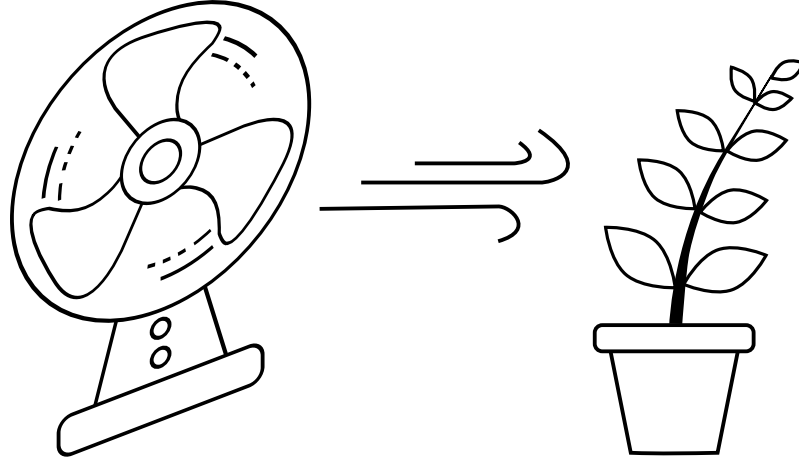


Figure 4.2: Schematic representation of a simple wind environment created by a fan that was employed in numerous studies on wind-plant interaction.

experimental group subjected to the wind treatment were placed in a circle around this wind loading device. Thus, a periodical wind treatment with a constant flow speed was applied to each plant for a certain amount of time when the arm with the fan was passing by. Based on the aforementioned studies, the flow speed created by the fan as well as the angular velocity of an arm can be adjusted according to the requirements of the conducted experiment. The maximum reported flow speed in these experiments was 5.5 m/s. The control group plants were grown on the same site nearby the experimental group.

Portable wind tunnels are more suitable for experiments with smaller plants and plant canopies as in the case of wheat, while a rotating arm with an attached fan can induce wind treatment on bigger plants like trees. Compared to the approach with natural wind, experiments with field setups that generate artificial wind can be conducted at most field sites and make factorial experiments with a control group easier. At the same time, this type of experiment ensures that environmental conditions are the same for both control and experimental groups in all parameters but the wind treatment. However, among all the environmental factors, only the wind speed can be controlled, although within a limited range. In addition, continuous or at least periodic characterisation of the environment is required throughout all types of the field experiments.

The other main approach used in wind-plant interaction studies, which is opposite to field investigations, is to subject plants to wind in a more controlled lab environment. A simple and widely used method (see e.g. Pigliucci, 2002; Smith and Ennos, 2003; Bossdorf and Pigliucci, 2009; Gladala-Kostarz et al., 2020) is to

place the plant in front of a fan that creates an air flow (Figure 4.2). This type of wind environment is normally poorly characterised since usually only the value of the velocity at a single point located at certain distance from the fan is provided. However, the air stream created by a fan is non-uniform, swirling, expanding, and its velocity is decreasing along the centreline with the distance from the fan. Thus, the characteristics of the flow created by the fan are not the same as those created by natural wind and a single point measurement is not sufficient to characterise the wind environment experienced by the plants. Another significant difference is that in the natural environment plants grow inside the atmospheric boundary layer, i.e. the wind speed is increasing with the distance from the ground. When a pot with a plant is simply placed in front of a fan, the plant's location inside the boundary layer and the velocity distribution along its height differ. Moreover, the presence of pots in the flow can induce disturbances into the flow.

A fan was also utilised in a more complex way to induce wind stress on cacao plants by Reis et al. (2018). In the reported setup, the fan was placed in front of a 4 m long channel with a cross-section of 0.5×0.4 m and blew air inside. The plants were inserted through the opening in the floor in the middle of the channel eliminating one of the aforementioned problems with wind environment created by fans, i.e. the pots were not exposed to the flow. However, additional issues were introduced by the presence of the channel walls that also create boundary layers. Judging by the photos of the plants provided in the paper and the schematic drawing of the setup, the plants placed inside the test section reached almost to the wind tunnel ceiling and walls and consequently some of their parts were subjected to velocity gradients created by the boundary layers on those surfaces.

A more elaborate setup, a purpose built wind tunnel, was used by Wadsworth (1959, 1960) to study the influence of wind on plants' growth rate and determine an optimum wind speed for plant growth. A detailed description of this wind tunnel is available in Wadsworth (1960). The wind tunnel is of an open circuit type with four rectangular test sections whose size is reducing in the downstream direction. The test sections are connected by contraction pieces with meshes that reduce disturbances to the flow created by the plants. This design allows for experiments in which plants in each test section are subjected to a higher flow speed compared to the preceding section. The maximum flow speed reported in the experiments was 12 m/s. It should be noted that no control groups were used in these experiments. As pointed out by the author, this is due to significant difficulties in creating a controlled environment with conditions (temperature and humidity) that match those inside the wind tunnel

(Wadsworth, 1960).

A wind tunnel with a well controlled growth and wind environments suitable for continuous growth of plants was reported in Grace (1974). Unfortunately, in this paper the description of the wind tunnel is limited, but from the provided schematic drawing and other studies where this wind tunnel was used, approximate characteristics of the wind tunnel can be inferred. The wind tunnel is of closed return type, with an approximately 2.5 m long test section of rectangular cross-section of approximately 1.6×1.4 m. The air flow is created by an axial fan and the maximum flow speed is 10 m/s (Russell and Grace, 1979). The environmental conditions inside the wind tunnel are controlled in terms of temperature, humidity, light intensity, and photoperiod. This provides growth conditions not only suitable for growing plants but also comparable to the control group that is grown elsewhere, e.g. in a growth room (Rees and Grace, 1980). In addition, it is possible to increase turbulence intensity of the flow in the test section by insertion of cross members that generate eddies. This wind tunnel was used for a large number of studies related to wind-plant interaction, including investigations on cuticular and stomatal transpiration in grasses (Grace, 1974), mechanical damage induced by wind on grasses (Thompson, 1974), diffusive leaf resistance in leaves of Sitka spruce (Grace et al., 1975), boundary layer over a leaf of a poplar (Grace and Wilson, 1976), effects of wind speed on the growth of grasses (Russell and Grace, 1979), and others.

Another complex setup designed to study wind and rain dispersal of plant pathogens can be found in Fitt et al. (1986). It consists of a wind tunnel and a rain tower. Since the effects of rain and its generation are beyond the scope of this thesis, the description of the rain tower is omitted in this overview. The wind tunnel's test section is approximately 5.5 m long with 1×1 m cross-section. In order to provide a suitable level of light for the experiments with plants, which extend over several days, lights are installed in the ceiling of the test section. The air flow, with a maximum speed of 8 m/s, is created by an axial fan installed downstream of the test section. The main feature of this experimental setup is that it can be operated in either closed or open circuit configuration. In the former configuration it is possible to control the environmental conditions (temperature and humidity) inside the wind tunnel within a certain range by means of an air conditioning unit and humidifiers. The latter configuration provides the possibility to connect a rain tower for simulation of rain inside the wind tunnel's test section. This rain/wind tunnel complex was used in a number of studies, e.g. Mann et al. (1995), Geagea et al. (2000), Calderon et al. (2002). Although this wind tunnel provides a suitable environment for the growth

and development of plants, to the best of author's knowledge, no experiments were conducted to investigate the effects of continuous wind exposure on plants.

Molina-Aiz et al. (2006) also reported a purpose-built low speed wind tunnel for experiments focussed on greenhouse agriculture. The wind tunnel is of an open-circuit type with a maximum flow speed of 10 m/s. The test section has a circular cross-section and is 0.39 m in diameter. In the aforementioned study, the wind tunnel was used to determine the drag coefficient of four widespread horticultural species as a function of flow speed. However, to the author's knowledge, this is the only study related to plants that was conducted in this wind tunnel, and in future studies it was used for investigations of insect-proof screens for glasshouses (Martínez et al., 2006, 2014; López et al., 2016). Also, the circular cross-section of the test section is not ideal for growing plants under wind, especially multiple plants at the same time. This is due to issues with placing plants on a curved surface which may require modifications to the test section.

There are a few studies where plants were actually grown in the wind tunnels which are primarily designed and used for various types of aerodynamic investigations. A series of experiments in which maize and sunflower plants were grown under a constant wind inside the wind tunnel are reported in Whitehead and Luti (1962), Whitehead (1962), Whitehead (1963a), and Whitehead (1963b). In these experiments plants were exposed to various wind speeds ranging from 0.45 m/s to 14.75 m/s for up to 40 days and the plants' growth and anatomy were studied. In addition to the wind speed, light intensity and photoperiod were controlled in terms of the growth conditions.

All experiments, where plants are continuously grown inside the wind tunnels, require additional equipment to be installed in order to provide suitable conditions for normal development of the plants inside the test section. Where a control group is required, this equipment should allow for control and modification of the environmental parameters to match those experienced by the control group. This presents a challenge in the implementation of this approach.

In addition, there are numerous studies where plants were placed in wind tunnels for tests that do not involve growth and development under constant wind inside the test section. For example, Mayhead (1973) determined drag coefficients for a number of conifer trees as a function of flow speed in the 24 ft wind tunnel at the Royal Aircraft Establishment at Farnborough. Utilisation of this wind tunnel allowed for conducting tests with trees of height up to 8 m. Tadrist et al. (2018) investigated foliage motion in a cherry tree that was around 3 m tall. Additional

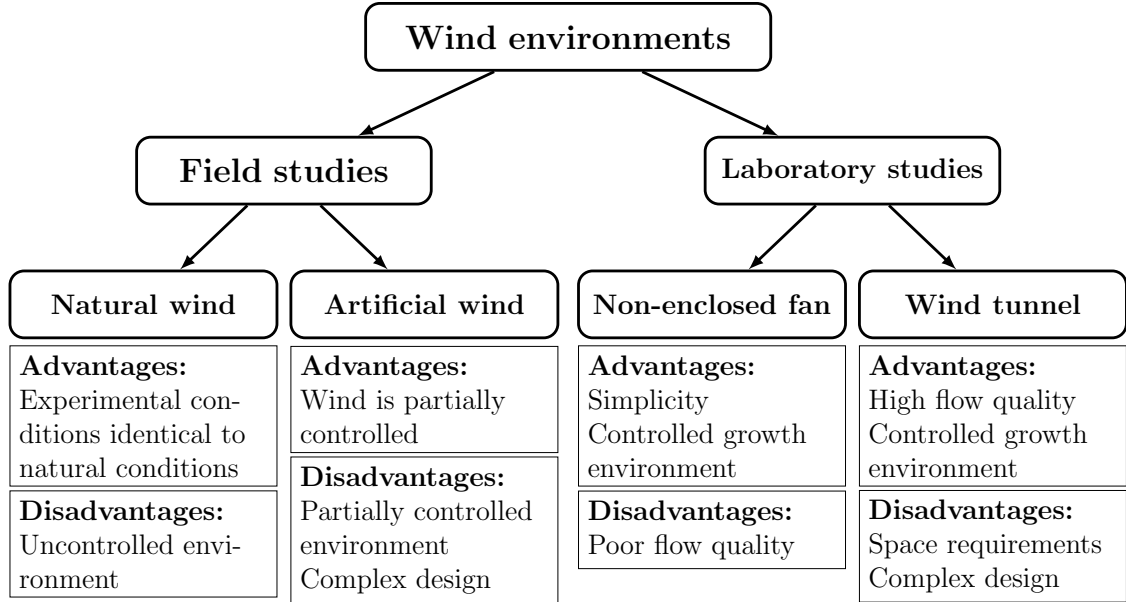


Figure 4.3: Overview of the wind environments that are used for studies on wind influence on plants.

parameters, such as drag and light interception of the tree as functions of wind speed were reported. The tests were conducted in a wind tunnel with a test section of 5×6 m. Other examples of wind tunnel utilisation for investigations of various aspects of wind-plant interaction can be found in Caldwell (1970), Etnier and Vogel (2000), Gillies et al. (2002), Vollsinger et al. (2005), and Cao et al. (2012) to name few. In general, these are short term experiments that do not involve growing plants under constant wind treatment inside these facilities, and thus do not require additional equipment to provide a suitable environment for plants.

In conclusion, it is clear that in plant sciences context no universal approach to the generation of a wind environment exists. Every approach offers certain advantages but also has drawbacks (Figure 4.3). For the model plant *Arabidopsis*, used in this project, experiments in a controlled laboratory environment are preferable since the influence of many variables can be eliminated (light intensity, day cycle) or minimised (temperature, humidity). Moreover, field experiments require additional site preparations to ensure absence of any other growth forms that can shelter *Arabidopsis* from the wind. From a fluid dynamics viewpoint, a wind tunnel is the best option for generating a well-characterised wind environment for plants provided that suitable conditions for growing plants can be ensured and, therefore, this option was chosen for the present project. There are a number of wind tunnels at the University of Glasgow; however, they are not suitable for the intended experiments. First,

due to high economical cost of running these wind tunnels it is not feasible to carry out experiments that involve continuous wind treatment of plants for several weeks. Second, the existing wind tunnel facilities have busy schedules, significantly limiting the number of experiments that could be conducted. Third, additional equipment and modifications to the wind tunnel test sections would be required in order to create a suitable growth environment. Based on these considerations it was decided to design and build a bespoke wind tunnel for investigation of the wind influence on the model plant *Arabidopsis*.

4.2 Bespoke wind tunnel

4.2.1 Wind tunnel design

The new, bespoke wind tunnel that was designed and built during the initial phase of this PhD project is shown in Figure 4.4. This wind tunnel is mainly dedicated to the experiments with *Arabidopsis*, where growth response and acclimation of this model plant to the windy environment are investigated, but it is also suitable for studies on other plants of small size. At the design stage the following objectives for the wind tunnel were established:

- Controllable wind environment with a constant uniform flow.
- Maximum flow speed inside the test section up to 10 m/s.
- Suitable environment inside the wind tunnel test section for growing plants (temperature, light intensity, day cycle, etc.).
- Suitable for continuous operation for several weeks.
- Possibility to accommodate multiple *Arabidopsis* plants.

In addition, the design of the wind tunnel was based on the choice of its primary location, i.e. the glasshouse in the Bower building at the University of Glasgow, which already provides a suitable growth environment for plants. The wind tunnel is of an open return type with a closed test section (Figure 4.4). The choice of an open circuit design was motivated by the fact that, when placed inside the glasshouse, the properties of air in terms of temperature and humidity are the same for the plants grown inside the wind tunnel and those grown in the same glasshouse

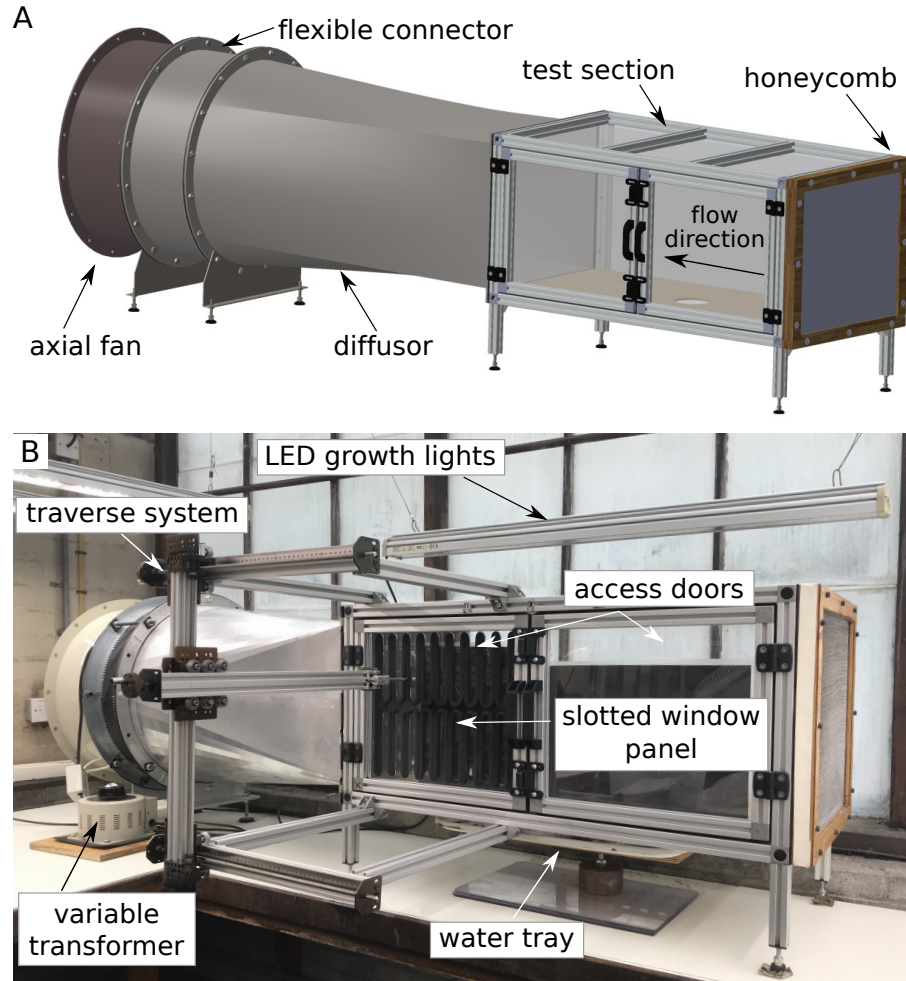


Figure 4.4: Bespoke wind tunnel for investigations on wind-plant interaction. (A) Wind tunnel CAD model showing its main components. (B) Actual wind tunnel inside the Bower building glasshouse.

but without wind influence. Thus, no auxiliary temperature control units and humidifiers are required to be installed in the wind tunnel as in the case of a closed return circuit type. In addition, an open return design is more compact and has lower construction costs. A typical open circuit wind tunnel is comprised of the following elements: flow conditioners (honeycombs, turbulence screens), contraction, test section, diffuser, and fan (Barlow et al., 1999). Due to space limitations inside the glasshouse, the wind tunnel was designed without a contraction. The main purpose of the contraction section is to increase the speed of the flow entering the test section (Barlow et al., 1999). However, the fan chosen for the present wind tunnel is powerful enough to generate flow speeds within the established design requirements without a contraction. If required for future experiments, a contraction section can

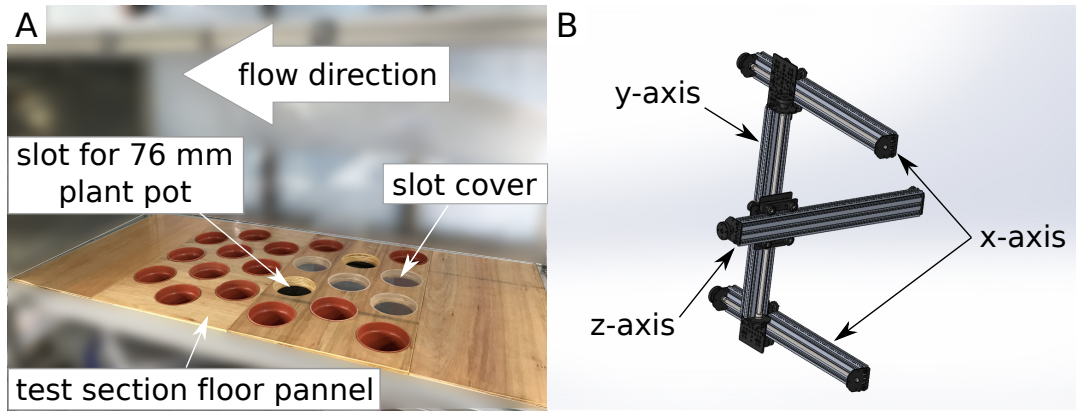


Figure 4.5: (A) Wind tunnel test section floor. (B) CAD model of the bespoke traverse system for the wind tunnel. The x-axis spans in the streamwise, y-axis in the wall normal, and z-axis in the spanwise direction.

be added to the wind tunnel, thus increasing the maximum achievable flow speed. All the other elements, that are typical for an open return design, are present in the wind tunnel and are discussed below.

Test section

The wind tunnel test section (Figure 4.4A) is one metre long with a rectangular cross-section of 450×400 mm. These dimensions allow for growing of multiple *Arabidopsis* plants simultaneously avoiding wall effects and extensive interference between neighbouring plants. The test section frame is assembled from 30×30 mm extruded aluminium profiles connected by bolts. The ceiling and side walls of the test section are made of 6 mm thick acrylic glass, which has excellent light transmission properties, is lightweight and break resistant, and provides optical access to the test section. The ceiling of the test section has an access point to insert a Pitot tube to measure the flow speed. Access to the test section is provided by the two doors (Figure 4.4B). The floor of the test section (Figure 4.5A) is comprised of interchangeable varnished plywood panels that can accommodate up to 21 single pots ($D = 76$ mm) with *Arabidopsis* plants in six staggered rows (4 pots in even and 3 pots in odd rows). Each individual slot is machined to fit the pot flush to the floor surface, ensuring no interference to the air flow from the pots. Additionally, acrylic covers can be used to block pot slots in case the number of plants in an experiment is less than 21. The test section is mounted on adjustable feet that allow it to be levelled with the rest of the wind tunnel.

Honeycomb

To reduce the turbulence level, straighten the flow, and increase its uniformity, an aluminium honeycomb with a cell size of 6 mm is installed upstream of the test section (Figure 4.4A). The cell length (honeycomb thickness) of 20 mm gives a length to diameter ratio of 3.33, and is less than the optimum value which is suggested to be in the range from 6 to 8 (Mehta and Bradshaw, 1979). However, these dimensions are suitable for the intended purpose of the wind tunnel as complete suppression of the turbulence at the test section inlet is not necessary for this project, since under realistic wind conditions, some level of turbulence is unavoidably present. For the same reason turbulence suppression screens are not installed after the honeycomb.

Axial fan

The air is drawn through the wind tunnel by a Rosenberg ER-560-4 cased axial fan (Figure 4.4A), that is able to achieve a flow rate of over 10,000 m³/h through a channel of the same cross-section as used for the test section. The fan is driven by a single phase motor and controlled by a MULTICOMP MCCMV 5E-1 variable transformer (Figure 4.4B). The choice of a single phase fan motor for this project is justified by the requirement to reduce electromagnetic noise from the experimental setup to minimise interference with sensitive equipment used for other research in the Bower building. Adjustable feet were manufactured to support the fan, level it with the rest of the wind tunnel, and damp fan vibrations.

Transition piece and flexible connector

Downstream of the test section a rectangular to round transition piece is installed to connect the test section to the fan (Figure 4.4A). This transition piece plays a role of the diffuser, reducing the speed of the flow entering the fan. Because of space limitations inside the glasshouse the equivalent conical angle of the diffuser is approximately 4.9° with an area ratio of 5.47, while the optimum values for the corresponding parameters are 3° and 3 (Barlow et al., 1999). However, the area ratio is below the maximum recommended value of 6 (Barlow et al., 1999) and thus is low enough to prevent separation of turbulent boundary layer entering the diffuser. In addition, upstream of the diffuser a mesh screen is installed to smooth out velocity variations and remove the effects of boundary layer growth (Mehta and Bradshaw, 1979). To prevent the spread of vibrations from the fan to the transition piece and further to the test section, a flexible connector is installed between the first two. In

addition, rubber sealing rings are installed between all parts of the wind tunnel to seal the joints.

Traverse system

A bespoke traverse system that was used for characterisation of the test section (see section 4.2.2) was designed and built. The three-axis manual traverse system consists of ACME lead screw linear actuators to ensure high precision movements (Figure 4.5B). The x-axis of the traverse system is made of two parallel linear actuators to increase rigidity and stability of the entire system. The length of the x-axis is 500 mm (travel length 400 mm) enables measurements along half of the test section length. This design provides easy access to the test section through the access doors and is lighter compared to the option where the x-axis spans along the full length of the test section. The y-axis length, 500 mm (travel length 400 mm), allows measurements at any point along the wind tunnel height excluding the 30 mm sections close to the floor and ceiling that are blocked by the door frame. The z-axis is chosen to be 600 mm (travel length 500 mm) to ensure measurements at any point between the wind tunnel side walls. Each axis is equipped with rulers to monitor the current positions. The linear actuators are made of extruded aluminium and are easily attached to the wind tunnel frame using extruded aluminium beams and corner brackets (Figure 4.4B). During the assembly and attachment process, alignment of all traverse system axes between themselves and with the wind tunnel axes were ensured with a level tool.

4.2.2 Characterisation of the test section

An initial characterisation of the wind tunnel's test section was conducted to determine the range of achievable flow speeds. The measurements were taken at the central point of the test section with a Pitot tube connected to a dry cell standard micromanometer (DP Measurements TT570SV) for different settings of the variable transformer output. The tests were repeated four times and the flow speed readings obtained for each value of the variac output were averaged. The mean flow speed as a function of the variac output is presented in Figure 4.6. The maximum achievable flow speed satisfies the established design objectives and is approximately 10.5 m/s. The low standard deviations for each value of the variac output suggest a good repeatability of set flow speed. Nevertheless, before each experiment with plants, the flow speed inside the wind tunnel was set using a Pitot tube.

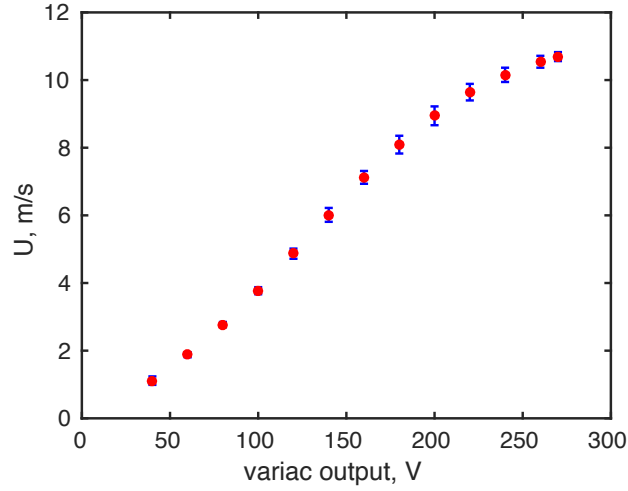


Figure 4.6: Mean flow speed at the centre of the wind tunnel test section over four independent measurements as a function of the variac output. Error bars represent standard deviations.

An in-depth characterisation of the flow within the wind tunnel test section was performed using a Dantec Dynamics StreamLine Pro System. Measurements were conducted with a straight, single sensor probe (55P11) that was attached to the z-axis of the traverse system. To provide access for the probe, the standard acrylic glass panels in the doors were replaced with slotted acrylic glass panels (Figure 4.4B).

In-situ calibration of the probe was performed before and after each measurement against Pitot tube data. The Pitot tube was connected to a dry cell standard micromanometer (DP Measurements TT570SV) and was inserted through a port in the top wall for the calibration procedure. The relationship between the squared sensor voltage and effective cooling velocity was established using King's law (King, 1914).

$$E^2 = E_0^2 + BU^n, \quad (4.1)$$

where E_0 - is the sensor voltage measured at zero velocity, B and n are King's law coefficients. B and n were determined using a simple linear regression method after measuring the voltage across the sensor over a range of known flow velocities.

The flow inside the test section was characterised in terms of the flow speed and turbulence intensity at several locations along its length. Measurements were taken in 2D planes normal to the flow direction. Each plane consisted of 80 points (10 in the horizontal direction and 8 in the vertical direction) with 40 mm spacing in

each direction. Due to the wind tunnel test section frame, the offsets from the wind tunnel walls were: 45 mm from the side walls and 60 mm from the top and bottom walls. Data was sampled at 100 kHz for 10 s at each measuring point.

The hot-wire measurements showed that the flow velocity inside the wind tunnel is stable over time. In Figure 4.7 representative results of the velocity distributions at three downstream locations ($x/h = 0.875$, $x/h = 2.775$ and $x/h = 3.975$, where h is the test section half height) along the wind tunnel test section are shown. The measurements were taken at three settings of the variable transformer, that correspond to flow velocities of 2.2 m/s, 5.3 m/s, and 10 m/s. The flow speed is normalised by the average across the entire test section at the corresponding variable transformer setting, while the axes are normalised by the test section half height. The results of the hot-wire measurements demonstrate that the distribution of the velocity is uniform along the wind tunnel test section. The average turbulence intensity inside the test section is approximately 2% for all tested flow speeds. Overall, the quality of the flow inside the wind tunnel is relatively uniform and plants will experience similar conditions regardless of their location.

4.2.3 Plant growth environment

The wind tunnel test section must have a suitable environment for growing plants in terms of temperature, humidity, light intensity, and photoperiod. For factorial experiments with an experimental and a control group, these conditions should be comparable in both groups. As previously mentioned, the wind tunnel was placed inside the Bower building glasshouse; thus, the air, drawn through the tunnel, is the same as the air inside the bigger volume of the glasshouse and has the same properties. This was confirmed by placing data loggers to record temperature and humidity inside the test section (Lascar EL-GFX-2) and outside (Elitech RC-61) at the location of the control group. To control light intensity inside the test section, professional LED grow lights (Valoya B100) were installed above it (Figure 4.4B). The light intensity can be regulated by adjusting the distance between the test section and the lights. The photoperiod is controlled by a programmable timer that switches the growth lights on and off at preset times. The light intensity level and photoperiod were set to the same values for both experimental and control groups in all conducted experiments. Overall, it was ensured that the growth conditions, except for the wind speed, were closely matched for the plants in the experimental and control groups.

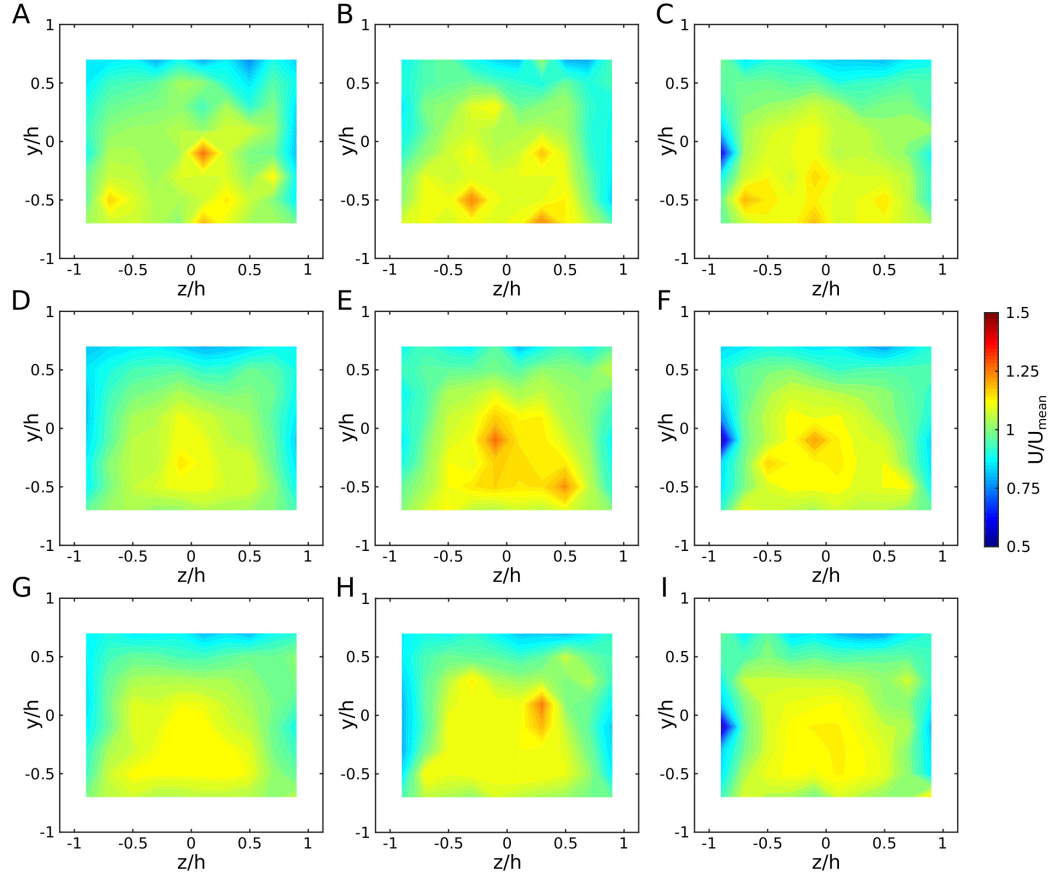


Figure 4.7: Representative examples of the mean velocity contours at several location along the test section length for three settings of the variable transformer. The flow direction is into the page. (A) Variac setting 70, $x/h = 0.875$. (B) Variac setting 70, $x/h = 2.775$. (C) Variac setting 70, $x/h = 3.975$. (D) Variac setting 130, $x/h = 0.875$. (E) Variac setting 130, $x/h = 2.775$. (F) Variac setting 130, $x/h = 3.975$. (G) Variac setting 230, $x/h = 0.875$. (H) Variac setting 230, $x/h = 2.775$. (I) Variac setting 230, $x/h = 3.975$. Velocity is normalised by the mean flow velocity in the test section, and where h - is the test section half height.

The temperature and humidity inside the glasshouse vary with the time of the day (diurnal variation) and depend on the outside conditions. Only minimum and maximum temperatures are controlled by the heating system and air conditioning unit. Thus, the results of experiments conducted at different times of the year (e.g. in July and December) are not quantitatively comparable. However, the qualitative comparison of the results and observed trends is still possible. Placing the wind tunnel in a fully controlled environment, e.g. a growth chamber, or modifications to the glasshouse environment control systems to maintain constant levels of all parameters could potentially reduce the variability of the recorded parameters between the experiments but would not guarantee comparability due to the natural varia-

tion between individual plants. In addition, the aforementioned approach would significantly increase the cost of the setup and conducted experiments.

In addition to the growth conditions, plants require water for their normal growth and development. To minimise disturbances to the plants other than from the wind, the plants were watered from below. For this purpose a tray was installed on an adjustable table under the test section (Figure 4.4B).

4.2.4 Summary

A bespoke wind tunnel was designed and built according to the specified requirements of the present project. The wind tunnel allows the study growth and development of *Arabidopsis* under continuous wind of a constant speed. The wind influence was quantified during the experiment and at the end of each experimental campaign by assessing a number of parameters (e.g. plant phenotype, mechanical properties). Statistical tests were used to establish whether the differences in the recorded parameters in each experiment were statistically significant. The details of the experiments are given in the corresponding chapters of this thesis.

Chapter 5

A new perspective on mechanical characterisation of Arabidopsis stems through vibration tests

This chapter is based on the following publication:

Zhdanov, O., Blatt, M.R., Cammarano, A., Zare-Behtash, H. and Busse, A., 2020. A new perspective on mechanical characterisation of Arabidopsis stems through vibration tests. *Journal of the Mechanical Behavior of Biomedical Materials*, **112**, p.104041.

DOI: 10.1016/j.jmbbm.2020.104041

Abstract The mechanical properties of plants are important for understanding plant biomechanics and for breeding new plants that can survive in challenging environments. Thus, accurate and reliable methods are required for the determination of mechanical properties such as stiffness and Young's modulus of elasticity. Much attention has been paid to the application of static methods to plants, while dynamic methods have received considerably less attention. In the present study, a dynamic forced vibration method for mechanical characterisation of Arabidopsis inflorescence stems was developed and validated against the conventional three-point bending test. Compared to dynamic tests based on free vibration, the current method allows to determine simultaneously more than one natural frequency, thus increasing the overall accuracy of the results. In addition, this method can be applied to the top parts of the stems that are more flexible, and where application of the three-point bending test is often limited. To demonstrate one of the potential applications of this method, it was applied to evaluate the influence of turgor pressure on the mechanical properties of Arabidopsis stems. Overall, the new dynamic testing approach has been shown to provide reliable data for the local mechanical properties along the Arabidopsis inflorescence stem.

Keywords: Arabidopsis, dynamic testing, mechanical properties, modulus of elasticity, multiple resonant frequency, vibration

5.1 Introduction

A key element of the Green Revolution in the 1950s and 1960s was the incorporation of dwarfing genes to breed plants with higher yields and shorter, stiffer straws that are less susceptible to lodging (Evenson and Gollin, 2003). An increase in global food production by 60% will be required by 2050 compared to 2005/2007 levels to feed the growing population of the world (Alexandratos and Bruinsma, 2012). To improve future food security mechanical as well as other physical/osmotic characteristics of plants have been identified as important (Connor, 2015). Understanding the mechanical properties of a plant, such as its modulus of elasticity, is therefore of high importance for breeding accessions that are more resilient to challenging environments.

In mechanical engineering there are a number of testing methods that can be used to determine the mechanical properties of materials and structures. In general, they can be divided into two groups: static and dynamic methods. In static tests,

e.g. tensile and three-point bending tests, a uni-axial stress is applied to the studied specimen and its response, e.g. elongation or deflection, is recorded. The mechanical properties are then determined from analysis of the stress-strain relationship. In dynamic tests, e.g. impulse excitation of vibration (ASTM, 2015) and sonic resonance (ASTM, 2003), a stress is applied to excite a dynamic response of the specimen, based on which a mechanical characterisation is performed.

Static methods have been successfully adapted to study mechanical properties of various plants. The most widely used are the three-point bending (Ennos, 1993; Robertson et al., 2015; Al-Zube et al., 2018) and the four-point bending tests (Ennos et al., 2000; Robertson et al., 2015) that have been used on bamboo, banana petioles, giant reed, maize, sedge and other plant stems. The main advantage of these methods is the minimal preparation of the specimens required for testing.

Other types of static tests such as tensile (Greenberg et al., 1989; Al-Zube et al., 2018) and compressive tests (Al-Zube et al., 2017, 2018) have also successfully been applied to plants. However, they need a considerably higher amount of preparatory work compared to three- and four-point bending tests. A comprehensive overview of static mechanical tests for plants is given by Shah et al. (2017b).

The main types of dynamic tests applied for the mechanical characterisation of plants are forced vibration and free vibration tests. Forced vibration tests have been applied to study the mechanical properties of plants since the pioneering works of Virgin (1955) and Burström et al. (1967). Niklas and Moon (1988) were first to use a multiple resonant frequency method to evaluate the flexural stiffness and the modulus of elasticity of a plant using a garlic flower stalk. This method was later applied to other plants and plant parts (Niklas, 1993, 1997). The free vibration method was utilised by Zebrowski (1991), Spatz and Speck (2002), Spatz and Theckes (2013) on winter wheat, triticale, giant reed and trees. In addition, vibration methods have found a number of applications on plants beyond the quantitative evaluation of their mechanical properties. For example, recently, free vibrations were utilised for the development of a non-destructive, high-throughput phenotyping method that can be applied on various plants (de Langre et al., 2019). An overview of vibrations in plants, including experimental methods for measuring them, is given by de Langre (2019).

Model plants are widely used in plant sciences to investigate and understand various processes and mechanisms in plants. *Arabidopsis thaliana* is widely used in this context due to its small size, short life cycle, and the availability of various mutants with altered parameters. In most cases, the mechanical characterisation of

Arabidopsis stems is performed using static methods such as three-point bending (Paul-Victor and Rowe, 2011), four-point bending (Goubet et al., 2009), tensile (Ryden et al., 2003), and compression tests (Verhertbruggen et al., 2013). The testing methods used for mechanical characterisation of Arabidopsis are reviewed in Brulé et al. (2016).

Historically, dynamic methods have found limited application for mechanical characterisation of Arabidopsis stems, e.g. a forced vibration method was utilised for modal analysis for phenotyping (Der Loughian et al., 2014) and the measurement of bending stiffness was performed using free vibrations method (Nakata et al., 2018). The former method does not give the possibility to evaluate the modulus of elasticity, a key parameter for determining the overall mechanical properties of a plant stem. On the other hand, it may be possible to extend the method described by Nakata et al. (2018) to the determination of the modulus of elasticity by adding the evaluation of the mass and geometrical properties of the studied stem, but these steps are not discussed in the aforementioned work.

The aim of this paper is to present a new type of multiple resonant frequency dynamic testing method for mechanical characterisation of Arabidopsis inflorescence stems. The developed dynamic testing approach was validated against static three-point bending tests. The new dynamic method requires the same amount of preparation time on specimens as a three-point bending test and only one additional measurement, the mass of the stem, for processing of the results. However, compared to the static and free vibration-based dynamic methods that have previously been applied to plants, the presented method allows for multiple estimations of the modulus of elasticity to be determined, hence increasing the accuracy of the results. In addition, a lower level of deformation of the tested specimen is achieved compared to previous dynamic tests, through implementation of the clamped-clamped boundary condition. For the first time, tests were performed on different sections of the same stem, that, as expected, showed a clear difference between their mechanical properties. Moreover, the presented dynamic method provides reliable data for the upper part of the stem, that is more flexible and where static methods usually fail to provide the average mechanical properties. Understanding of these local differences in the mechanical properties along the stems is important for studying changes in plants due to various factors, e.g. thigmomorphogenesis or turgor pressure variation. In addition, insight into the variation of the mechanical properties will also help to inform the breeding of plants to be grown in extreme environments (e.g. subjected to high wind), where mechanical properties averaged over the whole stem are not

sufficient to determine the susceptibility of the plants to lodging and other forms of mechanical damage.

5.2 Materials and methods

5.2.1 Plants

Arabidopsis thaliana seeds of ecotype Columbia-0 were sown in a single pot, which was kept for 48 hours at 4 °C, prior to moving it to a growth chamber. The conditions in the growth chamber were as follows: long day cycle (16 h of light and 8 h of darkness), temperature at 22 °C, light intensity at 150 $\mu\text{mol m}^{-2} \text{s}^{-1}$, and humidity at 60%. After 14 days, the seedlings were transplanted into individual pots (pot diameter = 76 mm) and were kept in the growth chamber for the next four weeks before the mechanical tests. At the time of the mechanical tests the plants were in the developmental stage where stems are mature and growth rate is reduced (Boyes et al., 2001); none of the plants showed any signs of senility. A total of 71 plants were used for the comparison of the dynamic and static testing methods. Taking into account that the mechanical properties of freshly cut *Arabidopsis* stem segments vary in time (Paul-Victor and Rowe, 2011) it was decided not to conduct both tests on the same segment. The plants were randomly separated into two groups and 40 plants were characterised using the dynamic method and 31 using the three-point bending test. For the study of the influence of turgor pressure on the mechanical properties of *Arabidopsis* inflorescence stems a separate group of 20 plants was grown under the same conditions.

5.2.2 Sample preparation

The tests were conducted on the primary inflorescence stem from which two segments were cut using a razor blade. The first segment was taken from the base of each stem and hereafter is referred to as “bottom part of the stem” while the second was taken from the tip of the stem and hereafter referred to as “top part of the stem”. Both segments, where necessary, were cleared from branches, fruits, flowers, and young floral buds prior to the tests using the same razor blade and taking care not to damage the tested part. In addition, a 15-20 mm segment that contains the growth zone was removed from the apex of the top part of the stem. Paul-Victor and Rowe (2011) reported that 15 minutes after cutting, the loss in stiffness of *Arabidopsis* stems is around 10% due to loss in turgor pressure as a result of

moisture evaporation. Taking into account that the time required for both tests in this study is significantly lower (less than 2 minutes from stem cutting to the end of the test), the stem ends were not sealed and all tests were performed immediately after the stem segments were cut.

In this study, the widely used approximation that an Arabidopsis stem segment has a circular cross-section of constant diameter along its length (see e.g. Turner and Somerville, 1997; Bichet et al., 2001) was adopted. Consequently, the second moment of area, I , of the stem segment is given by:

$$I = \frac{\pi}{64} D^4, \quad (5.1)$$

where D is the diameter of the stem cross-section. After each test, a photograph of the tested stem segment on a calibration ruler was taken using a USB digital microscope (UM012C, Mustech Electronics Co., Ltd). The diameter was determined using the ImageJ software (Schneider et al., 2012) as the averaged diameter over several locations along the tested segment.

5.2.3 Three-point bending tests

Three-point bending tests were performed using a Zwick Roell Z2.0 uni-axial tension compression machine (Zwick Testing Machines Ltd.) equipped with a 5 N load cell (Figure 5.1a). The anvil had a rounded end to minimise artificial cross-section deformation (Robertson et al., 2015) and was displaced at a speed of 2 mm min⁻¹. The distance between supports, L , was 50 mm. This value gives a span-to-depth ratio of the tested specimens, depending on the stem part, between 30 and 65. These values minimise the influence of shear on the measured deflection and are in line with recommendations by Shah et al. (2017b). For calculation of the Young's modulus of elasticity¹, E , which characterises the ability of a material to resist elastic deformations, the slope, c , of the steepest linear part of the force-displacement curve was determined. This ensures that the response of the sample remains in its elastic regime. The bending rigidity, EI , which quantifies the ability of a material to resist bending, of the stem parts was determined as:

$$EI = \frac{L^3 c}{48}, \quad (5.2)$$

¹Although the three-point bending test provides the flexural modulus, the flexural modulus is equal to the Young's modulus of elasticity under the assumption that the stem material is isotropic. This assumption is widely used in plant biomechanics.

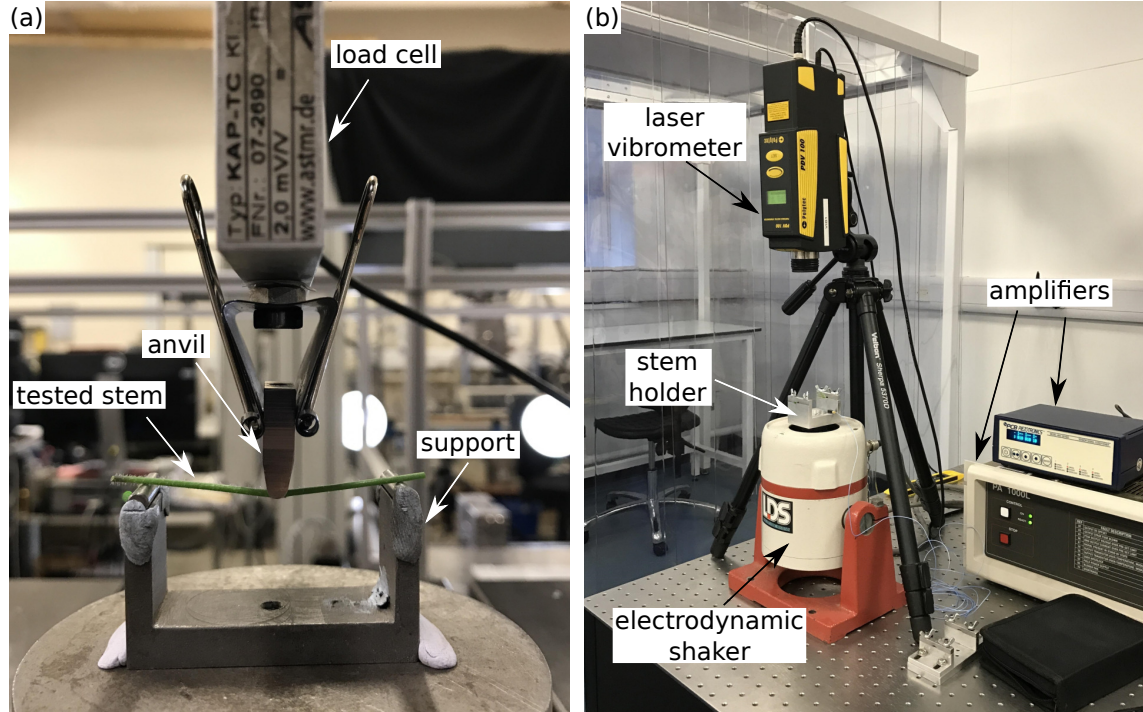


Figure 5.1: Experimental setups used for the mechanical tests. (a) Three-point bending test; (b) Vibration test.

and the value of elastic modulus was then calculated as $E = EI/I$.

5.2.4 Vibration tests

Multiple resonant frequency dynamic tests, namely base excited vibration tests, in a clamped-clamped configuration were used to determine the mechanical properties of the stems from their natural frequencies. The experimental setup shown in Figures 5.1b and 5.2 includes a dynamic signal analyser (Quattro, Data Physics, USA), a permanent magnet electrodynamic shaker (LDS V406) with an amplifier (LDS PA1000L), a piezoelectric accelerometer with amplifier (482C Series, PCB Piezoelectronics, USA) and a laser vibrometer (PDV 100, Polytec, Germany).

A random signal from the signal analyser is fed through amplifier 1 (Figure 5.2) to the shaker. The accelerometer measures the acceleration of the base of the shaker and sends signal to the signal analyser through amplifier 2. The laser vibrometer records the response of the tested structure to the applied vibrations and this signal is also fed to the signal analyser. The transfer function from the accelerometer and laser vibrometer signals is built using a specialised software for the signal analyser (SignalCalc, Data Physics, USA). A representative example of a transfer function is

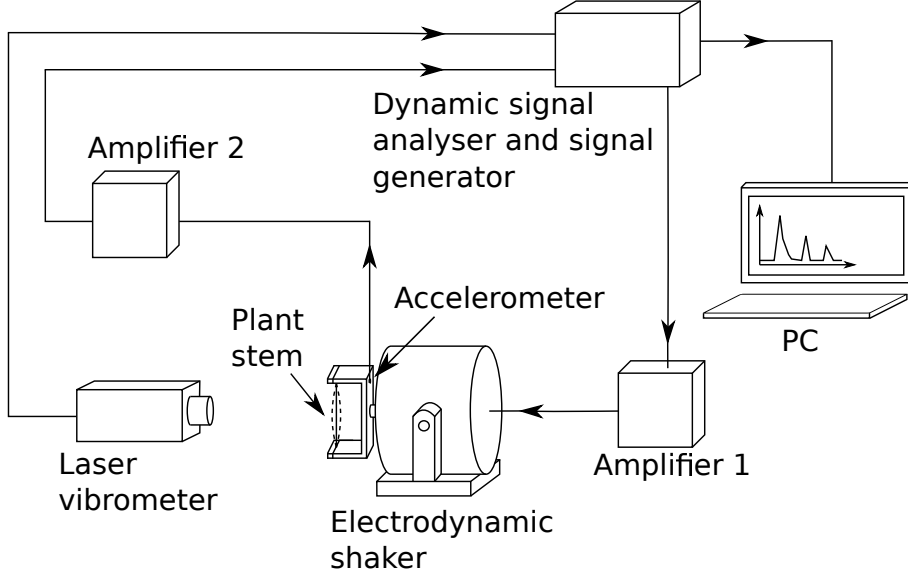


Figure 5.2: Schematic diagram of the experimental setup used for multiple resonant frequency dynamic tests.

presented in Figure 5.3. The peaks on the transfer function correspond to the natural frequencies (f_i) of the tested stems². The Young's modulus is then calculated from each value of f_i using the formula for the natural frequency of a beam, based on the Euler-Bernoulli beam theory (Blevins, 1979):

$$f_i = \frac{\lambda_i^2}{2\pi L^2} \sqrt{\frac{EI}{m}}, \quad i = 1, 2, 3, \dots, n \quad (5.3)$$

where L - length of the stem, I - second moment of area, m - mass per unit length, and λ_i is a dimensionless parameter that is obtained from the characteristic equation corresponding to the applied boundary conditions and vibration mode. In the current setup, i.e. a clamped-clamped beam, tabulated values from Blevins (1979) have been used (see also Table 5.1).

To evaluate the mass per unit length, m , the mass of the stem segment, cut from the holder using a razor blade, was determined using a precision balance and divided by the stem length (50 mm in this case) directly after the vibration test. This minimised changes in stem mass due to moisture evaporation.

The number of resonant frequencies that can be determined from this type of

²The experimentally measured values of the damped natural frequency (f_d) using the developed method are considered to be the same as the natural frequencies (f_n) due to the low damping ratios associated with the peaks on the obtained transfer functions. For example, for the first peak on the transfer function in Figure 5.3, the damping ratio (ζ) estimated using the 3-dB down point analysis (Inman, 2013) is 0.0135. As a result, the relation between the damped natural frequency and the natural frequency is $f_d = f_n \sqrt{1 - \zeta^2} = 0.9999 f_n$ justifying the aforementioned assumption.

Table 5.1: Values of λ_i for different vibration modes from Blevins (1979).

i	1	2	3	4
λ_i	4.73004074	7.85320462	10.9956079	14.1371655

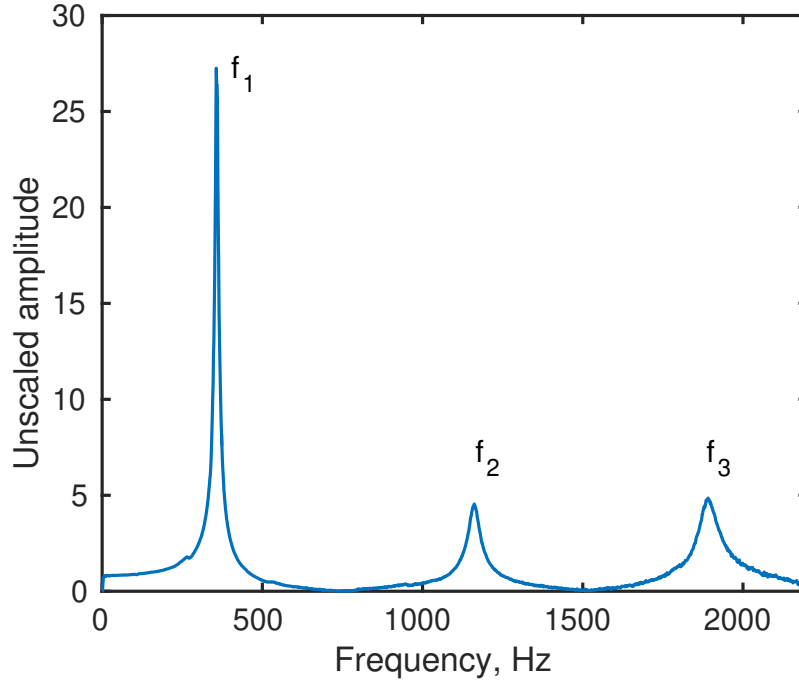


Figure 5.3: Representative example of a transfer function. This transfer function was obtained from one of the vibration tests performed on the bottom part of the stem. Peaks on the transfer function correspond to the natural frequencies of a tested stem.

vibration test depends on the stiffness and size of the tested specimen and the resolution of the measurement system. The stiffer and shorter the tested stem, the higher are the values of its natural frequencies. Since the length of the tested stem segments is fixed, the number of determined natural frequencies depends on the stem diameter. From the vibration tests on the bottom part of the stem three natural frequencies were determined, while from tests on the top part of the stem four could be measured due to the lower rigidity of the top part of the stem.

The final value of the modulus of elasticity for each tested stem segment was determined as an average of the values obtained from each natural frequency.

5.2.5 Examining the influence of stem clamping in the vibration test holder

For a vibration test with clamped-clamped boundary condition it is necessary to fix both ends of the tested specimen in the holder to prevent both linear displacement and rotation. The simplest way to fix a stem in the holder is to squeeze both ends between clamps. However, this will damage the tissues of the stem ends due to flattening and could affect the measured values for the stem natural frequencies. Therefore, preliminary tests were conducted, with and without squeezing of the stem ends, on *Arabidopsis* inflorescence stems.

In order to prevent squeezing of the stem ends, spacers of different thickness, based on the diameter of the stem, were placed between the top and bottom clamps of the holder (Figures 5.8a and b). This ensured secure fixation of the stem for testing without substantial damage to the stem ends from the clamping system. Since the damage by clamping is irreversible, first the stem was tested with the inserted spacers and straight after the test was repeated for the same stem but with spacers removed.

5.2.6 Investigation of influence of turgor pressure on the mechanical properties

To demonstrate a potential application of the presented dynamic method, it was applied to investigate the influence of turgor pressure on the mechanical properties of *Arabidopsis* stems. For this study 20 segments were cut from the bottom part of the *Arabidopsis* inflorescence stems as described in the sample preparation section. Immediately after cutting, segments were treated with carborundum powder (fine, about 180 grit) to create micro scratches on their surfaces making them permeable to the hyperosmotic solution that would be applied in the second stage of this test (see e.g. Cosgrove and Steudle, 1981). After the treatment, segments were submerged into distilled water prior to testing to prevent their dehydration. The baseline dynamic test was conducted according to the procedure described earlier. After the test, each stem was carefully removed from the holder's clamps and its mass and diameter were measured. The stems were then subjected to hyperosmotic stress (300 mM mannitol treatment) to decrease their cell turgor pressure. After one hour, the vibration tests were repeated to measure the natural frequencies of the stems with reduced turgor pressure. At this stage the evaluation of the mass of the stem segment was carried out again to account for a potential change in mass between the two tests. Finally,

after the completion of the second test, the mass of the 50 mm segment between the clamps was measured.

5.2.7 Statistical analysis

Differences in the modulus of elasticity values determined using static and dynamic methods for the same parts of the stem as well as differences between mechanical properties of bottom and top parts of the stems were investigated using a non-parametric Wilcoxon rank-sum test. The choice of this test is explained by small sample sizes of different lengths and by the fact that some of the data was not normally distributed. To examine the influence of stem clamping on the detected natural frequencies of the same stem tested with and without inserted spacers paired *t*-test was utilised. This test was also applied to study differences in the mechanical properties of the stems associated with the decrease of turgor pressure. Tests were carried out using Matlab (R2015b, MathWorks, USA) ranksum and ttest functions correspondingly. Statistically significant difference was established at $p \leq 0.05$.

5.3 Results

5.3.1 Bottom part of the stem

The bottom part of an Arabidopsis stem consists of mature tissues and cells that have stopped growing. Consequently, a more uniform distribution of the mechanical properties is expected along the length of the tested segment and variation between different stems is expected to be relatively low. Three natural frequencies were obtained from the vibration tests for this part of the stem based on which mechanical properties were determined.

In Figure 5.4 bending rigidity (EI) of each tested stem is plotted against stem diameter raised to the fourth power (D^4) using data from both vibration and three-point bending tests. The EI values for the vibration test correspond to the average of the EI_i values computed from the determined natural frequencies f_i for each stem. In both cases, EI shows statistically significant positive correlation with D^4 ($r^2 = 0.85$ for three-point bending test and $r^2 = 0.763$ for vibration). In addition, standard deviations of the E values determined from each natural frequency in the vibration tests are small (Figure 5.5a). These observations support the assumption that there is a low variation in the modulus of elasticity in the bottom part of the different tested stems.

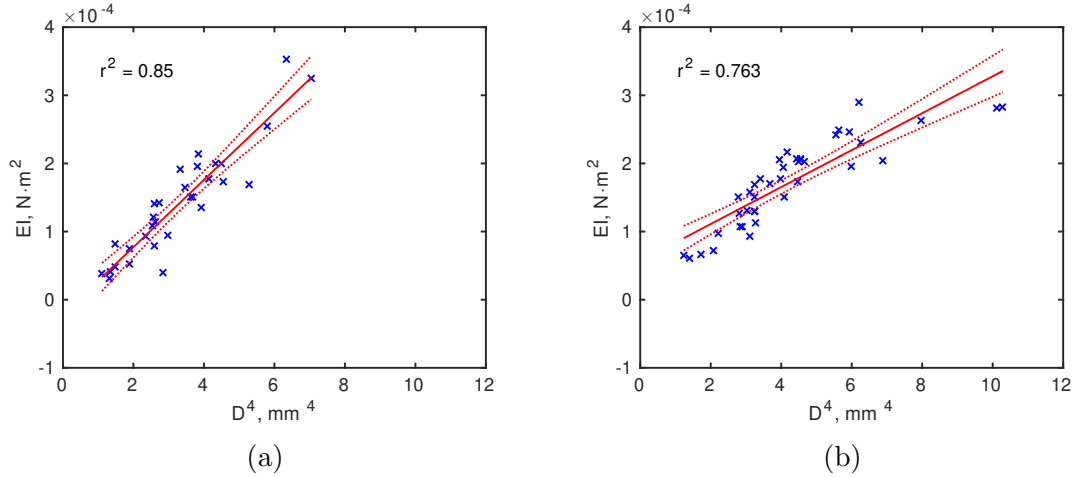


Figure 5.4: Scatter diagrams showing bending rigidity vs stem diameter raised to the fourth power for the bottom parts of the Arabidopsis stems. (a) Scatter diagram based on the results of the three-point bending tests; (b) Scatter diagram based on the results of the vibration tests.

The mean values of the modulus of elasticity, together with standard deviations are presented in Table 5.2. \overline{E}_i represents the mean of all values of E determined from the i^{th} natural frequency, while \overline{E} is the mean value of the modulus of elasticity averaged first over all values of E_i for each stem and then over all tested stems. The variation between \overline{E}_i values is low. The small differences in the obtained values of \overline{E}_i can be attributed to the fact that different mode shapes have participation from different sections of the stem segment. This together with any heterogeneity along the segment results in an uneven stress distribution.

Figure 5.5b shows that there is no statistically significant difference ($p > 0.8$) in the modulus of elasticity values obtained by the three-point bending and vibration methods for the bottom part of the stem. Both tests show good agreement in terms of mean values (difference $< 2\%$) and standard deviations (table 5.2). In case only the first natural frequency was used for the calculation of the modulus of elasticity, the discrepancy between the two methods would be higher (3-4%).

5.3.2 Top part of the stem

In contrast to the bottom part, the top part of Arabidopsis stems consists of young tissues and cells. In addition, along the length of the tested segments, variation of mechanical properties is expected, since closer to the tip tissues are younger compared to those at the lower end of the tested segment. The smaller diameter and

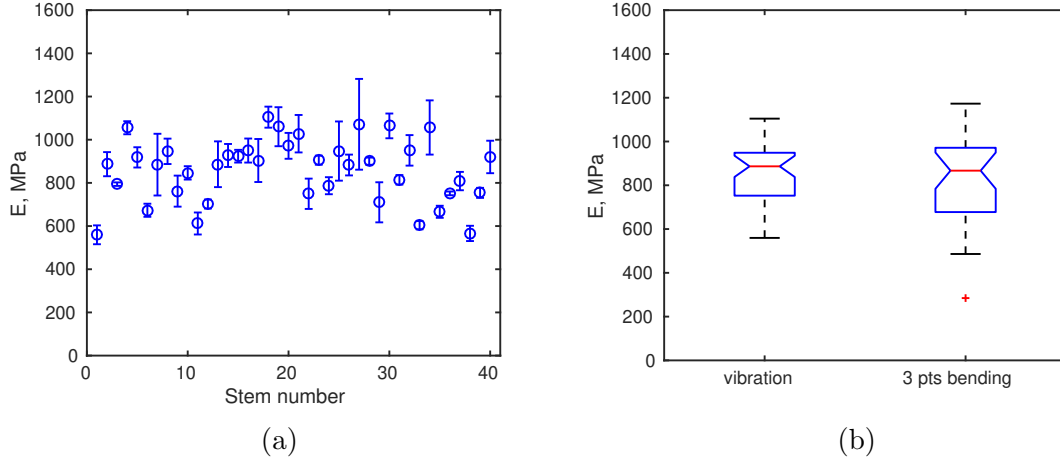


Figure 5.5: Modulus of elasticity determined for the bottom parts of the Arabidopsis stems. (a) Mean values of the modulus of elasticity, E , determined using the vibration method, errorbars represent standard deviations; (b) Box plots presenting E , determined from vibration ($n=40$) and three-point bending tests ($n=31$).

Table 5.2: Modulus of elasticity determined from mechanical tests for the bottom part of Arabidopsis inflorescence stems. Data is presented as mean \pm standard deviation. \overline{E}_1 , \overline{E}_2 and \overline{E}_3 mean values of the modulus of elasticity determined from corresponding natural frequencies in the vibration tests. \overline{E} mean values of the elastic modulus.

type of the test	\overline{E}_1 , MPa	\overline{E}_2 , MPa	\overline{E}_3 , MPa	\overline{E} , MPa
vibration	875 ± 156	872 ± 173	826 ± 150	858 ± 147
bending	-	-	-	842 ± 211

lower rigidity of the top part of the stems allowed to determine the first four natural frequencies for each tested stem. These frequencies were used for calculation of the mechanical properties. However, it was not possible to test the top parts of some stems using the three-point bending technique because of their shape and excessive flexibility. This led to sagging of the stem segments under their own weight and slipping of the stem ends between supports during the tests. In addition, in some cases, the point of maximum deflection was not the same as the point of force application. In the present study, the three-point bending test failed in approximately 45% of cases when applied to the top part of the stem. Thus, the results for this type of tests are given only for those specimens that could be tested. On the other hand it was possible to test all top parts of the stems using the vibration method

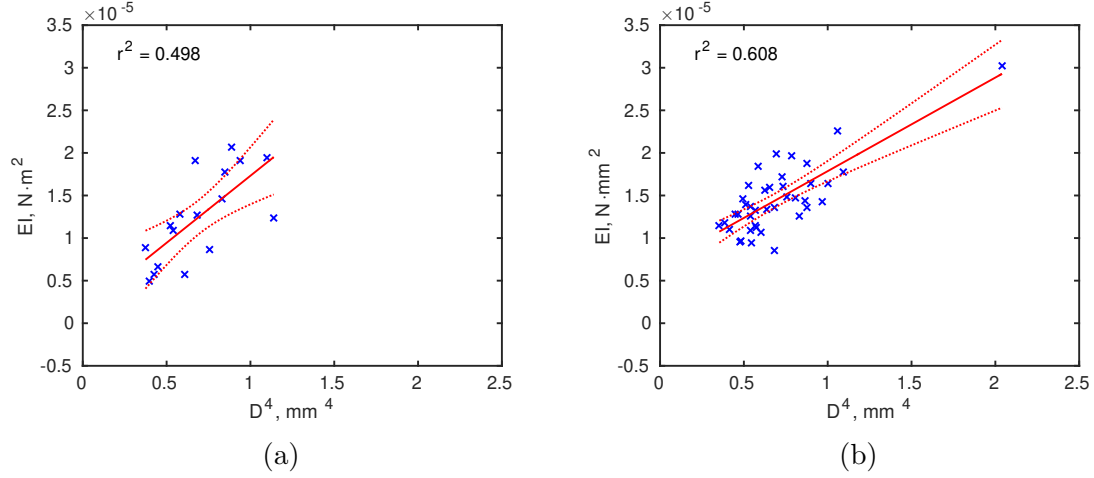


Figure 5.6: Scatter diagrams showing bending rigidity vs stem diameter raised to the fourth power for the top parts of the Arabidopsis stems. (a) Scatter diagram based on the results of the three-point bending tests; (b) Scatter diagram based on the results of the vibration tests.

due to the clamped-clamped boundary condition and the high resolution of the laser vibrometer.

The bending rigidity for each tested top part of the stem is plotted against stem diameter raised to the fourth power in Figure 5.6. For both tests there is weaker positive correlation ($r^2 = 0.608$ for the stems tested using vibration method, $r^2 = 0.498$ for the stems tested using three-point bending method) between these values which can be explained by the non-uniform properties of the tested segments compared to the bottom part of the stem. The standard deviations of the E values, determined from each natural frequency in the vibration tests, are significantly higher than those determined for the bottom part (Figure 5.7a). This confirms that material properties along the top parts of the Arabidopsis stems are not uniform.

Values of \overline{E}_i determined from each natural frequency (Table 5.3) show a stronger variation compared to the bottom part of the stem associated with the non-uniform mechanical properties along their lengths. For the top part of the stem both tests show a statistically significant difference in the results ($p < 0.05$) (Figure 5.7b). However, this can be attributed to the fact that even though three-point bending test provided results for 55% of the tested stems, this results might be biased by the same reasons that led to the failure of obtaining results in other 45% of tested stems.

Overall, values of the modulus of elasticity of the top part of the stem are signif-

Table 5.3: Modulus of elasticity determined from mechanical tests for the top part of Arabidopsis inflorescence stems. Data is presented as mean \pm standard deviation. \overline{E}_1 , \overline{E}_2 , \overline{E}_3 and \overline{E}_4 mean values of the modulus of elasticity determined from corresponding natural frequencies in the vibration tests. \overline{E} mean values of the elastic modulus.

type of the test	\overline{E}_1 , MPa	\overline{E}_2 , MPa	\overline{E}_3 , MPa	\overline{E}_4 , MPa	\overline{E} , MPa
vibration	525 ± 161	384 ± 103	404 ± 146	482 ± 135	449 ± 108
bending	-	-	-	-	369 ± 109

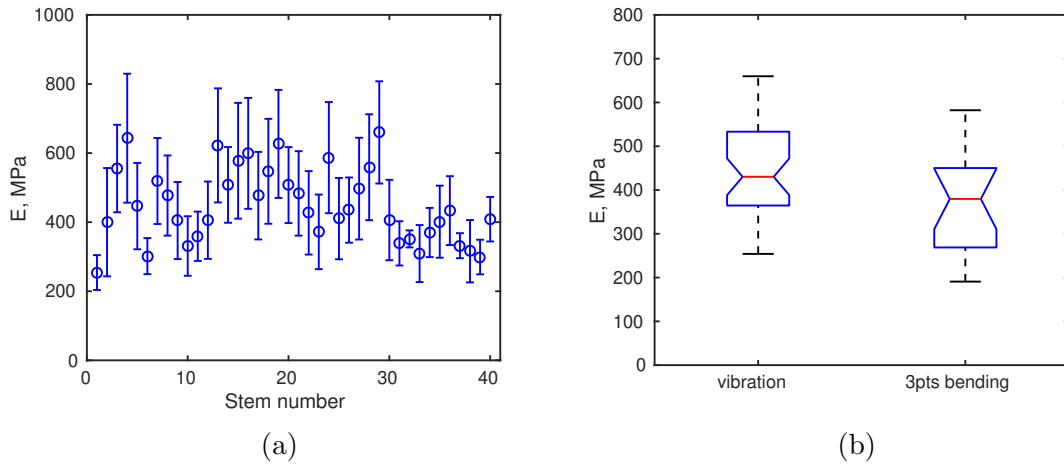


Figure 5.7: Modulus of elasticity determined for the top parts of the Arabidopsis stems. (a) Mean values of the modulus of elasticity, E , tested using the vibration method, errorbars represent standard deviations; (b) Box plots presenting E , determined from vibration ($n=40$) and three-point bending tests ($n=17$).

icantly different ($p < 0.0001$) from those for the bottom part of the stem, showing approximately twice lower values. This, as expected, shows that the material properties of an Arabidopsis inflorescence stem vary along its length.

5.3.3 Influence of stem clamping

The effect of squeezed stem ends on the natural frequencies is presented in Figure 5.8c. As expected, flattened stem ends reduced all detected natural frequencies of the stems. The observed differences are statistically significant with $p < 0.001$ for the first and $p < 0.0001$ for the second and third natural frequencies. The mean decrease for all three determined frequencies is around 15%. Since for calculation of

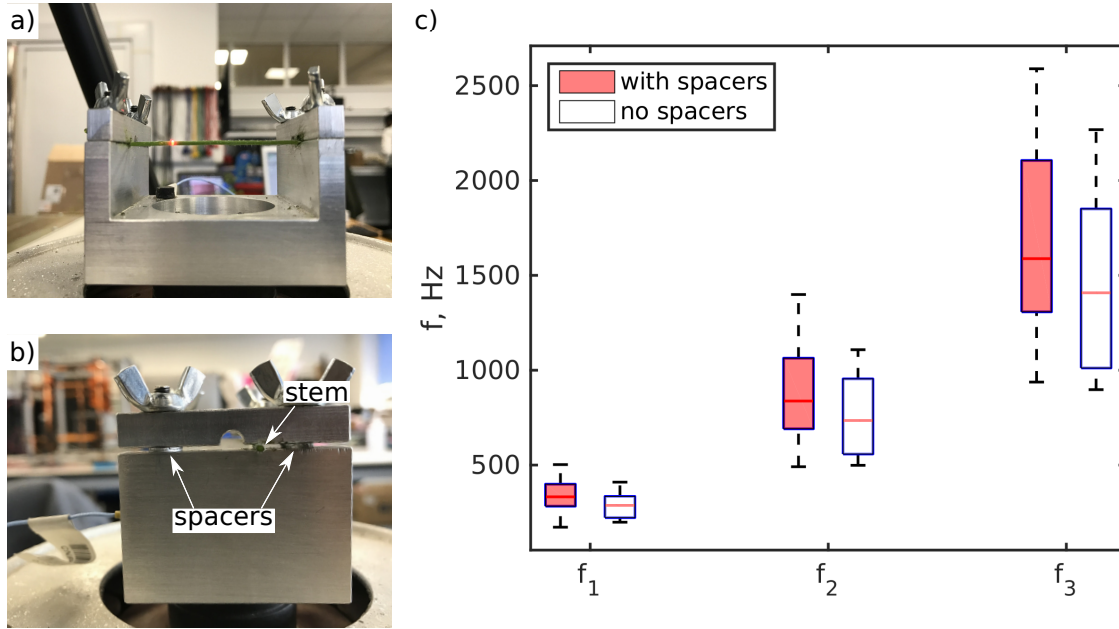


Figure 5.8: Examination of the effect of clamping in the holder on the measured natural frequencies of Arabidopsis stems. (a) Stem ends are squeezed by the clamps; (b) Spacers are inserted to prevent squeezing of stem ends; (c) Box plots representing the effect of squeezing of stem ends on the natural frequencies of the tested stems ($n=25$).

flexural rigidity from formula (5.3) f_i should be squared, according to propagation of uncertainty this will result in an error of more than 20% in EI and consequently in E values.

Thus, for vibration tests in a clamped-clamped configuration, attention should be paid to the conditions of the clamped stem ends and the clamping system should be designed in a way that prevents damage. In the current study, all tests were carried out with inserted spacers to mitigate the effect of damaged stem ends on the results.

5.3.4 Influence of turgor pressure on the mechanical properties of Arabidopsis stems

The mass of the whole tested segment did not show a significant change between the two tests as the observed difference was close to the resolution limit of the precision balance used for its determination. Consequently, for the calculations of the bending rigidity and modulus of elasticity, the mass of the 50 mm segment determined after the second test was used. Also, significant differences were not

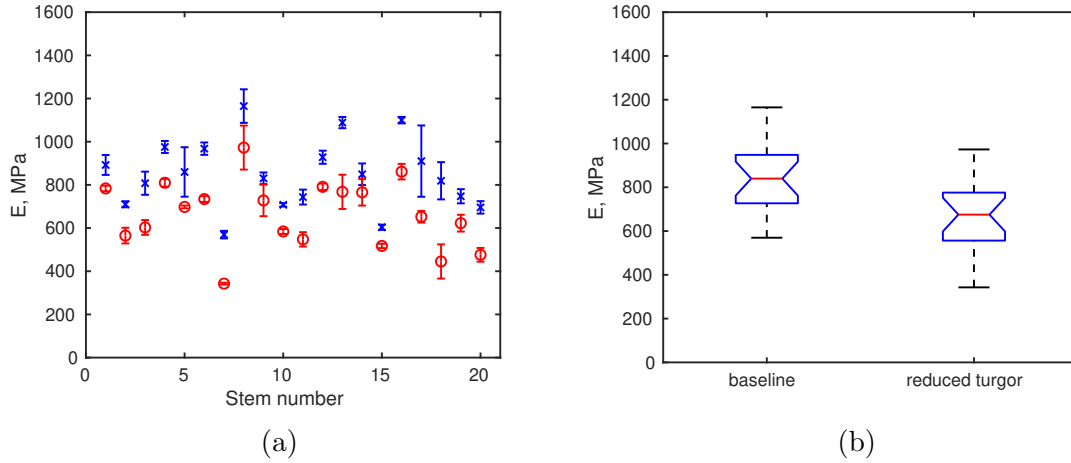


Figure 5.9: Influence of turgor pressure on the modulus of elasticity of Arabidopsis stems. (a) Mean values of the modulus of elasticity determined for the baseline case (\times) and after hyperosmotic treatment (\circ), errorbars represent standard deviations; (b) Box plot representing E , determined for the baseline tests ($n=20$) and after hyperosmotic treatment ($n=20$).

observed in the values of the stem diameters from both tests. However, taking into account manual image processing that is required to measure the diameter, and some degree of inaccuracy associated with this, the diameter for each segment was averaged between two tests and the second moment of area was based on this value. Taking all the aforementioned points into account, all the changes in the mechanical properties of the tested segments of Arabidopsis stems were associated with the decrease in their cell turgor pressure as a result of hyperosmotic stress. With the decrease of the turgor pressure the flexibility will increase, hence the modulus of elasticity is expected to decrease.

After the stems were treated with mannitol, a consistent decrease in their modulus of elasticity was observed in all cases (Figure 5.9a). This is in line with previous studies on the influence of turgor pressure on the mechanical properties of various plant parts and tissues (e.g. Falk et al., 1958; Faisal et al., 2010). On average the modulus of elasticity decreased by 185 ± 77 MPa due to the reduction of turgor pressure. Figure 5.9b shows that this change is statistically significant ($p < 0.0001$). Since the stem diameter remained unchanged the bending rigidity followed the same trend as modulus of elasticity. The decrease in cell turgor pressure made the stems more susceptible to elastic deformations and reduced their resistance to bending through decrease of the modulus of elasticity and bending rigidity, respectively.

5.4 Discussion

5.4.1 Design of the holder for vibration tests

As any other structure the stem holder for vibration tests has its own natural frequencies that may overlap and interfere with the natural frequencies of the tested stems and consequently affect the results. Thus, the design of the holder must ensure that its natural frequencies are not within the frequency range of interest for the planned tests.

Finite element modelling (FEM) could be used during the design stage of the holder to establish its natural frequencies. Existing holders can be tested separately from the plant stems to determine their suitability.

The holder used in the present study is made of aluminium, and the distance between supports is 50 mm. Based on the results obtained in FEM modelling software, Abaqus (Dassault Systemes, France), the base of the holder was made approximately 2.5 times thicker than the side walls. This aspect ratio results in its first natural frequency being over 6500 Hz. An aspect ratio of 1:1 between the thickness of the base and the wall would lower the first natural frequency to 2800 Hz, hence affecting the vibration tests. Preliminary vibration tests of the holder in isolation confirmed that no peaks are present within testing range (0-4000 Hz).

5.4.2 Clamped-clamped boundary conditions

Although it is more intuitive to test plant stems in a clamped-free (cantilever) configuration, since this is how most plants grow in nature, in this study clamped-clamped boundary conditions were used. Clamped-clamped boundary conditions reduce maximum deflection (Blevins, 1979) thus leading to a more linear response, and therefore avoiding modal-coupling energy transfer (Hill et al., 2015). In addition, compared to a cantilever, a clamped-clamped configuration gives more control over the measurement system thanks to the aforementioned lower deformation levels and the existence of at least two nodes with zero displacement in fixed locations along the structure, namely the extremities. This allows for the use of a laser vibrometer which offers an inherently high resolution and sampling rate but also requires that the motion occurs along the direction of the laser beam. The nodes permit to identify two neighbourhoods where the displacements are sufficiently small so that the target movements can be kept perpendicular to the laser beam.

The perfect implementation of any boundary condition is very difficult to achieve

in an experimental setup and some degree of uncertainty will be introduced due to this fact. For example, if some degree of flexing was allowed at one or both clamping points, the boundary condition would correspond to clamped-pinned or pinned-pinned, respectively. In this case, for the calculation of the mechanical properties of the tested stem segments, values of the parameter λ that correspond to these boundary conditions should be used in equation 5.3. However, in our current experimental setup we closely approximate clamped-clamped boundary condition as demonstrated by the successful validation against the three-point bending test. Use of λ -values corresponding to clamped-pinned or pinned-pinned boundary conditions would result in a significant mismatch to three-point bending test results.

5.4.3 Comparison with other recently developed dynamic methods

Recently two other vibration-based methods for characterisation of plants have been developed, namely the methods described in Nakata et al. (2018) and de Langre et al. (2019). In the following section we give a comparison of these methods with the current approach that is summarised in Table 5.4.

de Langre et al. (2019) presented a method that allows to measure the first natural frequency of free vibration of a whole plant. In addition, it gives the possibility to determine the frequency of each stem in case of multi stem plants. The method is non-destructive, allowing to examine the same plant over a period of time as it grows. The primary purpose of this method is phenotyping of various plants including Arabidopsis. Theoretically, this approach could be extended to the mechanical characterisation of plants, provided the mass of the plant can be measured. As pointed out by the authors non-destructive measurement of the mass of a plant with complex structure is challenging.

The method presented by Nakata et al. (2018) was designed primarily for the characterisation of Arabidopsis stems and allows to determine the first natural frequency from free vibration. It can be applied for identification of Arabidopsis mutants (phenotyping) with altered cell wall properties. In addition, it provides data on bending rigidity of tested stems, and as it is a destructive method it could potentially be extended to the measurement of the modulus of elasticity. However, its capabilities for the mechanical characterisation still require validation against a standard testing method such as the three-point bending test to establish its reliability.

In contrast to the aforementioned methods, the method developed in this study

Table 5.4: Comparison of the current method with other recent dynamic methods that can be applied on Arabidopsis inflorescence stems.

Parameters	present method	Nakata et al. (2018)	de Langre et al. (2019)
determined frequencies	n natural frequencies $n \in [1..4]^*$	1 st natural frequency	1 st natural frequency
type of vibrations	forced	free	free
application	mechanical characterisation phenotyping	mechanical characterisation phenotyping	phenotyping
validation	yes	no	n/a
non-destructive	no	no	yes
measured quantities	f_i, EI, E	f_1, EI	f_1

* depending on the mechanical characteristics of the stem

uses a forced vibration approach and provides data on multiple resonant frequencies of the Arabidopsis stems. This data is used for determination of their bending rigidity and modulus of elasticity. Utilisation of several frequencies for the calculation of the mechanical properties increases the overall accuracy of the results. In addition, the presented method was validated against the well-established three-point bending method. While the main purpose of the developed method is to measure mechanical properties, it could also be utilised to identify Arabidopsis mutants with different cell wall properties by measuring their natural frequencies.

5.4.4 Limitations

Despite a number of advantages, the developed method has also some limitations. As discussed previously, a carefully designed holder is required for clamping of the biological specimens. Attention should also be paid to the design of the clamping system as well as the clamping process itself, as damage to the specimen during clamping can affect the results. Proper clamping of the tested specimen with utilisation of spacers requires training of the operator. This can be considered as a drawback of the presented method compared to the static bending tests, where clamping is not involved.

5.4.5 Considerations for future studies

The presented method can be used for characterisation of mechanical properties of Arabidopsis stems and changes in them associated with thigmomorphogenesis caused by growth under different conditions mimicking challenging environments (e.g. with mechanical perturbation or subjected to wind). In addition, this method can be utilised for mechanical characterisation of Arabidopsis mutants with altered properties (e.g. mutant without secondary cell walls) and other plants. When applied to other plants and plant parts (e.g. roots), it should be taken into account that values of the natural frequencies depend on a number of parameters (see equation 5.3). For testing of plant parts that have similar diameter as tested Arabidopsis stems the current setup could be used in the present configuration. However, the number of detected frequencies can be reduced in case tested specimen has lower mass per unit length value or higher modulus of elasticity. A possible solution is to increase the resolution of the system to detect frequencies over a wider range. Stems of larger plants, such as wheat or rice, would require an appropriate scaling of the holder taking into account aforementioned considerations for the holder design and span-to-depth ratio limitations in order for Euler-Bernoulli beam theory to remain valid. Furthermore, when used without immediate frequency data post-processing, it can be applied as a high-throughput technique similar to the one presented by Nakata et al. (2018). The advantage of the current method is that it gives more than one natural frequency and consequently more information on tested plant is available.

Another advantage of the clamped-clamped boundary condition is that it allows to isolate the part of the stem under consideration for testing. Consequently, it would be attractive to evolve the described method into a non-destructive testing technique. However, the main challenge will be to develop a clamping system that minimises stem bruising, since damage to the plant stem will affect plant growth and properties after testing.

5.5 Conclusions

A new type of multiple resonant frequency dynamic testing method for characterisation of mechanical properties of the inflorescence stems of the model plant *Arabidopsis thaliana* was developed. This method enables the assessment of the bending rigidity as well as modulus of elasticity of the stems. The values obtained by this

method were compared to those obtained from more conventional three-point bending tests. For the bottom part of the stems, both methods show a good agreement in the modulus of elasticity values. However, for the top part of the stems the discrepancies between both methods are observed. The presented dynamic method gives the possibility to investigate mechanical properties for a top part of the stem that is more flexible in a more reliable way compared to the three-point bending test. The current samples show approximately 50% of the value of the elastic modulus of the bottom parts. In addition, the overall accuracy of the presented method is higher since more than one natural frequency is obtained simultaneously from each test. The possibility to test different parts of the stem gives an advantage to assess the variation of the properties along the stem instead of obtaining the net value. This will provide a better and more accurate understanding of plant material properties and their changes due to various factors such as mechanical stimuli, drought, etc. that are important for breeding of new plants of high resilience against challenging environmental conditions. Furthermore, one of the potential applications of the developed dynamic method was demonstrated through assessment of changes in the mechanical properties of Arabidopsis stems due to variation in their cell turgor pressure. These tests showed a consistent reduction of the modulus of elasticity and bending rigidity with decrease of turgor pressure.

CRedit authorship contribution statement

Oleksandr Zhdanov: Conceptualization, Investigation, Formal analysis, Data curation, Writing - original draft, Writing - review & editing, Visualization. Michael R. Blatt: Conceptualization, Supervision, Resources. Andrea Cammarano: Conceptualization, Methodology, Resources. Hossein Zare-Behtash: Conceptualization, Supervision. Angela Busse: Conceptualization, Supervision, Writing - review & editing.

Declaration of competing interest

The authors declare that they have no known competing financial interests or personal relationships that could have appeared to influence the work reported in this paper.

Acknowledgements

This work was supported by the University of Glasgow's Lord Kelvin/Adam Smith (LKAS) PhD Scholarship. The experimental data for this study is available at <http://dx.doi.org/10.5525/gla.researchdata.988>.

Chapter 6

Wind-evoked anemotropism affects the morphology and mechanical properties of Arabidopsis

This chapter is based on the following publication:

Zhdanov, O., Blatt, M.R., Zare-Behtash, H. and Busse, A., 2021. Wind-evoked anemotropism affects the morphology and mechanical properties of Arabidopsis. *Journal of Experimental Botany*, **72**(5), pp.1906-1918.

DOI: 10.1093/jxb/eraa541

Abstract Plants are known to exhibit a thigmomorphogenetic response to mechanical stimuli by altering their morphology and mechanical properties. Wind is widely perceived as mechanical stress and in many experiments its influence is simulated by applying mechanical perturbations. However, it is known that wind-induced effects on plants can differ and at times occur even in the opposite direction compared with those induced by mechanical perturbations. In the present study, the long-term response of *Arabidopsis thaliana* to a constant unidirectional wind was investigated. We found that exposure to wind resulted in a positive anemotropic response and in significant alterations to *Arabidopsis* morphology, mechanical properties, and anatomical tissue organization that were associated with the plant's strategy of acclimation to a windy environment. Overall, the observed response of *Arabidopsis* to wind differs significantly from previously reported responses of *Arabidopsis* to mechanical perturbations. The presented results suggest that the response of *Arabidopsis* is sensitive to the type of mechanical stimulus applied, and that it is not always straightforward to simulate one type of perturbation by another.

Keywords: Anemotropic response, *Arabidopsis thaliana*, biomechanics, mechanical properties, morphology, stem anatomy, thigmomorphogenesis, wind.

6.1 Introduction

Current predictions on global warming show that the global average temperature will increase by 1.5 °C compared with pre-industrial levels by 2030–2050 (Allen et al., 2018). Among other climatic changes, this will lead to alterations in wind speeds and patterns. Global climate simulation models show that the predicted increase in the global temperature will lead to a significant increase in surface wind speeds over the UK and Northern Europe (Hosking et al., 2018). Similar trends have been found for other parts of the world; for example, analysis of the wind speed data for China demonstrated an increase in the wind speeds measured during spring and summer months over the last 40 years (Zhang et al., 2020).

Strong winds and storms have a negative impact on food security, since for crop plants (e.g. wheat, rice, and maize) wind-induced stem and root lodging significantly affects yields (Berry et al., 2004). An overview of the reported yield reductions in major crop plants due to lodging shows that it can reach up to 80% in wheat, 83.9% in rice, 65% in barley, 40% in oats, and 20% in maize (Shah et al., 2017a). Wind also has an economic impact on wood production, since windthrow due to strong

winds poses a serious threat to forests (Mitchell, 2013). The review by Schelhaas et al. (2003) showed that damage from windstorms to forests in Europe contributes >50% to the total damage from all natural causes.

In their natural environment, plants are typically subjected to low and moderate wind conditions on a regular basis, since they cannot shelter themselves from wind. This interaction can have either beneficial or detrimental effects, and plants have developed a number of strategies to adapt and survive. Detailed reviews of these effects and strategies are given in de Langre (2008) and Gardiner et al. (2016).

Wind is a complex environmental factor (Ennos, 1997; Jones, 2013) that among other effects regulates the microclimate of plants, can alter photosynthesis (Smith and Ennos, 2003; Burgess et al., 2016), and can change heat and mass transfer in plants (Jones, 2013). One of the most direct effects of wind on plants is the mechanical stress exerted on plants through the drag force. This, as in the case of mechanical stress induced by mechanical perturbations (e.g. brushing or touching), evokes physiological and morphological responses in plants known under the term thigmomorphogenesis first introduced by Jaffe (1973). Typically, thigmomorphogenesis leads to the inhibition of the stem length and an increase of its diameter, thus plants develop shorter but thicker stems (see, for example, Biddington, 1986; Jaffe and Forbes, 1993). In addition, mechanical perturbations reduce a plant's above-ground biomass (Niklas, 1998; Kern et al., 2005). Similar effects were noticed in plants, especially trees, that are exposed to wind and experience mechanical stress, mainly in the form of bending (Lawton, 1982; Biddington, 1986). These observations inspired numerous studies where mechanical perturbations, such as bending or touching, were utilized to mimic the influence of wind on various plants (e.g. Gartner, 1994; Niklas, 1998).

However, the wind-plant interaction involves fluid (air) to solid (plant) contact and can be considered a fluid dynamic perturbation as opposed to a mechanical perturbation in the form of brushing or touching where direct solid to solid contact is present. Different types of perturbations may induce different effects on plants. Indeed, factorial experiments where the response to wind and mechanical perturbations was studied separately on the same plant species have shown that wind can have different and even opposite effects to mechanical perturbations (Smith and Ennos, 2003; Anten et al., 2010). The different response of the same plant to wind compared with mechanical perturbations suggests that implicit extrapolation of results obtained from tests with mechanical perturbations (e.g. brushing or flexing) to the effects of wind is not always correct (Anten et al., 2010).

Arabidopsis thaliana, a small annual herbaceous plant, is widely used in plant science as a model organism to study different processes and mechanisms especially in the field of plant genetics and molecular biology (Koornneef and Meinke, 2010). *Arabidopsis Columbia* (Col-0) is commonly utilized as the reference genotype in plant science, but many other natural accessions as well as mutants of this plant exist and have been subjected to a wide range of investigations (Lamesch et al., 2012). Brulé et al. (2016) suggested that *Arabidopsis* can be used, with certain limitations, as a model plant to investigate the influence of different parameters on plant stiffness. The response of *Arabidopsis* to various mechanical perturbations was explored in a number of studies and is well documented (Braam, 2005; Chehab et al., 2009; Paul-Victor and Rowe, 2011). In addition, investigation of thigmomorphogenesis in *Arabidopsis* at the molecular level identified a set of touch-induced genes whose expression is enhanced in response to various stimuli (Braam and Davis, 1990).

In general, mechanical perturbations of *Arabidopsis* result in a response that is common to many other plants, namely reduction of the stem length. Mechanical characterization of the primary inflorescence stems showed that perturbed plants were less rigid and had a decreased elastic modulus compared with the control group, thus suggesting that *Arabidopsis* follows the ‘short and flexible strategy’ for stem development in order to cope with mechanical stress (Paul-Victor and Rowe, 2011). From these experiments, it was conjectured that exposure to wind will have the same effects on *Arabidopsis Col-0*. However, as mentioned previously, wind can have different and even opposite effects on plants compared with those from mechanical stimuli. Indeed, a limited number of studies where periodic wind treatment was applied to *Arabidopsis* show that even where the response was in the same direction, the magnitude of changes was not the same (e.g. Bossdorf and Pigliucci, 2009). However, in these experiments, the response to wind was analysed as an average across a number of *Arabidopsis* ecotypes and the response specific to Col-0 cannot be inferred. In addition, the mechanical characterization of inflorescence stems did not form part of this study. Consequently, the question remains open as to whether the response of *Arabidopsis Col-0* to mechanical stress induced by fluid dynamic perturbations, namely wind, is the same as has been previously documented for mechanical stress induced by mechanical perturbations, such as brushing or touching. In addition, the effect of wind on mechanical properties of *Arabidopsis*, such as stem bending rigidity and Young’s modulus of elasticity, remains untested.

In the present study, the influence of a constant unidirectional wind on *Arabidopsis* ecotype Col-0 is investigated. The results show that wind-treated plants exhibit

a positive anemotropic response and their morphology is significantly altered. In addition, exposure to wind modified mechanical properties, anatomical tissue organization, and ion content of the primary inflorescence stems. The observed changes were related to the acclimation strategy of *Arabidopsis* to survive and develop under constant unidirectional wind. Overall, it was found that wind-induced changes to *Arabidopsis* differ from those reported previously as a result of mechanical perturbations in the form of brushing. These observations suggest that *Arabidopsis* is sensitive to the type of stimulus applied and that the substitution of one type of perturbation by another is not straightforward. This study contributes to the systematic understanding of the thigmomorphogenetic response of *Arabidopsis* and provides new insights into the response of plants to wind.

6.2 Materials and methods

6.2.1 Plants

In this study, the response of *Arabidopsis* to wind was characterized using a range of techniques. Two experiments were carried out in order to obtain all measurements since the number of plants that could be subjected to the wind treatment simultaneously was limited to 21 in each experiment. Because of the different preparations, the quantitative results differ between the two data sets although the qualitative results are the same. For this reason, we report the results from the two data sets separately. In the first experiment, seeds of *Arabidopsis* ecotype Col-0 were sown in a single pot and kept at 4 °C for 48 h. The pot was then placed in the growth chamber with a long-day cycle (16 h of light and 8 h of darkness), temperature at 22 °C, light intensity at 150 $\mu\text{mol m}^{-2} \text{s}^{-1}$, and humidity at 60%. After ~ 2 weeks, the seedlings were transplanted into individual pots and were kept in the same growth chamber. After 15 d, when the flower-bearing stem was about to start its development, plants were randomly separated into two groups and moved to the glasshouse. In the second experiment, the procedure was the same except that the plants were grown inside the glasshouse from its start. The first group (21 plants in both experiments) was subjected to a constant unidirectional flow in a purpose-built wind tunnel (experimental group), while the second group (19 plants in the first and 21 plants in the second experiment) was cultivated in the same glasshouse but without wind influence (control group). The conditions in the glasshouse for both groups were as follows, long-day cycle and minimum light intensity at 150 $\mu\text{mol m}^{-2} \text{s}^{-1}$.

The temperature and humidity inside the glasshouse exhibit diurnal variation and only minimum and maximum temperatures are controlled. However, when the wind tunnel was on, loggers placed inside the wind tunnel test section (Lascar EL-GFX-2) and outside of the test section (Elitech RC-61) showed that the conditions in terms of temperature and humidity experienced by the plants are the same in both groups.

6.2.2 Wind treatment

To study the influence of wind on *Arabidopsis*, a specialized wind tunnel was designed and built. The description of the wind tunnel together with the characterization of its test section using hot-wire anemometry is presented in the following section. The wind tunnel provides a well-controlled and characterized constant wind environment. In both experiments, plants were subjected to a unidirectional flow of a constant speed of 5 m s^{-1} with turbulence intensity of 2%. According to Bossdorf and Pigliucci (2009), who applied wind treatment of the same speed to *Arabidopsis*, this value is higher than the typical wind speed at a few decimetres above the surface, based on the mean wind speed data over Central Europe. In the UK, the mean wind speed at 10 m height above the surface level can reach up to 7.5 m s^{-1} (MetOffice, 2020). Assuming a logarithmic wind profile (Manwell et al., 2010), this value extrapolates to a maximum average speed of $2.4\text{--}3 \text{ m s}^{-1}$ at the height of 20–30 cm above ground in open agricultural areas. Consequently, the wind speed of 5 m s^{-1} utilized in this study can be considered as a high wind for small plants such as *Arabidopsis*.

The wind was applied for 24 h a day, and the total duration of the treatment was up to 17 d. Inside the test section, 21 pots with a single *Arabidopsis* plant were arranged in six staggered rows (four pots in the odd rows and three pots in the even). In order to minimize the influence of the pot position and ensure even exposure to the wind, the pots were swapped between rows and within each row every 4–5 d. The orientation of the plants with respect to the flow direction was preserved. The top edges of the pots were in line with the test section floor and the plants were regularly watered from the bottom.

6.2.3 Wind tunnel

The wind tunnel (Supplementary Fig. S1¹) is an open-circuit type with a closed test section and can be run continuously at a constant flow speed for the required

¹Supplementary Fig. S1 is the same as Figure 4.4 in this thesis.

duration of the experiment. The test section is 1 m long and has a rectangular cross-section of 0.45 m \times 0.4 m. The side walls and the ceiling of the test section are made of acrylic glass to provide optical access for monitoring the plants' development and conditions. To straighten the flow and increase its uniformity, an aluminium honeycomb (cell size=6 mm) is installed at the test section inlet. The flow is created by an axial fan connected to the outlet of the test section through a diffuser and flexible connector. The flow speed is controlled by a variable transformer and can be set to any value in the range from 0.8 m s⁻¹ to 10.5 m s⁻¹. LED grow lights with a programmable timer are installed over the test section to control light intensity and the growth cycle.

Characterization of the flow within the wind tunnel test section was performed using a Dantec Dynamics StreamLine Pro System. Measurements were conducted with a straight, single sensor probe (55P11). During the characterization procedure, the wind tunnel was equipped with a bespoke three-axis traverse system enabling a precise positioning of the hot-wire probe, and the standard acrylic glass panels in its doors were replaced with slotted panels to provide access for the probe to the interior.

In situ calibration of the probe was performed before and after each measurement against pitot tube data. The pitot tube was connected to a dry cell standard micromanometer (DP Measurements TT570SV) and was inserted through a port in the top wall for the calibration procedure. The relationship between the squared sensor voltage (E) and effective cooling velocity (U) was established using King's law (King, 1914):

$$E^2 = E_0^2 + BU^n, \quad (6.1)$$

where E_0 is the sensor voltage measured at zero velocity, B and n are King's law coefficients. B and n were determined using simple linear regression after measuring the voltage across the sensor over a range of known flow velocities.

The flow inside the test section was characterized in terms of the flow speed and turbulence intensity at several locations along its length. Measurements were taken in 2D planes normal to the flow direction. Each plane consisted of 80 points (10 in the horizontal and 8 in the vertical direction) with 40 mm spacing in each direction. Due to construction features of the wind tunnel test section frame, the offsets from the wind tunnel walls were 45 mm from the side walls and 60 mm from top and bottom walls. Data were sampled at 100 kHz for 10 s at each measuring point.

The hot-wire measurements showed that the flow velocity inside the wind tunnel

is stable over time and that the velocity distribution is uniform along the wind tunnel test section (see Supplementary Fig. S2²). The average turbulence intensity inside the test section is $\sim 2\%$ for all tested flow speeds. Overall, the quality of the flow inside the wind tunnel is quite uniform and the plants experience similar conditions regardless of their location.

6.2.4 Phenotyping

To investigate the morphological response of *Arabidopsis* to the wind treatment, phenotyping of plants in both experimental and control groups was conducted at two time points during each experiment. The recorded parameters were the length of the primary inflorescence stem, the number of stems (basal branches), and the number of branches. The first phenotyping was conducted 34–38 days after sowing (DAS) when the average length of the primary inflorescence stem in the control group plants was >170 mm. All the parameters were measured again at 40–48 DAS in both experiments (6–10 d after the first phenotyping). The second reported experiment was shorter in time compared with the first one (12 d and 17 d of the wind treatment, respectively); however, the duration of the experiment does not affect the trends in the wind-induced changes to the *Arabidopsis* phenotype. In addition, the average diameters of the top and bottom parts of the primary inflorescence stems were measured from the photographs taken during the mechanical tests in the first experiment. In the second experiment, after the end of the wind treatment, the aboveground fresh biomass of 10 plants from both groups was assessed³. After oven drying at 70 °C, the dry biomass was also determined.

6.2.5 Mechanical characterization

In the first experiment, the changes in mechanical properties of *Arabidopsis* primary inflorescence stems as a result of wind treatment were characterized by assessing their bending rigidity and Young’s modulus of elasticity. The former characterizes the ability of the material to resist bending, while the latter characterizes its resistance to elastic deformations. Mechanical characterization was conducted for all plants from

²Supplementary Fig. S2 is the same as Figure 4.7 in this thesis.

³The main challenge in assessing the belowground biomass of *Arabidopsis*, grown in soil, is associated with the root extraction process. *Arabidopsis* roots are quite delicate themselves and have a substantial number of tiny root hairs which significantly increase root diameter and surface area (Grierson et al., 2014). During the extraction most of them can be destroyed, thus affecting the measurements. Therefore, only the aboveground biomass was assessed in the experiments described in this thesis.

the experimental ($n=21$) and control ($n=19$) groups on two segments taken from the same stem. The first segment was taken from the basal part of the stem, where the cells and tissues are the oldest and were subjected to the wind for the longest time. This part of the stem is referred to as the ‘bottom part of the stem’. The second segment was taken from the apex part of the stem, that was subjected to wind for a shorter period of time compared with the bottom part and is comprised of younger cells and tissues. This part of the stem is referred to as the ‘top part of the stem’. By investigating two different segments of the same stem, it is possible to check the distribution of the mechanical properties along its length and to study whether the changes resulting from the wind treatment are consistent. Both segments were cut using a razor blade and, if necessary, cleared of branches, fruits, flowers, and young floral buds. The tip part of the stem, containing the growth zone, was removed from the top part of the stem prior to testing.

Mechanical characterization of Arabidopsis primary inflorescence stems was conducted using the dynamic forced vibration method (Zhdanov et al., 2020). In this method, the mechanical properties of the tested stem segments are estimated through their multiple resonant frequencies (f_i) using Euler–Bernoulli beam theory (Blevins, 1979):

$$f_i = \frac{\lambda_i^2}{2\pi L^2} \sqrt{\frac{EI}{m}}, \quad i = 1, 2, 3, \dots, n \quad (6.2)$$

where L is the length of the stem, I is the second moment of area, m is the mass per unit length, and λ_i is a dimensionless parameter that is obtained from the characteristic equation corresponding to the applied boundary conditions and vibration mode. In the present study, stem segments were tested with clamped-clamped boundary conditions. In all tests, the length of the tested stem segment was equal to 50 mm, corresponding to the distance between the clamping points. To evaluate I , a widely used approximation that a segment of Arabidopsis stem has a circular cross-section of constant diameter along its length was utilized (see, for example, Turner and Somerville, 1997; Bichet et al., 2001). The diameter was determined from the photographs of the tested stem segment taken after each test using ImageJ software (Schneider et al., 2012) as the averaged diameter over several locations. The mass of the segment was determined directly after each test using a precision balance; m was then evaluated as the ratio between the mass and the length of the segment. For the bottom part of the stem, the determined mechanical proprieties were averaged over the first three natural frequencies while for the top part the first four natural

frequencies were used. The multiple resonant frequency method was previously validated against a standard three-point bending test (Zhdanov et al., 2020). The tests were performed immediately after the cutting of each segment to avoid changes in the mechanical properties of the stem segments due to dehydration and decrease in turgor pressure.

6.2.6 Anatomical measurements

In the second experiment, the anatomical tissue composition of the primary inflorescence stem was investigated for 10 plants from each group. Segments were taken from the basal and apex ends; that is, the same two parts of the stem were considered as for the mechanical characterization. The transverse segments were sectioned manually from the centre of these stem parts using a razor blade and stained with 0.02% toluidine blue. As a result of histochemical staining it was possible to differentiate three representative tissues, namely the outer part that consists of epidermis and cortex, the middle part that mostly accommodates lignified tissues (coloured in blue), and the innermost part – pith (coloured in purple). The samples were observed on a Zeiss Stemi SV11 microscope and photos were captured. The relative areas of the three aforementioned representative tissues were measured from the images using ImageJ software.

6.2.7 Ca^{2+} measurements

In the second experiment, bottom stem segments from eight plants in each group were collected and their fresh weight was determined. After drying for 48 h and recording the dry weight, the stems were homogenized, and dry material was extracted in 1 M HCl. The insoluble material was removed through centrifugation, retaining the supernatant. Aliquots of the supernatant were used to determine the Ca^{2+} content utilizing flame photometry (Model 410 flame photometer, Sherwood). All measurements were quantified against calibration standards.

6.2.8 Statistical analysis

All statistics of measured quantities are reported as the mean \pm SD of n observations. The post-hoc statistical analysis was carried out with a non-parametric Wilcoxon rank-sum test. This test was chosen due to the small sample sizes of different lengths and because some of the data did not follow the normal distribution. The tests

were performed in Matlab (R2015b, MathWorks, USA) using the in-built ranksum function. A statistically significant difference was established at $P \leq 0.05$.

6.3 Results

Due to the destructive nature of most of the conducted tests and limited room inside the wind tunnel test section, two sets of experiments were conducted in this study. The experiments were carried out at two different times of the year, hence the conditions inside the glasshouse were slightly different in terms of temperature and maximum light intensity. In addition, performing two sets of experiments provided the possibility to increase the sample size for statistics of the reported parameters. Where possible, the same tests were conducted in both sets of experiments (phenotyping). Despite the quantitative differences between the results obtained in the reported experiments, qualitatively they led to the same conclusions.

6.3.1 Wind treatment induces changes in Arabidopsis phenotype

The effect of wind treatment on the recorded morphological parameters was low compared with the control group during the first phenotyping in both experiments (see Fig. 6.1). The primary inflorescence stem of plants in the experimental group was on average shorter by 8.81% and 10.52% in the first and second experiments, respectively (Fig. 6.1A). However, the observed decrease is statistically significant ($P < 0.05$) only in the second experiment. The average number of stems in the wind-treated plants at this stage was 2.33 ± 0.73 and 2.24 ± 0.78 in the first and second experiments, respectively (Fig. 6.1B). These values were lower compared with the control group where the number of stems was 2.79 ± 1.13 and 3.95 ± 0.86 , respectively. The difference in average number of stems between the wind-treated plants and the control group was statistically significant only in the second experiment. The same effect was observed for the number of branches (Fig. 6.1C), namely plants from the experimental group had fewer branches in both experiments, 2.81 ± 0.6 and 4.95 ± 1.47 , respectively, compared with 3.26 ± 0.81 and 9.14 ± 2.43 in the control groups. As in the case of the number of stems, this difference was statistically significant in the second experiment only.

During the second phenotyping, which was conducted 10 d and 6 d after the first one in the first and second experiments, respectively, the wind effects became

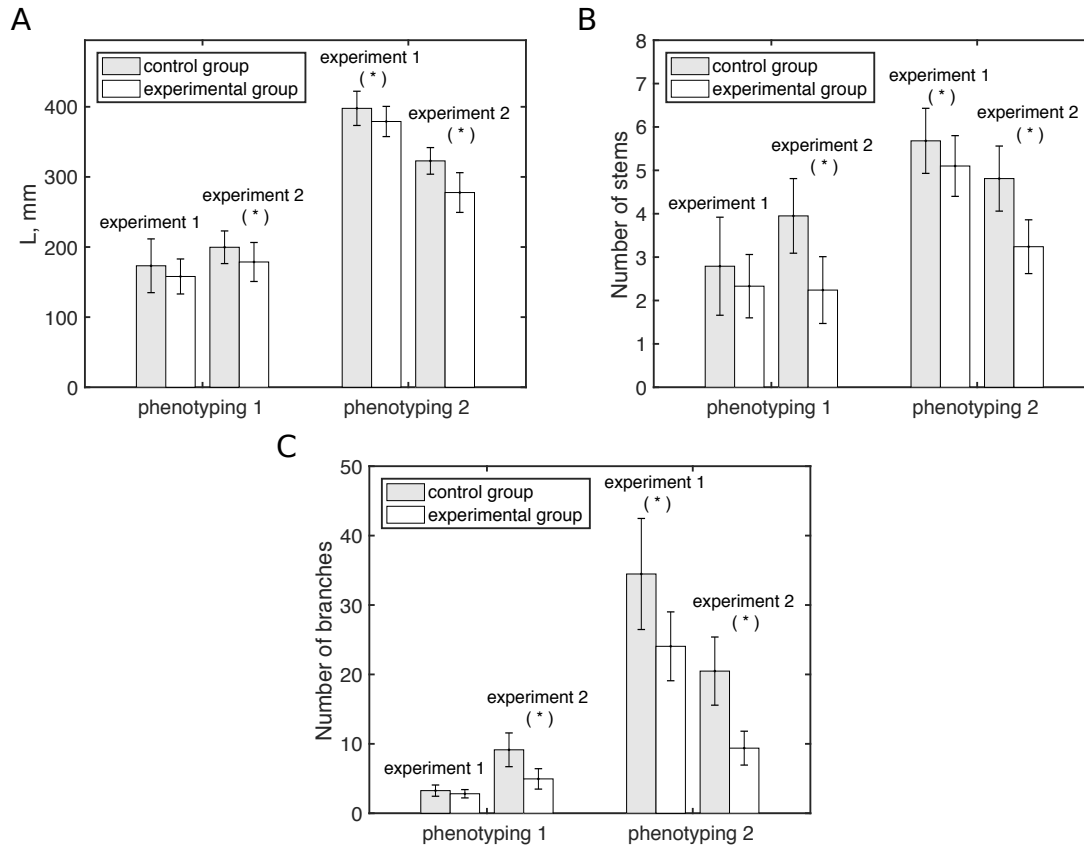


Figure 6.1: Changes to the morphological parameters as a result of unidirectional wind treatment with a constant flow speed of 5 m s^{-1} in both conducted experiments. (A) Length of the primary inflorescence stem. (B) Number of stems. (C) Number of branches. Error bars represent the SD. Statistically significant difference ($P \leq 0.05$) from the two-sided Wilcoxon rank sum tests comparing medians of the corresponding parameters in the control ($n=19$ and $n=21$ for the first and second experiments, respectively) and experimental ($n=21$ for both experiments) groups is marked with (*).

more substantial and statistically significant (see Fig. 6.1). The length of the primary inflorescence stem in both experiments was reduced only slightly compared with the control group plants (4.71% and 13.98%), but, in contrast to the first phenotyping, this difference became statistically significant ($P < 0.05$) in all cases (Fig. 6.1A). In addition, both experiments showed that plants subjected to the unidirectional constant wind have fewer stems and branches compared with the untreated plants (Fig. 6.1B, C). The number of stems in the wind-treated plants recorded in both experiments was 5.1 ± 0.7 and 3.24 ± 0.62 , respectively. These values are significantly lower ($P < 0.05$) compared with 5.68 ± 0.75 and 4.81 ± 0.75 observed in the plants from the corresponding control groups. The highest effect of the wind treat-

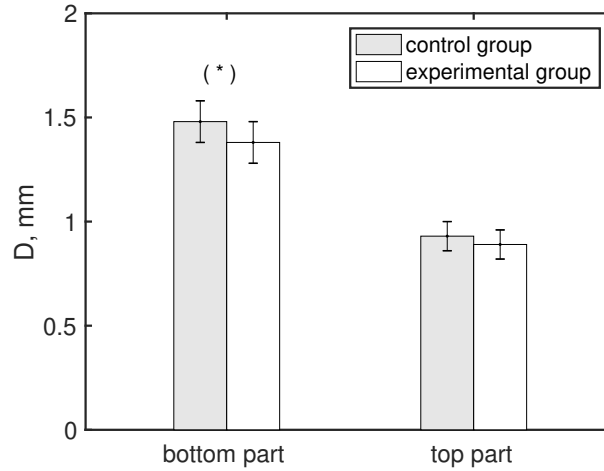


Figure 6.2: Changes to the Arabidopsis stem segments diameter as a result of the unidirectional wind treatment with a constant flow speed of 5 m s^{-1} measured in the first experiment. Error bars represent the SD. A statistically significant difference ($P \leq 0.05$) from the two-sided Wilcoxon rank sum tests comparing medians of the corresponding parameters in the control ($n=19$) and experimental ($n=21$) groups is marked with (*).

ment was measured for the number of branches. Plants from the experimental group had on average 24.05 ± 4.96 and 9.38 ± 2.44 branches (in experiments 1 and 2, respectively); this is lower by approximately one-third compared with the average number of branches in the plants from the control group (34.47 ± 8.0 and 20.48 ± 4.91), and this difference is statistically significant ($P < 0.0001$).

Wind treatment also resulted in a decrease in the diameter of the primary inflorescence stem segments that was measured after the first experiment (see Fig. 6.2). The bottom parts of the stem had significantly ($P < 0.05$) lower diameter compared with those of the control group plants. The diameter of the top parts of the stem was also reduced, but the difference was statistically insignificant ($P > 0.05$).

The plants grown under a constant unidirectional wind had a significantly ($P < 0.05$) lower aboveground fresh biomass (see Table 6.1). Fresh weight of the Arabidopsis Col-0 exposed to wind was less than half of the weight of the control plants. In addition, a significant ($P < 0.01$) reduction by almost 48% in the dry aboveground biomass of the plants from the experimental group was also observed. On the other hand, the biomass ratio that was calculated as the percentage of moisture evaporated during oven drying was almost the same in both groups.

Table 6.1: Overview of the changes to the Arabidopsis biomass (mean \pm SD) that were assessed after the end of the unidirectional wind treatment with a constant flow speed of 5 m s⁻¹ in the second experiment.

	Experiment 2		
	control plants	wind treated plants	p-value
fresh biomass, g	1.78 \pm 0.55	0.87 \pm 0.33	0.001
dry biomass, g	0.23 \pm 0.06	0.12 \pm 0.04	0.001
biomass ratio, %	86.7 \pm 0.6	85.6 \pm 0.3	0.0312

P-values are obtained from the two-sided Wilcoxon rank sum tests comparing medians of the corresponding parameters in the control (n=10) and experimental (n=10) groups.

6.3.2 Wind changes mechanical properties of Arabidopsis stems

The primary inflorescence stems of Arabidopsis plants grown under constant wind were inclined in the direction of the wind but did not show any signs of mechanical damage. The mechanical properties, namely bending rigidity and Young's modulus of elasticity, of segments taken from the tip and basal parts of the same stems were evaluated using the dynamic forced vibration method (Fig. 6.3). Wind treatment resulted in a significant increase ($P < 0.05$) in Young's modulus of elasticity of both tested segments (Fig. 6.3B). The average value of the elastic modulus of the bottom part of the stem of plants exposed to the wind was 1119 MPa, that is 17% higher compared with the untreated plants. The increase in the modulus of elasticity of the segments taken from the top part of the stem was $>12\%$ in the same stems. While the intensive property (E) of the stem material increased, its extensive property (EI) was only slightly ($P > 0.05$) lower for all tested stem parts (Fig. 6.3A).

6.3.3 Wind changes anatomical structure of Arabidopsis stems

Exposure to wind induced substantial changes to the anatomical structure of Arabidopsis primary inflorescence stems in terms of their tissue organization (see Table 6.2; Fig. 6.4). Plant stems from the experimental group have significantly ($P < 0.05$) more lignified interfascicular tissue compared with the control group in their bottom part. In addition, wind treatment resulted in a significant ($P < 0.05$) decrease of the pith tissue area in the same part of Arabidopsis stems. On the other hand, the relative area of cortex together with epidermis was not affected by the wind treatment

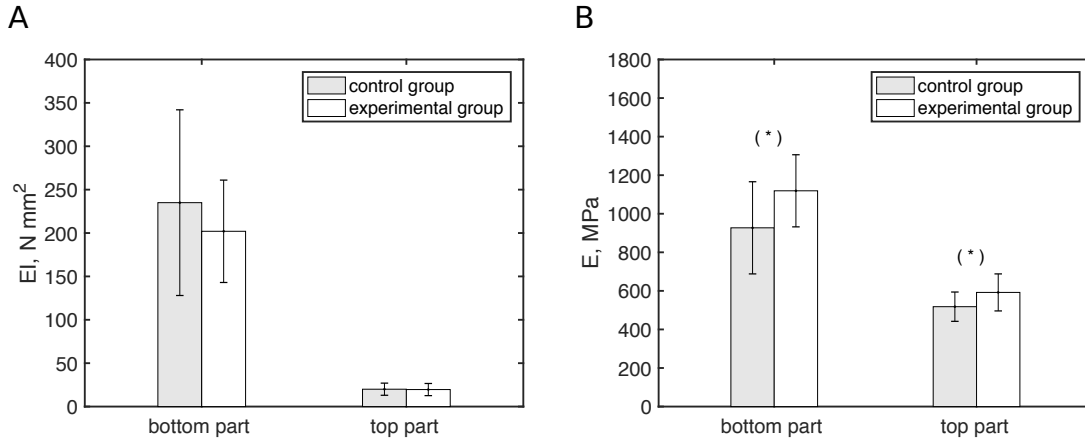


Figure 6.3: Changes to the mechanical properties of Arabidopsis stem segments as a result of the unidirectional wind treatment with a constant flow speed of 5 m s^{-1} in the first experiment. (A) Bending rigidity. (B) Young's modulus of elasticity. Error bars represent the SD. Statistically significant difference ($P \leq 0.05$) from the two-sided Wilcoxon rank sum tests comparing medians of the corresponding parameters in the control ($n=19$) and experimental ($n=21$) groups is marked with (*).

and remained almost the same in the bottom part of the stems in the experimental and control groups. The changes in the tissue organization in the top part of the primary inflorescence stems demonstrate the same trends as those observed in the bottom part as a result of exposure to wind (Table 6.2).

6.3.4 Wind changes Ca^{2+} content of Arabidopsis stems

Ion content measurements conducted after the second experiment showed that wind treatment resulted in a significant increase ($P < 0.001$) in Ca^{2+} content in the Arabidopsis primary inflorescence stems (Fig. 6.5). The weight of calcium per gram of the fresh weight on average was almost twice higher in the stems of plants grown under constant unidirectional wind compared with the stems of control group plants.

6.4 Discussion

6.4.1 Morphological response of Arabidopsis

As was shown in previous studies (Smith and Ennos, 2003; Anten et al., 2010), the effect of wind can differ considerably from the effect of mechanical perturbations in the same plants. Indeed, the changes to Arabidopsis Col-0 that were observed in this study differ from those reported for the same ecotype in previous investigations where

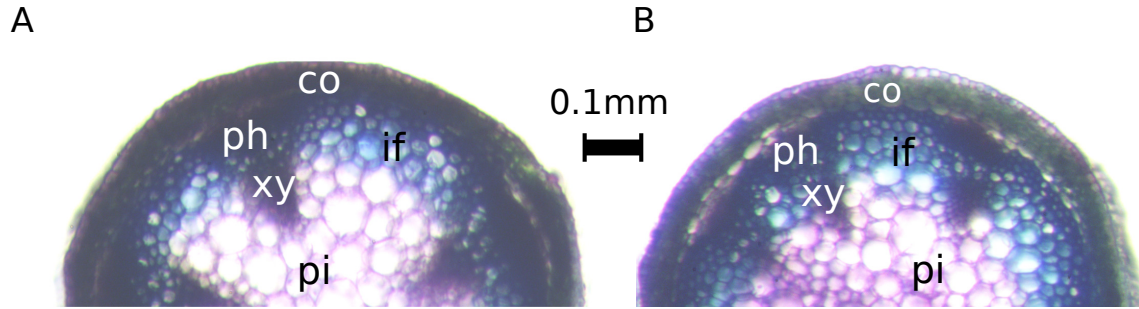


Figure 6.4: Representative examples of the primary inflorescence stem cross-section showing anatomical tissue organisation of its bottom part: (A) plant from the control group. (B) plant from the experimental group. co, cortex; ph, phloem; xy, xylem; if, interfascicular tissue; pi, pith.

wind influence was mimicked by mechanical perturbations. Regular brushing of *Arabidopsis* led to the reduction of the stem length by $\sim 50\%$ (Paul-Victor and Rowe, 2011), and a similar response was recorded as a result of physical touch (e.g. Braam and Davis, 1990). In contrast, in the present experiments, the highest observed decrease in the length of the primary inflorescence stem subjected to a constant wind was only 14% compared with the untreated plants. These observations are consistent with those reported by Bossdorf and Pigliucci (2009) where the average reduction of the plant height of various natural populations of *Arabidopsis* was $\sim 13.2\%$ when subjected to a periodic wind treatment.

In addition to the inhibition of the stem length, a common thigmomorphogenetic response in many plants includes an increase in the stem diameter. This was reported for numerous plants as a result of mechanical bending (see, for example, Goodman and Ennos, 1996; Telewski, 2006; Coutand et al., 2010). However, the present results show that the mean diameter of the primary inflorescence stem measured for its bottom and top parts was reduced in the wind-exposed plants compared with the control group. Lower stem diameter was also reported in trees as a result of wind influence. For example, exposure of *Cecropia schreberiana* to the natural wind environment resulted in significantly lower stem diameters in wind-exposed plants compared with those in plants sheltered from the wind (Cordero, 1999). Slightly lower stem diameter was also observed in lodgepole pine (*Pinus contorta* Douglas ex Loudon) subjected to a constant wind in a controlled wind tunnel environment (Rees and Grace, 1980). In addition, the influence of wind, without mechanical flexure, led to a decrease in the stem diameter of sunflowers (*Helianthus annuus* L.) in factorial experiments conducted by Smith and Ennos (2003). When both wind and flexure were combined, a slight increase in the stem diameter was observed; however,

Table 6.2: Contribution of tissues to the total cross-sectional area of the Arabidopsis primary inflorescence stem segments (mean \pm SD) that was assessed after the end of the unidirectional wind treatment with a constant flow speed of 5 m s⁻¹ in the second experiment.

	Tissue contribution %		
	control plants	wind treated plants	p-value
Bottom part of the stem			
Pith	38.92 \pm 3.33	31.64 \pm 3.23	< 0.001
Lignified tissues	24.76 \pm 2.69	31.02 \pm 2.33	< 0.001
Cortex+epidermis	36.43 \pm 3.06	37.34 \pm 3.6	0.68
Top part of the stem			
Pith	35.6 \pm 1.88	31.47 \pm 2.4	< 0.01
Lignified tissues	22.99 \pm 1.83	26.21 \pm 1.08	< 0.001
Cortex+epidermis	41.41 \pm 2.3	42.32 \pm 1.96	0.32

P-values are obtained from the two-sided Wilcoxon rank sum tests comparing medians of the corresponding parameters in the control (n=10) and experimental (n=10) groups.

as pointed out by the authors, the amount of mechanical flexure received by plants in this group was considerably higher than the wind could create. Interestingly, a reduction of the stem diameter in Arabidopsis Col-0 was also reported as a result of brushing (Paul-Victor and Rowe, 2011), showing, in this respect, similarities of the response to the wind and brushing in these plants.

We found that plants grown under constant unidirectional wind had a significantly lower number of stems and branches compared with the untreated plants. As will be discussed below, this can be a part of the acclimation strategy of Arabidopsis to deal with wind loadings. The reduced branching in Arabidopsis was also reported as a result of a periodic wind exposure of different flow speeds (Bossdorf and Pigliucci, 2009), but not for all 17 tested natural populations. The same behaviour was reported earlier by Pigliucci (2002) for 11 natural accessions of Arabidopsis that were subjected to a periodic wind treatment of different durations. While the number of branches in some accessions decreased, a similar or even increased number was observed in others. On the other hand, increased branching was reported for *Potentilla reptans* L. as a response to the mechanical brushing that was applied to mimic a wind environment (Liu et al., 2007).

Another effect of mechanical perturbations on plants is the decrease of above-ground biomass (Niklas, 1998; Kern et al., 2005). This can be linked to the overall

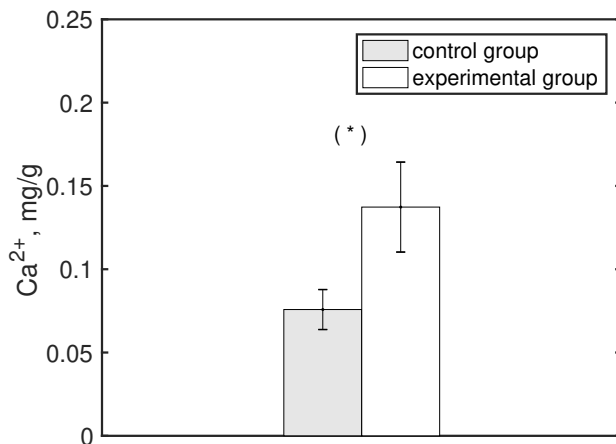


Figure 6.5: Changes to the Ca^{2+} content of Arabidopsis stems as a result of the unidirectional wind treatment with a constant flow speed of 5 m s^{-1} in the second experiment. Error bars represent the SD. A statistically significant difference ($P \leq 0.05$) from the two-sided Wilcoxon rank sum tests comparing medians of the corresponding parameters in the control ($n=8$) and experimental ($n=8$) groups is marked with (*).

reduction of the plant's size as a result of thigmomorphogenesis. In the present study, both fresh and dry aboveground biomass was reduced for plants grown under a constant unidirectional wind. This is attributed to the changes in the Arabidopsis morphology where a lower number of stems and branches together with slightly shorter stems of reduced diameter were observed in plants subjected to wind. The decrease of Arabidopsis dry biomass as a result of wind treatment is consistent with previous observations by Bossdorf and Pigliucci (2009). Although changes in the biomass were not quantified for Arabidopsis subjected to mechanical perturbations in the studies by Braam and Davis (1990) and Paul-Victor and Rowe (2011), it can be reasonably presumed that it was decreased due to the significant reduction in size of the plants. The very close values of the biomass ratio in both experimental and control groups in the present study point to the same amount of water in both groups at the time of harvest and throughout the experiments. Thus, the changes observed as a result of wind treatment were not due to the water loss in plants from the experimental group through increased evaporation. In addition, a similar water content can be associated with water-saving strategies of plants under wind, but further investigation of this aspect is required.

Comparing the changes in Arabidopsis morphology, some similarities between responses to wind and mechanical brushing can be noted. In both cases, a reduction

of the plant biomass and decrease in the stem diameter are observed, even though the latter is not a common response to mechanical bending in plants. However, the inhibition of the stem length is much lower in wind-exposed plants compared with those subjected to brushing. The observed differences in the responses to constant unidirectional wind as in the current study and mechanical contact (e.g. Paul-Victor and Rowe, 2011) can be attributed to the fact that in the first case *Arabidopsis* can adapt to the constant stress coming from a single direction by adapting its shape and structure, while it is not possible to achieve this when stress is applied from multiple directions, as in the case of brushing.

6.4.2 Anemotropic response of *Arabidopsis* to a constant unidirectional wind

Environmental stimuli have an effect on the specific orientation of plant growth, which is known as tropism. A tropic response can be either positive, towards the stimulus, or negative, away from it. The response of plants to touch and other mechanical contacts is known as thigmotropism. By analogy, the response of plants to wind can be termed as anemotropic or anemotropism. In the present experiments, *Arabidopsis* ecotype Col-0 grown under the constant unidirectional wind exhibited an anemotropic response (Fig. 6.6). The young seedlings demonstrated a positive anemotropic response to wind, by directing their primary growth in the direction opposite to the direction of the flow (Fig. 6.6A, B). To the best of our knowledge, this is the first time an anemotropic response to a unidirectional wind has been documented in any plant system (Telewski, 2012), although previous work on conifers already suggested the existence of this type of tropic response (Rees and Grace, 1980; Berthier and Stokes, 2006). As *Arabidopsis* developed under the wind and its size increased, the shape of the plants became windswept; however, the upwind bending of the stems was preserved (Fig. 6.6C, D). The windswept growth form is widely found in trees for which it is a crucial acclimation response to the wind environment (Telewski, 2012). It should be noted that the *Arabidopsis* stem is known to exhibit gravitropism when inclined at an angle from the vertical orientation. In the case of the gravitropic response, the stem returns back to the vertical orientation within a few hours (Fukaki et al., 1996a). Curvature of *Arabidopsis* stems grown under constant unidirectional wind was preserved over time (see Fig. 6.6), suggesting that the observed response is mainly due to anemotropism. However, an interaction between anemotropic and gravitropic responses cannot be fully excluded since gravity was

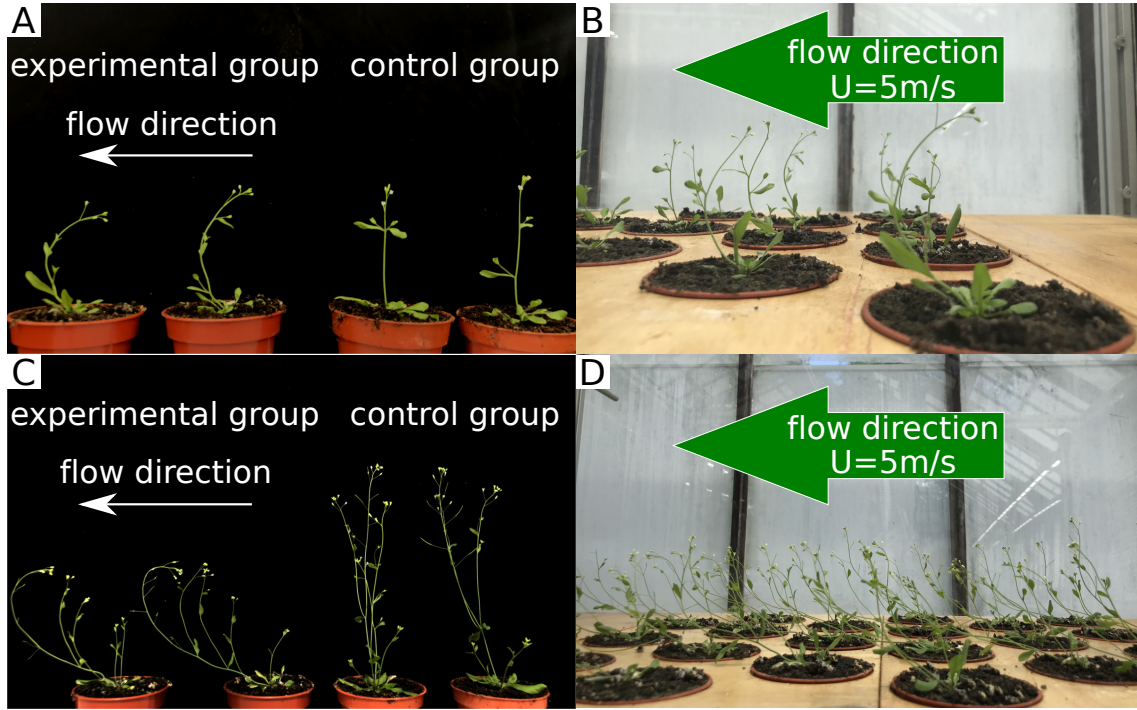


Figure 6.6: Arabidopsis ecotype Col-0 grown under the constant unidirectional wind exhibits positive anemotropic response. (A) Young Arabidopsis seedlings (30 DAS) from experimental and control groups. (B) Young Arabidopsis seedlings (30 DAS) inside the wind tunnel test section. (C) Arabidopsis plants (34 DAS) from experimental and control groups. (D) Arabidopsis plants (34 DAS) inside the wind tunnel test section. Note that in (A) and (C) plants from the experimental group were removed from the wind tunnel and the curvature of their stems is increased compared to plants in (B) and (D) where Arabidopsis is subjected to a constant unidirectional wind of 5 m s^{-1} . For reference in all parts of the figure the diameter of the pot is 76 mm.

inevitably present in the experiments. As was shown in the studies where Arabidopsis was grown in a centrifuge (e.g. Dümmer et al., 2015; Chauvet et al., 2016), the combination of gravity with an additional force results in a growth response in the direction parallel to their resultant force. In the present study, the additional force was exerted by the wind, which could explain the observed curvature of the stem and the fact that Arabidopsis grown under constant wind did not develop parallel to the wind direction.

6.4.3 Acclimation of Arabidopsis to a constant unidirectional wind

To grow and survive in windy environments, plants have developed a number of acclimation strategies. These strategies include streamlining and reconfiguration, damping, and wind-induced pruning (Gardiner et al., 2016). Reconfiguration, the term introduced by Vogel (1984) to describe the change of plant shape under wind, and streamlining are common for most plants regardless of size and growing environment. In terms of this strategy, plants reduce their frontal area and aerodynamically optimize their shape to experience less force from the wind. The details of the physics and mechanics behind streamlining and reconfiguration can be found in, for example, Gosselin (2019). Plants mainly experience force from the wind in the form of fluid dynamic drag, which is defined as:

$$D = \frac{1}{2}\rho AC_D U_\infty^2, \quad (6.3)$$

where ρ is the density of the fluid, A the frontal area of the plant, C_D the drag coefficient, and U_∞ flow velocity. For plants it was shown that drag does not scale as U_∞^2 but rather as U_∞^{2+v} , where v is the Vogel exponent (Vogel, 1984, 1989). In order to reduce the drag force experienced from wind, plants can modify only two parameters in Equation 6.3, namely their drag coefficient and frontal area.

In the present study, Arabidopsis is expected to exhibit a long-term acclimation strategy to a unidirectional wind environment. As mentioned above, Arabidopsis grown inside the wind tunnel developed in the downstream direction and its shape became windswept. In trees, a windswept form is a result of long-term streamlining that occurs as a response to regular wind exposure. Trees with windswept crowns are known to experience substantially less drag (Telewski and Jaffe, 1986a); that is, values of their C_D in Equation 6.3 are reduced. Taking into account similarity in the long-term response to continuous wind, it can be presumed that Arabidopsis optimized its shape into a more streamlined one and thus experienced less drag.

In addition, phenotyping showed a significantly lower total number of branches (including basal branches) in the wind-exposed plants. This in turn decreased their frontal area compared with the untreated plants that had more branches and stems. From Equation 6.3, a reduction in the frontal area directly leads to a decrease in the drag force the plant experiences from the wind. Hence, the reduced number of stems and branches in the experimental group compared with the control group can be considered as part of the long-term acclimation strategy of Arabidopsis Col-0 to

constant unidirectional wind.

6.4.4 Changes in the mechanical properties of *Arabidopsis* stems

The observed changes to the mechanical properties of *Arabidopsis* are opposite to those reported as a result of brushing, where bending rigidity and Young's modulus of elasticity of inflorescence stems were significantly reduced (Paul-Victor and Rowe, 2011). In the present study, only a marginal decrease in the bending rigidity of *Arabidopsis* stems was recorded for the experimental group (Fig. 6.3A). It should be noted that this property is dependent on the stem geometry, namely the second moment of area. This parameter, in turn, is a function of the stem diameter, which was lowered as a result of the wind treatment (Fig. 6.2). As was discussed earlier, plants experience a drag force from the wind that is dependent on the characteristic dimension of the plant (projected frontal area). Consequently, the reduced stem diameter is also important for reducing the wind-induced drag force. Paul-Victor and Rowe (2011) suggest that changes in mechanical properties are related to changes in the developmental rate and, combined with alterations in plant morphology, are adaptive to the growth environment. Therefore, a possible explanation for the contrasting results between the two types of treatment may be the fact that under unidirectional wind *Arabidopsis* did not bend in opposite directions as in the case of brushing, and hence increased flexibility was not required to adapt to the growth environment. On the other hand, wind treatment increased the modulus of elasticity of the primary inflorescence stems of *Arabidopsis* (Fig. 6.3B). A higher elastic modulus means that a larger stress needs to be applied in order to produce the same strain (deformation). This may also form a part of the acclimation strategy, making the plant material more rigid so it can withstand the loads from the continuous wind exposure. In addition, an increased modulus of elasticity compensates the influence of lower stem diameter on the bending rigidity, so stems sway less in the wind compared with the case where both E and D are reduced.

Other studies where the influence of different types of perturbations (wind, flexing, rubbing, etc.) on the mechanical properties of plants was assessed show that the changes can be in any direction. Bending rigidity of stems was reported to decrease (e.g. Telewski and Jaffe, 1986b; Cordero, 1999), increase (e.g. Hepworth and Vincent, 1999; Kern et al., 2005; Niez et al., 2019), or remain unaffected (e.g. Jaffe et al., 1984). Young's modulus of elasticity also can increase (e.g. Telewski and Jaffe,

1986a; Gladala-Kostarz et al., 2020) or decrease (e.g. Jaffe et al., 1984; Cordero, 1999; Kern et al., 2005) as a result of various mechanical treatments including wind. The present results support the hypothesis proposed by Newcombe (1895) that there is no universal change in the mechanical properties of plants as a response to mechanical stress (for a review, see Telewski (2016)). The changes are likely to adjust to the exact type of perturbation and depend on many factors, such as frequency of perturbations, amount of stress induced per perturbation, direction of perturbation, etc. Thus, as discussed in Coutand and Moulia (2000), it is important to characterize perturbations experienced by plants as well as their growth environment. In the present study, the wind conditions inside the test section were characterized using hot-wire anemometry and it was ensured that other environmental variables were the same for both groups. Experiments conducted at different times of the year (see the Materials and methods) confirmed that changes to the mechanical properties of Arabidopsis primary inflorescence stems resulting from continuous exposure to wind at a constant flow speed of 5 m s^{-1} are repeatable. In addition, as was shown for loblolly pines (Telewski and Jaffe, 1986b) and hybrid poplars (Pruyn et al., 2000), the response to mechanical perturbations depends on the plant genotype.

In future studies, various Arabidopsis ecotypes and mutants can be subjected to different wind speeds, and the corresponding changes to their mechanical as well as morphological properties can be quantified. This will give the possibility to assess how Arabidopsis adapts to different wind conditions and how these conditions affect the aforementioned properties.

6.4.5 Changes in the stem anatomy and ion content related to the changes in the mechanical properties

Lignin is known to strengthen cell walls and supportive fibres, and thus provides rigidity to plants (Smith et al., 2013; Brulé et al., 2016). As was shown with the lignin deficit Arabidopsis mutants, *irx4*, reduction of lignin leads to the decrease in the mechanical properties of Arabidopsis stems (Jones et al., 2001). Consequently, the observed changes in the relative areas of structural tissues as a result of wind influence in the present study suggest direct correlation between an increase in the area of the lignified tissues and an increase in the modulus of elasticity of the tested stem segments.

The larger relative area of lignified tissues in Arabidopsis stems observed in wind-exposed plants is opposite to the effects of mechanical perturbations in the form of

brushing. Paul-Victor and Rowe (2011) reported a decrease in this parameter in the stems of brushed plants. This was partially attributed to the recorded reduction in the mechanical properties of perturbed plants compared with the control group.

Ko et al. (2004) showed that lignification in *Arabidopsis* inflorescence stems is related to their weight and length. Furthermore, it was found that an artificial increase of stem weight promoted further formation of lignified tissues. As in the experiments by Ko et al. (2004), where addition of the weight to the stem tip increased the gravitational force exerted on *Arabidopsis* stems, in the present study, stems were also made to experience an additional force, namely the drag force that was induced by the constant unidirectional wind. This suggests a possible explanation for the observed increase of the lignified tissues in the wind-treated plants compared with the control group.

In addition to an increase in the area of lignified tissues, stems of wind-exposed plants had a higher Ca^{2+} content. An increase in Ca^{2+} is known to occur in response to different types of mechanical stress in plants (Telewski, 2006). Furthermore, Ca^{2+} ions contribute to cell wall stiffening by taking part in the formation of pectate gels (Jiang et al., 2005; Höfte et al., 2012). Based on this, it can be presumed that elevated levels of Ca^{2+} may also contribute to the increased modulus of elasticity of plant stems from the experimental group.

6.4.6 Wind and water stress in plants

In general, it can be expected that wind leads to water stress in plants through an increase in transpiration from plant surfaces. In many cases, the increased evaporation from plants in wind is a result of the decrease in cuticle resistance which occurs through abrasive wear and damage due to flexing of leaves and collisions with other leaves (Jones, 2013). This was experimentally shown for a number of plants, such as *Festuca arundinacea* (Grace, 1974), *Picea sitchensis*, and *Pinus sylvestris* (Van Gardingen et al., 1991). However, several theoretical and experimental studies show that, in certain cases, wind has a small influence on the evaporation rate in plants and even a decrease in transpiration has been observed (Monteith, 1965; Drake et al., 1970; Rees and Grace, 1980; Dixon and Grace, 1984). It should be noted that Rees and Grace (1980) and Dixon and Grace (1984) conducted experiments in a wind tunnel and their findings thus are directly relevant to the current study.

The present study focuses on the changes in the *Arabidopsis* morphology and

mechanical properties as a result of continuous unidirectional wind treatment at a constant speed. The growth conditions between the control and experimental groups were identical except for the wind treatment. Moreover, the wind environment was created in a purpose-built wind tunnel, that was precisely characterized, and through repeated experiments the results were shown to be reproducible. Any changes in the plant microclimate came directly from the wind and are expected to occur in the natural environment under the same conditions, resulting in similar changes to the plant structure and mechanical properties. The top edges of the plant pots were in line with the wind tunnel floor, hence the leaf rosettes were located very close to the wind tunnel floor inside the boundary layer, where flow speed is significantly reduced. Consequently, the disturbance from wind to the leaf rosettes of *Arabidopsis* was reduced to a minimum throughout the experiments and neither flexing nor rubbing of leaves against each other was observed. The other aboveground parts of *Arabidopsis* swayed in the wind but did not touch parts of neighbouring plants or other parts of the same plant. Based on this, it can be presumed that damage to the cuticle was also reduced or even eliminated, thus avoiding an increase in transpiration from the plants through a decrease in the cuticle resistance.

6.5 Conclusions

In this study, *Arabidopsis* ecotype Col-0 was subjected to a continuous wind treatment in a purpose-built wind tunnel. Exposure to wind resulted in a positive anemotropic response, recorded for the first time in any plant system, and in pronounced changes to the plant structure. In addition, mechanical properties, anatomical tissue organization, and ion content of the primary inflorescence stems were modified. Overall, the observed changes can be interpreted as a part of the acclimation strategy of *Arabidopsis* to wind.

Acknowledgements

This work was supported by the University of Glasgow's Lord Kelvin/ Adam Smith (LKAS) PhD Scholarship. Hot-wire anemometry instrumentation used in this study was provided by the National Wind Tunnel Facility funded by EPSRC, grant no. EP/L024888/1. We would like to thank Amparo Ruiz-Prado for help with growing plants, and Naomi Donald for help with flame photometry tests.

Author contributions

OZ: conceptualization, investigation, formal analysis, visualization, writing – original draft, writing – review and editing. MRB: conceptualization, supervision, resources. HZB: conceptualization, supervision. AB: conceptualization, supervision, writing – review and editing.

Chapter 7

Unidirectional versus bidirectional brushing: simulating wind influence on *Arabidopsis thaliana*

This chapter is a draft manuscript to be submitted:

Zhdanov, O., Blatt, M.R., Zare-Behtash, H. and Busse, A., 2021. Unidirectional versus bidirectional brushing: simulating wind influence on *Arabidopsis thaliana*. (In preparation)

Abstract Plants acclimate to various types of mechanical stresses through thigmomorphogenesis and alterations in their mechanical properties. Although resemblance between wind- and touch-induced responses provides the foundation for studies where wind influence was mimicked by mechanical perturbations, factorial experiments revealed that it is not always straightforward to extrapolate results induced by one type of perturbation to the other. To investigate whether wind-induced changes in morphological and biomechanical traits can be reproduced, we subjected *Arabidopsis thaliana* to two vectorial brushing treatments. Both treatments significantly affected the length, mechanical properties, and anatomical tissue composition of the primary inflorescence stem. While some of the morphological changes were found to be in line with those induced by wind, changes in the mechanical properties exhibited opposite trends irrespective of the brushing direction. Overall, a careful design of the brushing treatment gives the possibility to obtain a closer match to wind-induced changes, including a positive tropic response.

Keywords: *Arabidopsis thaliana*, biomechanics, morphology, mechanical perturbations, mechanical properties, thigmomorphogenesis, tropic response.

7.1 Introduction

Plants respond to mechanical perturbations through morphological and physiological changes termed ‘thigmomorphogenesis’ by Jaffe (1973). The most common responses found in many plant species are inhibition of the stem length, increase in stem radial growth, and redistribution of biomass from above- to below-ground (Chehab et al., 2009; Telewski, 2016). Other reported responses include alterations in flowering time, chlorophyll content, number of leaves, senescence, and development of stress resistance (see Biddington, 1986). In addition, plants alter their mechanical properties to cope with the induced mechanical stress. However, the nature of this response, i.e. whether the plant becomes more rigid or flexible, is not universal and depends on the type of perturbation and the plant genotype (Telewski and Jaffe, 1986b; Pruyn et al., 2000; Telewski, 2016)

Initially, thigmomorphogenesis was recorded as a result of the application of artificial mechanical stress in the form of rubbing (Jaffe, 1973). Other types of mechanical perturbations, such as bending (Coutand et al., 2010), brushing (Paul-Victor and Rowe, 2011), flexing (Pruyn et al., 2000), shaking (Niklas, 1998), which also involve solid to solid contact (e.g. brushing material to plant), evoke similar

responses in plants and have been widely used in thigmomorphogenetic studies.

In their natural environment, terrestrial plants regularly experience perturbations from various natural sources, such as wind, rain, snow, animals; among which wind is widely considered as the major one. Plants acclimate to windy environments through morphological changes that are similar to thigmomorphogenetic response resulting from artificial mechanical perturbations (Biddington, 1986; Jaffe and Forbes, 1993; Gardiner et al., 2016), although wind exerts perturbations through fluid (air) to solid (plant) interaction. Based on these similarities various types of mechanical perturbations have been applied to plants in many studies to mimic the effects of wind (e.g. Niklas, 1998; Paul-Victor and Rowe, 2011; Niez et al., 2019).

However, the results of factorial experiments suggest that wind and mechanical perturbations can have significantly different effects on the same plants when applied separately. Smith and Ennos (2003) showed that while exposure of sunflowers (*Helianthus annuus* L.) to airflow resulted in taller plants with less rigid stems, mechanical flexure had opposite effects. Similarly, the effects of wind and brushing on *Plantago major* L. were shown to be opposite in terms of the morphology of petioles and laminae (Anten et al., 2010). Consequently, as concluded by Anten et al. (2010) it is not always correct to extrapolate the effects of mechanical perturbations to the effects of wind.

In our recent study (Zhdanov et al., 2021), we demonstrated that the response of the widely used model plant *Arabidopsis* to a constant unidirectional wind is significantly different compared to those reported as a result of brushing (Paul-Victor and Rowe, 2011) in terms of changes in plant morphology, mechanical properties, and anatomical tissue composition of its primary inflorescence stem. Moreover, *Arabidopsis* exhibits a positive anemotropic response to this type of treatment. A possible source of these discrepancies could be the difference in the direction of the applied stress, i.e. the wind treatment in Zhdanov et al. (2021) was unidirectional, while Paul-Victor and Rowe (2011) applied bidirectional brushing.

Based on these observations, it can be hypothesised that a careful design of the brushing experiment, especially in terms of the direction of applied perturbations, could allow for a closer mimicking of a unidirectional wind treatment and hence the observed response of *Arabidopsis*, including a positive tropic response, will be similar. The aim of the present study is to investigate the possibility to mimic the effects of a constant unidirectional wind through mechanical perturbations. To address this question, *Arabidopsis* ecotype Col-0 was subjected to two types of vectorial brushing treatment, namely bidirectional and unidirectional, in separate experiments. In

addition, two different brushing materials were applied in each experiment to investigate possible differences in the plant response. The use of two brushing materials is motivated by the variety of materials that have been used in brushing experiments, e.g. paper (Wang et al., 2009), cardboard (Latimer, 1990), wooden bar (Keller and Steffen, 1995), duster (Anten et al., 2010), polythene (Paul-Victor and Rowe, 2011), which have different surface textures and thus could result in different effects on plants. The tropic response and thigmomorphogenetic changes to *Arabidopsis* morphology, mechanical properties, and anatomical tissue composition of the primary inflorescence stem were assessed and compared between and within the experiments.

7.2 Materials and methods

7.2.1 Plants

Seeds of *Arabidopsis* (ecotype Columbia-0) were sown in a single pot and kept at 4 °C for 48 hours. The pot was then placed in the growth chamber with a long-day cycle (16 hours of light and 8 hours of darkness), temperature at 22 °C, light intensity at 150 $\mu\text{mol m}^{-2} \text{s}^{-1}$, and humidity at 60%. After approximately 1 week, the seedlings were transplanted into individual pots (pot diameter = 76 mm) and moved into the growth room where the experiments were conducted. The conditions in the growth room were as follows: long-day cycle, temperature at 19 °C, light intensity at 150 $\mu\text{mol m}^{-2} \text{s}^{-1}$. After approximately 20 to 25 days, when the flower bearing stem started to develop, plants were randomly separated into three groups. Two groups (20 plants each) were subjected to mechanical perturbations (experimental groups 1 and 2) by two different brushing materials. The third group (20 plants) was grown on the same shelf in the growth room under the same conditions but without any perturbations (control group). The same growth procedure was used in both conducted experiments.

7.2.2 Mechanical perturbations

Mechanical perturbations in the form of brushing were performed by a bespoke brushing machine (Figure 7.1). The machine has two belt-driven linear actuators which enable movements along horizontal and vertical axes (Figure 7.1A). The actuators are controlled by individual step motors with controllers allowing for separate and fully automated operation based on a preset programme. A beam mounted on the belt-driven gantry of the vertical axis is used for attaching the brushing material

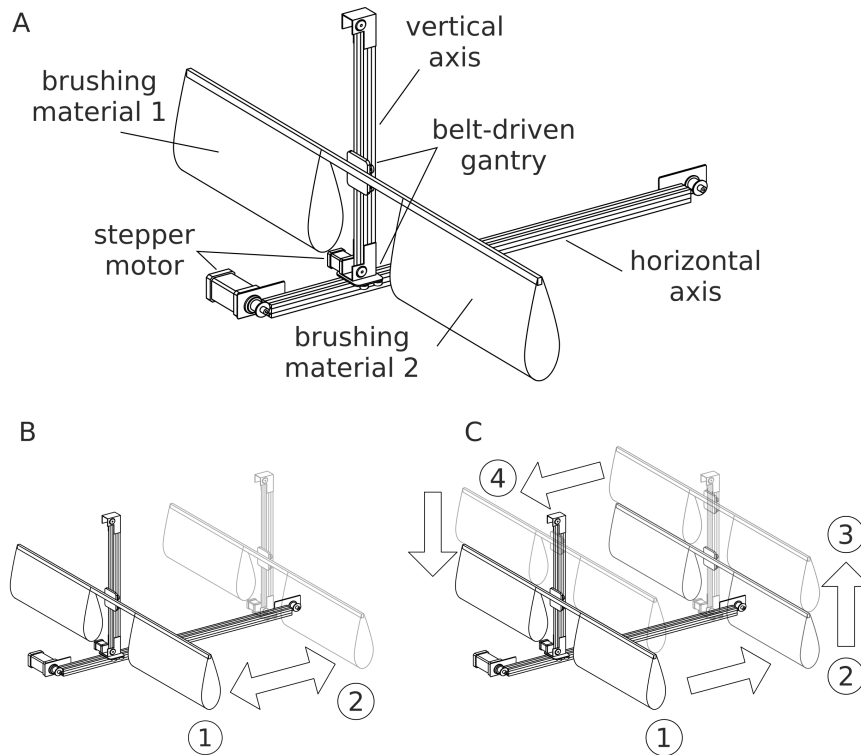


Figure 7.1: Brushing machine and its operational modes used in the present study. (A) Schematic diagram of the brushing machine and its components. (B) Bidirectional brushing mode: the plants are brushed in both directions by moving brushing material back and forth (from position 1 to position 2). (C) Unidirectional brushing mode: the plants are brushed in a single direction by moving the brushing material from position 1 to position 2. Upon reaching the end of the horizontal axis (position 2), the brushing materials is lifted to position 3, moved back to the beginning of the axis (position 4) and returned to the initial position 1. The plants are placed under the brushing material on both sides of the brushing machine. The position of the beam with brushing material is adjusted in the vertical direction as the plants grow.

for the experiments. The beam extends on both sides of the machine and thus allows to use two different materials within a single experiment.

In the present study two sets of brushing experiments were carried out. In both cases, the experimental groups were placed on opposite sides of the machine along its horizontal axis and subjected to brushing by different materials for two weeks. Plants from the experimental group 1 were brushed with smooth plastic, while the second group was brushed by a textured jute fabric. The brushing elements were made by combining plastic sheets with jute fabric pieces of the same size and folding them with one or the other side up. This ensured they had the same mass, and the plants were brushed with equal force. Consequently, any morphological changes or alterations observed in the mechanical properties, were expected to be solely a result

of differences in the surface texture of the brushing material.

In the first experiment, plants were subjected to bidirectional brushing (Figure 7.1B). Every four hours the plants in both experimental groups were brushed 20 times (10 times in each direction). In the second experiment, unidirectional brushing was applied (Figure 7.1C): in this case plants were subjected to the same number and frequency of mechanical perturbations (20 brushes every 4 hours), but all brushes were made in one direction. In both modes, only the stems and not the rosettes were mechanically perturbed. The height of the beam with the brushing material was adjusted as plants grew so that the primary inflorescence stems were deflected by 45° to 65° from their vertical orientation during the brushing.

7.2.3 Phenotyping

Morphological changes in *Arabidopsis* phenotype as a result of mechanical perturbations were assessed at the end of each experiment. For each plant in the control and experimental groups the length of the primary inflorescence stem, number of stems (basal branches), and the number of branches were determined. The above-ground fresh biomass was assessed for 10 randomly chosen plants from each group. In addition, after oven drying at 70°C their dry biomass was also determined. For the other 10 plants from each group, the average diameters of their bottom and top parts were evaluated as part of their mechanical characterisation.

7.2.4 Mechanical characterisation

Mechanical characterisation of the primary inflorescence stems of perturbed and control plants was carried out using the dynamic forced vibration method (Zhdanov et al., 2020) for 10 plants from each group. Two segments of the primary inflorescence stem were characterised. The first segment, referred to as “bottom part of the stem”, was taken from the basal part of the stem. The second segment was taken from the apex part of the stem excluding the growth zone and is referred to as “top part of the stem”. The tests were conducted directly after the segment under consideration was cut from the stem using a razor blade and, if required, cleared from branches, fruits, flowers, and young floral buds. This eliminated the influence of turgor pressure reduction and dehydration on the determined mechanical properties. In addition, at the time of the tests none of the stems showed any sign of senescence that could also affect their mechanical properties.

The dynamic forced vibration method allows to determine multiple resonant frequencies (f_i) of the tested stem segment that are related to its mechanical properties through Euler-Bernoulli beam theory (Blevins, 1979):

$$f_i = \frac{\lambda_i^2}{2\pi L^2} \sqrt{\frac{EI}{m}}, \quad i = 1, 2, 3, \dots, n \quad (7.1)$$

where E is the Young's modulus of elasticity which characterises the ability of the material to resist elastic deformations, L is the length of the stem, I is the second moment of area, m is the mass per unit length, and λ_i is a dimensionless parameter that is obtained from the characteristic equation corresponding to the vibration mode and applied boundary conditions. The product of EI is known as bending rigidity and characterises the ability of the material to resist bending. In the present study, both E and EI were determined for each tested stem segment.

The cross-section of Arabidopsis was approximated as a circle (Turner and Somerville, 1997; Bichet et al., 2001), thus I was calculated as:

$$I = \frac{\pi}{64} D^4 \quad (7.2)$$

where D is the diameter of the tested stem segment that was determined as an average value over several measurements of the stem diameter at different locations along its length. The measurements were done post-hoc using ImageJ (Schneider et al., 2012) from the photographs of the tested stem segments taken after each test. The mass of the tested segments was also measured after each test using a precision balance to evaluate m , which is required to estimate the mechanical properties using equation 7.1.

7.2.5 Anatomical measurements

Anatomical tissue organisation was observed on the next day after mechanical characterisation for the same stem segments. Prior to this, the stem segments were stored in individual falcon tubes filled with distilled water at 4 °C. Manually sectioned transverse segments from the central parts of each stem segment were stained with 0.02% toluidine blue. Histochemical staining enabled visual differentiation between the structural tissues of the studied segments. The samples were observed on a Zeiss Stemi SV11 microscope and photographs were captured. The relative areas of the outer part (epidermis and cortex), middle part (lignified tissues coloured in blue), and innermost part (purple coloured pith) were measured from the images

using the ImageJ software.

7.2.6 Statistical analysis

All statistics of measured quantities are reported as mean \pm standard deviation of n observations. Due to the small sample sizes of different lengths and because some of the data did not follow the normal distribution a non-parametric Wilcoxon rank-sum test was applied for post-hoc statistical analysis. The tests were performed in Matlab (R2020a, MathWorks, USA) using the in-built ranksum function. A statistically significant difference was established at $P \leq 0.05$.

7.3 Results

Due to the availability of only one brushing machine two sets of experiments were conducted to explore the influence of vectorial brushing treatment on Arabidopsis. Although both experiments were conducted following the same procedure in the same growth room, the differences observed between some parameters are believed to be due to the natural variability. However, comparison of the parameters between different groups within a single experiment and comparison of the absolute effects between two brushing treatments led to valuable and reliable conclusions.

7.3.1 Arabidopsis morphology

Both bi- and unidirectional types of brushing treatment resulted in a statistically significant ($P < 0.0001$) inhibition of the primary inflorescence stem length (Figure 7.2A). The reduction of the stem length appears to be dependent on the applied type of brushing. Compared with the control group, plants subjected to the bidirectional brushing on average were shorter by 27%, while in the unidirectional brushing experiment the average reduction was only 16.5%. In contrast, no significant changes ($P > 0.05$) to the number of stems and branches were imposed by any type of the applied brushing treatment and values of these parameters were only slightly reduced in the experimental plants compared to the controls (Figure 7.2B and C).

In addition, mechanical perturbations in the form of brushing had only minor effects on the other measured morphological traits (Table 7.1). While the brushing treatment resulted in a reduction of the diameter of the bottom part of the stem, this reduction was marginal and, in most cases, not statistically significant ($P > 0.05$) compared to the control group, except for the experimental group 2 in the

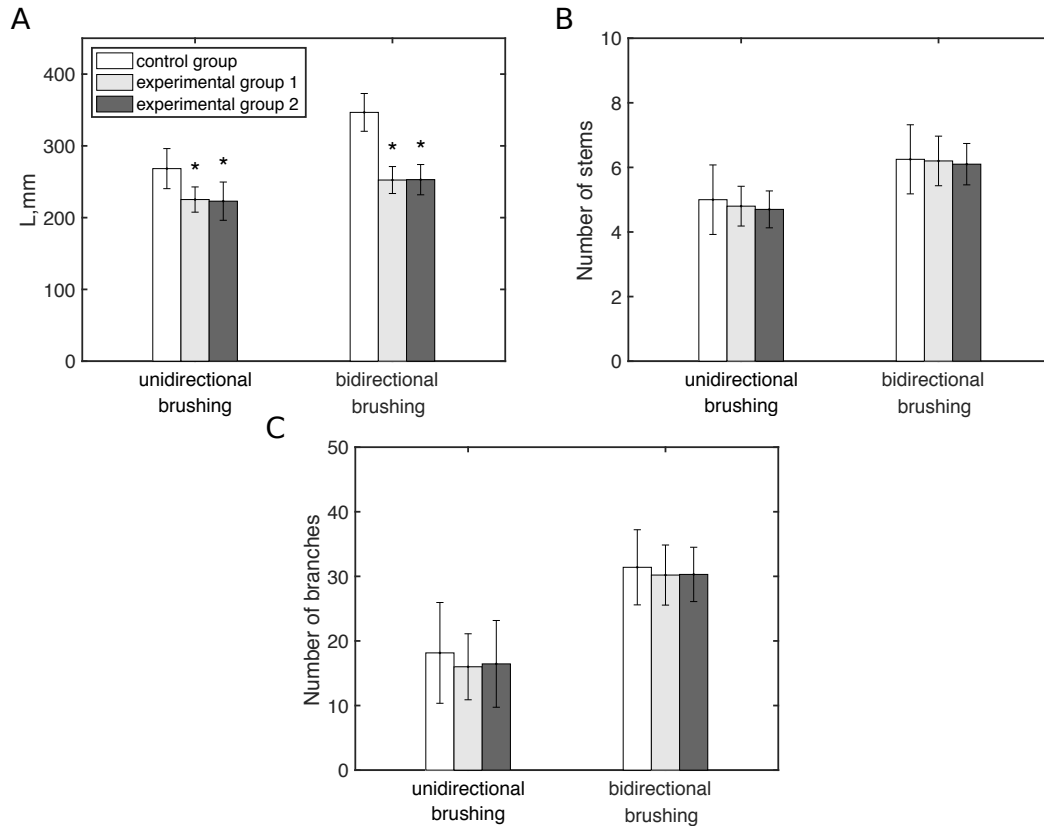


Figure 7.2: The effect of mechanical perturbations by different types of brushing treatment and brushing material on Arabidopsis morphology. (A) Primary inflorescence stem length. (B) Number of stems. (C) Number of branches. The legend in part (A) applies to all parts of this figure. Experimental group 1 was brushed with textured jute fabric while experimental group 2 with a smooth plastic in both experiments. Statistically significant differences ($P \leq 0.05$) were identified using the two-sided Wilcoxon rank sum test comparing medians of the corresponding parameters between groups. * marks statistically significant difference compared with the control group in the respective experiment.

unidirectional brushing experiment ($P=0.026$). Furthermore, no consistent effect of both types of brushing was observed for the top part of the stem and the diameters of these segments were similar in all groups. Mechanically perturbed plants also had slightly lower fresh and dry biomass compared to the plants from the control group in both conducted experiments. However, this reduction was not statistically significant ($P>0.05$).

No significant difference in the effects induced by different types of brushing material, namely textured jute fabric (experimental group 1) and smooth plastic (experimental group 2), was observed in both experiments. All recorded morphological parameters had similar values (see Figure 7.2 and Table 7.1) irrespective of

Table 7.1: The effect of mechanical perturbations by different types of brushing and brushing material on morphological and biomechanics parameters of Arabidopsis.

	Unidirectional brushing			Bidirectional brushing		
	control	experimental group 1	experimental group 2	control	experimental group 1	experimental group 2
	whole plant					
fresh biomass, g	6.04 ± 0.95	5.33 ± 0.35	5.74 ± 0.49	7.99 ± 1.17	7.22 ± 0.97	6.95 ± 1.27
dry biomass, g	0.55 ± 0.07	0.50 ± 0.05	0.52 ± 0.06	0.85 ± 0.21	0.71 ± 0.11	0.66 ± 0.15
	bottom part of the stem					
D, mm	1.20 ± 0.15	$1.04 \pm 0.10^*$	1.10 ± 0.09	1.86 ± 0.25	1.68 ± 0.26	1.71 ± 0.22
EI, N mm ²	117 ± 70	$49 \pm 18^*$	$60 \pm 17^*$	625 ± 281	$268 \pm 170^*$	$328 \pm 219^*$
	top part of the stem					
D, mm	1.01 ± 0.08	0.99 ± 0.10	1.06 ± 0.07	1.07 ± 0.06	1.09 ± 0.06	1.11 ± 0.08
EI, N mm ²	22 ± 6	21 ± 6	27 ± 8	31 ± 10	30 ± 8	32 ± 8

Experimental group 1 was brushed with textured jute fabric while experimental group 2 with smooth plastic in both experiments. Values are presented as mean \pm SD with n=10 for each case. Statistically significant differences ($P \leq 0.05$) were identified using the two-sided Wilcoxon rank sum test comparing medians of the corresponding parameters between groups.

* marks statistically significant difference compared with the control group in the respective experiment.

the used brushing material.

7.3.2 Mechanical properties of primary inflorescence stems

At the time of the mechanical characterisation, the primary inflorescence stems were upright and self-supporting. No signs of damage, inflicted by mechanical perturbations in the form of brushing, were observed in plants from the experimental groups in both conducted experiments. Unidirectional and bidirectional brushing treatments resulted in significant changes ($P < 0.05$) to the intensive (independent of the object's size), and extensive (proportional to the object's size), mechanical properties of the bottom part of the primary inflorescence stem. Compared to the control group, the unidirectional brushing decreased E of this part of the stem by approximately 20%, while a reduction of more than 30% was observed due to bidirectional brushing (Figure 7.3A). The EI of the bottom parts of the perturbed plants was approximately half of the values determined for the control group in both conducted experiments (Table 7.1).

In contrast, the Young's modulus of elasticity (Figure 7.3B) and bending rigidity (Table 7.1) of the top parts of the stems were not significantly ($P > 0.05$) affected by any type of the applied brushing treatments. In addition, no significant differences ($P > 0.05$) in the mechanical properties were found within a single experiment

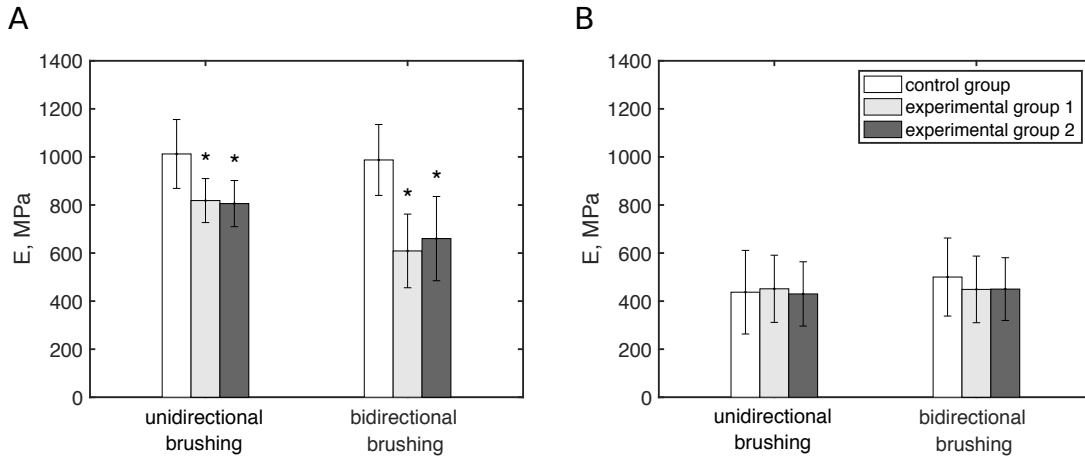


Figure 7.3: The effect of mechanical perturbations by different types of brushing treatment and brushing material on the intensive mechanical properties of Arabidopsis primary inflorescence stem. (A) Modulus of elasticity of the bottom part of the stem. (B) Modulus of elasticity of the top part of the stem. The legend in part (B) applies to both parts of this figure. Experimental group 1 was brushed with textured jute fabric while experimental group 2 with smooth plastic in both experiments. Statistically significant differences ($P \leq 0.05$) were identified using the two-sided Wilcoxon rank sum test comparing medians of the corresponding parameters between groups. * marks a statistically significant difference compared with the control group in the respective experiment.

between plants from experimental groups brushed with either smooth plastic or textured jute fabric. For both tested stem segments, the values of E and EI had similar values irrespective of the brushing material.

7.3.3 Anatomical tissue composition

Both types of vectorial brushing treatment resulted in significant changes to the anatomical tissue organisation of the bottom part of the primary inflorescence stem of Arabidopsis (Table 7.2). Brushed plants developed proportionally more cortex and epidermis compared to the control group. In addition, a reduction of the relative area of lignified tissues was observed in the plants from both experimental groups. In both cases the observed alterations are statistically significant ($P < 0.05$). However, the brushing treatment did not show significant effects on pith in this part of the stem.

Similar to the other aforementioned parameters that were recorded for the top part of the stem, anatomical tissue organisation was not affected either. All relative areas of the considered tissues had similar values in all groups (Table 7.2). Moreover,

Table 7.2: The effect of mechanical perturbations by different types of brushing and brushing material on the contribution of anatomical tissues to the total cross-sectional area of the the primary inflorescence stem of Arabidopsis.

	Unidirectional brushing			Bidirectional brushing		
	control	experimental group 1	experimental group 2	control	experimental group 1	experimental group 2
	bottom part of the stem					
Pith	37.06 \pm 4.01	36.66 \pm 3.24	37.54 \pm 2.12	44.78 \pm 1.84	47.78 \pm 1.09	46.61 \pm 2.94
Lignified tissues	28.52 \pm 4.19	23.91 \pm 2.20*	24.02 \pm 2.08*	28.44 \pm 1.88	22.04 \pm 2.70*	23.36 \pm 2.69*
Cortex & epidermis	34.42 \pm 4.20	39.43 \pm 3.45*	38.44 \pm 3.48*	26.78 \pm 2.23	30.18 \pm 2.64*	30.03 \pm 2.34*
	top part of the stem					
Pith	44.61 \pm 3.32	42.39 \pm 3.04	42.93 \pm 3.42	44.56 \pm 2.77	44.18 \pm 2.16	43.81 \pm 2.08
Lignified tissues	22.42 \pm 1.84	22.79 \pm 1.37	21.68 \pm 1.84	23.42 \pm 1.81	22.26 \pm 1.63	22.17 \pm 2.49
Cortex & epidermis	32.97 \pm 3.10	34.82 \pm 2.67	35.39 \pm 3.09	32.02 \pm 2.12	33.56 \pm 1.51	34.02 \pm 2.67

Experimental group 1 was brushed with textured jute fabric while experimental group 2 with a smooth plastic in both experiments. Values are presented as mean \pm SD with n=10 for each case. Statistically significant differences ($P \leq 0.05$) were identified using the two-sided Wilcoxon rank sum test comparing medians of the corresponding parameters between groups.

* marks statistically significant difference compared with the control group in the respective experiment.

no significant differences were found between tissue contributions due to different texture of the brushing material in both experiments.

7.4 Discussion

7.4.1 Morphological changes

The observed inhibition of the stem length due to different types of mechanical perturbations is consistent with the previously reported results for various herbaceous and woody plants, such as *Brachypodium distachyon* (Gladala-Kostarz et al., 2020), *Helianthus annuus* (Smith and Ennos, 2003), *Zea mays*, *Cucumis sativus* (Jaffe, 1973), *Pinus taeda* (Telewski and Jaffe, 1986b), *Abies fraseri* (Telewski and Jaffe, 1986a). Moreover, a reduction of the primary inflorescence stem length by approximately 50% was observed in an earlier study where Arabidopsis was subjected to a bidirectional brushing treatment (Paul-Victor and Rowe, 2011). On one hand, the decrease of the stem length in the present bidirectional brushing experiment is in line with these results, however, the inhibition relative to the control group is lower, namely 27%. This difference can be related to the higher total number of perturbations received by Arabidopsis plants in the study by Paul-Victor and Rowe (2011), where 80 additional brushes were made at the end of each day. In addition,

Paul-Victor and Rowe (2011) started the mechanical perturbation of *Arabidopsis* at an earlier developmental stage, i.e. at the leaf developmental stage, whereas in the present study, brushing treatment commenced from the inflorescence emergence stage, to be consistent with the previously conducted wind treatment experiments (Zhdanov et al., 2021). On the other hand, the inhibition of the stem length in the present unidirectional brushing experiment is found to be similar to the effects of exposure to constant unidirectional wind (Zhdanov et al., 2021) and periodic multidirectional wind (Bossdorf and Pigliucci, 2009) of 5 m/s, where stem length reductions of 14% and 13.2% were reported, respectively.

In contrast to many other plants, (see e.g. Biddington, 1986; Telewski and Jaffe, 1986a; Coutand et al., 2010), where increase in the stem radial growth is a common thigmomorphogenetic response to various types of mechanical stress including wind, both types of the applied brushing treatment decreased the diameter of the bottom part of the stem even though this effect was statistically insignificant in most cases. A statistically insignificant reduction of the stem radial growth was also reported for *Arabidopsis* in a result of bidirectional brushing (Paul-Victor and Rowe, 2011). However, no effect of the brushing treatment was found on the diameter of the top part of the stem in the present study. This can be attributed to the fact that during the brushing treatment the stem was bent in its bottom part, while the top part was subjected solely to brushing, i.e. brushing material was dragged along this part of the stem. Studies of wind effects on *Arabidopsis* also reported reduction in the radial growth of the bottom part of the stem (Bossdorf and Pigliucci, 2009; Zhdanov et al., 2021), but this effect was statistically significant. In addition, an insignificant decrease of the diameter of the top part of the stem was observed (Zhdanov et al., 2021).

No alterations to the number of stems and branches were observed by any type of applied brushing treatment. These parameters were not reported in Paul-Victor and Rowe (2011), but from the presented photographs, the number of branches in the experimental and control groups appears to be similar. However, at this developmental stage of the plants, the number of branches is quite low and for possible effects longer experiments would be required. In case of the constant unidirectional wind treatment (Zhdanov et al., 2021), a significant reduction in both of these parameters was observed, which was linked to the acclimation strategy of *Arabidopsis* to reduce experienced wind loadings through the reduction of its frontal area. In case of a brushing treatment, this does not apply and thus *Arabidopsis* would not benefit from reduction of the number of stems and branches.

Mechanical perturbations are also known to affect the aboveground biomass due to its reallocation to the below ground part of the plant (Kern et al., 2005; Coutand et al., 2008). The significant decrease in *Arabidopsis* aboveground biomass has also been reported in the literature as a result of wind treatment (Bossdorf and Pigliucci, 2009; Zhdanov et al., 2021). However, the none of the applied types of brushing treatment resulted in significant effect on the biomass in the present study, with only slight reduction observed in all experimental groups. There are several factors that can explain these observations. First, as mentioned above, the brushing treatment was applied when the primary inflorescence stem started to emerge. At this developmental stage the significant part of the rosette has already been formed (Boyes et al., 2001). Second, the rosettes were not affected by the brushing treatment, since with the present configuration of the brushing material this could result in the irreversible damage to the primary inflorescence stems. Finally, brushing had no significant effect on the number of stems and branches and the diameter of the primary inflorescence stem, hence the rest of the aboveground biomass, apart from rosette, was affected only slightly. However, based on the photographs of *Arabidopsis* after brushing treatment in (Paul-Victor and Rowe, 2011), it can be presumed that application of mechanical perturbations at an earlier developmental stage might result in the significant decrease of the aboveground biomass. Furthermore, a different configuration of brushing materials, which would allow to brush rosette together with the stem could result in the changes to this parameter.

Overall, brushing of *Arabidopsis* can reproduce effects of wind on the length of the primary inflorescence stem and partially on the alterations to the stem radial growth and plant biomass. Furthermore, match in the wind and brushing directions gives closer match in the inhibition of the primary inflorescence stem. However, the brushing treatment does not mimic wind-induced changes to the number of stems and branches.

7.4.2 Changes to mechanical properties and anatomical tissue organisation

The observed reduction in the bending rigidity and Young's modulus of elasticity of the stem are consistent with the previous findings in plants subjected to mechanical stress, e.g. Telewski and Jaffe (1986b), and Anten et al. (2010). However, it should be noted that changes to the mechanical properties are plant specific and also vary between different genotypes of the same plants (see e.g. Pruyn et al. 2000). Conse-

quently, it is more informative to compare changes in the mechanical properties to those reported for Arabidopsis Col-0.

The decrease in bending rigidity and Young's modulus of elasticity was reported for this Arabidopsis ecotype in the result of the bidirectional brushing experiment by Paul-Victor and Rowe (2011), however, the decrease in the mechanical properties observed in the present study is lower. Paul-Victor and Rowe (2011) attributed the reduction in the mechanical properties to the inhibition of the net development due to perturbations in the form of brushing. The evidence for this can be found in the present results by comparing values of the elastic modulus between the present experiments and those reported in Paul-Victor and Rowe (2011): while the values are similar for the bottom part of the stem in the control groups in both studies, the value of E in the experimental group of Paul-Victor and Rowe (2011) is similar to those for the top part in the present study. Thus, it can be suggested that reduction in the E and EI in the bottom part of the stem is a result of bending due to the brushing treatment and not due to differences in the developmental stages. This also provides an explanation for the negligible effect of the brushing treatment on the top part of the stem, which was subjected to brushing rather than bending.

In contrast, a constant unidirectional wind treatment resulted in the increase of the elastic modulus (Zhdanov et al., 2021). This change was attributed to the acclimation strategy of Arabidopsis in which more rigid plant material is beneficial for withstanding constant wind loadings from the same direction. The current results are in line with the study of Paul-Victor and Rowe (2011) and confirm that the acclimation strategy of Arabidopsis to brushing treatment is to produce shorter and more flexible stems with reduced modulus of elasticity. In the present study, the reduction in E in unidirectionally brushed plants was lower compared to bidirectionally brushed and may be related to the vectorial influence of perturbations, where in the second case bending of the stem occurred in two directions compared to only a single direction in the first case.

The changes to mechanical properties are consistent with the modifications to the anatomical tissue organisation of the primary inflorescence stems of the perturbed plants. A decrease in the relative area of the lignified tissues, which are known to strengthen the cell walls and increase stiffness of Arabidopsis stems (see e.g. Huang et al., 2001), provides an explanation for the observed decrease in E and consequently EI in the bottom part of the stem. The significant reduction in the area of lignified tissues in brushed Arabidopsis together with an increase of cortex and epidermis were also reported by Paul-Victor and Rowe (2011). In contrast, no changes to the

area of pith were observed in the present study, while a decrease was found by Paul-Victor and Rowe (2011) due to mechanical perturbations. These observations can also be related to the difference in the developmental rate, since at the earlier growth stages *Arabidopsis* has less pith, whose relative area increases as the plant grows. Furthermore, as in the case of the mechanical properties no significant changes to the anatomical tissue organisation of the top part of the stem due to brushing were found.

Overall, both applied types of brushing treatment induce opposite effects on the modulus of elasticity and relative area of lignified tissues of the *Arabidopsis* stems compared to wind. Consequently, changes to these parameters cannot be directly extrapolated from experiments where the latter stress is mimicked by the former, at least in the case of constant unidirectional wind.

7.4.3 Tropic response

Depending on the direction of the brushing treatment, *Arabidopsis* exhibits a tropic response. While no tropic response was observed in the bidirectional brushing experiment (Figure 7.4A and C), unidirectional brushing evoked a positive tropic response in *Arabidopsis* (Figure 7.4 B and D), and young seedlings curved in the direction opposite to the direction of brushing. The observed positive thigmotropic response resembles the positive anemotropic response of *Arabidopsis* to a constant unidirectional wind treatment (Zhdanov et al., 2021), but without a windswept shape of the plant. Therefore, a careful selection of the type of brushing treatment allows to mimic the tropic response in *Arabidopsis* as in the case of exposure to unidirectional wind, although this response is thigmotropic rather than anemotropic.

In each brushing instance, the stems were deflected from their vertical orientation and returned back to the initial vertical position immediately after. As a result of this inclination, the position of the inflorescence stem with respect to the direction of gravity vector changes and could evoke a gravitropic response. It is widely known that *Arabidopsis* shoots exhibit negative gravitropism and reorient themselves back to a vertical position within a few hours after permanent inclination (see e.g. Morita, 2010). Moreover, gravitropic responses in plants can be evoked by temporary changes to their orientation. Caspar and Pickard (1989) and Kiss et al. (1989) estimated the minimum induction time, i.e. the time to evoke gravitropic curvature, for *Arabidopsis* roots to be 30s by extrapolating data obtained for different durations of gravitropic stimulation. Unfortunately, no measurements of this type have been performed

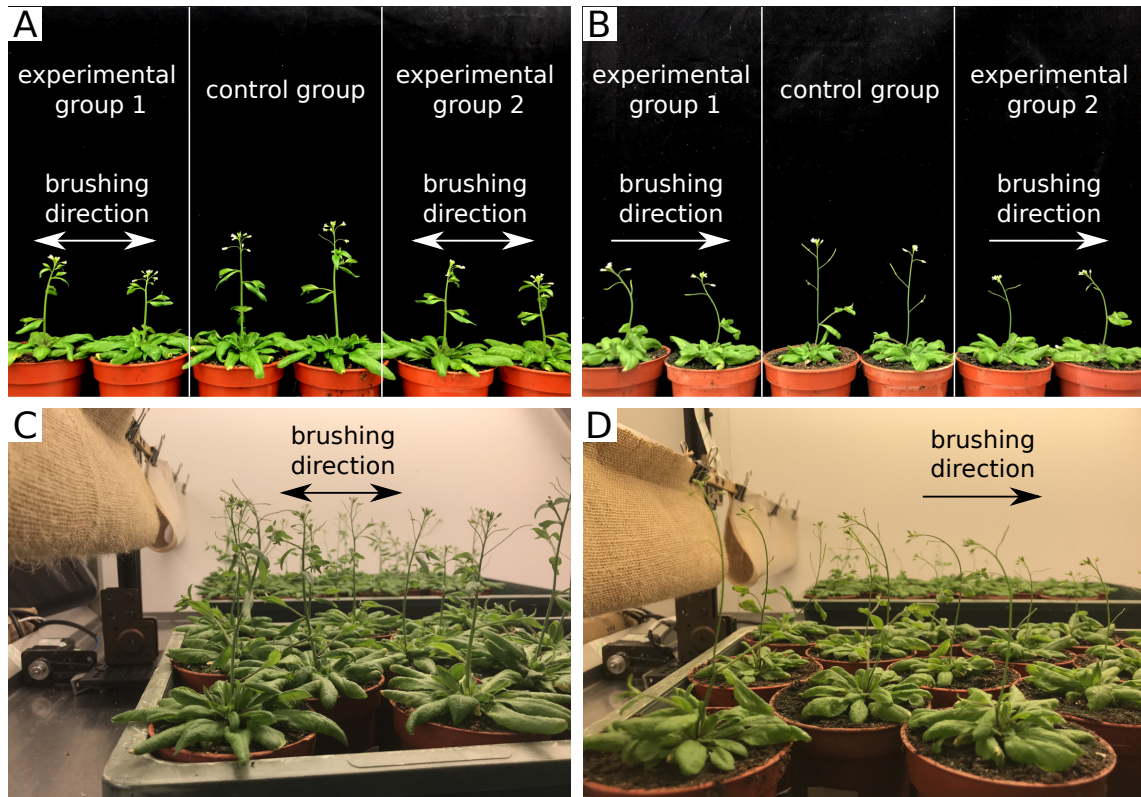


Figure 7.4: Depending on the direction of brushing treatment it is possible to evoke a tropic response in *Arabidopsis* similar to that observed as a result of constant unidirectional wind. (A and C) *Arabidopsis* does not exhibit any tropic response in the bidirectional brushing experiment. (B and D) *Arabidopsis* exhibits a positive tropic response in the unidirectional brushing experiment. Experimental group 1 was brushed with a smooth plastic while a textured jute fabric was used as brushing material for experimental group 2 in both experiments. The photos were taken on the fourth day after the start of the brushing treatment.

for *Arabidopsis* inflorescence stems. In the present experiments, the gravitropic stimulation due to brushing was intermittent with the duration in the order of 1s and it is highly unlikely to result in such curvature of the stem as observed in Figure 7.4. In addition, experiments exploring the dose response of plants to gravitropic stimulation usually involve clinorotation to minimise the influence of gravity after stimulation and to isolate the evoked gravitropic response (Perbal et al., 1997), while in the present study after the end of brushing cycle the plants continued to grow in the vertical positions under constant gravity. Thus, the observed directional growth response of *Arabidopsis* inflorescence stems as a result of unidirectional brushing treatment is considered to be thigmotropic, i.e. due to contact between the brushing material and plant stem.

A thigmotropic response is known to occur in *Arabidopsis* roots (see Massa and Gilroy, 2003), but to the best of our knowledge it has not been reported for its shoots. However, thigmotropic responses were recorded in the aboveground parts of various other plants, e.g. the common bean (*Phaseolus vulgaris* L. (Huberman and Jaffe, 1986), and cucumbers (*Cucumis sativus* L.) (Takahashi and Jaffe, 1990). For the reviews of thigmotropic responses in plants see Jaffe et al. (2002), Braam (2005), and Telewski (2012).

The uni- and bi-directional brushing treatments applied to *Arabidopsis* in the present study resemble those described in Huberman and Jaffe (1986) and Takahashi and Jaffe (1990) where plant parts were rubbed on one or both sides to evoke thigmotropic responses. The resemblance is particularly close for the top part of the stem, which was brushed, i.e. the brushing material was dragged along this part of the stem on one or both sides depending on the applied type of treatment, without bending, which occurred in the bottom part of the stem. In case of symmetric stem rubbing on both sides no thigmotropic response was observed in Takahashi and Jaffe (1990). This observation is similar to the absence of a thigmotropic response in *Arabidopsis* subjected to bidirectional brushing treatment in the present study. These similarities provide additional evidence that the observed response is thigmotropic. The presence of a thigmotropic response in *Arabidopsis* gives the possibility to conduct studies focussed on the mechanosensing and thigmotropic response mechanism, since a wide selection of *Arabidopsis* mutant lines are readily available. In addition, experiments with nonphototropic (nph) (Liscum and Briggs, 1995) and shoot gravitropic (sgr) (Fukaki et al., 1996b) mutants could be conducted to investigate the interaction between different tropic responses in *Arabidopsis* shoots and how these responses affect thigmotropism.

7.5 Conclusions

Artificial vectorial mechanical perturbations in the form of uni- and bidirectional brushing were applied to *Arabidopsis* to investigate the possibility to mimic influence of the unidirectional wind. The results suggest that some of the changes to morphological parameters and mechanical properties can be reproduced (inhibition of the primary inflorescence stem length, decrease of bending rigidity) or partially reproduced (decrease of stem diameter and biomass) through both types of brushing applied in this study. In contrast, the changes in the modulus of elasticity and relative area of lignified tissues were found to exhibit opposite trends compared to

the unidirectional wind treatment. Furthermore, the magnitude of the decrease of E is dependent on the brushing direction, but not on the surface texture of the brushing material. However, all these changes affect only the bottom part of the stem, which is bent during the brushing, while no significant difference between the recorded morphological and biomechanical parameters were found in the top part of the stem, which was brushed but not bent. Branching of Arabidopsis was not affected by the vectorial type of brushing treatment confirming that reduction in number of branches is an acclimation response to wind which is not evoked by brushing. Arabidopsis exhibited a positive tropic response to unidirectional brushing, which to the best of our knowledge is reported for the first time for the Arabidopsis shoot. This response resembles the anemotropic response to constant unidirectional wind but is considered thigmotropic since it is a result of brushing that involves solid to solid contact.

Overall, brushing treatments can be employed to mimic some aspects of wind influence on Arabidopsis. Moreover, a careful experimental design allows for a closer match between responses to these two types of stresses, including a positive tropic response. However, attention must be paid to the interpretation of the results of brushing experiments and their extrapolation to wind-induced effects.

Acknowledgements

This work was supported by the University of Glasgow's Lord Kelvin/Adam Smith (LKAS) PhD Scholarship. We would like to thank Amparo Ruiz-Prado for the help with growing plants and Liam Anderson for the help in the design and assembly of the brushing machine.

Part II

**Aerodynamics of
succulent-inspired cylinders**

Chapter 8

Introduction

This chapter provides a brief introduction to the second part of this thesis, which presents an investigation of the aerodynamics of succulent-inspired cylinders. The basic background on flow past bluff bodies is provided, since from the fluid mechanics point of view, these types of cylinders are considered bluff bodies.

Bluff bodies form part of many engineering applications, such as tall buildings, chimneys, heat exchangers, overhead lines, oil risers, wind turbine towers, to name a few. Many of the aforementioned examples can be approximated as slender cylinders with either a circular or a square cross section. These two types of cylinders are the most widespread representatives of bluff bodies and have received considerable attention in fluid dynamics research.

The flow past bluff bodies is a complex phenomenon that is characterised by flow separation, wake formation, vortex shedding, etc. (Williamson, 1996). In the circular cylinder case, the aerodynamic properties and the flow field are significantly dependent on the Reynolds number (Achenbach, 1971; Roshko, 1993). For $Re > 1,000$ four flow regimes are distinguished, namely subcritical, critical, supercritical, and post-critical (transcritical) (Roshko, 1961; Williamson, 1996) (see Figure 8.1). In the subcritical regime ($1 \times 10^3 < Re < 2 \times 10^5$) the drag coefficient has an almost constant value and a laminar boundary layer separates over the upstream part of the cylinder. With increasing of Reynolds number, a sharp reduction in the drag and absolute value of base pressure coefficients to their minimum values is observed. This phenomenon occurs in the critical flow regime ($2 \times 10^5 < Re < 5 \times 10^5$) and is associated with the shift of the separation point to the downstream side of the cylinder due to the presence of a separation-reattachment bubble. Further increase in Re leads to the transition to the supercritical regime ($5 \times 10^5 < Re < 2 \times 10^6$), where gradual recovery of the drag coefficient takes place together with slow decrease of

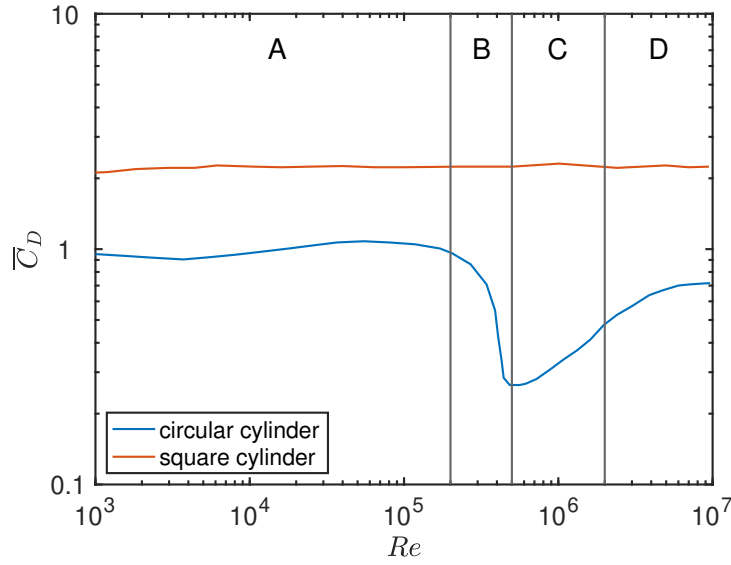


Figure 8.1: Reynolds number dependence of the mean drag coefficient of a circular cylinder and a square cylinder at $\alpha = 0^\circ$. The data is taken from Bai and Alam (2018). Flow regimes for the circular cylinder are marked: A - subcritical, B - critical, C - supercritical, and D - post-critical.

the base pressure coefficient. In addition, the separation point moves upstream and the transition of the boundary layer from laminar to turbulent occurs immediately after separation. In the post-critical regime $2 \times 10^6 < Re < 1 \times 10^7$, the drag coefficient again attains an almost constant value, which is lower than the value for the subcritical regime. The boundary layer on the cylinder surface becomes fully turbulent and separation points move further upstream.

In contrast to the circular cylinder, for a square cylinder the separation points are fixed at the leading edge corners. As a result, its aerodynamic characteristics are insensitive to Reynolds number variation for $Re > 1,000$ (Bai and Alam, 2018) (Figure 8.1). However, whereas a circular cylinder has an infinite number of lines of symmetry passing through its centre, a square cross-section has the symmetry of order eight. Thus, its rotation in the range from 0° to 45° with respect to the direction of free-stream will change the surrounding flow field and hence alter its aerodynamics properties, i.e. a strong angle of attack dependence is present for the square cylinder case. The general convention applied in most square cylinder studies is that $\alpha = 0^\circ$ when its side is normal to the flow, and $\alpha = 45^\circ$ when a corner is facing the flow.

Igarashi (1984) classified the flow past the square cylinder into four distinct regimes depending on the angle of attack (Figure 8.2). At zero angle of attack,

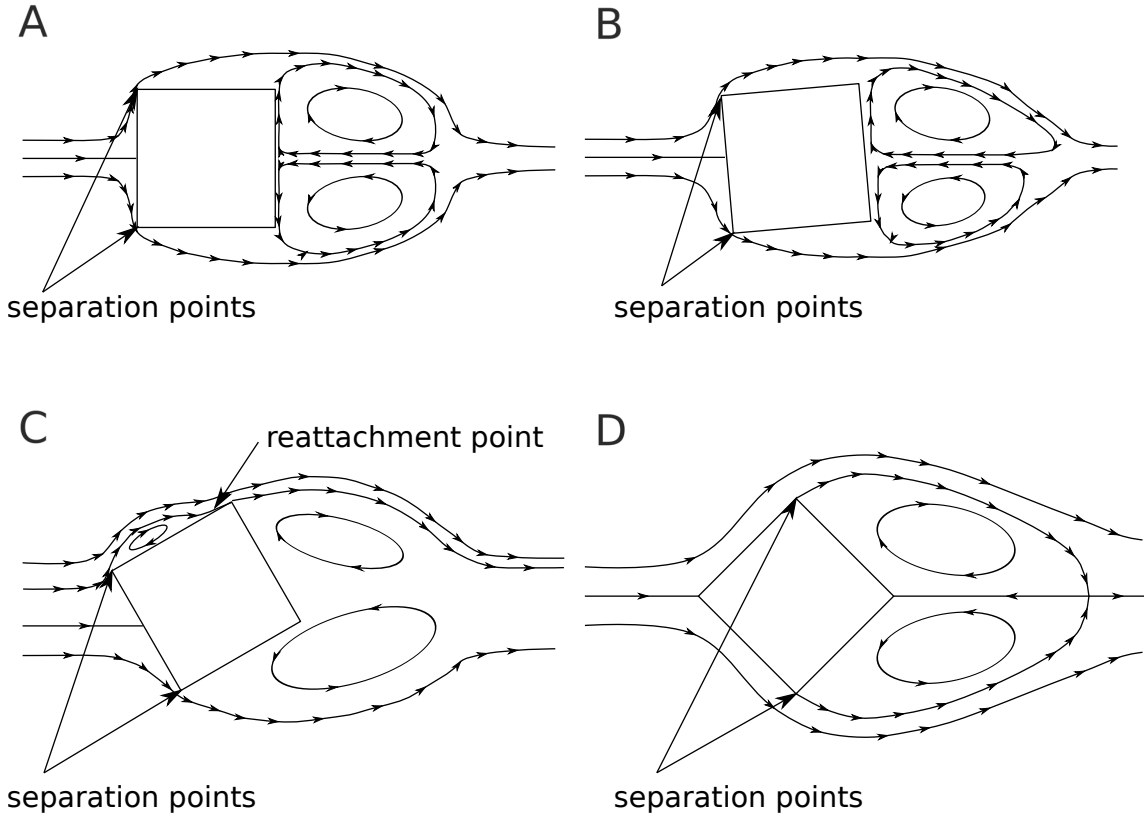


Figure 8.2: Schematics of the average flow patterns around a square cylinder at different angles of attack illustrating the classification by Igarashi (1984). (A) ‘Perfect separation type with symmetric flow’ ($0^\circ \leq \alpha \leq 5^\circ$). (B) ‘Perfect separation type with asymmetric flow’ ($5^\circ < \alpha < \alpha_{cr}$). (C) ‘Reattachment type’ ($\alpha_{cr} \leq \alpha < 35^\circ$). (D) ‘Wedge flow type’ ($35^\circ \leq \alpha \leq 45^\circ$). The critical angle of attack (α_{cr}) varies between 12° and 15° depending on experimental conditions.

the flow separates at both leading edge corners and the flow patterns around the square cylinder are symmetric. The same features are observed up to $\alpha = 5^\circ$ and the flow in this range is therefore classified as ‘perfect separation type with symmetric flow’ (Figure 8.2A). With further increase in α the flow symmetry is broken, but shear layer separation without reattachment is still observed. Hence, this regime is known as ‘perfect separation type with asymmetric flow’ (Figure 8.2B). These two flow regimes, which sometimes are considered together as one subcritical regime, are characterised by a reduction of the mean drag (C_D) and fluctuating lift (C'_L) coefficients and increase in Strouhal number and absolute value of the mean lift coefficient ($|C_L|$) with increasing α .

At the critical angle of attack (α_{cr}) the shear layer that separates from one of the leading edge corners starts to reattach to the wind exposed side of the square

cylinder (Lee, 1975). The exact value of α_{cr} is dependent on the test conditions, e.g. the level of free stream turbulence, and is usually reported to be in the range of 12° – 15° (Lee, 1975; Igarashi, 1984; Carassale et al., 2014). At α_{cr} the mean drag, and fluctuating lift coefficients of the square cylinder attain their minima, while the absolute mean lift coefficient reaches its maximum. In addition, the Strouhal number also reaches its highest peak, which together with the drop in C_D is associated with the reduction of the wake width due to the flow reattachment (Lee, 1975). Due to the reattachment phenomenon, the flow is classified as ‘reattachment type’ (Figure 8.2C) at angles of attack beyond critical and up to 35° . In this regime, the reattachment point on the cylinder side moves upstream with increasing α . In angle of attack range from 35° to 45° the flow patterns resemble those around a triangular cylinder, hence this regime has been named ‘wedge flow type’ (Figure 8.2D). In the supercritical regimes, an increase in the mean drag coefficient is observed while St attains almost constant value after initial reduction. On the other hand, the mean value of C_L decreases to nearly zero at approximately 30° . With a further increase in α , small but finite values of lift of opposite sign to those generated in the subcritical regime are observed, followed by a drop to zero at $\alpha = 45^\circ$. The fluctuating lift coefficient initially demonstrates a small recovery from its minimum but attains an almost constant value at $\alpha > 20^\circ$.

Many studies on circular and square cylinders explore flow control mechanisms to reduce the aerodynamic forces (e.g. Bearman and Harvey, 1993; Igarashi, 1997; Owen et al., 2001; Tsutsui and Igarashi, 2002). For example, biomimetic modifications to the circular cylinder, based on the Saguaro cactus, showed that the presence of ribs on the cylinder surface decreases the mean drag and the amplitude of the lift force fluctuations (Talley et al., 2001; Talley and Mungal, 2002).

In the second part of the thesis, the aerodynamic properties of succulent-inspired cylinders are explored using numerical and experimental methods. Compared to the Saguaro cactus, which has up to 30 ribs, tall arborescent succulents have a similar plant structure but with a considerably lower number of ribs. In chapter 9 two succulent-inspired cylinders with three and four ribs, respectively, are studied using 2D URANS simulations. This chapter gives as part of its introduction an overview of the literature on cactus-inspired cylinder modifications. In the following chapter 10, the same four-ribbed cylinder, which represents a modified square cylinder, is investigated using wind tunnel experiments. In the introductory section of this chapter the most common modifications to the square cylinder are reviewed.

Chapter 9

Angle of attack dependence of flow past cactus-inspired cylinders with a low number of ribs

This chapter is based on the following publication:

Zhdanov, O. and Busse, A., 2019. Angle of attack dependence of flow past cactus-inspired cylinders with a low number of ribs. *European Journal of Mechanics-B/Fluids*, **75**, pp.244-257.

DOI: 10.1016j.euromechflu.2018.09.008

Abstract The aerodynamic coefficients and the Strouhal number of cylinders with three and four ribs, inspired by succulents *Euphorbia trigona* and *Euphorbia Abyssinica* are investigated using 2D Unsteady Reynolds-Averaged Navier-Stokes simulations at Reynolds number 20,000. Both configurations show a significant dependence of the studied characteristics on the angle of attack. The obtained results are compared to the smooth circular cylinder, previous results for cylinders with 24 ribs based on the Saguaro cactus, and cylinders with triangular and square cross-sections. Relative to the circular cylinder, the mean drag coefficient is lowered only for the four-rib case at high angles of attack. However, at some angular positions, the ability to reduce unsteady force fluctuations exceeds Saguaro-inspired cylinders. For both shapes studied, the Strouhal number at most angles of attack is lower compared to both the circular cylinder and cylinders with 24 ribs at the same Reynolds number. The minimum values of the aerodynamic coefficients for both configurations are related to the angular orientation. For the four-rib case a critical angle of $\alpha_{cr} \approx 40^\circ$ is observed, at which the mean drag coefficient and the fluctuating lift coefficient attain their minima. The mean lift coefficient reaches at this angle its maximum value before a sudden drop for higher angles of attack. Therefore, for cactus-shaped cylinders with four ribs high angles of attack give the optimum orientation relative to prevailing winds.

Keywords: Cactus-inspired cylinder, bluff bodies, aerodynamic coefficients, Strouhal number

9.1 Introduction

The shape and structural features of cacti have significant importance for their survival in the natural environment. For example, ribs and spines play a vital role in fog collection (Ju et al., 2012) and control of moisture evaporation from the surface of the plants. Moreover, ribs and cavities have another function, as they can help to decrease wind loads and to prevent wind damage and uprooting by modifying the flow field around the plant.

In terms of aerodynamics, cacti are classified as bluff-bodies that resemble cylinders with ribs. Research on flow past cylindrical type structures has wide engineering applications to buildings, structural elements, risers, cables, etc. A widely studied grooved cylinder shape, investigated first by Talley et al. (2001), is a biomimetic shape based on the cross-section of the Saguaro cactus. Originating from the deserts

of the South-West of the United States and the Mexican State of Sonora, these tall, tree-like and ribbed (10 to 30 ribs) plants have the ability to withstand high winds without being broken or uprooted, despite having only a shallow root system (Pierson and Turner, 1998).

Talley et al. (2001) and Talley and Mungal (2002) conducted numerical and experimental studies using Saguaro-like cylinders with 24 V-shaped ribs at Reynolds numbers of 20,000 up to 100,000. They found a reduction of the mean drag coefficient, lower lift and drag force fluctuations and an increase in the Strouhal number compared to the smooth cylinder.

Extensive experimental and numerical research by Liu and co-authors (Liu et al., 2011; Wang et al., 2014; Jie and Liu, 2016) on the 24 V-shaped grooves cactus cylinder configuration also confirmed the previous observations in terms of the ability of ribbed cylinders to damp fluctuations of longitudinal (up to 50%) and cross-flow unsteady forces at low (Liu et al., 2011) and high (Wang et al., 2014; Jie and Liu, 2016) Reynolds numbers. The visualisations by Liu et al. (2011) showed small recirculation flows within the cavities of the grooved cylinder, similar to those discovered previously by Babu and Mahesh (2008). The presence of these vortices was also demonstrated experimentally (Wang et al., 2014) and numerically (Jie and Liu, 2016) at a higher Reynolds number of 54,000.

Recent experiments by Letchford et al. (2016) on cactus-shaped cylinders placed in smooth and rough boundary layers at Reynolds numbers from 10,000 to 20,000 showed the reduction of the aerodynamic coefficients and an increase in the Strouhal number, which is consistent with the two-dimensional results by Talley et al. (2001). This indicates that the results from previous studies for the two-dimensional case also translate to three-dimensional structures. In addition, the dependence of the cactus orientation with respect to the flow direction was reported to show little variation.

The studies discussed above are all focused on the ‘classical’ ribbed cylinder configuration with 24 V-shaped grooves introduced by Talley et al. (2001). The effect of the number and the shape of grooves was first studied by Yamagishi and Oki (2004, 2005) for Reynolds numbers ranging from 10,000 to 400,000 using experiments and numerical simulations. Both cylinders with U- and V-shaped grooves yielded significant reduction in drag compared to the smooth cylinder, but drag reduction for cylinders with V-shaped grooves was found to be up to 15% higher than for cylinders with U-shaped grooves. The critical Reynolds number was found to decrease with increasing number of grooves.



Figure 9.1: *Euphorbia trigona*, a member of the Euphorbiaceae family, in Glasgow Botanic Gardens.

Zhou et al. (2015) experimentally determined aerodynamic properties of the cylinders with 16 rectangular grooves in the Reynolds number range from 7,400 to 18,000. As in the case of other groove shapes, significant drag reduction was found together with the property of the grooved cylinder to mitigate vortex shedding.

The lowest number of ribs investigated so far has been the configuration used by Abboud et al. (2011) and El-Makdah and Oweis (2013), a cylinder with eight U-shaped grooves. Visualisation of the flow (El-Makdah and Oweis, 2013) near the cactus surface showed the presence of counter-rotating vortices, similar to those discovered numerically by Babu and Mahesh (2008). The authors suggest that there may be significant dependence of the flow field on the angle of attack for cacti with a low number of ribs, but they give results only for an angle of attack of zero degrees.

As discussed above, most studies on the aerodynamic characteristics and flow around cacti have focussed on cactus-shaped cylinders with many grooves, a shape inspired by the Saguaro cactus. However, a number of cacti have only three or

four ribs, e.g., *Cereus*, *Trichocereus pachanoi*, and *Calymmanthium*. Moreover, a number of succulents from the Euphorbiaceae family (Figure 9.1) from the Eastern Hemisphere, which in the process of convergent evolution developed a similar plant structure, including ribs and spines, as members of the Cactaceae family in the Western Hemisphere (McGhee, 2011), have only a low number of ribs (e.g. *Euphorbia trigona*, *Euphorbia Abyssinica*). Considering similar wind conditions in their natural environment, succulents may have similar aerodynamic benefits from their shape as the Saguaro cactus.

The present study focusses on the flow past cylinders with a low number of ribs based on the succulents *Euphorbia trigona* and *Euphorbia Abyssinica* at the biologically relevant Reynolds number of about 20,000. The goal is to establish whether the shapes adopted by these succulents have similar aerodynamic features as the Saguaro cactus. Unlike the cactus-shaped cylinders with many ribs in most of previous studies, the aerodynamic characteristics of cacti with a low number of ribs should be strongly dependent on the angle of attack (El-Makdah and Oweis, 2013).

In the present work, the dependence of the aerodynamic coefficients and Strouhal number on the angle of attack is studied numerically. The investigated shapes, a three-rib and a four-rib cylinder, are described in Section 9.2, and the numerical methodology is discussed in Section 9.3. In Sections 9.4.1 – 9.4.3 the dependence of the aerodynamic coefficients and of the Strouhal number on the angle of attack are discussed for both investigated geometries. The influence of the projected frontal width is discussed in Section 9.4.4, where the force coefficients and the Strouhal number of the four-rib and three-rib cactus-shaped cylinders are also compared to results for square cylinders and triangular prisms. In Section 9.4.5 flow visualisations are employed to gain insight into the angle of attack dependence of the mean flow fields. In the last Section general conclusions are given.

9.2 Investigated geometries

Following the approach of previous work on cacti with many ribs (Talley et al., 2001; Talley and Mungal, 2002), we approximate the shape of *Euphorbia Trigona* (Figure 9.2a) and *Euphorbia Abyssinica* (Figure 9.2b) using two-dimensional configurations where the cross-section shape is described using simple geometrical relations (see Figure 9.3). The equivalent circle of diameter D was divided into three or four parts by an equilateral triangle or square depending on the configuration. At the intersection points with the circle, ribs with minimum thickness of $0.075D$ and tip radius

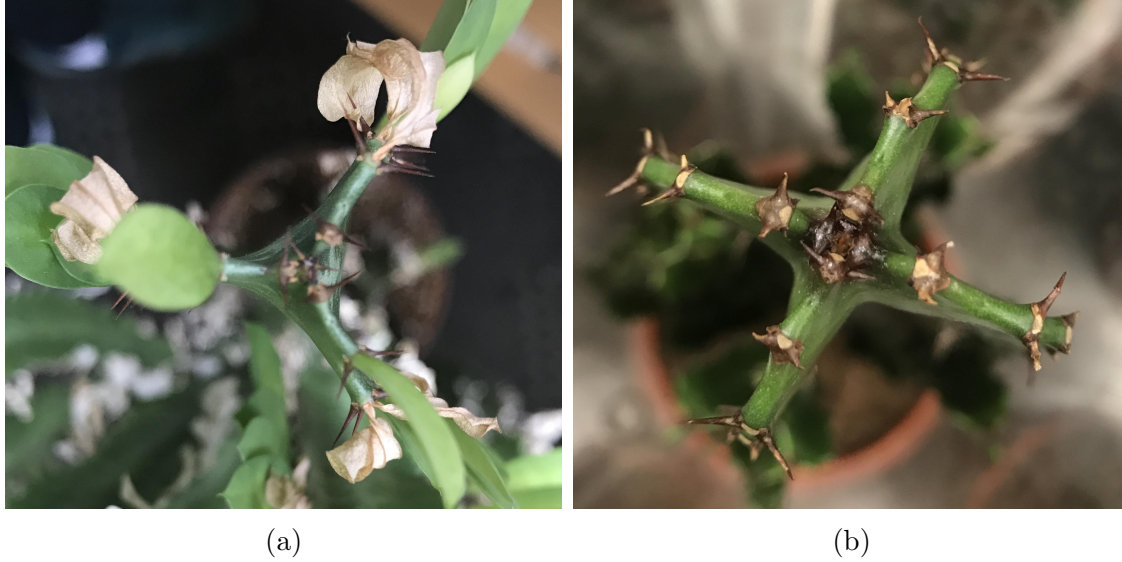


Figure 9.2: Succulents with low number of ribs: a - *Euphorbia trigona*, b - *Euphorbia Abyssinica*.

of half of the thickness were constructed. The grooves between ribs correspond to approximate representations of cross-sections of *Euphorbia Trigona* and *Euphorbia Abyssinica*. In the three-rib case the grooves are formed by conjugating ribs with the fillets of radius $0.65D$ while the four-rib case has fillets of $0.15D$ between neighbouring ribs. We will refer to these shapes as ‘cactus-shaped cylinders’ in the following, even though *Euphorbia trigona* and *Euphorbia Abyssinica* are not members of the Cactaceae family, i.e. they are succulents and not cacti in the botanical classification.

In the following, numerical simulations will be used to investigate the flow past the described three-rib and four-rib cylinders at a Reynolds number of 20,000. For example, for a succulent stem of diameter $D = 0.08$ m this would correspond to a wind speed of ≈ 4 m/s in dry air at 27°C . This velocity falls into the range of mean summer wind speed measured in the natural environment of succulents (Teboho et al., 2017).

9.3 Numerical method

As in the studies by Yamagishi and Oki (2004, 2005) and Talley et al. (2001) in the present study unsteady Reynolds-Averaged Navier-Stokes (URANS) simulations are used. The CFD solver Star-CCM+ v11.04 by Siemens PLM Software (Siemens, 2017) was employed. For the spatial discretisation a second order accurate finite volume discretisation with second order upwind scheme for the convective flux was

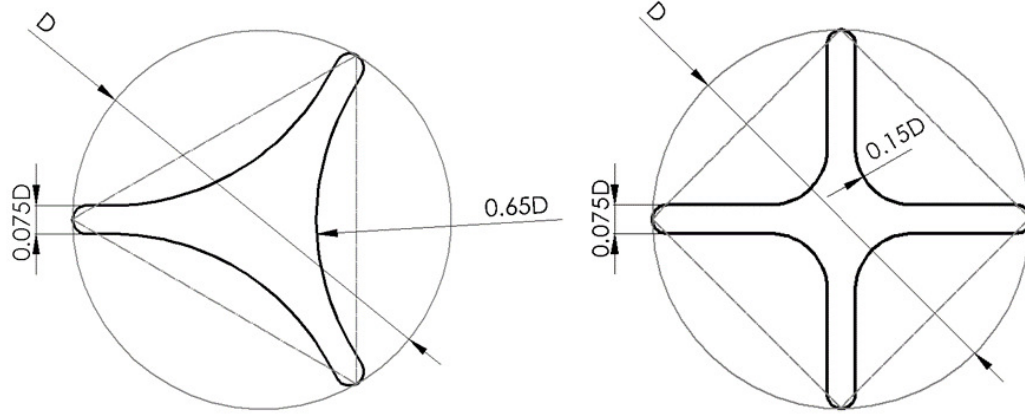


Figure 9.3: Geometrical representation of the tested cactus shapes. Left: three-rib configuration approximating *Euphorbia trigona*; right: four-rib configuration approximating *Euphorbia Abyssinica*.

used; a second order implicit scheme was selected for the discretisation in time. The Spalart-Allmaras turbulence model was used in combination with a low y^+ approach. This is known to give satisfactory results for the smooth cylinder case (Apaçoğlu and Aradağ, 2011).

The computational domain is shown in Figure 9.4. The size of the domain is $32.5D$ in the streamwise direction leaving $20D$ behind the cylinder. In the cross-stream direction, the computational domain has an extent of $25D$. Benim et al. (2008) found that blockage effects of a cylinder become negligible for $H/D > 6$, where H is half of the domain size in the cross-stream direction for Reynolds-Averaged Navier-Stokes (RANS) simulations. In this study $H/D = 12.5$, so blockage effects are expected to be very low. This was confirmed by a simulation with doubled domain size in streamwise and cross-stream direction for the smooth cylinder case ($H/D = 25$), which showed negligible influence of the domain size effect on the drag and lift coefficients (Table 9.1).

An unstructured mesh consisting of polyangular cells was used for the discretisation of the domain (see Figure 9.4). The use of polyangular cells allows the construction of meshes with low cell skewness (Siemens, 2017) for the cactus-shaped cylinder cases. The mesh was refined close to the cylinder and in the wake of the cylinder. Prismatic cells were placed on solid boundaries, i.e. on the surface of the cylinder, for improved resolution of the near wall flow (Figure 9.5). The prismatic layers were stretched with a geometric stretching factor of 1.11, yielding wall y^+ values < 1 at the solid boundaries and gradually increasing in size to match the size

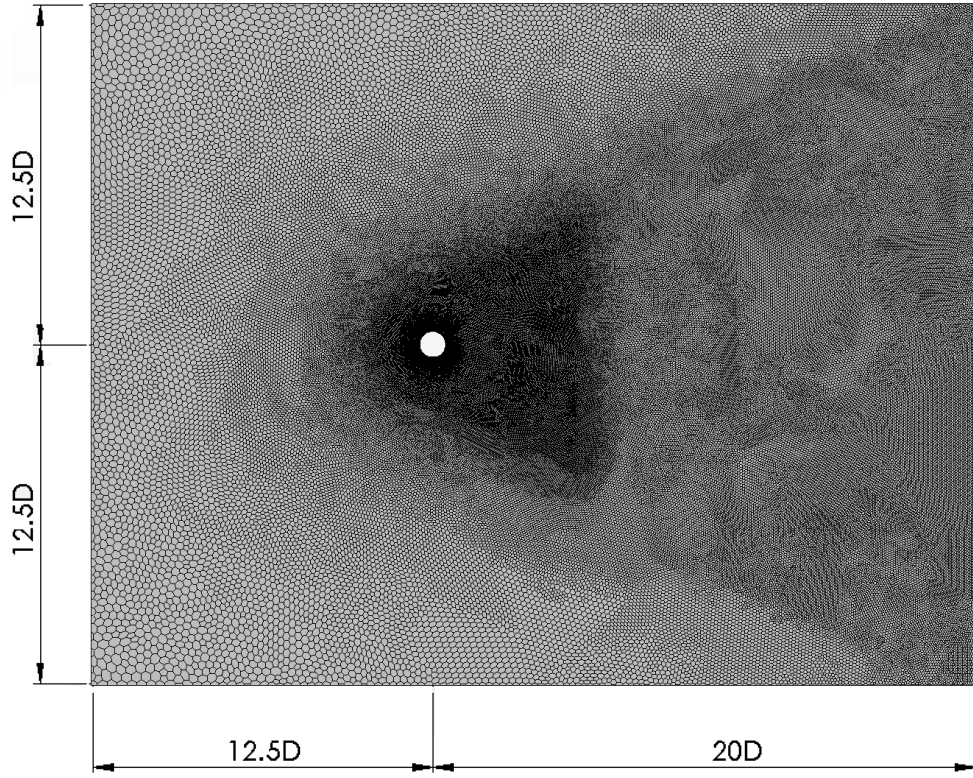


Figure 9.4: Computational domain with grid used for the simulations.

of the polyangular cells close to the cylinder. The typical number of cells used for the simulations is $\approx 110,000$ for the circular cylinder, $\approx 180,000$ for the three-rib cases, and $\approx 310,000$ for the four-rib cases.

The inlet was placed at the left side of the computational domain, and a uniform inlet velocity of U_∞ was applied at this boundary. Standard pressure outlet conditions were applied on the outlet of the domain. Symmetry boundary conditions were applied at the top and bottom boundaries of the computational domain.

The Reynolds number of the flow, based on free-stream velocity U_∞ and outer diameter D was set at 20,000. This, biologically relevant, Reynolds number has already been used in a number of studies related to the Saguaro cactus (Talley et al., 2001; Talley and Mungal, 2002; Letchford et al., 2016). A non-dimensional time step of $\Delta t U_\infty / D = 7.833 \times 10^{-3}$ was used for the numerical simulations. Results were extracted once the unsteady force coefficient fluctuations settled down to a quasi-stationary pattern and the amplitude of the oscillations had attained constant values.

The computational approach was validated using the standard smooth cylinder

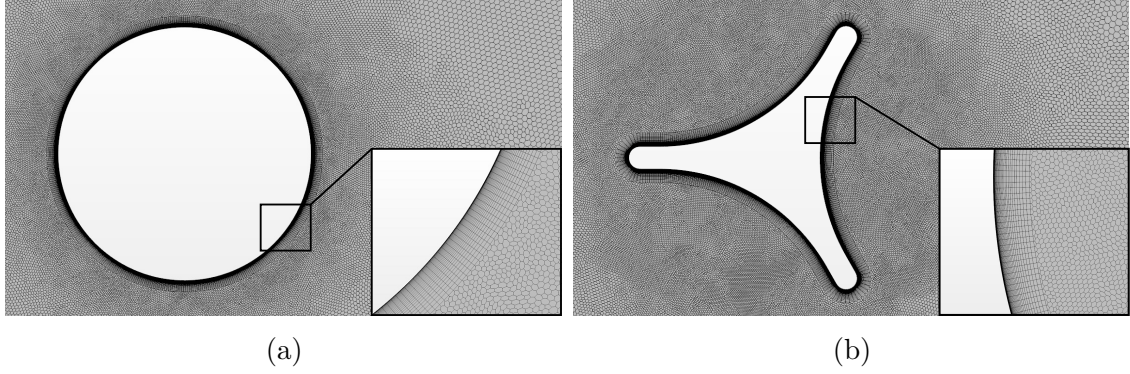


Figure 9.5: Mesh close to (a) circular cylinder and (b) three-rib cactus-shaped cylinder with enlarged prism layers.

due to the wealth of experimental and numerical data available for this case. The results for the mean drag coefficient C_d , rms lift coefficient C'_l , amplitude of the lift coefficient fluctuations C_l^{amp} , and Strouhal number St show overall good agreement with numerical and experimental studies (Table 9.1). All measured values are very close to the results of Apaçoğlu and Aradağ (2011) who used the same turbulence model. A comparison with the data by Talley et al. (2001), who used the $v^2 - f$ turbulence model, shows that the Spalart-Allmaras turbulence model gives overall a better match to experiments and LES. The determined magnitude of the drag coefficient is close to experimental studies conducted at the same Re (West and Apelt, 1993; Lim and Lee, 2002). The computed value of the rms lift coefficient is consistent with the LES results by Lysenko et al. (2014), but exceeds the experimental values of Norberg (2003) and West and Apelt (1993). However, even experimental results (Table 9.1) for these two parameters show a significant scatter. As discussed by West and Apelt (1993) and Lysenko et al. (2014) this is due to a number of factors such as cylinder surface roughness, blockage ratio, free stream turbulence, cylinder span, etc., which can affect experimental data.

9.4 Results and discussion

The investigated cactus-shaped cylinders have 3-fold rotational symmetry (three-rib configuration) or 4-fold rotational symmetry (four-rib configuration). Dependence of their flow properties on the angle of attack (α) (see Figure 9.6) was tested for the three-rib configuration in the range from 0° to 60° in 5° steps, while for the four-rib configuration the angle of attack was varied from 0° to 45° in 3.75° steps. In order to determine the angle of attack at which the drag force coefficient attains its minimum,

Table 9.1: Overview of the experimental and numerical values of the aerodynamic coefficients and Strouhal number for circular cylinder at $Re = 20,000$. Entries for the rms lift coefficient C'_l marked with * have been computed from the amplitude of the lift fluctuations C_l^{amp} assuming a sinusoidal signal.

	Method	C_l^{amp}	C'_l	C_d	St
Current simulation $H/D = 12.5$	URANS	1.12	0.80	1.17	0.228
Current simulation $H/D = 25$	URANS	1.12	0.79	1.15	0.225
Apaçoğlu and Aradağ (2011)	URANS	1.1	(0.78)*	1.17	0.22
Norberg (2003)	Experiment	-	0.47	-	0.194
Lysenko et al. (2014)	LES	-	0.61 – 0.75	1.30 – 1.39	0.17 – 0.20
West and Apelt (1993)	Experiment	-	0.49 – 0.68	1.14 – 1.4	0.195
Lim and Lee (2002)	Experiment	-	-	1.2	0.187
Talley et al. (2001)	URANS	1.923	(1.360)*	1.683 ± 0.164	0.217

additional simulations were performed with smaller steps in the corresponding angle of attack ranges. The $\alpha = 0^\circ$ configuration corresponds to the orientation where the rib at the windward side of the cactus is aligned with the direction of free-stream velocity. At 60° (three-rib configuration) and 45° (four-rib configuration) angle of attack the groove/cavity between ribs faces the free-stream flow. Due to the mirror symmetry of the studied configurations with respect to any rib axis, higher angles of attack ranging from 60° to 120° (three-rib configuration) or 45° to 90° (four-rib configuration) will give the same absolute values of the aerodynamic coefficients as the corresponding configuration at angle of attack $(120^\circ - \alpha)$ or $(90^\circ - \alpha)$, respectively. Therefore, in the following results will be shown as a function of $\alpha/\alpha_{\text{max}}$, where $\alpha_{\text{max}} = 60^\circ$ for the three-rib case and $\alpha_{\text{max}} = 45^\circ$ for the four-rib case.

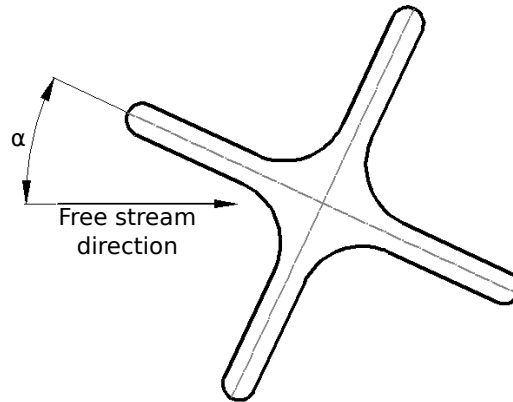


Figure 9.6: Angle of attack definition for the cactus-shaped cylinder.

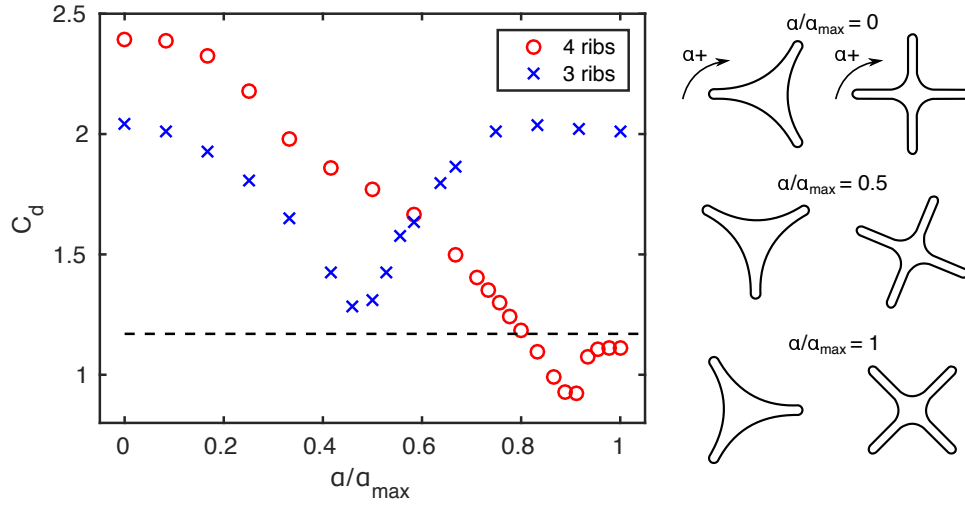


Figure 9.7: Mean drag coefficient versus angle of attack. The angle of attack has been normalised with the maximum angle of attack (three-rib case: $\alpha_{\max} = 60^\circ$, four-rib case: $\alpha_{\max} = 45^\circ$). The dashed line indicates the value for the smooth circular cylinder case.¹

The force coefficients were calculated during the simulations as

$$C_{d,l} = \frac{\overline{f_{x,y}}}{\frac{1}{2}\rho U_\infty^2 D} \quad (9.1)$$

$$C'_{d,l} = \frac{\sigma(f_{x,y})}{\frac{1}{2}\rho U_\infty^2 D}, \quad (9.2)$$

where $\overline{f_{x,y}}$ is the mean value of the force in the respective direction (x for the drag and y for the lift), $\sigma(f_{x,y})$ the root mean square deviation of $f_{x,y}$, and D the equivalent circle diameter. As expected, the aerodynamic coefficients and the Strouhal number exhibit a strong dependence on the angle of attack for both the three-rib and the four-rib configuration.

9.4.1 Drag coefficient

The dependence of the mean drag coefficient, C_d , on the angle of attack is shown in Figure 9.7. In both cases C_d shows strong variations with angle of attack. In the three-rib case, C_d attains its lowest values close to an intermediate angle of attack at $\alpha = 27.5^\circ$ ($\alpha/\alpha_{\max} \approx 0.46$) and its maximum values for 0° and 50° ($\alpha/\alpha_{\max} \approx 0.83$).

¹This figure has been modified for the thesis by adding schematics of angle of attack orientations of the studied cylinders.

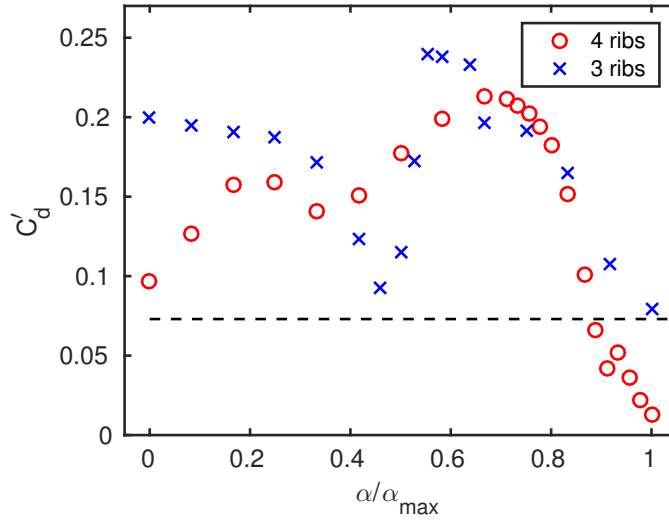


Figure 9.8: Rms drag coefficient versus angle of attack. The angle of attack has been normalised with the maximum angle of attack (three-rib case: $\alpha_{\max} = 60^\circ$, four-rib case: $\alpha_{\max} = 45^\circ$). The dashed line shows the value for the smooth cylinder case.

A difference of over 60% was found between the maximum and the minimum values of the drag coefficient. Compared to the smooth cylinder case, the C_d value is increased for all angles of attack for the three-rib configuration.

In contrast, the C_d values of the four-rib configuration are lower than the value for the smooth cylinder case at high angles of attack $\alpha > 36^\circ$ ($\alpha/\alpha_{\max} > 0.8$). As the angle of attack is decreased for this configuration, the value of C_d increases, and C_d attains its maximum value for $\alpha = 0$. The maximum value of C_d is more than double compared to the C_d value for the circular cylinder case and also exceeds the maximum values observed for the three-rib configuration.

Unlike in previous studies on cactus-shaped cylinders with many ribs (Talley et al., 2001; Yamagishi and Oki, 2004, 2005; Letchford et al., 2016) significant drag reduction compared to the circular cylinder was not observed in the present study. However, the four ribbed configuration showed between $\alpha = 36^\circ$ ($\alpha/\alpha_{\max} = 0.8$) and 45° ($\alpha/\alpha_{\max} = 1$) C_d values below the value for a smooth circular cylinder.

In order to assess the fluctuations in the streamwise force, root mean square (rms) values of the fluctuating part of the drag coefficient C_d' were determined for both cactus shapes (see Figure 9.8). Like the mean drag coefficient, C_d' shows significant variation as the angle of attack is changed. For both the three-rib and the four-rib configuration C_d' attains its minimum value at α_{\max} , i.e. for the orientation where

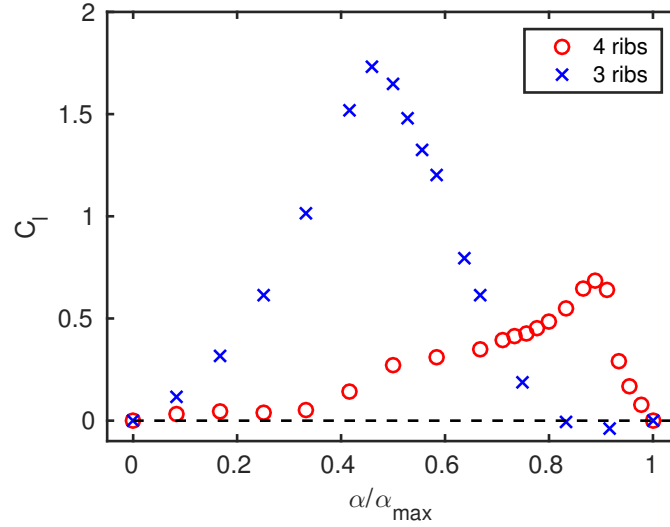


Figure 9.9: Mean lift coefficient versus angle of attack. The angle of attack has been normalised with the maximum angle of attack (three-rib case: $\alpha_{\max} = 60^\circ$, four-rib case: $\alpha_{\max} = 45^\circ$). The dashed line shows the value for the smooth cylinder case.

a cavity is centred at the windward side of the cactus. For the three-rib case the C_d' value at α_{\max} is close to the value for the smooth cylinder case. In contrast, a substantial reduction in C_d' compared to the smooth cylinder case is observed for the four-rib case at $\alpha > 39^\circ$ ($\alpha/\alpha_{\max} > 0.86$). At lower angles of attack, C_d' is significantly higher than in the smooth cylinder case for both the three-rib and the four-rib configuration, and no simple dependence on the angle of attack can be observed. Moreover, a sudden increase in C_d' is observed between $\alpha = 27.5^\circ$ ($\alpha/\alpha_{\max} \approx 0.46$) and $\alpha = 40^\circ$ ($\alpha/\alpha_{\max} \approx 0.66$) in the three-rib case. For cactus configurations with many ribs reduction in the unsteady drag forces was found by Talley et al. (2001), Letchford et al. (2016) for the same Reynolds number and by Babu and Mahesh (2008) for the laminar regime. In the current study, a significant reduction is observed only for the four-rib configuration at high angles of attack. Taking into account the behaviour of the C_d and C_d' it can be conjectured that stems of succulents and cacti may be orientated with respect to the prevailing winds in the natural environment in a way to minimise their wind loading as they grow.

9.4.2 Lift coefficient

Figure 9.9 shows the variation of the mean lift coefficient C_l with angle of attack. For angles of attack where symmetry with respect to the mean flow direction is given, a zero mean lift coefficient is found, as expected. Thus at zero and maximum angle

of attack the mean lift coefficient is zero. At all other angles of attack, symmetry with respect to the mean flow direction is not preserved, and we therefore expect non-zero values for the lift coefficient.

The change of the mean lift coefficient with the angle of attack in the three-rib case demonstrates an opposite trend to the mean drag coefficient for the same configuration. The maximum value of C_l is attained close to an intermediate angle of attack ($\alpha = 27.5^\circ$) ($\alpha/\alpha_{\max} \approx 0.46$), while minimum values occur for $\alpha = 0^\circ$ and α_{\max} . Compared to the drag coefficient, the lift coefficient shows a stronger variation with angle of attack for the three-rib configuration.

For the four-rib configuration, the maximum mean lift coefficient is attained for $\alpha = 40^\circ$ ($\alpha/\alpha_{\max} \approx 0.89$), but its value is still more than two times lower compared to the maximum value in the three-rib case. The maximum value of C_l is followed by a sudden drop. In general, the four-rib case demonstrates a lower dependence of C_l on the angle of attack.

Most previous studies on flow past cactus-shaped cylinders with many ribs did not report on angle of attack dependence (Talley et al., 2001; Yamagishi and Oki, 2004, 2005; Liu et al., 2011; Wang et al., 2014; Jie and Liu, 2016) or stated that the influence of the angular position is insignificant (Letchford et al., 2016). Oweis et al. (2011, 2013), who studied the flow around a cactus-shaped cylinder with eight ribs, pointed out that a change in the angular position will have an effect on the flow characteristics. However, they did not investigate the angle of attack dependence for their configuration.

In the current study, a decrease in angle of attack dependence was found when proceeding from a three-rib to a four-rib configuration. We expect that this trend will continue as the number of ribs of a cactus is increased, since with increasing number of ribs the range of possible different angular orientations decreases and the configuration approaches a more circular shape. Thus the angle of attack dependence of the mean lift coefficient should be lower but still noticeable for a cylinder with eight ribs compared to the current configurations, and attain negligible variation with angle of attack, i.e. approach $C_l = 0$, for the classical cactus configuration with 24 ribs.

The rms value of the fluctuating part of the lift coefficient, C'_l , is shown in Figure 9.10. For most angles of attack, the rms lift coefficient is reduced compared to the smooth cylinder. The cactus-shaped cylinders demonstrate opposite trends in C'_l behaviour with angle of attack for the three- and the four-rib configuration. For the three-rib configuration, C'_l increases with angle of attack, whereas the four-rib

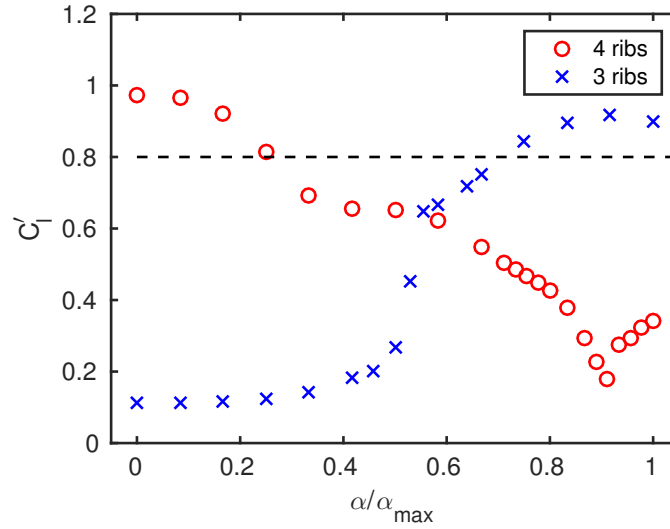


Figure 9.10: Rms lift coefficient versus angle of attack. The angle of attack has been normalised with the maximum angle of attack (three-rib case: $\alpha_{\max} = 60^\circ$, four-rib case: $\alpha_{\max} = 45^\circ$). The dashed line shows the value for the smooth cylinder case.

configuration shows a decrease of C_l' with increasing angle of attack up to $\alpha = 41^\circ$ ($\alpha/\alpha_{\max} \approx 0.91$) followed by slight increase towards α_{\max} . The lift force fluctuations are reduced by up to 85% compared to the smooth cylinder case in the range of angles of attack ranging from $\alpha = 0^\circ$ to $\alpha = 45^\circ$ ($\alpha/\alpha_{\max} = 0.75$) for the three-rib case. The four-rib configuration also shows reduction of the lift force fluctuations. This effect starts from $\alpha = 15^\circ$ ($\alpha/\alpha_{\max} \approx 0.33$) and increases with angle of attack reaching 77% reduction compared to the smooth cylinder case at $\alpha = 41^\circ$ ($\alpha/\alpha_{\max} \approx 0.91$). The results for C_l' are consistent with the observation that has been made for a cylinder with many ribs (Talley et al., 2001; Babu and Mahesh, 2008; Wang et al., 2014; Jie and Liu, 2016; Letchford et al., 2016) in terms of the ability of cactus-shaped cylinders to mitigate unsteady lift force fluctuations. The maximum decrease in C_l' observed in the current study is higher than in other works where the maximum reduction reported by Wang et al. (2014) and Jie and Liu (2016) was 50%.

Representative sections of the time histories of the lift force fluctuations are shown in Figure 9.11. As expected, a clear periodic behaviour can be observed in all cases. Some higher frequency content can be observed, which is stronger for the three-rib cylinder at low angle of attack. A similar observation has been made in the experiments by Nakagawa (1989), who showed that pressure fluctuations around a triangular prism have a more regular pattern at $\alpha = 60^\circ$ compared to $\alpha = 0^\circ$. This is consistent with the present results for the three-rib case. The angle of attack

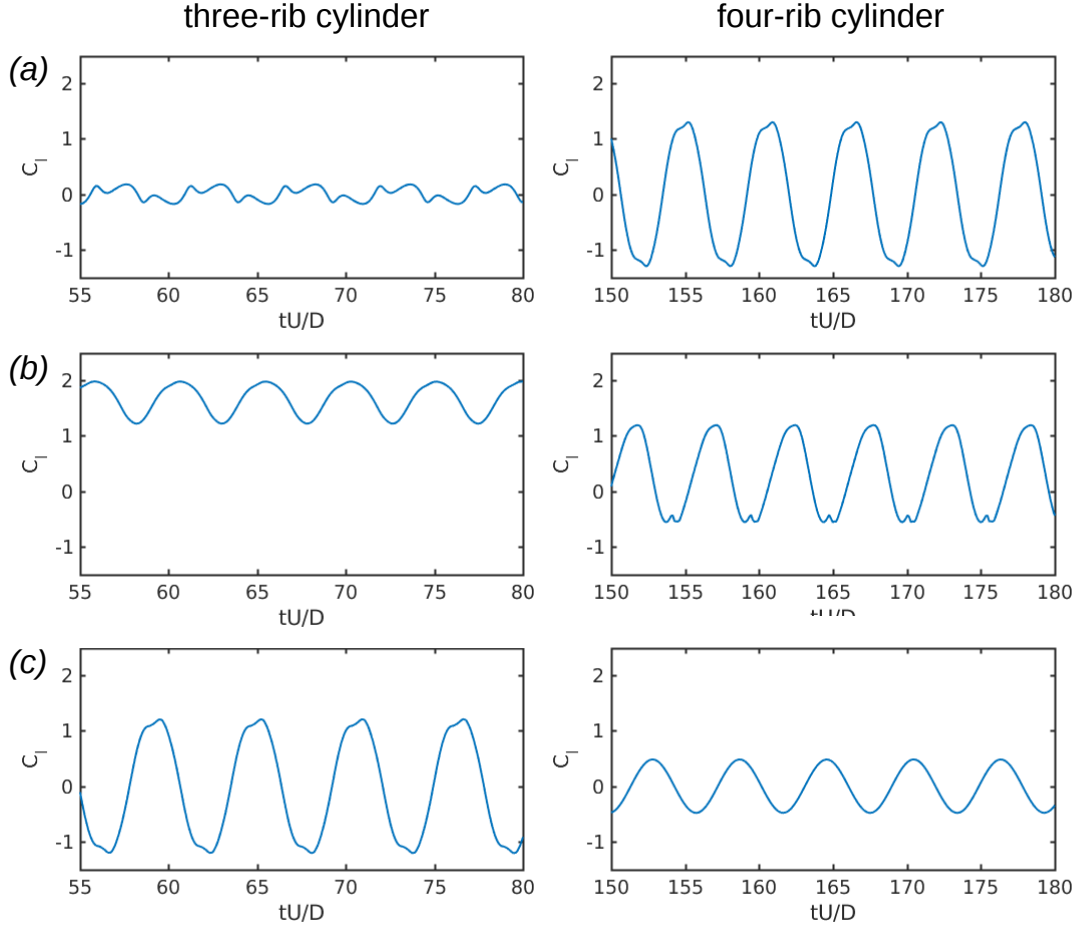


Figure 9.11: Time history of C_l for three- and four-rib cylinders at angles of attack normalised with maximum angle of attack: (a) - $\alpha/\alpha_{\max} = 0$, (b) - $\alpha/\alpha_{\max} = 0.5$, (c) - $\alpha/\alpha_{\max} = 1$.

dependency of the lift force coefficient support the conjecture that the plant can minimise the possibility of wind damage by orientating itself with the prevailing wind direction. This is discussed in more detail in section 9.4.5.

9.4.3 Strouhal number

The Strouhal number (Figure 9.12) was determined using Fast Fourier Transformation of the lift coefficient fluctuation as a function of time. Following the approach for the force coefficients calculation, the equivalent circle diameter was used as the characteristic length for St . Cactus-shaped cylinders of both configurations yield lower Strouhal numbers compared to the smooth cylinder over the whole range of angle of attack, except for the three-rib case between $\alpha = 20^\circ$ ($\alpha/\alpha_{\max} \approx 0.33$) and $\alpha \approx 27.5^\circ$ ($\alpha/\alpha_{\max} \approx 0.46$). In the four-rib case a maximum decrease of 25%

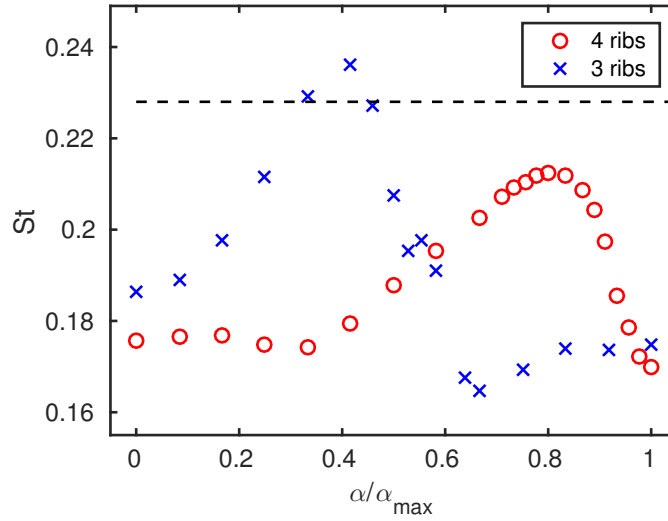


Figure 9.12: Strouhal number versus angle of attack. The angle of attack has been normalised with the maximum angle of attack (three-rib case: $\alpha_{\max} = 60^\circ$, four-rib case: $\alpha_{\max} = 45^\circ$). The dashed line shows the value for the smooth cylinder case.

in Strouhal number occurs at α_{\max} , while in the three-rib case the lowest value is observed at $\alpha = 40^\circ$ ($\alpha/\alpha_{\max} \approx 0.67$). At this angle of attack St is 28% lower compared to the circular cylinder. Babu and Mahesh (2008) observed a decrease in Strouhal number by 6.25% and 10.6% for flow past cylinders with many ribs in the laminar regime. However, it is difficult to relate their findings to the current results as the present study was performed in the turbulent flow regime and at a considerably higher Reynolds number. Previous experimental (Letchford et al., 2016) and numerical (Talley et al., 2001) results for the same Reynolds number (20,000), as used in this study, showed an increase of St for a classical ribbed cylinder compared to the smooth cylinder case.

9.4.4 Influence of the projected frontal width

Whereas for a smooth, circular cylinder the cylinder diameter is the obvious choice for the characteristic linear dimension in the computation of aerodynamic coefficients and Strouhal number, in the case of non-circular two-dimensional cross-sections there are several possible choices for the characteristic linear dimension. For example, in the context of square and equilateral triangular cylinders both the side of the square/triangle or its projected width are in wide use as characteristic linear dimension. The projected width of a non-circular object will change with angle of attack, and therefore the angle of attack dependence of its aerodynamic coefficients will be

influenced by the choice of the characteristic linear dimension.

In the following, the current results are revisited using the projected frontal width D^* instead of the equivalent circle diameter as characteristic linear dimension and then compared to the angle of attack dependence of the force coefficients of similar bluff bodies, i.e. square cylinders and equilateral triangular prisms. The projected frontal widths were based on the inscribed triangle and square (see Figure 9.3) used in their construction. This gives for the three-rib case

$$D^* = \frac{\sqrt{3}D}{2} \cos(|\alpha - 30^\circ| - 30^\circ), \quad (9.3)$$

and for the four-rib case

$$D^* = D \cos(\alpha). \quad (9.4)$$

Force-coefficients and Strouhal numbers that have been computed with the projected frontal width as a characteristic dimension are marked with asterisks, e.g., C_d^* and St^* , to distinguish them from the results discussed in the previous sections.

As expected substitution of the projected frontal width instead of the equivalent circle diameter increased the values of the force coefficients at all angles attack except $\alpha = 0^\circ$ for the four-rib case, where the projected frontal width is equal to the diameter $D = D^*$, and at angles of attack where the value of the force coefficients is 0 in both studied configurations (see Figure 9.13 and 9.14). The values of C_d^* in the four-rib case exceed those for the circular cylinder at all angles of attack, but are close to it at $\alpha \approx 40^\circ$. The decreased values of the fluctuating force coefficients compared to the circular cylinder were preserved for both configurations at most angles of attack when projected frontal width was used as characteristic linear dimension. The change of characteristic linear dimension led to further reduction in Strouhal number compared to the circular cylinder. This indicates that the observed reduction of the Strouhal number is consistent with the general trend of bluff bodies with non-circular cross-section, which yield lower Strouhal number values compared to smooth, circular cylinders (Roshko, 1955).

As for the cactus-shaped cylinders, C_d^* , C_l^* , and $C_l'^*$ for the square cylinder show a strong dependence on the angle of attack (see Figure 9.14). It should be noted that in the investigation on flow past square cylinders, a different convention for the angle of attack is used, i.e. $\alpha_{sq} = 45^\circ$ when a corner of the square is facing the flow, while in our definition this corresponds to $\alpha = 0^\circ$, consequently $\alpha = 45^\circ - \alpha_{sq}$. In Figure 9.14, this relationship was used to convert results from the cited studies of square cylinders to our definition of the angle of attack α .

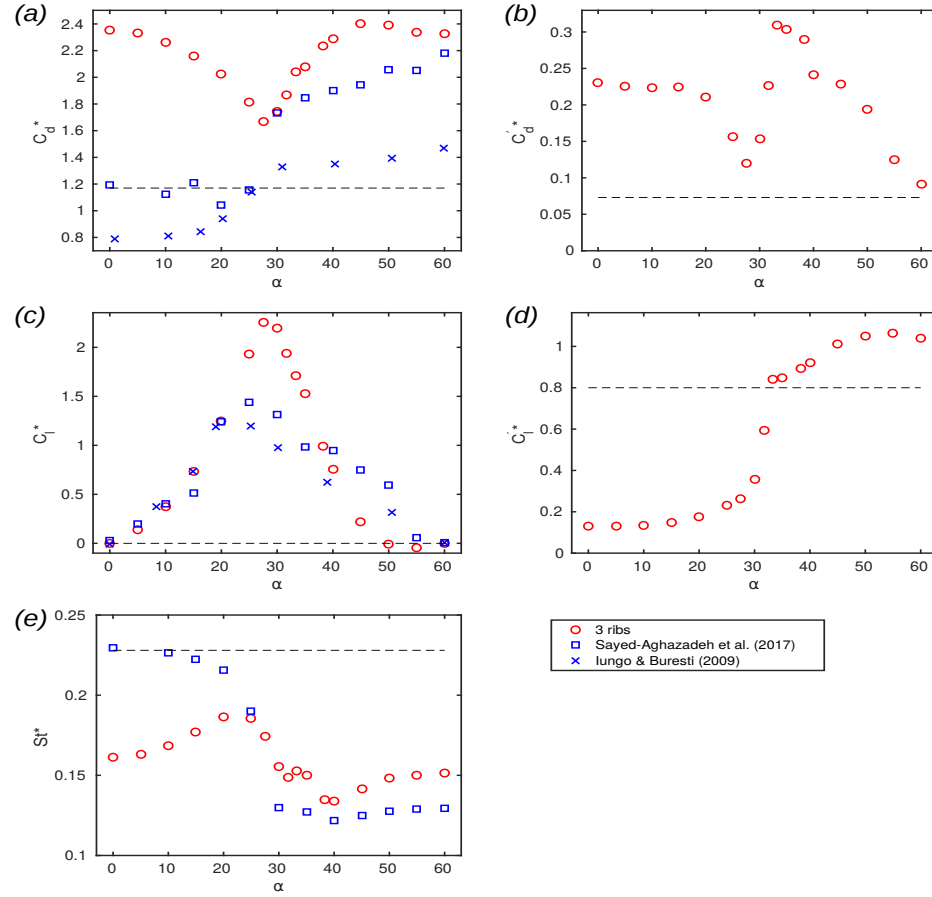


Figure 9.13: Mean and fluctuating lift force coefficients and Strouhal number calculated using projected frontal width as characteristic linear dimension versus angle of attack for the three-rib case and triangular prism: a) C_d^* , b) $C_d'^*$, c) C_l^* , d) $C_l'^*$, e) St^* . The dashed line shows the value for the smooth cylinder case. Data from experimental studies for low-aspect ratio triangular cylinders Iungo and Buresti (2009) and high-aspect ratio cylinders Seyed-Aghazadeh et al. (2017) are shown for comparison where available.

For the square cylinder, a critical angle of attack α_{cr} is observed. At this angle of attack, the mean drag and fluctuating lift force coefficients attain their minimum and the mean lift coefficient and the Strouhal number their maximum values. This behaviour is attributed to the reattachment of the flow that separates at the front corner of the square cylinder to the back corner at this angle of attack. Similar features in the angle of attack dependence of C_d^* , C_l^* , $C_l'^*$, and St^* can be observed in the four-rib cylinder data. However, the critical angle of attack for the four-rib cylinder is higher ($\alpha_{cr} \approx 40^\circ$) compared to the value for the square cylinder, where $\alpha_{cr} \approx 32^\circ$ (Igarashi, 1984). This may be a combined effect of the corner rounding of the rib tips and of the flow within the cavities for the four-rib cylinder. Corner

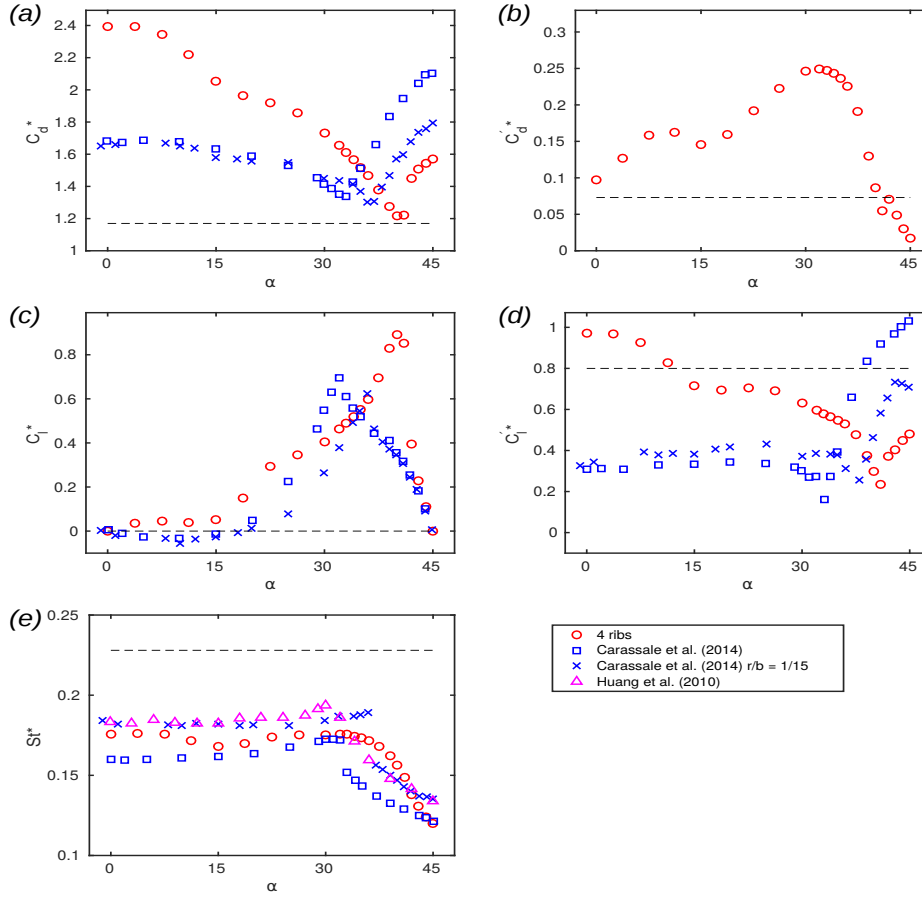


Figure 9.14: Mean and fluctuating lift force coefficients and Strouhal number calculated using projected frontal width as characteristic linear dimension versus angle of attack for the four-rib case and square prism: a) C_d^* , b) $C_d'^*$, c) C_l^* , d) $C_l'^*$, e) St^* . The dashed line shows the value for the smooth cylinder case. Data from Huang et al. (2010) (standard square cylinder) and Carassale et al. (2014) (standard square cylinder and square cylinder with rounded corners; datasets for smooth flow conditions) are shown for comparison where available.

rounding is known to increase the critical angle for the square cylinder (Carassale et al., 2014). When comparing the four-rib cylinder results to the square cylinder with the corner rounding closest to the four-rib case ($r/b = 1/15.5$, where r is the corner radius and b is the side of the square) from Carassale et al. (2014)'s study, a stronger effect is observed in the four-rib cylinder case, even though it has a slightly smaller corner rounding radius ($r/b = 1/18.8$). In addition, the values of C_d^* and $C_l'^*$ for $\alpha > \alpha_{cr}$ in the four-rib case are lower compared to those of the square with rounded corners. These differences in the angle of attack dependence compared to square cylinders with rounded corners are likely to be an effect of the cavities between the ribs, as they are the main difference in shape between the two geometries. The

presence of cavities is probably also the cause of the increased values of the drag force coefficient and fluctuating lift force coefficient at lower angles of attack relative to the square cylinder. The results for the angle of attack dependence of the Strouhal number show the same trends as observed for square cylinders. At low angles of attack the Strouhal number has an approximately constant value and a decrease of St^* is observed for high angles of attack. The drop in St^* around the critical angle appears more gradual for the four-rib cylinder compared to the square, where a more sudden drop in St^* is observed.

For the three-rib cylinder, the angle-of-attack dependence of the force coefficients and Strouhal number also suggest the presence of a critical angle of attack at $\alpha_{cr} \approx 27.5^\circ$. As for the four-rib case, the minimum value of C_d^* and the maximum values of C_l^* and St^* are observed at this angle of attack. However, in contrast to the four-rib case a minimum value of $C_l'^*$ is not attained at α_{cr} , but a sudden increase is observed. Published data on the angle-of-attack dependence of the aerodynamic characteristics of equilateral triangular cylinders is limited, as most studies focus on the 0° and 60° cases. Therefore, the three-rib case is compared to experimental results for a wall-mounted, low-aspect ratio triangular prism with a free end at higher Reynolds number ($Re = 1.2 \cdot 10^5$) (Iungo and Buresti, 2009) and for a high aspect ratio triangular cylinder at lower Reynolds number ($Re = 2,700$) (Seyed-Aghazadeh et al., 2017). Due to the three-dimensionality of the former flow configuration and the large differences in Reynolds numbers no detailed quantitative comparison with the three-rib cylinder results can be made. However, the behaviour of the mean lift and drag coefficients is qualitatively consistent with the referenced results, namely the maximum of C_l^* and the minimum of C_d^* was found close to intermediate angles of attack both in the three-rib case and in the referenced studies (see Figure 9.13 (a) and (c)).

At low angles of attack, higher values of C_d^* are observed for the three-rib cylinder compared to the triangular prism, which may be an effect of the cavities, as discussed above for the four-rib cylinder. For the Strouhal number (Figure 9.13 e), matching trends are observed for higher angles of attack $\alpha > 27.5^\circ$, but for low angles of attack the three-rib cylinder case shows a decreasing trend and lower St^* values than the triangular cylinder at lower Reynolds number (Seyed-Aghazadeh et al., 2017). For a more detailed comparison of the three-rib case to an equilateral triangle further comparative studies of infinitely long triangular cylinders, including cases with rounded corners, are required which are beyond the scope of the current investigation.

The minimum values of the determined aerodynamic coefficients for both configurations have been related to their angular orientation with respect to the flow. In both the three- and four-rib cases minimum values of C_d^* are observed at a critical angle of attack ($\alpha_{cr} \approx 40^\circ$ for the four-rib case and $\alpha_{cr} \approx 27.5^\circ$ for the three-rib case). At this angle of attack C_l^* reaches its maximum value for both configurations. In addition, at $\alpha \geq \alpha_{cr}$ in the four-rib case relatively low values of the drag coefficient and fluctuating force coefficients are observed. Therefore, a high angle of attack $\alpha > \alpha_{cr}$ relative to the prevailing wind would minimise the wind loadings experienced by the *Euphorbia Abyssinica* based cylinder as C_l^* drops off rapidly for $\alpha > \alpha_{cr}$. For a three-rib cactus there is no single optimal orientation, as low C_d^* values correlate with high C_l^* . Considering the fluctuating loads on the three-rib cylinder, an angle of attack just below the critical angle may be the most favourable orientation for the *Euphorbia trigona* based cylinder, as here C_d^* , C_l^* , and $C_d'^*$ all have relatively low values.

9.4.5 Flow visualisations

To gain further insight into the angle of attack dependence of the flow, in the following key features of the mean flow fields are discussed. Figure 9.15 shows the mean velocity field and the mean streamlines for the three-rib case at different angular orientations. At $\alpha = 0^\circ$ the mean flow is symmetrical and two vortices are formed behind the three-rib cylinder (Figure 9.15 a). This is consistent with experimental and numerical results by Yagmur et al. (2017) for a triangular prism at the same angular orientation. With the increase of angle of attack the symmetry is broken and an additional vortex starts to form in the top cavity (Figure 9.15 b). At the angle $\alpha = 27.5^\circ$ the flow detached at the front rib still reattaches to the top trailing rib, while at $\alpha = 30^\circ$ this is no longer observed (Figure 9.15 c, d). The reattachment of the flow supports the conjecture regarding the critical angle of attack for the three-rib cylinder and explains minimum value of the drag coefficient and maximum value of the lift coefficient at this angle of attack. In addition, at intermediate angle of attack up to $\alpha < 50^\circ$ a secondary vortex is observed in the top cavity (Figure 9.15 c-e) close to the front rib. At $\alpha = 50^\circ$ an additional vortex starts to form in the trailing bottom cavity (Figure 9.15 f). When the cavity of the cactus shaped cylinder with three ribs is facing the flow, the symmetry of the flow is restored and in addition to the vortices formed at the top and bottom ribs smaller vortices are formed at the back rib (Figure 9.15 g). These features are consistent with the flow

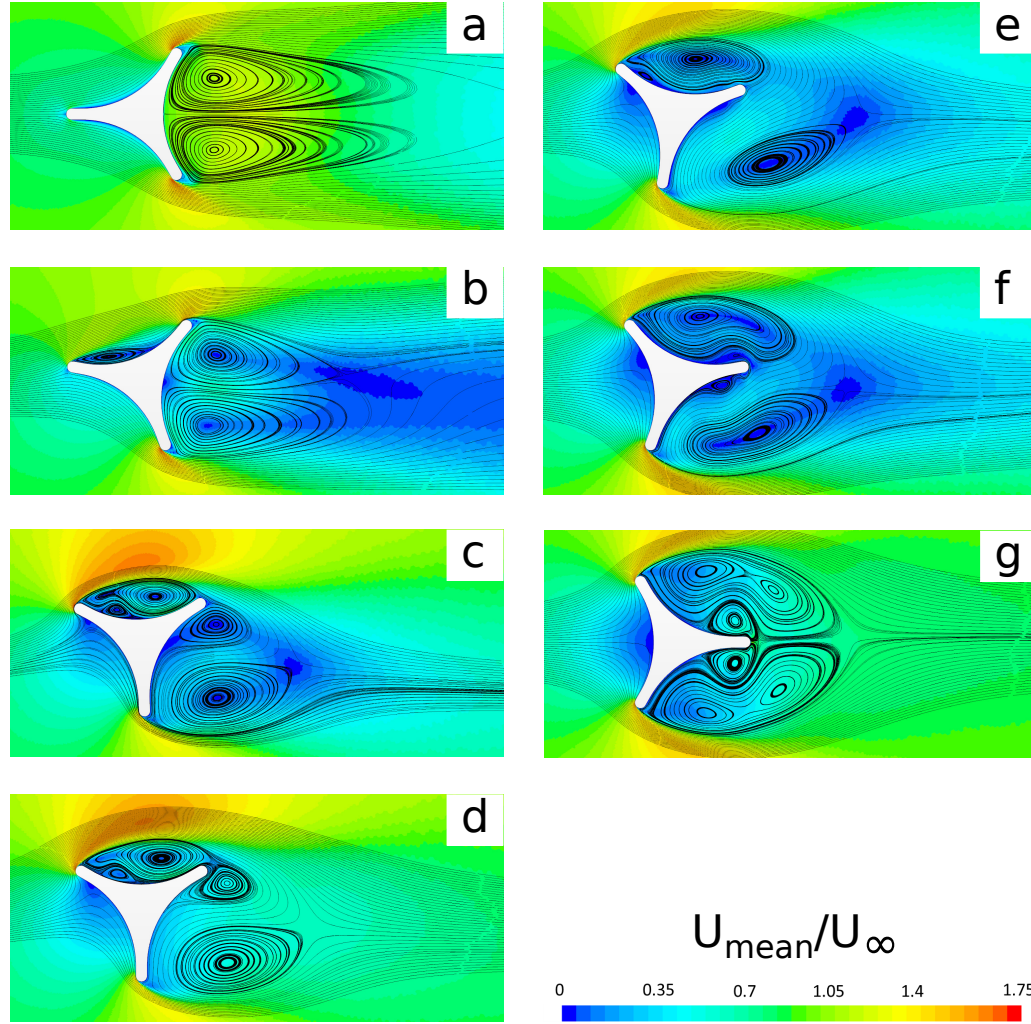


Figure 9.15: Mean streamlines variation with angle of attack for the three-rib cylinder case: a) $\alpha = 0^\circ$, b) $\alpha = 10^\circ$, c) $\alpha = 27.5^\circ$, d) $\alpha = 30^\circ$, e) $\alpha = 40^\circ$, f) $\alpha = 50^\circ$, g) $\alpha = 60^\circ$.

visualisations of Nakagawa (1989) for the same orientation of the triangular prism.

The mean velocity field and mean streamlines for the four-rib cylinder are shown in Figure 9.16. The mean streamlines at $\alpha = 45^\circ$ in the four-rib case (Figure 9.16 a) indicate the presence of recirculation zones within the cavities tangential to the flow, i.e. in the lower and the upper cavities, similar to those reported by Wang et al. (2014) and Jie and Liu (2016) for cylinders with many ribs. Deep within the cavity a secondary recirculation zone can be observed, a similar feature observed in the numerical study by Babu and Mahesh (2008) at low Re . With the decrease of the angle of attack this secondary recirculation zone in the top cavity shrinks (see Figure 9.16 b and c) and disappears when $\alpha < 30^\circ$. In contrast, a secondary recirculation zone in the bottom cavity is present until $\alpha = 22.5^\circ$ (Figure 9.16 d).

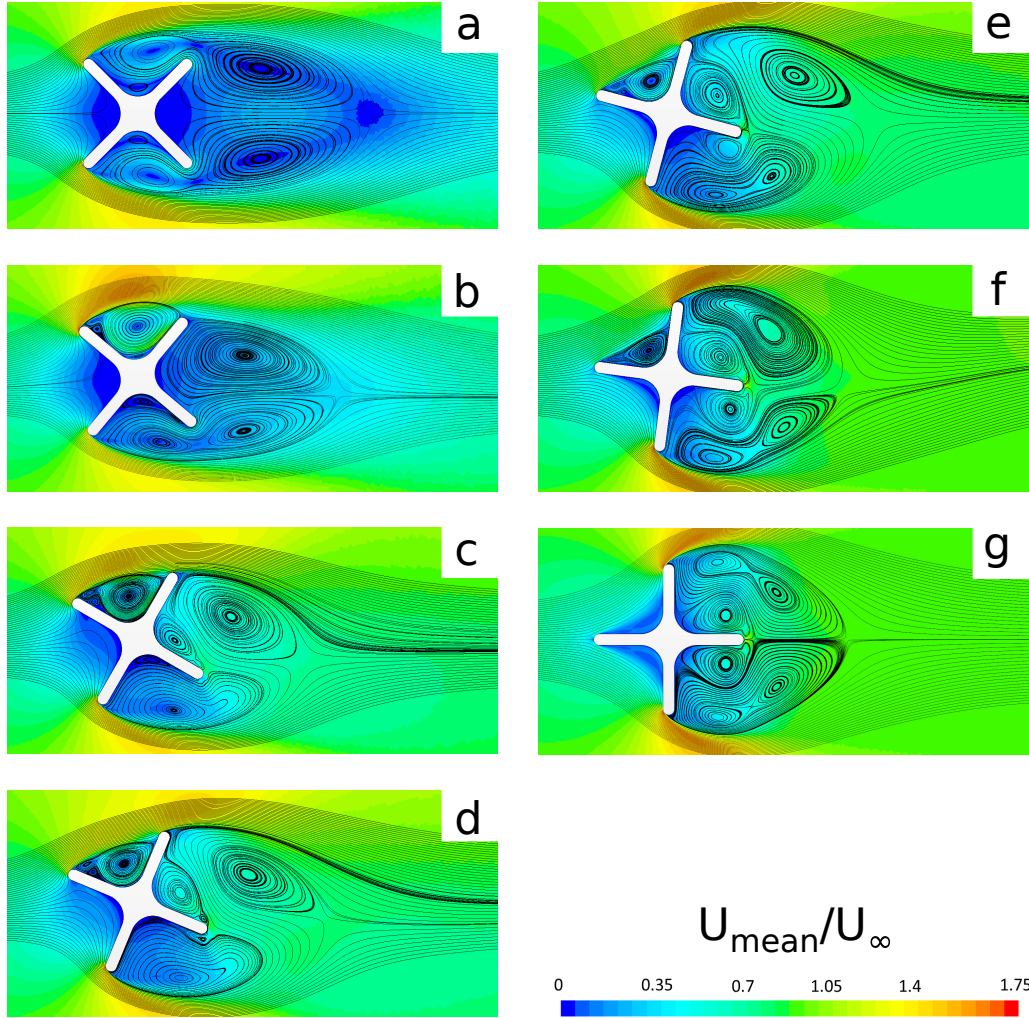


Figure 9.16: Mean streamlines variation with angle of attack for the four-rib cylinder case: a) $\alpha = 45^\circ$, b) $\alpha = 40^\circ$, c) $\alpha = 30^\circ$, d) $\alpha = 22.5^\circ$, e) $\alpha = 15^\circ$, f) $\alpha = 7.5^\circ$, g) $\alpha = 0^\circ$.

Igarashi (1984) classified the flow around a square prism into four regimes with respect to angle of attack and his classification will be used in the following. Angles of attack ranges from Igarashi (1984)'s paper given below were converted to the angle of attack definition adopted in the current paper (see also section 9.4.4). Visualisations with streamlines of the flow past square cylinders are given in Oka and Ishihara (2009). At $\alpha = 45^\circ$ the flow around the square prism is characterised by a 'perfect separation' from the leading edge and by symmetric flow. The same is observed in the four-rib case at the same angle of attack (Figure 9.16 a). However, compared to the numerical results by Oka and Ishihara (2009) the recirculation bubble in the four-rib case is significantly elongated behind the cylinder, delaying the development of a von Kármán vortex street.

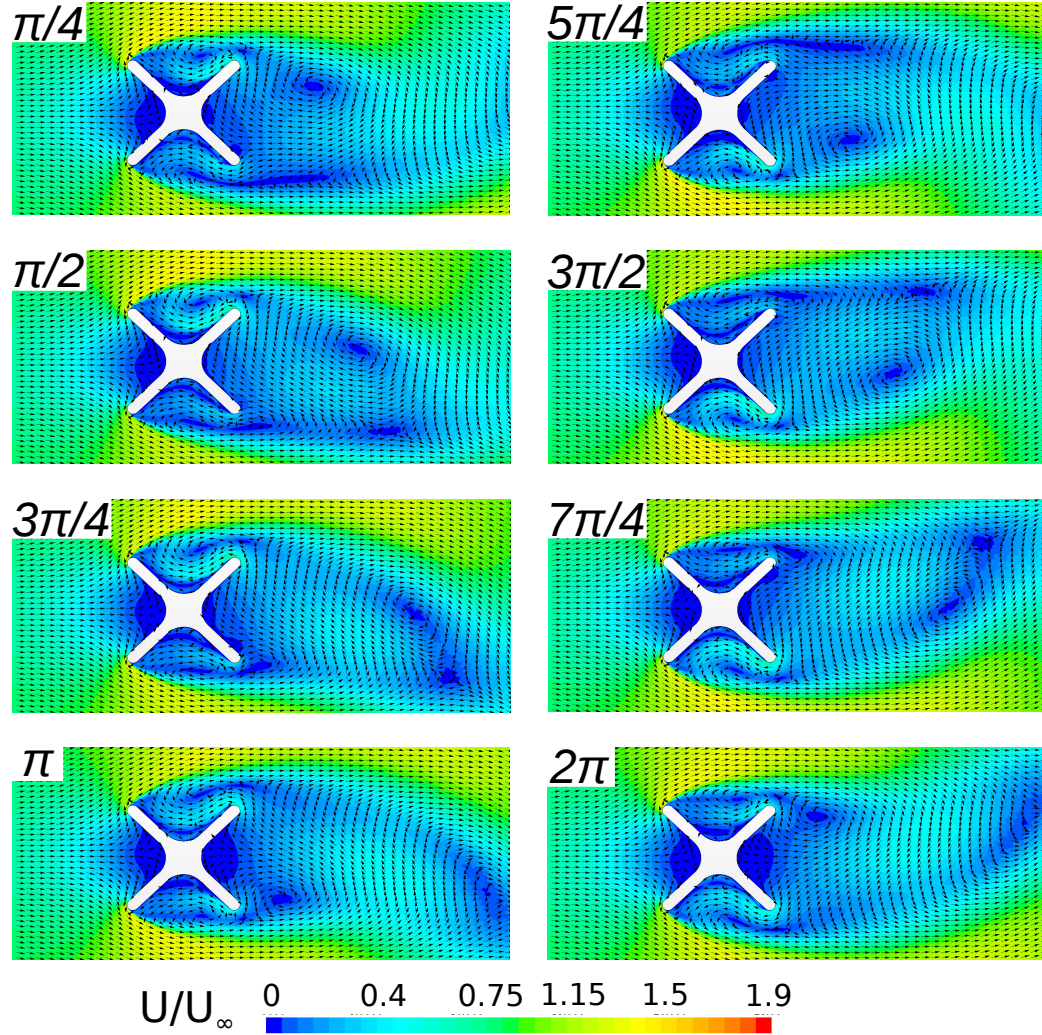


Figure 9.17: Vortex development around the four-rib cylinder at $\alpha = 45^\circ$ at different phases in the shedding cycle.

For the square cylinder at angles of attack values $32^\circ < \alpha < 40^\circ$, the flow is characterised by a ‘perfect separation’ type without symmetry of the flow, while reattachment of the flow is observed in α range of 10° to 31° . For the cactus-shaped cylinder with four ribs the reattachment of the flow at the back rib appears to be delayed to higher angles of attack ($\alpha = 40^\circ$) (Figure 9.16 b) compared to the square cylinder. This could be caused by the combined effect of the rounding of the tips of the ribs compared to the sharp corners of a classical square cylinder and the stronger development of the separated flow due the cavities. The sudden jumps in the aerodynamic coefficients and Strouhal number values in this α range are consistent with these observations (see Figure 9.14).

To obtain further insight into the flow field variation around the four-rib cylinder,

the velocity field is shown at eight different phases within the shedding cycle of the velocity field for two different angles of attack, $\alpha = 45^\circ$ and $\alpha = 22.5^\circ$ (see Figures 9.17 and 9.18). During the formation of a new vortex in the near wake for the $\alpha = 45^\circ$ case, this vortex interacts with the flow inside the cavity. Stronger interaction between the cavity flow and the near wake is observed than for the 24-rib cylinder due to the much wider cavities for the four-rib case. No separated flow is observed in the leading and trailing cavities. As has been discussed above, flow separation occurs at the front ribs. This is consistent with the square cylinder case where flow separates from the leading edge corners (Huang et al., 2010). In the corresponding snapshots of the velocity for $\alpha = 22.5^\circ$ reattachment of the flow at the back ribs and asymmetric vortex shedding can be observed. For both angles of attack, the flow in the trailing cavity undergoes complete reversal as the shedding cycle progresses. High acceleration of the flow close to the back rib can be observed for the $\alpha = 22.5^\circ$ case before this flow reversal occurs (Figure 9.18 π and 2π). In contrast, velocity changes at the back ribs are much lower for the $\alpha = 45^\circ$ case.

9.5 Conclusions

The flow past cylinders with a low number of ribs has been studied at Reynolds number 20,000 using unsteady Reynolds-Averaged Navier-Stokes simulations. Two different configurations, a three-rib configuration based on *Euphorbia trigona* and a four-rib configuration based on *Euphorbia Abyssinica*, were used for the investigation. Both shapes demonstrated strong dependence of their aerodynamic coefficients on the angle of attack. In contrast to many-rib cylinders, drag reduction was found only in the four rib case at high angles of attack.

We found that cactus-inspired cylinders with a low number of ribs can mitigate lift force fluctuations which is consistent with previous results for Saguaro-inspired cylinders with many ribs. The maximum reduction is higher, reaching up to 85% in the three-rib and up to 77% in the four-rib case compared to the smooth cylinder values. However, this is not observed over the whole angle of attack range. Reduction of the unsteady drag forces was observed only for the four-rib case at high angles of attack. Overall, the cylinder with four ribs showed at high angle of attack values of the aerodynamic coefficients superior to those at other orientations and to all tested three-rib case angular positions. In addition, it yielded mean force coefficients similar to the smooth cylinder case, while also yielding a considerable reduction of the fluctuating lift and drag coefficients. These observations remained valid when

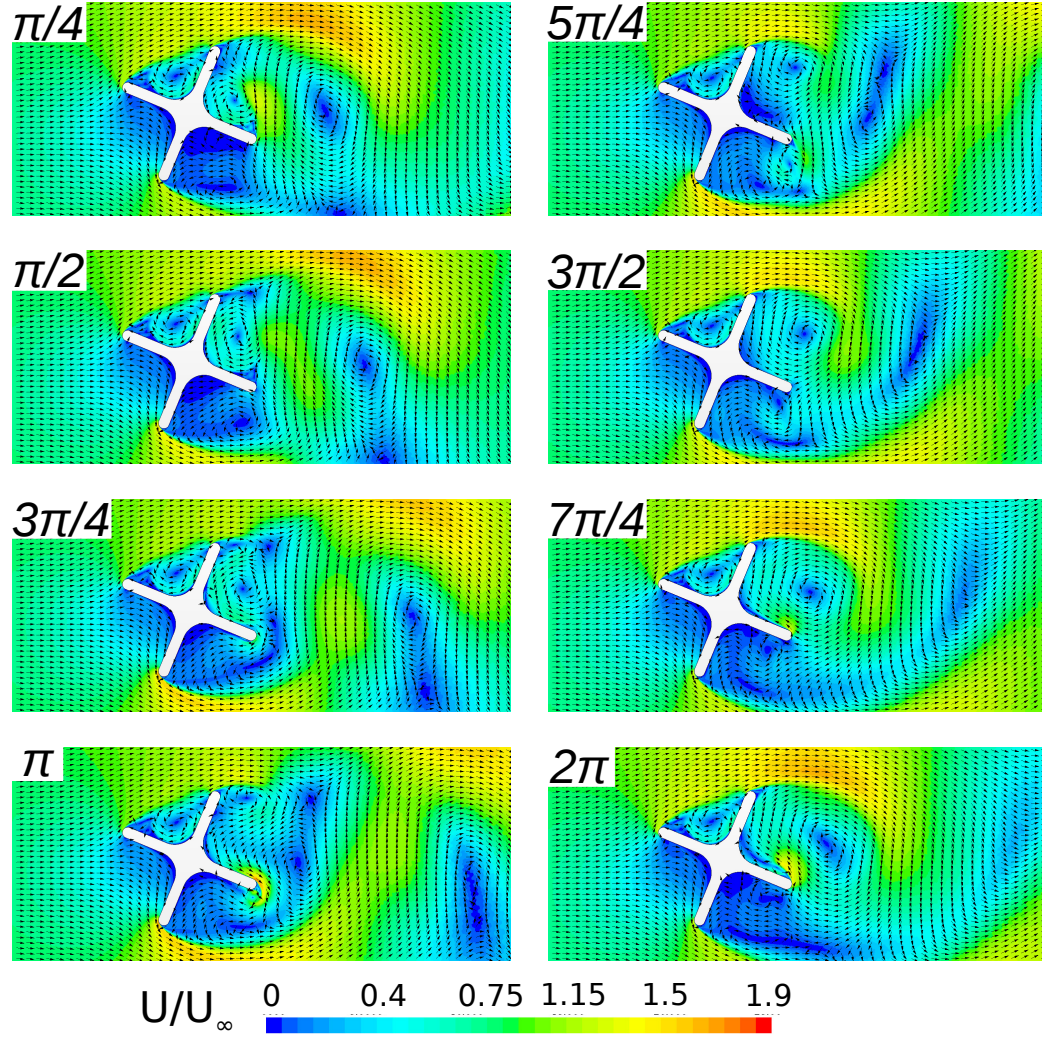


Figure 9.18: Vortex development around the four-rib cylinder at $\alpha = 22.5^\circ$ at different phases in the shedding cycle.

the characteristic linear dimension for calculation of the aerodynamic coefficients was changed from equivalent circle diameter to projected frontal width.

The relation between cavity orientation and minimum values of the aerodynamic coefficients shows that drag is minimised at a critical angle of attack α_{cr} while minimum lift is observed when the symmetry of the body with respect to the flow is preserved. The presence of cavities at the front and the back of the cylinder reduces unsteady drag and lift forces. This suggests that in the natural environment the orientation of the four-rib succulent stem at which aerodynamic loadings are minimised is for angles of attack higher than critical ($\alpha > \alpha_{cr} \approx 40^\circ$). On the other hand there is no clear optimum orientation for the single stems of the three-rib succulents, although angular orientations just below the critical angle $\alpha_{cr} \approx 27.5^\circ$ for the three-rib

case appear to be the most desirable for decreasing the fluctuating loads and the mean drag.

Comparisons of the flow field around the four-rib cylinder to the square cylinder and the three-rib cylinder to triangular prisms have been performed due to their similar outer shapes. At high angles of attack the mean streamlines of the four rib-case showed features resembling the square cylinder case. However, the reattachment of the flow in the four-rib cactus-shaped cylinder case is observed at higher angle of attack compared to the square cylinder. In addition, a significant difference in flow patterns is observed at lower angles of attack, due to the more complex vortex patterns formed at cactus cylinder ribs and their interaction with vortices formed at the trailing rib.

The significant dependence of the aerodynamic characteristics on the cactus orientation with respect to the flow direction may have an effect on plants in the real world. The stems of the succulents and cacti with a low number of ribs may be oriented relatively to the prevailing wind in order to minimise negative impact from the wind loadings, however no relevant information was found in the literature. Moreover, unlike the Saguaro cactus, which usually grows as a single stem plant with a couple of branches, succulents with a low number of ribs tend to form a bush-like structure with many branched stems. Another conjecture, which could be investigated in future work, is that the collective aerodynamic behaviour of multiple stems may have an effect similar to many-rib cylinders, consequently minimising angle of attack dependence of the aerodynamic coefficients. Previous studies of a small groups of cylinders, such as two cylinders in tandem (Alam et al., 2003b) and side-by-side arrangements (Alam et al., 2003a), as well as the investigation by Taddei et al. (2016) on large groups of cylindrical objects show that the interaction between neighbouring cylinders can have a profound effect on their aerodynamic coefficients. Therefore, we expect that interaction between multiple stems of a succulent will influence the force coefficients experienced by the individual stems as well as the plant as the whole².

Acknowledgment

The authors gratefully acknowledge support by the University of Glasgow's Lord Kelvin-Adam Smith scholarship scheme.

²The conclusions related to the possible evolution of the succulent shape as an adaptive mechanism to windy environments are discussed further in Chapter 10.

Chapter 10

Experimental investigation of the angle of attack dependence of the flow past a cactus-shaped cylinder with four ribs

This chapter is based on the following publication:

Zhdanov, O., Green, R. and Busse, A., 2020. Experimental investigation of the angle of attack dependence of the flow past a cactus-shaped cylinder with four ribs. *Journal of Wind Engineering and Industrial Aerodynamics*, **208**, p.104400

DOI: 10.1016/j.jmbbm.2020.104041

Abstract The aerodynamic properties of a two-dimensional cactus-shaped cylinder with four ribs are studied experimentally. The cross-section of the cylinder corresponds to a modified square cylinder with rounded corners and concave sides inspired by tall succulents with four ribs. The mean aerodynamic coefficients, fluctuating lift coefficient, Strouhal number, and mean surface pressure distribution are measured as a function of the angular orientation for Reynolds numbers ranging from 50,000 to 150,000. Hot-wire measurements are conducted at two locations in the wake for several angles of attack to provide insight into the vortex shedding frequencies. The results show that the studied shape exhibits a strong angle of attack dependence while no Reynolds number dependence is found within the tested range. As for the square cylinder, a critical angle of attack of approximately 13° is observed at which drag and fluctuating lift forces are minimised while mean lift and Strouhal number reach their highest values. Reattachment of the shear layer at and above the critical angle of attack is confirmed using PIV. Overall, succulents with four ribs retain some of the aerodynamic benefits that have been observed for cactus-shaped cylinders with many ribs, albeit over a limited range of angles of attack.

Keywords: bluff body, cactus-shaped cylinder, square cylinder, nature inspired

10.1 Introduction

Flow past bluff bodies has been a long-standing subject of fluid mechanics research due to its numerous practical applications in engineering. Bluff bodies, especially circular and square cylinders, are very common shapes that are present in various structures (e.g. tall buildings, suspension bridges, risers, heat exchangers). It is well known that the aerodynamic characteristics as well as the wake of the circular cylinder are strongly dependent on the Reynolds number ($Re = U_\infty D / \nu$, where U_∞ is freestream velocity, D is the cylinder diameter, and ν is the kinematic viscosity of the fluid). With increasing Reynolds number the location of the separation points on the cylinder surface changes and four distinctive flow regimes, namely subcritical, critical, supercritical and transcritical exist (see e.g. Achenbach, 1971).

In contrast, for the square cylinder, the separation points are fixed at the leading edge corners and its aerodynamic behaviour does not depend on Reynolds number for $Re > 1,000$ (see e.g. Bai and Alam, 2018). While the circular cylinder is insensitive to angular orientation due to its symmetry, strong angle of attack (α) dependence is observed for flow past the square cylinder. The general convention applied for

the angle of attack definition is that the 0° case is when the freestream is normal to a side of the cylinder and maximum angle of attack (45° case) is attained when one of the corners of the square cylinder is facing the flow. One of the distinctive features of the angle of attack dependence of the square cylinder is the presence of a critical angle of attack (α_{cr}), at which the shear layer that separates from the front corner reattaches to the side face of the cylinder (Lee, 1975). As a result of the reattachment, minimum values of drag and fluctuating lift coefficients together with maximum Strouhal number and absolute lift coefficient are observed at this angle of attack. Flow patterns around the square cylinder also change with angular orientation and can be subdivided into two main regimes, the perfect separation and reattachment flow regimes, separated by the critical angle of attack (Igarashi, 1984).

Various drag reduction and passive flow control techniques have been applied to circular and square cylinders. Splitter plates placed along the wake centreline alter vortex shedding and reduce drag of both circular (Apelt et al., 1973) and square cylinders (Bearman and Trueman, 1972). Another way to reduce drag of the square cylinder is through corner modifications. Naudascher et al. (1981) studied the influence of recessed corners on the mean aerodynamic forces. Experimental investigations were carried out for square-shaped recesses of two different sizes. Both configurations provided drag reduction over the full angle of attack range, and decrease in the lift force was observed at most angular orientations.

Tamura and Miyagi (1999) investigated the effect of rounded and chamfered corners on the flow past square cylinders. Both modifications reduce the aerodynamic drag experienced by the square cylinder over all reported angles of attack. However, a reduction of the lift force and its fluctuations was observed only at some angular orientations. With the increase of the freestream turbulence intensity this trend was sustained but the difference in lift force fluctuations between the standard square cylinder and those with modified corners was reduced compared to uniform inflow. In addition, a decrease in the critical angle of attack was observed as a result of the corner modifications.

A square cylinder can be transformed into a circular cylinder by increasing the radius of corner rounding. An experimental study on a set of cylinders with various corner roundings at zero angle of attack was conducted by Hu et al. (2006). Their results show that as a square is morphed into a circular cylinder, mean drag decreases while an increase in Strouhal number is observed. Carassale et al. (2014) studied the angle of attack dependence of square cylinders with two different corner roundings. Both studied modifications showed an increase in Strouhal number compared to the

square cylinder for all angles of attack. On the other hand, it was reported that small corner rounding leads to reduction of drag only below the critical angle of attack. For the higher corner rounding drag reduction was observed for all angular orientations. In addition, it was shown that while rounded corners reduce the fluctuating lift coefficient at angles of attack below critical, an increase was observed for angles of attack above α_{cr} . As in the case of other corner modifications, a reduction of the critical angle of attack was found for both cylinders with rounded corners.

He et al. (2014) investigated the effect of another type of corner modification by recessing the corners of the leading edge of a square cylinder. At zero angle of attack, drag reduction was achieved for all studied configurations of rectangular recesses. However, drag was found to be dependent on the size and orientation of the recesses. Rectangular recesses where the longer side was aligned with the direction of the flow provided higher drag reduction compared to the same recesses where the longer side was normal to the freestream direction. As for other types of corner modifications, an increase in Strouhal number compared to the square cylinder was observed.

The natural world has been a source of inspiration for a number of drag reduction and passive flow control approaches including modifications to the cross-sections of bluff bodies (Bushnell and Moore, 1991; Choi et al., 2012). For example, Hanke et al. (2010) and Wang and Liu (2016) showed that a cylinder shape inspired by the vibrissae of harbour seals suppresses vortex-induced vibrations compared to a regular circular cylinder. Another modification to the cross-section of the circular cylinder has been inspired by the Saguaro cactus, a tall slender plant with ribbed, approximately circular cross section, that can have up to 30 ribs. Experimental and numerical investigations showed that the ribs on the cactus trunk help to reduce drag and the magnitude of unsteady force fluctuations (Talley et al., 2001; Cheng et al., 2018) compared to the smooth circular cylinder. In the plant kingdom, there are a number of tall, cactus-like succulents that have only four ribs, e.g. *Euphorbia abyssinica*, *Euphorbia ammak*, or *Euphorbia ingens*. Their cross sections resemble a square cylinder with concave sides and rounded corners. Taking into account that these succulents have developed their plant features, including ribs, independently from cacti through the process of convergent evolution (McGhee, 2011), their shape may provide aerodynamic benefits similar to those of cactus-shaped cylinders with many ribs. In a 2D URANS study it was found that a succulent-inspired cylinder with four ribs has superior aerodynamic behaviour compared to the regular square cylinder at certain angles of attack (Zhdanov and Busse, 2019).

In the present study, the aerodynamic properties of a succulent-inspired cylinder with four ribs are measured in a wind tunnel to investigate its ability to reduce drag and modify force fluctuations and Strouhal number. Force and surface pressure measurements were carried for 17 angular orientations ranging from 0° to 45° at Reynolds numbers 50,000, 100,000, 120,000, and 150,000. Hot-wire measurements were performed in the wake at Reynolds number 100,000 to provide further insight into the vortex shedding frequencies. Flow visualisation was conducted using particle image velocimetry for a range of angular orientations at Reynolds number 50,000.

The current paper is organised into four sections: In Section 10.2 the details of the tested model and the experimental setup are described. The experimental results for mean force coefficients, fluctuating lift coefficient, mean surface pressure distribution, Strouhal number, hot-wire measurements in the wake and PIV flow visualisations are presented in Section 10.3. Finally, in Section 10.4 general conclusions on the ability of ribs to help tall succulents to cope with high wind loads are given.

10.2 Experimental setup

Force, surface pressure and wake hot-wire measurements were conducted in the low-speed deHavilland tunnel at the University of Glasgow, a closed-return type wind tunnel facility. The wind tunnel test section has a $2.66 \text{ m} \times 2.1 \text{ m}$ octagonal cross-section and is 5.5 m long with 5 : 1 contraction ratio. Turbulence intensity in the empty test section is below 0.2%.

The tested model, a cactus-shaped cylinder with four ribs, is based on the succulent *Euphorbia abyssinica*. The plant's cross section was approximated using simple geometrical relations (Figure 10.1a). The model has a 3D printed central section, where pressure taps are installed. The end parts were made from model foam. To strengthen the model it was reinforced by a steel tube along its central axis. The surface of the model was painted and polished to give a smooth finish. The dimensions of the cactus-shaped cylinder model are $110 \times 110 \times 1250 \text{ mm}^3$ (width \times height \times length). At zero angle of attack these dimensions give an aspect ratio of 11.4% and a blockage ratio of 5.16%. Blockage corrections were not applied to the experimental data, following the approach by Tamura and Miyagi (1999) for a 2D square cylinder with blockage ratio of 5% at $\alpha = 0^\circ$.

To achieve two-dimensional flow conditions, a 2D insert was installed in the wind tunnel test section. The model was mounted horizontally between the walls of the 2D insert at approximately the mid-height of the wind tunnel test section (Figure

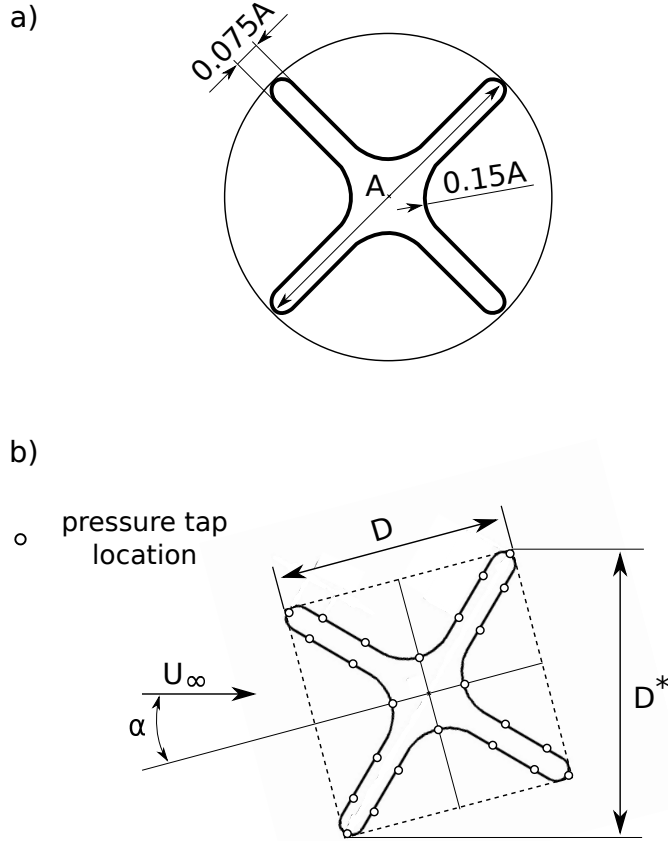


Figure 10.1: a) Geometrical representation of the studied geometry. b) Definitions of length scales, angle of attack, and location of the pressure taps on the model of the cactus-shaped cylinder with four ribs.

10.2).

The orientation of the model with respect to the incoming flow was varied manually and checked by a digital inclinometer at several positions along the model span. The angle of attack (α) definition was adopted from the square cylinder studies, namely zero angle of attack is when the flow is normal to the cavity of the cactus-shaped cylinder, while $\alpha = 45^\circ$ when the rib tip is facing the flow (Figure 10.1b). In the present study data have been acquired at 17 angular orientations: 0° , 5° , 7.5° , 10° , 11° , 12° , 13° , 14° , 15° , 20° , 22.5° , 25° , 30° , 35° , 37.5° , 40° , and 45° . First, the measurements were carried out with 5° steps. Next, to increase resolution, the data was acquired with 7.5° steps excluding repetitive orientations. Finally, in the range $10^\circ \leq \alpha \leq 15^\circ$ the data was recorded with 1° steps to capture the critical angle of attack.

Wind tunnel dynamic pressure was measured with Pitot-static probe at the work-

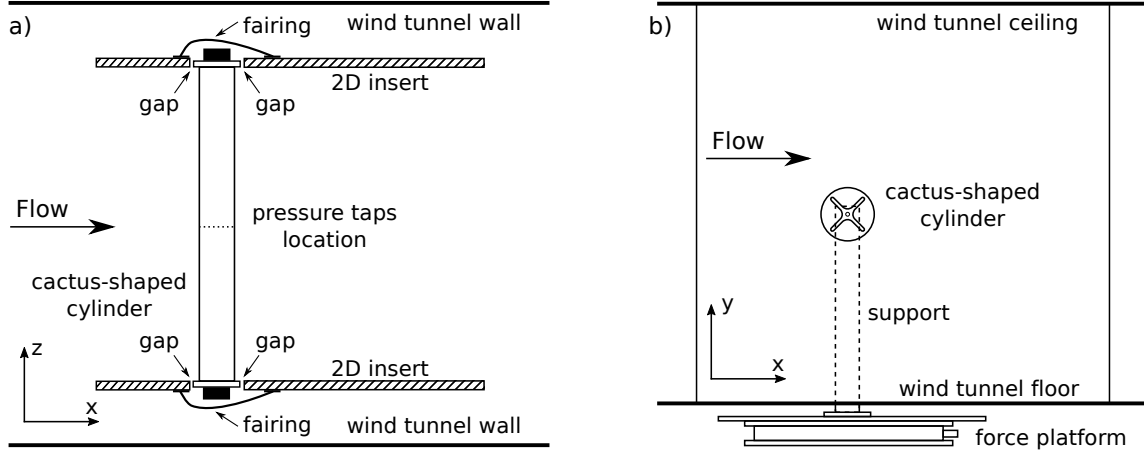


Figure 10.2: Schematic diagram of the experimental setup. a) Top view, showing 2D insert to the test section and location of pressure taps on the cactus-shaped cylinder model. b) Side view, showing force platform mounted beneath the wind tunnel test section.

ing section entry and using pressure tappings in the wind tunnel settling chamber and contraction. The experiments were conducted at four Reynolds numbers, namely 50,000, 100,000, 120,000 and 150,000. The Reynolds number was based on the distance between adjacent rib tips (D), i.e. the length of the side of the equivalent square cylinder (Figure 10.1b).

10.2.1 Force measurements

The forces were measured by an AMTI OR6-7-1000 force platform, installed under the wind tunnel floor, at 1 kHz rate for at least 100 s. This corresponds to a minimum of approximately 700 shedding cycles at the lowest tested Reynolds number of 50,000 in $\alpha = 45^\circ$ configuration. The accuracy of the measurements is $\pm 0.25\%$ of the applied load. To eliminate interference between the model ends and the walls of the 2D insert they were separated by a small gap (see Figure 10.2a).

10.2.2 Pressure measurements

In the central plane of the cactus-shaped cylinder 24 pressure taps were installed. Pressure taps were located at the tip of each rib and at the centre of each cavity. In addition, each rib had 2 taps on each side (Figure 10.1b). All pressure taps were connected to a Scanivalve ZOC23b miniature pressure scanner (range ± 2.5 kPa) through PVC tubes. Surface pressure was determined at every measuring point as

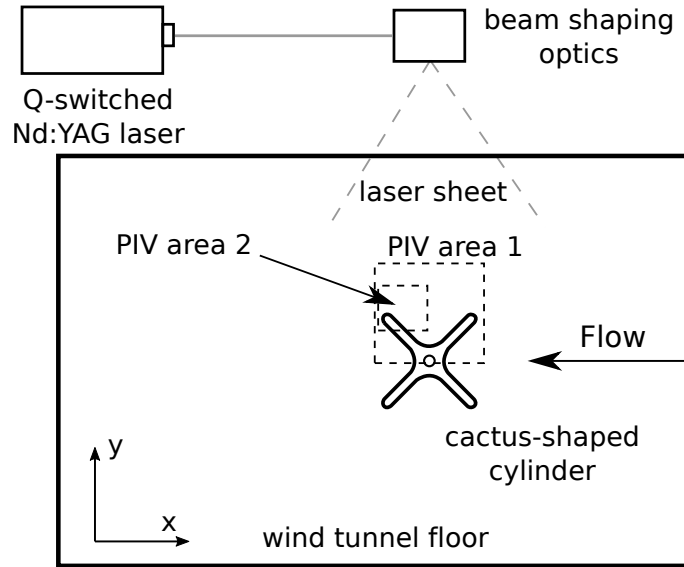


Figure 10.3: Schematic diagram of the experimental setup used for PIV quantitative visualisations of the flow over the top part of the cactus-shaped cylinder with four ribs.

an average over 1600 data points. Resolution of the pressure scanner of around 1 Pa provided accuracy of the pressure coefficient close to 1%.

10.2.3 Hot-wire measurements

Hot-wire measurements were conducted using a Dantec Dynamics StreamLine Pro System with X-probe (55P61) at Reynolds number 100,000. The probe sensors are tungsten wires with diameter of $5\ \mu\text{m}$ and length 1.25 mm. Data was sampled at 10 kHz rate for 60 s. Before and after each set of measurements the probe was calibrated using a StreamLine Pro automatic directional calibrator. The estimated accuracy of the hot-wire measurements is around 1% based on the results reported in Kawall et al. (1983).

10.2.4 PIV measurements

Quantitative flow visualisation was performed using two-dimensional, two-component particle image velocimetry (PIV) in a $1.15\ \text{m} \times 0.85\ \text{m}$ low speed, closed-return wind tunnel with turbulence intensity of approximately 0.3% at the University of Glasgow (Green et al., 2005). The same model, as in the aforementioned experiments, was mounted in a cantilever configuration with model's axis spanning across the mid-height of the tunnel in the horizontal plane. The span of the model was adjusted to

fit flush to both sides of the tunnel. The PIV measurements were performed around the model (indicated as PIV area 1 in Figure 10.3) at Reynolds number of 50,000 for six angular orientations, namely 0° , 5° , 10° , 13° , 15° , and 30° . In addition, for two orientations, 13° and 10° , i.e. at the critical angle of attack and at an angle just below, close up quantitative flow visualisations (indicated as PIV area 2 in Figure 10.3) were carried out to capture the reattachment of the separated shear layer.

Illumination for the PIV was provided by a Quanta-Ray, single cavity, Q-switched Nd:YAG pulsed laser with frequency doubler that produced a pulsed output of 8 ns duration with 532 nm wavelength. The laser was directed into the wind tunnel working section from above and expanded into a thin sheet using beam shaping optics and a cylindrical lens. The light sheet was in the vertical plane coincident with the lateral symmetry plane of the wind tunnel test section. A 10-bit, Redlake Megaplus 4 2048×2048 pixel CCD camera was used to capture images for the PIV, with each image synchronised with a laser Q-switch pulse. The camera was fitted with a selection of lenses for the PIV including an 85 mm focal length lens at $f/2$ for the PIV area 1 and a 200 mm focal length lens at $f/4$ for the PIV area 2. The PIV setup was spatially calibrated by taking a photograph of a grid of 2 mm diameter dots with a 5 mm pitch, and performing a least-squares fit to the centroids of the dot images. PIV seeding was generated by a Concept Systems Viscount fog generator that heated a light smoke oil (density 700 kg m^{-3}) and was pumped into the wind tunnel circuit using carbon dioxide. The notional seeding particle size was $< 1 \text{ }\mu\text{m}$. The PIV inter-pulse time delay was set between 40 and 80 μs depending on the field of view, flow speed, and required accuracy and resolution for analysis. The field of view was set to $150 \text{ mm} \times 150 \text{ mm}$ for the PIV area 1 and $50 \text{ mm} \times 50 \text{ mm}$ for the PIV area 2. In total, 144 image pairs were recorded for each tested configuration.

Image analysis for the PIV was performed using the well-established cross-correlation technique with image shifting for improved accuracy and data validation and to avoid the peak-locking bias effect inherent in digital PIV. Correlation peak detection accuracy was improved to around 0.1 pixel by using a local Gaussian fit. Image tile (sub-window) size was initially selected at 32×32 pixels and reduced to 16×16 pixels for higher spatial resolution where required. Use of this PIV system and image analysis technique has been reported in detail in Green et al. (2005). Spatial calibration error and PIV timing errors were negligible. The major source of error in the PIV was the digital bias, which itself was dependent upon the field of view. The maximum field of view used for this study ($150 \text{ mm} \times 150 \text{ mm}$) gives an accuracy of around 2% at the wind tunnel speed that is required to attain a Reynolds number

of 50,000 (approximately 8ms^{-1}). Spatial resolution according to vector spacing was around $1\text{ mm} \times 1\text{ mm}$.

10.3 Experimental results

10.3.1 Mean force coefficients

Mean drag and lift force coefficients of the cactus-shaped cylinder with four ribs were calculated from the experimental data as:

$$\begin{aligned} C_D &= \frac{\overline{F}_D}{0.5\rho U_\infty^2 A}, \\ C_L &= \frac{\overline{F}_L}{0.5\rho U_\infty^2 A}, \end{aligned} \tag{10.1}$$

where \overline{F}_D and \overline{F}_L are the measured mean values of drag and lift force, respectively, ρ is the density of air determined based on the temperature inside the wind tunnel, and A is the projected frontal area of the cactus-shaped cylinder.

The mean drag and lift coefficients are presented as a function of angle of attack for the four tested Reynolds numbers in Figure 10.4. No significant Reynolds number dependence of the force coefficients is observed within tested range. On the other hand, both C_D and C_L show strong variation with the angle of attack. With an increase of α in the range from 0° to 13° , the drag coefficient decreases, reaching its minimum value at $\alpha = 13^\circ$. With further increase of the angle of attack, a monotonic increase of the drag coefficient is observed.

An opposite trend is observed for the absolute value of the lift coefficient which increases with angle of attack from 0 at $\alpha = 0^\circ$, where the mean flow around the cactus-shaped cylinder is symmetric, to its absolute maximum value at $\alpha = 13^\circ$. At higher angles of attack the value of the lift coefficient decreases and returns to 0 at $\alpha = 45^\circ$, where symmetry of the mean flow is restored.

Similar trends in the behaviour of the mean force coefficients with the increase of an angle of attack are observed in both cactus-shaped and square cylinders (Figure 10.4). However, compared to the square cylinder, a reduction of the drag coefficient is observed for the cactus-shaped cylinder at angles of attack up to 30° (Figure 10.4a). The absolute value of the lift force coefficient is higher for the cactus-shaped cylinder at all angles of attack, except for 0° and 45° , where zero lift is observed for both shapes (Figure 10.4b).

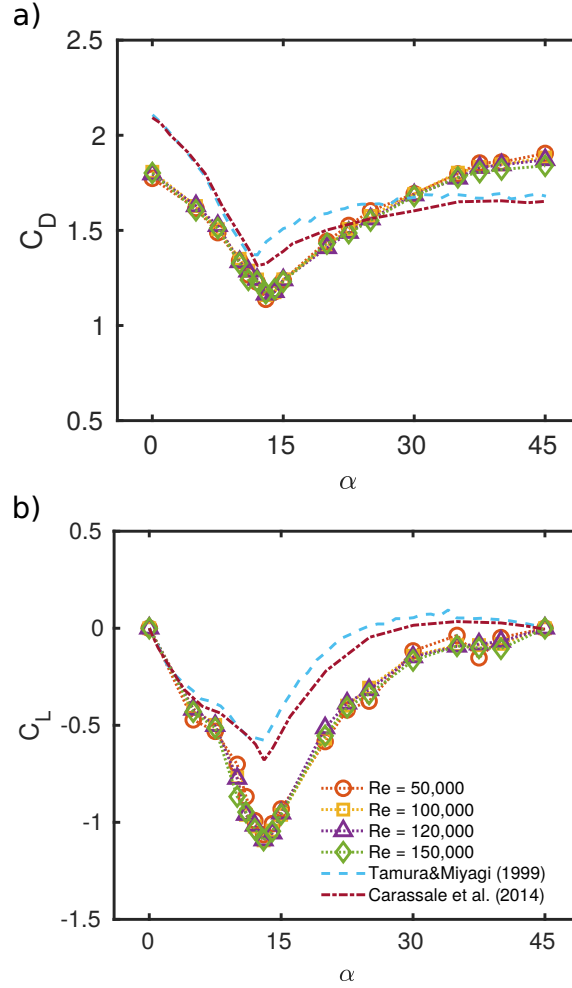


Figure 10.4: Mean aerodynamic force coefficients as a function of angle of attack. (a) mean drag coefficient; (b) mean lift coefficient. Data for the square cylinder from Tamura and Miyagi (1999) (Re=30,000) and from Carassale et al. (2014) (Re=37,000) was recalculated with projected frontal width for comparison purposes. (The legend in part b) applies to both parts of this figure.)

The presence of extrema in the mean force coefficients at a certain angle of attack shows that critical behaviour, similar to that of the square cylinder, is also present in the cactus-shaped cylinder. The minimum value of C_D as well as maximum absolute value of the lift coefficient are attained at the same angle of attack $\alpha_{cr} = 13^\circ$ (Figure 10.4).

10.3.2 Unsteady lift force

The time history of the lift force fluctuations was recorded at all tested angular positions for Reynolds number 100,000. The unsteady lift force coefficient (C'_L) is

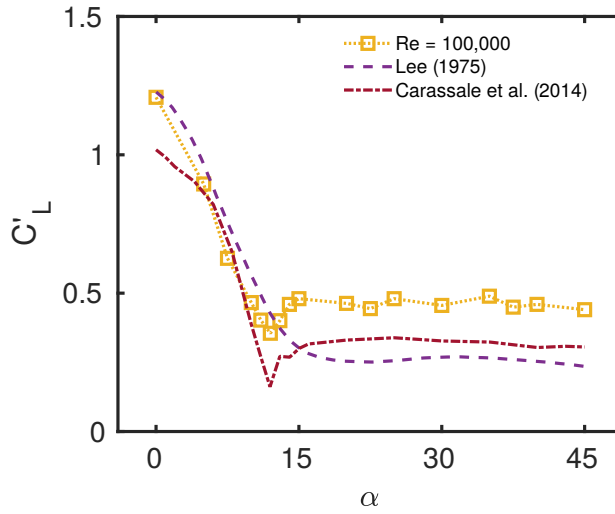


Figure 10.5: Unsteady lift force coefficient of the cactus-shaped cylinder as a function of angle of attack at $Re = 100,000$. Data for the square cylinder from Lee (1975) ($Re=176,000$) and from Carassale et al. (2014) ($Re=37,000$) was recalculated with projected frontal width for comparison purposes.

presented in Figure 10.5 as a function of angle of attack. The maximum value of C'_L is observed at zero angle of attack, followed by a reduction to its minimum value at $\alpha = 12^\circ$. This value is slightly lower than α_{cr} obtained from the mean force coefficients. With further increase in α , the fluctuating lift force coefficient recovers slightly and then remains close to constant over the range $15^\circ \leq \alpha \leq 45^\circ$.

Before comparing to the square cylinder it should be noted that there is a limited number of studies where C'_L dependence on the angle of attack is reported, since many studies on the square cylinder consider only the mean force coefficients. In addition, significant deviations between C'_L values reported in the literature can be observed (see Figure 10.5).

Overall, C'_L dependency on the angle of attack of the cactus-shaped cylinder follows the same trend as that of the square cylinder (Figure 10.5). Below the critical angle of attack a good match between the C'_L values for the two different shapes can be observed. At $\alpha = \alpha_{cr}$ reduction in fluctuating lift is higher in the square cylinder case (the minimum value of C'_L at α_{cr} is not captured in Lee (1975) because of the coarse steps in the angle of attack). At angles of attack above the critical, C'_L values of the cactus-shaped cylinder are consistently higher but also settle down to a constant value as observed for the square cylinder case.

10.3.3 Surface pressure distribution

As expected from the mean force data, no Reynolds number dependency was observed for the surface pressure distribution. In Figure 10.6 the variation of the time-averaged pressure coefficient around the cactus-shaped cylinder is presented at different angles of attack for Reynolds number 100,000. The pressure coefficient was determined from the experimental data as

$$C_p = \frac{p - p_\infty}{0.5\rho U_\infty^2} = \frac{p - p_\infty}{p_0 - p_\infty} \quad (10.2)$$

where p is the static pressure at the point of measurement, p_∞ the static pressure in the freestream, and p_0 the freestream total pressure. The pressure distribution shows significant variation with angle of attack. Both for the 0° and 45° cases, a symmetric pressure distribution is recovered as expected for a cylinder with 4-fold symmetry. Since the front cavity (between points A and B) is always upstream for all tested angular orientations ($0^\circ \leq \alpha \leq 45^\circ$), the pressure coefficient inside shows positive values (Figures 10.6a and 10.6b). For the bottom (between points D and A) and rear (between points C and D) cavities the pressure coefficient has negative values at all angular positions. This can be explained by the fact that flow separating from rib A does not reattach to the surface of the bottom cavity at any angle of attack, and a recirculation zone is present downstream of the rear cavity. The pressure coefficient behaviour is more complex for the top cavity surface (between points B and C), showing negative values for angles of attack lower than 30° . For $\alpha > 30^\circ$ the pressure coefficient inside the top cavity has positive values since at this orientation the front of rib C starts to be exposed to the flow.

As inferred from the mean force measurements, the critical angle for the cactus-shaped cylinder is attained at $\alpha_{cr} = 13^\circ$. Focusing on the surface pressure coefficient distribution for angles below critical (see Figure 10.6a), it is observed that the pressure coefficient inside cavity AB shows negligible variation with angular orientation. While the absolute value of the pressure coefficient measured at the tip of rib A slightly decreases, a small increase of C_p is observed at the equivalent location at the tip of rib B. The maximum value of the pressure coefficient inside cavity AB is observed at its centre and is close to unity. C_p inside cavities CD and DA and on tips of ribs C and D increases with angle of attack reaching maximum values at $\alpha = \alpha_{cr}$. The pressure coefficient inside cavity BC does not show significant variation for $0^\circ \leq \alpha \leq 7.5^\circ$. With further increase of angle of attack, the pressure inside this cavity drops, reaching its minimum at $\alpha = \alpha_{cr}$.

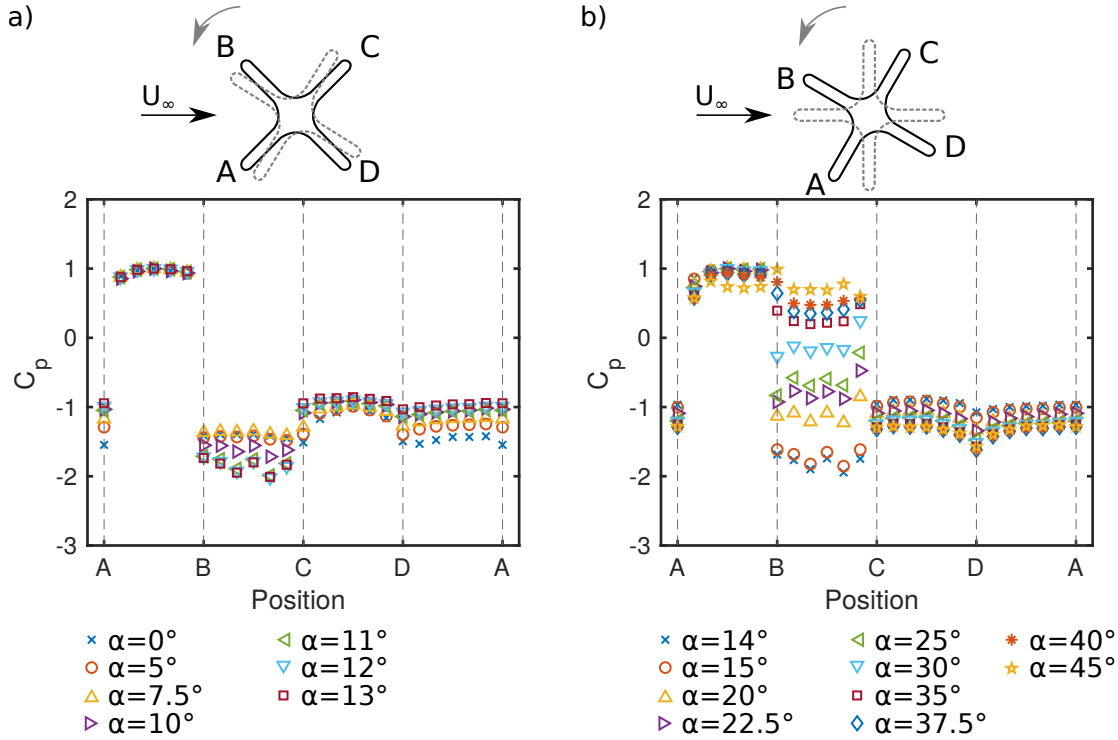


Figure 10.6: Distribution of the pressure coefficient on the surface of the cactus-shaped cylinder with four ribs at $Re=100,000$. a) angular orientations up to critical angle of attack ($\alpha = 0^\circ - 13^\circ$); b) angular orientations above critical angle of attack ($\alpha = 14^\circ - 45^\circ$).

At critical angle of attack, the pressure coefficient inside the top cavity BC attains its absolute highest value while inside the opposite bottom cavity DA it reaches its absolute lowest value, thus maximizing the pressure difference. This explains the maximum lift force generated by the cactus-shaped cylinder at the critical angle of attack. Similarly, at α_{cr} the lowest absolute value of the pressure coefficient on the surface of the rear cavity CD contributes to the reduced drag at this angle of attack.

For angles of attack higher than critical (Figure 10.6b), the pressure coefficient inside cavity AB tends to show a small decrease in C_p with increasing α . Values of the pressure coefficient inside cavity BC and on rib tip B show a considerable increase with α reaching maximum values at $\alpha = 45^\circ$. On the other hand, C_p inside cavities CD and DA and on rib tips C,D, and A decreases with α up to $\alpha = 37.5^\circ$ and starts to recover at higher angles of attack.

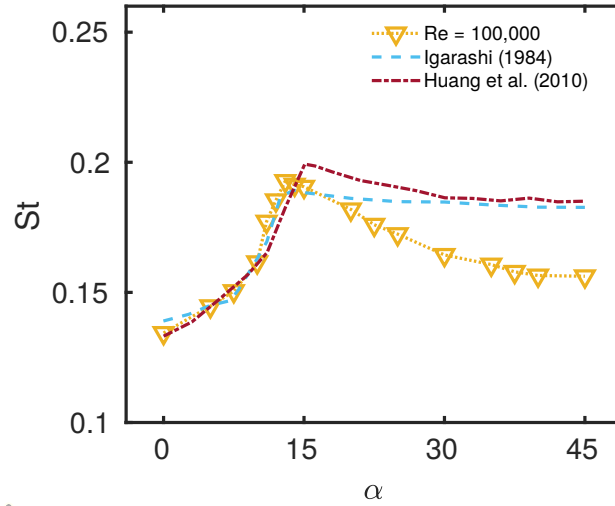


Figure 10.7: Strouhal number of the cactus-shaped cylinder with four ribs as a function of angle of attack. Data for the square cylinder from Igarashi (1984) ($Re=37,000$) and Huang et al. (2010) ($46,000 \leq Re \leq 94,000$) is presented for comparison.

10.3.4 Strouhal number

As for the mean force and surface pressure coefficients, no Reynolds number dependency is observed for the Strouhal number. St as a function of angle of attack at Reynolds number of 100,000 is presented in Figure 10.7. The value of the Strouhal number increases with α and reaches its maximum at $\alpha = 13^\circ$. This matches the critical angle of attack observed in the mean force measurements. With further increase in the angle of attack up to $\alpha = 45^\circ$, the Strouhal number gradually decreases.

For comparison, data on St of the square cylinder (Igarashi, 1984; Huang et al., 2010) is also presented in Figure 10.7. Up to the critical angle of attack, the Strouhal numbers of both shapes follow the same increasing trend and have closely matched values. However, at angles of attack above the critical the cactus-shaped cylinder has lower values of St compared to the square cylinder and this difference increases with α .

10.3.5 Quantitative flow visualisations

To gain further insight into the flow patterns and reattachment behaviour of the cactus-shaped cylinder PIV measurements were performed around its top part. Contours of the mean vorticity with superimposed mean flow streamlines are shown in Figure 10.8 for six angles of attack. For all tested angular orientations separation of

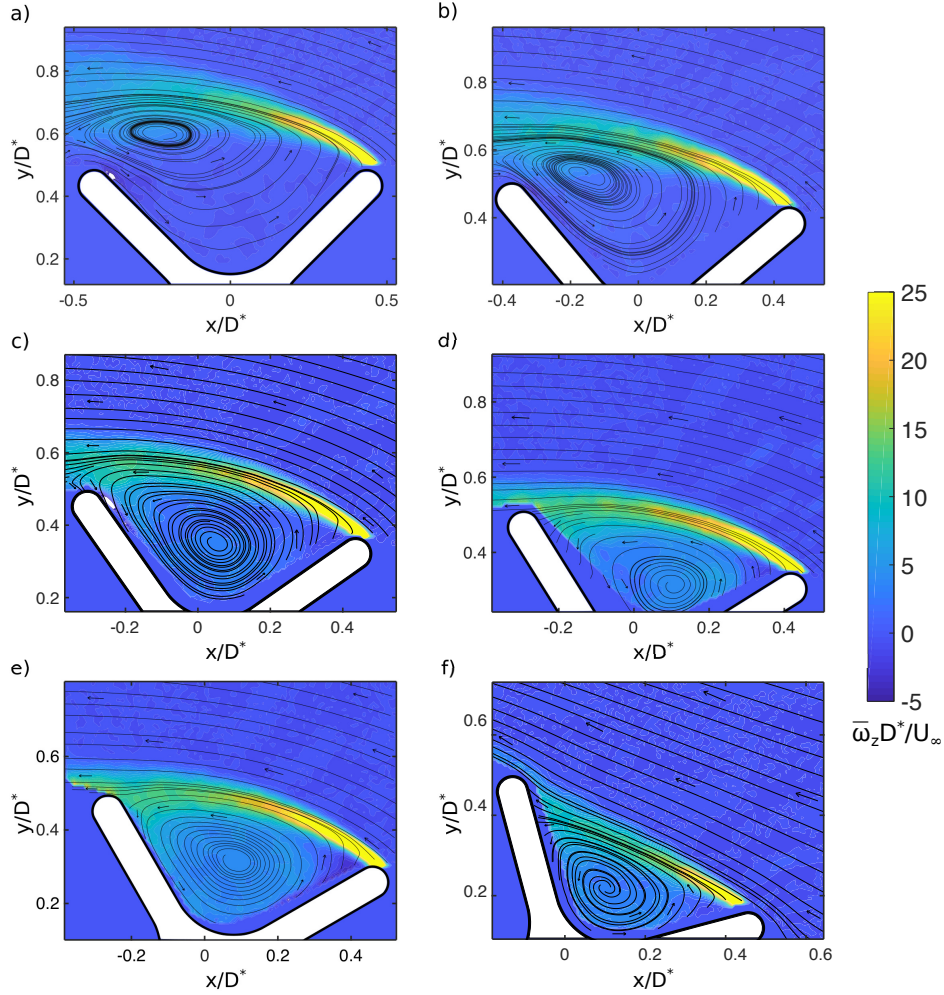


Figure 10.8: Contours of the mean vorticity fields and mean flow streamlines around the top part of the cactus-shaped cylinder with four ribs at $Re=50,000$. a) $\alpha = 0^\circ$; b) $\alpha = 5^\circ$; c) $\alpha = 10^\circ$; d) $\alpha = 13^\circ$; e) $\alpha = 15^\circ$; f) $\alpha = 30^\circ$. The freestream velocity is in the negative x-direction.

the shear layer from the front rib is observed. In addition, a recirculation bubble is formed inside the cavity between the front and back ribs. The separated mean shear layer follows the boundary of this recirculation bubble and $\bar{\omega}_z$ is decreasing in the downstream direction.

In the range $0 \leq \alpha < 13^\circ$ (see Figure 10.8a-c), the separated shear layer moves closer to the tip of the back rib with increasing angle of attack, but no reattachment is observed. The size of the recirculation bubble decreases with increasing α and its centre shifts more deeply inside the cavity. At angle of attack of 13° , i.e. the critical angle, the separated shear layer reattaches to the back rib of the cactus-shaped cylinder and the recirculation bubble becomes fully enclosed inside the cavity. This is

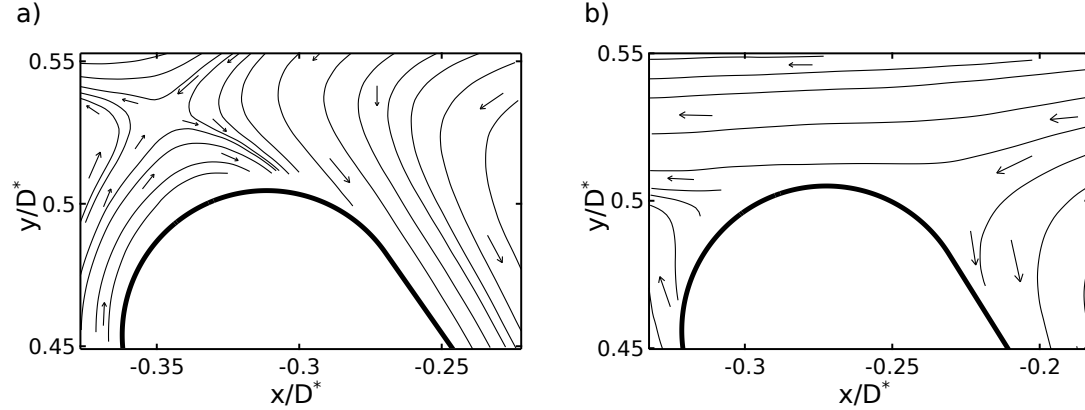


Figure 10.9: Mean flow streamlines around the back rib of the cactus-shaped cylinder with four ribs at $Re=50,000$. a) $\alpha = 10^\circ$; b) $\alpha = 13^\circ$. The freestream velocity is in the negative x-direction.

more clearly demonstrated in Figure 10.9 where mean flow streamlines are presented in a close up view in the region around the back rib at two angular orientations of 10° and 13° . At $\alpha = 10^\circ$ (Figure 10.9a) no reattachment at the back rib is observed, while with an increase of α to 13° (Figure 10.9b) the reattachment occurs. This angular orientation of 13° corresponds to the critical angle of attack that was observed in the mean force coefficients and Strouhal number data. In addition, the critical angle of attack separates two distinctive flow regimes around the cactus-shaped cylinder, namely perfect separation and reattachment, that are also distinguished in the square cylinder case (Igarashi, 1984). Reattachment of the shear layer is observed with the increase of α above the critical value (see Figure 10.8e, f). Moreover, the length of the reattachment zone on the back rib expands towards the centre of the cavity with an increase in angle of attack, while the size of recirculation bubble inside the cavity decreases.

10.3.6 Critical angle of attack

As discussed in the previous sections, a critical angle of attack α_{cr} is present for the studied cactus-shaped cylinder where C_D and C_L' attain their minimum values, while C_L and St reach maxima. While mean aerodynamic coefficients and Strouhal number reach their extrema at $\alpha = 13^\circ$, the fluctuating lift coefficient attains its lowest value at a slightly lower angle of $\alpha = 12^\circ$. Similar dispersion of the critical angle values of attack was observed for the square cylinder (see Table 10.1), where reported values of α_{cr} are between 12° and 15° . As in the case of the square cylinder, critical behaviour

Table 10.1: Overview of the extreme values of aerodynamic coefficients and Strouhal number at critical angle of attack for cactus-shaped cylinder and previously reported data on the square cylinder.

	Re	$C_{Dmin}(\alpha_{cr})$	$ C_L _{max}(\alpha_{cr})$	$C'_{Lmin}(\alpha_{cr})$	$St_{max}(\alpha_{cr})$
Present case	100,000	1.138(13°)	1.064(13°)	0.187(12°)	0.192(13°)
Square cylinder					
Lee (1975)	176,000	1.26(12°)	0.67(13°)	-	0.18(15°)
Igarashi (1984)	56,000	1.36(14°)	0.64(14°)	-	0.19(14°)
Tamura and Miyagi (1999)	30,000	1.37(12°)	0.60(13°)	0.15(11°)	0.18(15°)
Carassale et al. (2014)	37,000	1.32(12°)	0.68(13°)	0.16(12°)	0.18(14°)
Square cylinder with modified corners					
Tamura and Miyagi (1999)*	30,000	0.80(5°)	0.64(5°)	0.15(4°)	0.22(5°)
Tamura and Miyagi (1999)**	30,000	1.02(7°)	0.28(8°)	0.13(6°)	0.21(7°)
Carassale et al. (2014)***	27,000	1.28(8°)	0.61(9°)	0.13(8°)	0.19(9°)
Carassale et al. (2014)****	27,000	1.10(6°)	0.57(7°)	0.15(5°)	0.20(7°)

If necessary, force coefficients and Strouhal numbers from the literature were recalculated with the projected frontal area and projected side length, respectively, for comparison purposes.

* - square cylinder with rounded corners, $r = D/6$,

** - square cylinder with chamfered corners, $size = D/6$,

*** - square cylinder with rounded corners, $r = D/15$,

**** - square cylinder with rounded corners, $r = D/7.5$,

where r - radius of the corner rounding

of the studied cactus-shaped cylinder is associated with the reattachment of the shear layer, which separates from the front rib, to the the back rib and which was confirmed by the flow visualisations discussed in the previous section. Modifications to the corners of the square cylinder are known to have a strong influence on the reattachment of separated shear layers, and tend to shift the critical angle of attack to lower values (Tamura and Miyagi, 1999; Carassale et al., 2014) (see Table 10.1). This effect is not observed in case of the cactus-shaped cylinder, where the critical angle of attack is in the range reported for the square cylinder.

10.3.7 Power spectra

The power spectral density (E_u) of the streamwise component of the velocity based on hot-wire measurements at two downstream positions behind the cactus-shaped cylinder is shown in figure (Figure 10.10) for four angles of attack at Reynolds number

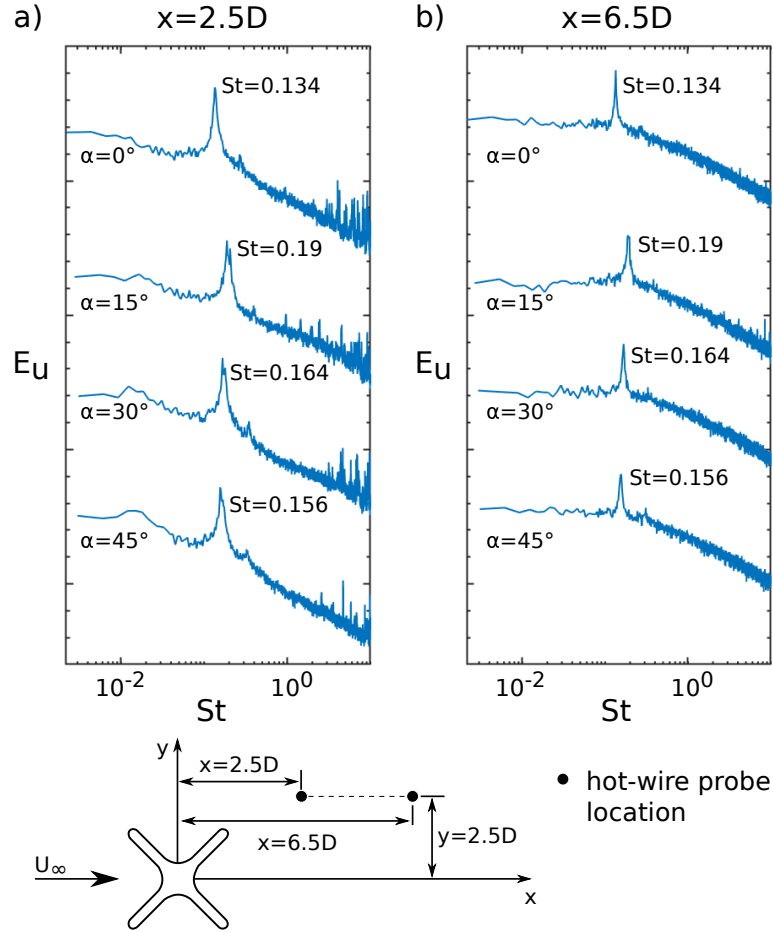


Figure 10.10: Power spectra of the u -component of the velocity determined for four angular orientations at two locations behind the cactus-shaped cylinder at $Re=100,000$. a) $x = 2.5D$, $y = 2.5D$ b) $x = 6.5D$, $y = 2.5D$. The scale on the vertical axis is arbitrary but the same scale is used for each spectrum. For clarity, the spectra have been shifted relative to each other along the vertical axis.

100,000. The first position was located at $x = 2.5D$ downstream of the centre of the cylinder with cross-stream offset $y = 2.5D$ with respect to the centreline, and the second position at $x = 6.5D$ using the same cross-stream offset. The data was averaged with Bartlett's method using 16 segments. The ordinate axis in Figure 10.10 has arbitrary scale but the same scale was used for all presented spectra for comparison purposes.

At both locations ($x = 2.5D$ and $x = 6.5D$) a dominant peak in E_u is present for all angles of attack. These peaks indicate spanwise vortex shedding and correspond to the Strouhal numbers of the cactus-shaped cylinder at these particular angular orientations. In addition, in all cases at least one higher harmonic can be observed. At intermediate angles of attack ($\alpha = 15^\circ$ and $\alpha = 30^\circ$), a further peak can be

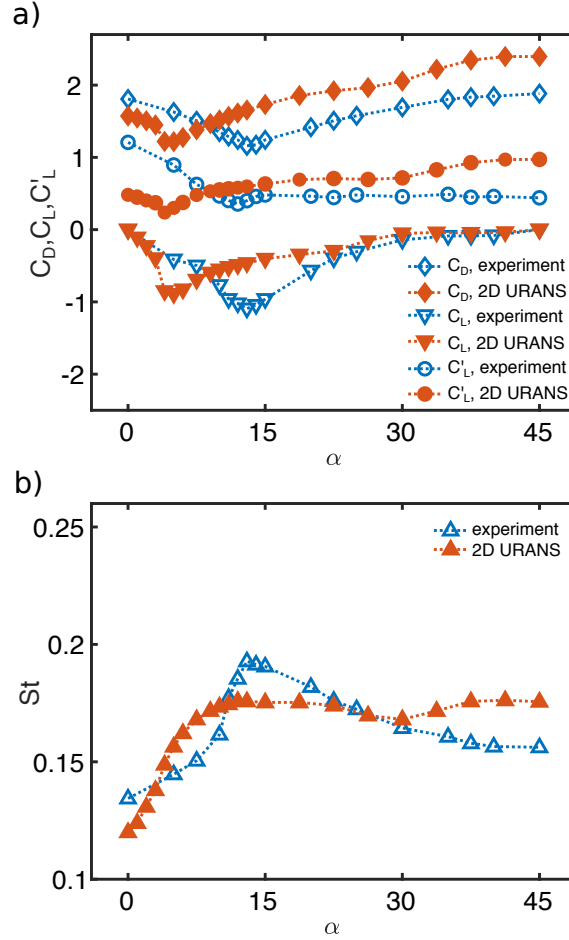


Figure 10.11: Aerodynamic force coefficients and Strouhal number as a function of an angle of attack obtained from the present experiments at representative Reynolds number of 100,000 compared to the URANS results (Zhdanov and Busse, 2019) for the same shape at Reynolds number of 20,000. (a) Force coefficients; (b) Strouhal number.

observed that is close to the primary one. This can be attributed to secondary vortex shedding at these angles of attack. Similar behaviour was previously observed in a URANS-based investigation of a cactus-shaped cylinder with four ribs (Zhdanov and Busse, 2019).

10.3.8 Comparison with earlier 2D URANS results

In the present section, the current experimental results are compared to an earlier 2D URANS-based investigation of the same cactus-shaped cylinder at a Reynolds number of 20,000 (Zhdanov and Busse, 2019). Whilst this previous investigation was at a Reynolds number below the range studied in the experiments, a comparison of

results obtained at different Re can be justified by the similarities of the aerodynamic behaviour between the studied shape and the square cylinder. The cactus-shaped cylinder does not exhibit Re dependence within the range of 50,000 to 150,000, and in investigations of the square cylinder no Reynolds number dependence is observed at $Re > 1,000$ (Bai and Alam, 2018). Therefore, it can be reasonably presumed that no significant changes would be observed at $Re = 20,000$.

Both experimental and 2D URANS investigations capture the presence of the critical angle of attack for the studied cactus-shaped cylinder, but its actual value is underpredicted by the 2D URANS simulations. In both experiments and URANS simulations α_{cr} is associated with the reattachment of the separated shear layer from the front rib to the back rib. Qualitatively, experimental and 2D URANS results demonstrate the same trends in the behaviour of aerodynamic coefficients and Strouhal number with angle of attack (Figure 10.11). With the change of α from 0° up to the critical angle, values of C_D and fluctuating lift coefficient decrease to their minima, whilst St and the absolute value of C_L increase and reach their maxima. With further increase of the angle of attack from α_{cr} to 45° an increase in the mean drag coefficient is observed, while C'_L attains an approximately constant value after an initial increase. The Strouhal number and absolute mean lift coefficient decrease over the same range. A mismatch in the behaviour of St and C'_L between experimental and 2D URANS results is present at angles of attack $> 30^\circ$.

At most angular orientations, quantitative differences are observed for the aerodynamic coefficients and Strouhal number when comparing experimental and URANS results (Figure 10.11), which can be related to the underprediction of the critical angle of attack by the 2D URANS simulations. Fairly good quantitative agreement is observed for the mean lift coefficient at angles of attack up to 4° and at $\alpha > 22.5^\circ$ (Figure 10.11a).

The observed quantitative differences between experimental results and 2D URANS simulations are in line with conclusions of the work of Mannini et al. (2010), who studied URANS modelling of the flow past a rectangular cylinder: the quantitative match tends to be better at $\alpha = 0^\circ$ compared to a finite angle of attack. In addition, the URANS simulations are able to predict the physical behaviour found in the experiments in a qualitative way, but for unsteady bluff-body flows 2D URANS has limited accuracy. Overall, the 2D URANS approach provides useful insight into key features of the flow past a cactus-shaped cylinder, but for a close quantitative agreement to experimental data 3D eddy-resolved methods, e.g. Large-Eddy Simulations, are required.

10.4 Conclusions

An experimental investigation of the aerodynamic properties of a cactus-shaped cylinder with four ribs was conducted in low speed wind tunnels. The studied shape is a modification to the cross section of a square cylinder inspired by a number of tall succulents that have four ribs. The cactus-shaped cylinder showed strong angle of attack dependence of aerodynamic coefficients and Strouhal number. No Reynolds number dependence was observed within the tested range from 50,000 to 150,000.

With an increase of the angle of attack, reduction of the mean drag and fluctuating lift coefficients was observed, while Strouhal number and the absolute value of the lift coefficient were found to increase. At angle of attack of 13° C_D reached its minimum, and $|C_L|$ and St attained their maxima. The highest reduction in C'_L was observed at $\alpha = 12^\circ$. Taking into account previous studies on square cylinders, a critical angle of attack exists for the studied cactus-shaped cylinder between 12° and 13° . Similar to the square cylinder, the critical behaviour is caused by a reattachment of the shear layer that separates at the front rib to the back rib as was confirmed by quantitative flow visualisations using PIV. These observations are also supported by the mean surface pressure distribution at this angle of attack, which showed the highest pressure difference between top and bottom cavities, resulting in the maximum lift coefficient value. In addition, at the critical angle the absolute lowest C_p was recorded inside the rear cavity contributing to the lowest drag.

Previous studies on the square cylinder with modified corners found a shift of the critical angle of attack towards lower values compared to the square cylinder. This effect was not observed in the present study where α_{cr} of the cactus-shaped cylinder falls within the reported range of the square cylinder. This could be attributed to the small tip radius of the ribs as well as to the effect of large vortices trapped in the side cavities.

Comparing values of the aerodynamic coefficients of the cactus-shaped cylinder to those of the square cylinder a reduction of the mean drag was observed for $\alpha \leq 30^\circ$. The mean lift coefficient was higher for the studied shape at all angles of attack except for the two extreme orientations where mean lift vanishes due to the symmetry. At angles of attack below critical, both C'_L and St showed similar values to those of the square cylinder. Moreover, a reduction in Strouhal number was observed with further increase in α .

Studies on Saguaro-inspired cylinders with many ribs demonstrated their ability to reduce drag and unsteady lift fluctuations, thus helping Saguaro cacti to deal with

aerodynamic loads in their environment. The present study on a succulent-inspired cylinder with four ribs suggests that this shape also provides aerodynamic benefits to actual plants albeit over a limited range of angular orientations. Typically, natural evolution is a result of a competition between various biotic and abiotic factors that affect survival and development of an organism. In complex living systems, like plants, the minimum requirement for their survival and normal functioning is usually determined by a single factor that limits the development of other functions and features (Niklas, 1992). Therefore, while aerodynamics may be one of the factors driving the adaptation of succulents to their environment, it is probably not the critical one and other factors, e.g. heat transfer and water collection and retention may be more dominant.

In the current succulent-inspired study, as well as in previous investigations on cacti with many ribs (Talley et al., 2001; Wang et al., 2014; Letchford et al., 2016), the plant geometry was simplified to a 2D cylinder as the focus was on the aerodynamic influence of the plant's ribs. However, cacti and succulents exhibit further features that may influence their aerodynamics, such as ridges, spines, and branches. In future studies, these elements could be successively added to explore their potential to further enhance the aerodynamic properties of these plants.

CRedit authorship contribution statement

Oleksandr Zhdanov: Conceptualization, Methodology, Investigation, Formal analysis, Data curation, Writing – original draft, Writing – review&editing, Visualization. Richard Green: Methodology, Investigation, Formal analysis, Supervision, Resources, Writing – review&editing. Angela Busse: Conceptualization, Resources, Supervision, Writing – review&editing

Acknowledgements

The authors gratefully acknowledge access to the low-speed National Wind Tunnel Facility funded by the Engineering and Physical Sciences Research Council, grant number EP/L024888/1, and support by the University of Glasgow's Lord Kelvin/Adam Smith (LKAS) PhD scholarship scheme.

Chapter 11

Conclusions and future work

11.1 Conclusions

This PhD thesis presents the results of plant biomechanics and fluid dynamics based research on different aspects of wind-plant interaction. In the first part, the focus is on the influence of various types of mechanical stresses, in particular wind, on a widely used model organism in plant science – *Arabidopsis*. A bespoke wind tunnel facility alongside a dedicated mechanical characterisation method were developed. The results of the conducted experiments on continuous exposure of *Arabidopsis* to wind and brushing treatments contribute to systematic studies on the effects of wind and other types of mechanical stresses on plants expanding the current knowledge in these fields. In the second part of this thesis, the aerodynamic properties of succulent-inspired cylinders with a low number of ribs were investigated using experimental and numerical techniques. This study provides new insights into the passive flow control mechanism of cacti and succulents and the potential for biomimetic modifications to bluff bodies of similar cross-sections.

All research objectives outlined in chapter 2 were achieved. In addition to the summaries and conclusions provided in each chapter of the present thesis, the key conclusions are compiled below followed by suggestions for future work. Following the structure of the thesis, this section is separated into two parts on the two distinct studies that comprise this project.

11.1.1 Response of *Arabidopsis* to wind-induced and other types of mechanical stress

- A bespoke wind tunnel with a suitable environment for the growth and development of small plants was designed and built. The wind tunnel provides a well characterised and controlled environment for experiments on the effects of continuous wind exposure on the model plant *Arabidopsis*. In this PhD project, it was successfully used for the investigations of the acclimation response of *Arabidopsis* to a constant unidirectional wind. Moreover, this bespoke facility proved its versatility during a dandelion seed dispersal study that was carried out in collaboration with the University of Edinburgh (the latter study does not form part of this thesis).
- The dynamic forced vibration method which was developed for the mechanical characterisation of *Arabidopsis* inflorescence stems proved its robustness and reliability in the later studies of this PhD project, where effects of wind and mechanical perturbations on the growth and development of *Arabidopsis* were investigated.
- A positive anemotropic response of young *Arabidopsis* seedlings to a constant unidirectional wind was discovered. This is the first clear demonstration of this type of tropic response in any plant system.
- The experiments on continuous exposure to a constant unidirectional wind revealed the acclimation response of *Arabidopsis* to this type of treatment. The observed changes to the whole plant morphology, as well as alterations in the mechanical properties of the primary inflorescence stem, are adaptive to this environment. They help *Arabidopsis* to reduce the force experienced from the wind and at the same time make the stem more rigid allowing it to withstand the applied mechanical stress. The characterisation of the anatomical tissue organisation and ion content of the stem also showed wind-induced changes that resulted in its strengthening. Moreover, the repeatability of the acclimation strategy and observed changes were confirmed through repeated experiments.
- The experiments where two different types of directional brushing treatments were applied to *Arabidopsis* demonstrated that some wind-induced effects can be reproduced by brushing. However, while the thigmomorphogenetic response

in terms of growth inhibition and reduction in stem diameter resembles those to the wind treatment, the changes in the modulus of elasticity were in the opposite direction. Furthermore, the magnitude of these responses is dependent on the brushing direction, but not on the surface texture of the brushing material. In contrast, none of the applied brushing treatments affected the branching of *Arabidopsis*, whereas a reduction in branching was observed in the experiments with wind exposure. This observation confirms that the reduction in the number of branches is an acclimation response to wind, which does not occur in the case of brushing. In addition, unidirectional brushing evoked a positive thigmotropic response in the *Arabidopsis* shoot, which has not been reported before for this plant, and resembles the anemotropic response to a constant unidirectional wind. Overall, the results suggest that a carefully designed brushing treatment can be used to mimic some aspects of wind influence on plants. But attention must be paid to the interpretation of results and their extrapolation to wind-induced effects.

11.1.2 Aerodynamics of succulent-inspired cylinders

Two different succulent-shaped ribbed cylinders were studied to extend previous research on Saguaro-inspired cactus-shaped cylinders to similar plants with a lower number of ribs. The 4-rib cylinder was investigated using both wind tunnel experiments and the 2D URANS simulations, whilst the 3-rib shape was investigated using 2D URANS approach only.

- The investigated succulent-inspired cylinder with four ribs, which resembles a square cylinder with modified cross-section, demonstrated no Reynolds number dependence of its aerodynamic characteristics within the experimentally tested range from 50,000 to 100,000. Based on the results of 2D URANS investigations the bottom limit of this range can be lowered to 20,000.
- The studied shape exhibited a strong angle of attack dependence with the presence of a critical angle of attack of approximately 13° , at which the shear layer separating from the front rib reattaches to the back rib. At this angle of attack, drag and fluctuating lift forces attain their minima, while mean lift and Strouhal number have their highest values. This behaviour was found to be similar to the conventional square cylinder.
- Compared to the square cylinder, the succulent-inspired cylinder with four

ribs demonstrated aerodynamic benefits in terms of reduced drag albeit over a limited range of angles of attack.

- In contrast to many other modifications to the square cylinder cross-section, e.g. corner rounding or chamfering, the value of the critical angle of attack remained unaffected for the studied shape.
- When comparing the 2D URANS investigation with experimental results for the same succulent-inspired cylinder with four ribs, qualitative agreement in the dependency of the aerodynamics coefficients and Strouhal number on the angle of attack was observed. However, quantitative differences in the values of these properties and in critical angle of attack were present.
- Overall, the 2D URANS approach can be employed to study key features of the flow past succulent-shaped cylinders with a low number of ribs, but for accurate quantitative results experiments or 3D eddy-resolved simulations are required.
- The 2D URANS investigation of the flow past a succulent-inspired cylinder with three ribs showed strong angle of attack dependence of this shape and its drag reduction potential compared to equilateral triangular cylinders. However, based on the previous conclusion further investigations are required.

11.2 Future work

While the results of the studies reported in this PhD thesis provided new insights to the fields of plant biomechanics and aerodynamics, they also raise new research questions that could be explored in future work.

11.2.1 Response of *Arabidopsis* to wind-induced and other types of mechanical stress

- The wind speed of 5 m/s used in the current work falls into a high but not extreme wind speed range experienced by *Arabidopsis* in its natural environment. To provide insight into the acclimation response of *Arabidopsis* to wind speeds ranging from more moderate to very extreme, investigations where *Arabidopsis* is subjected to higher and lower constant unidirectional wind could be carried out.

- Due to a large number of available *Arabidopsis* ecotypes and mutants, genotype dependent acclimation to wind could be explored. Furthermore, by selecting suitable mutants (e.g. agravitropic mutants, such as scarecrow (*scr*)), interaction between different types of tropic responses, i.e. gravitropic, phototropic, thigmotropic, and anemotropic, in *Arabidopsis* could also be studied. In addition, mutants such as PIN1 could help to explore dependency of acclimation strategy on the plant morphology.
- The wind tunnel floor could be modified by incorporation of a rotation mechanism for the plant pots. This would allow studies on bi- and multidirectional wind influence on *Arabidopsis*. Furthermore, this modification could be used to verify the observed anemotropic response by subjecting plants in slowly rotating pots to constant unidirectional wind. However, prior experiments on the potential influence of constant pot rotation on *Arabidopsis* would be required as well as tests to establish a suitable rotational speed.
- An upgrade of the fan control system would allow for digital and the fully automated adjustment of the flow speed inside the test section. This would enable experiments in which plants are subjected to variable wind speeds or wind gusts. In conjunction with the previous suggestion, it would also allow to expose plants to variable wind coming from different directions.
- The temporal evolution of the observed tropic responses could be investigated and compared with those reported for gravitropism. In addition, the influence of different types of mechanical stresses on the growth rate of *Arabidopsis* could be measured.
- The influence of the developmental stage of *Arabidopsis*, at which different types of mechanical stresses are applied, on the induced effects could be also explored.

11.2.2 Succulent-inspired passive flow control

- All the investigations on the succulent- and cactus-inspired cylinders reported in literature, as well as those carried out in this project, studied the influence of either ribs or spines on the aerodynamic properties separately. In addition to these two distinct features of cacti and succulents, their ribs have ridges that also modify the flow field around these plants and could provide

further aerodynamic benefits. In future studies, the combined potential of the aforementioned features of succulents and cacti to further enhance their aerodynamic properties and passive flow control ability could be explored.

- Studies with multiple succulent-inspired cylinders that resemble the actual bush-like structure of many succulents could be carried out. This would provide information on the collective aerodynamic behaviour of multiple stems and its influence on the forces experienced by the individual stems and the whole plant. In addition, while the investigations in this PhD project were carried on cylinders with infinite span, succulents in the natural environment have a free end. This could be taken into account in future studies.
- A parametric study of the cavity size and rib-tip curvature could be carried out to find the optimum values of these parameters for drag reduction. Since cacti and succulents shrink and swell depending on the water availability, which, as well as wind conditions, is seasonal, the findings of this investigation could answer the question whether these mechanisms are interdependent and present an evolutionary adaptation to the wind conditions and water availability changes in the local environment.
- Experiments on dynamic stability and vortex-induced vibrations of succulent-inspired cylinders with a low number of ribs would provide information whether their shape helps succulents to remain stable in the windy conditions.
- Previous studies show that the aerodynamic properties of circular cylinders and square cylinders with rounded corners are dependent on the test conditions. Based on this, the effect of turbulence intensity on the aerodynamic properties of the succulent-inspired cylinder with four ribs could be investigated.
- Wind tunnel tests using real cacti or succulents could be conducted. Alternatively, models based on the 3D scans of actual plants could be manufactured for this purpose. These studies could also take into account all of the aforementioned suggestions for future work on succulent-inspired passive flow control.

Bibliography

- Abboud, J. E., Karaki, W. S., and Oweis, G. F. Particle image velocimetry measurements in the wake of a cactus-shaped cylinder. *Journal of Fluids Engineering*, 133(9):094502, 2011. doi: 10.1115/1.4004824.
- Achenbach, E. Distribution of local pressure and skin friction around a circular cylinder in cross-flow up to $Re = 5 \times 10^6$. *Journal of Fluid Mechanics*, 34(4): 625–639, 1968. doi: 10.1017/S0022112068002120.
- Achenbach, E. Influence of surface roughness on the cross-flow around a circular cylinder. *Journal of Fluid Mechanics*, 46(2):321–335, 1971. doi: 10.1017/S0022112071000569.
- Al-Zube, L., Sun, W., Robertson, D., and Cook, D. The elastic modulus for maize stems. *Plant Methods*, 14(1):11, 2018. doi: 10.1186/s13007-018-0279-6.
- Al-Zube, L. A., Robertson, D. J., Edwards, J. N., Sun, W., and Cook, D. D. Measuring the compressive modulus of elasticity of pith-filled plant stems. *Plant Methods*, 13(1):99, 2017. doi: 10.1186/s13007-017-0250-y.
- Alam, M. M., Moriya, M., and Sakamoto, H. Aerodynamic characteristics of two side-by-side circular cylinders and application of wavelet analysis on the switching phenomenon. *Journal of Fluids and Structures*, 18(3-4):325–346, 2003a. doi: 10.1016/j.jfluidstructs.2003.07.005.
- Alam, M. M., Moriya, M., Takai, K., and Sakamoto, H. Fluctuating fluid forces acting on two circular cylinders in a tandem arrangement at a subcritical Reynolds number. *Journal of Wind Engineering and Industrial Aerodynamics*, 91(1-2):139–154, 2003b. doi: 10.1016/S0167-6105(02)00341-0.
- Alexandratos, N. and Bruinsma, J. World agriculture towards 2030/2050: the 2012 revision. 2012. doi: 10.22004/ag.econ.288998.

- Allen, M., Dube, O., Solecki, W., Aragón-Durand, F., Cramer, W., Humphreys, S., Kainuma, M., Kala, J., Mahowald, N., Mulugetta, Y., Perez, R., Wairiu, M., and Zickfeld, K. Framing and context. In: *Global Warming of 1.5 °C. An IPCC Special Report on the impacts of global warming of 1.5 °C above pre-industrial levels and related global greenhouse gas emission pathways, in the context of strengthening the global response to the threat of climate change* (eds Masson-Delmotte, V. et al.). *IPCC/WMO*, pages 47–92, 2018.
- Anten, N. P., Alcalá-Herrera, R., Schieving, F., and Onoda, Y. Wind and mechanical stimuli differentially affect leaf traits in *Plantago major*. *New Phytologist*, 188(2): 554–564, 2010. doi: 10.1111/j.1469-8137.2010.03379.x.
- Apaçoğlu, B. and Aradağ, S. CFD analysis of uncontrolled and controlled turbulent flow over a circular cylinder. In *6th International Advanced Technologies Symposium (IATS'11)*, volume 16-18, pages 60–65, 2011.
- Apelt, C., West, G., and Szewczyk, A. A. The effects of wake splitter plates on the flow past a circular cylinder in the range $10^4 < R < 5 \times 10^4$. *Journal of Fluid Mechanics*, 61(1):187–198, 1973. doi: 10.1017/S0022112073000649.
- ASTM. E1875-13 standard test method for dynamic Young's modulus, shear modulus, and Poisson's ratio by sonic resonance. 2003. doi: 10.1520/E1875-13.
- ASTM. E1876-15 standard test method for dynamic Young's modulus, shear modulus, and Poisson's ratio by impulse excitation of vibration. 2015. doi: 10.1520/E1876-15.
- Babu, P. and Mahesh, K. Aerodynamic loads on cactus-shaped cylinders at low Reynolds numbers. *Physics of Fluids*, 20(3):035112, 2008. doi: 10.1063/1.2887982.
- Badham, E. R. Tropisms in the mushroom *Psilocybe cubensis*. *Mycologia*, 74(2): 275–279, 1982. doi: 10.1080/00275514.1982.12021501.
- Bai, H. and Alam, M. M. Dependence of square cylinder wake on Reynolds number. *Physics of Fluids*, 30(1):015102, 2018. doi: 10.1063/1.4996945.
- Bailey, S., Walters, R. G., Jansson, S., and Horton, P. Acclimation of *Arabidopsis thaliana* to the light environment: the existence of separate low light and high light responses. *Planta*, 213(5):794–801, 2001. doi: 10.1007/s004250100556.

- Baker, C., Sterling, M., and Berry, P. A generalised model of crop lodging. *Journal of Theoretical Biology*, 363:1–12, 2014. doi: 10.1016/j.jtbi.2014.07.032.
- Bar-On, Y. M., Phillips, R., and Milo, R. The biomass distribution on Earth. *Proceedings of the National Academy of Sciences*, 115(25):6506–6511, 2018. doi: 10.1073/pnas.1711842115.
- Barlow, J. B., Rae, W. H., and Pope, A. *Low-speed wind tunnel testing*. John Wiley & Sons, 1999.
- Barros, J., Serk, H., Granlund, I., and Pesquet, E. The cell biology of lignification in higher plants. *Annals of Botany*, 115(7):1053–1074, 2015. doi: 10.1093/aob/mcv046.
- Bearman, P. and Harvey, J. Control of circular cylinder flow by the use of dimples. *AIAA Journal*, 31(10):1753–1756, 1993. doi: 10.2514/3.11844.
- Bearman, P. and Trueman, D. An investigation of the flow around rectangular cylinders. *The Aeronautical Quarterly*, 23(3):229–237, 1972. doi: 10.1017/S0001925900006119.
- Beauzamy, L., Nakayama, N., and Boudaoud, A. Flowers under pressure: ins and outs of turgor regulation in development. *Annals of Botany*, 114(7):1517–1533, 2014. doi: 10.1093/aob/mcu187.
- Bell, C. and Rose, D. Light measurement and the terminology of low. *Plant, Cell & Environment*, 4(2):89–96, 1981. doi: 10.1111/j.1365-3040.1981.tb01043.x.
- Benim, A., Pasqualotto, E., and Suh, S. Modelling turbulent flow past a circular cylinder by RANS, URANS, LES and DES. *Progress in Computational Fluid Dynamics, an International Journal*, 8(5):299–307, 2008. doi: 10.1504/PCFD.2008.019483.
- Berry, P. and Spink, J. A physiological analysis of oilseed rape yields: past and future. *The Journal of Agricultural Science*, 144:381, 2006. doi: 10.1017/S0021859606006423.
- Berry, P., Sterling, M., Spink, J., Baker, C., Sylvester-Bradley, R., Mooney, S., Tams, A., and Ennos, A. Understanding and reducing lodging in cereals. *Advances in Agronomy*, 84(04):215–269, 2004. doi: 10.1016/S0065-2113(04)84005-7.

- Berthier, S. and Stokes, A. Phototropic response induced by wind loading in Maritime pine seedlings (*Pinus pinaster* aït.). *Journal of Experimental Botany*, 56(413):851–856, 2005. doi: 10.1093/jxb/eri071.
- Berthier, S. and Stokes, A. Righting response of artificially inclined maritime pine (*Pinus pinaster*) saplings to wind loading. *Tree Physiology*, 26(1):73–79, 2006. doi: 10.1093/treephys/26.1.73.
- Bichet, A., Desnos, T., Turner, S., Grandjean, O., and Höfte, H. BOTERO1 is required for normal orientation of cortical microtubules and anisotropic cell expansion in *Arabidopsis*. *The Plant Journal*, 25(2):137–148, 2001. doi: 10.1111/j.1365-313X.2001.00946.x.
- Biddington, N. L. The effects of mechanically-induced stress in plants—a review. *Plant Growth Regulation*, 4(2):103–123, 1986. doi: 10.1007/BF00025193.
- Blevins, R. D. *Formulas for natural frequency and mode shape*. Van Nostrand Reinhold, 1979.
- Boldes, U., Golberg, A., Di Leo, J. M., Colman, J., and Scarabino, A. Canopy flow and aspects of the response of plants protected by herbaceous shelterbelts and wood fences. *Journal of Wind Engineering and Industrial Aerodynamics*, 90(11):1253–1270, 2002. doi: 10.1016/S0167-6105(02)00256-8.
- Bossdorf, O. and Pigliucci, M. Plasticity to wind is modular and genetically variable in *Arabidopsis thaliana*. *Evolutionary Ecology*, 23(5):669–685, 2009. doi: 10.1007/s10682-008-9263-3.
- Boyes, D. C., Zayed, A. M., Ascenzi, R., McCaskill, A. J., Hoffman, N. E., Davis, K. R., and Görlach, J. Growth stage-based phenotypic analysis of *Arabidopsis*: a model for high throughput functional genomics in plants. *The Plant Cell*, 13(7):1499–1510, 2001. doi: 10.1105/TPC.010011.
- Braam, J. In touch: plant responses to mechanical stimuli. *New Phytologist*, 165(2):373–389, 2005. doi: 10.1111/j.1469-8137.2004.01263.x.
- Braam, J. and Davis, R. W. Rain-, wind-, and touch-induced expression of calmodulin and calmodulin-related genes in *Arabidopsis*. *Cell*, 60(3):357–364, 1990. doi: 10.1016/0092-8674(90)90587-5.

- Brulé, V., Rafsanjani, A., Pasini, D., and Western, T. L. Hierarchies of plant stiffness. *Plant Science*, 250:79–96, 2016. doi: 10.1016/j.plantsci.2016.06.002.
- Brummell, D. A. Cell wall acidification and its role in auxin-stimulated growth. *Journal of Experimental Botany*, 37(2):270–276, 1986. doi: 10.1093/jxb/37.2.270.
- Burgess, A. J., Retkute, R., Preston, S. P., Jensen, O. E., Pound, M. P., Pridmore, T. P., and Murchie, E. H. The 4-dimensional plant: effects of wind-induced canopy movement on light fluctuations and photosynthesis. *Frontiers in Plant Science*, 7: 1392, 2016. doi: 10.3389/fpls.2016.01392.
- Burström, H., Uhrström, I., and Wurscher, R. Growth, turgor, water potential, and Young’s modulus in pea internodes. *Physiologia Plantarum*, 20(1):213–231, 1967. doi: 10.1111/j.1399-3054.1967.tb07157.x.
- Bushnell, D. M. and Moore, K. Drag reduction in nature. *Annual Review of Fluid Mechanics*, 23(1):65–79, 1991. doi: 10.1146/annurev.fl.23.010191.000433.
- Calderon, C., Ward, E., Freeman, J., and McCartney, A. Detection of airborne fungal spores sampled by rotating-arm and Hirst-type spore traps using polymerase chain reaction assays. *Journal of Aerosol Science*, 33(2):283–296, 2002. doi: 10.1016/S0021-8502(01)00179-3.
- Caldwell, M. M. Plant gas exchange at high wind speeds. *Plant Physiology*, 46(4): 535–537, 1970. doi: 10.1104/pp.46.4.535.
- Cao, J., Tamura, Y., and Yoshida, A. Wind tunnel study on aerodynamic characteristics of shrubby specimens of three tree species. *Urban Forestry & Urban Greening*, 11(4):465–476, 2012. doi: 10.1016/j.ufug.2012.05.003.
- Carassale, L., Freda, A., and Marre-Brunenghi, M. Experimental investigation on the aerodynamic behavior of square cylinders with rounded corners. *Journal of Fluids and Structures*, 44:195–204, 2014. doi: 10.1016/j.jfluidstructs.2013.10.010.
- Caspar, T. and Pickard, B. G. Gravitropism in a starchless mutant of Arabidopsis. *Planta*, 177(2):185–197, 1989. doi: 10.1007/BF00392807.
- Chaffey, N., Cholewa, E., Regan, S., and Sundberg, B. Secondary xylem development in Arabidopsis: a model for wood formation. *Physiologia Plantarum*, 114(4):594–600, 2002. doi: 10.1034/j.1399-3054.2002.1140413.x.

- Chauvet, H., Pouliquen, O., Forterre, Y., Legué, V., and Moulia, B. Inclination not force is sensed by plants during shoot gravitropism. *Scientific Reports*, 6:35431, 2016. doi: 10.1038/srep35431.
- Chehab, E. W., Eich, E., and Braam, J. Thigmomorphogenesis: a complex plant response to mechano-stimulation. *Journal of Experimental Botany*, 60(1):43–56, 2009. doi: 10.1093/jxb/ern315.
- Cheng, W., Pullin, D., and Samtaney, R. Large-eddy simulation of flow over a grooved cylinder up to transcritical Reynolds numbers. *Journal of Fluid Mechanics*, 835:327–362, 2018. doi: 10.1017/jfm.2017.767.
- Choi, H., Park, H., Sagong, W., and Lee, S.-i. Biomimetic flow control based on morphological features of living creatures. *Physics of Fluids*, 24(12):121302, 2012. doi: 10.1063/1.4772063.
- Chum, H. L., Warner, E., Seabra, J. E., and Macedo, I. C. A comparison of commercial ethanol production systems from Brazilian sugarcane and US corn. *Biofuels, Bioproducts and Biorefining*, 8(2):205–223, 2014. doi: 10.1002/bbb.1448.
- Connor, R. *The United Nations world water development report 2015: water for a sustainable world*, volume 1. UNESCO publishing, 2015.
- Cordero, R. A. Ecophysiology of *Cecropia schreberiana* saplings in two wind regimes in an elfin cloud forest: growth, gas exchange, architecture and stem biomechanics. *Tree Physiology*, 19(3):153–163, 1999. doi: 10.1093/treephys/19.3.153.
- Cosgrove, D. and Steudle, E. Water relations of growing pea epicotyl segments. *Planta*, 153(4):343–350, 1981. doi: 10.1007/BF00384253.
- Coutand, C. and Moulia, B. Biomechanical study of the effect of a controlled bending on tomato stem elongation: local strain sensing and spatial integration of the signal. *Journal of Experimental Botany*, 51(352):1825–1842, 2000. doi: 10.1093/jexbot/51.352.1825.
- Coutand, C., Dupraz, C., Jaouen, G., Ploquin, S., and Adam, B. Mechanical stimuli regulate the allocation of biomass in trees: demonstration with young *Prunus avium* trees. *Annals of Botany*, 101(9):1421–1432, 2008. doi: 10.1093/aob/mcn054.

- Coutand, C., Chevolot, M., Lacointe, A., Rowe, N., and Scotti, I. Mechanosensing of stem bending and its interspecific variability in five neotropical rainforest species. *Annals of Botany*, 105(2):341–347, 2010. doi: 10.1093/aob/mcp286.
- Cummins, C., Seale, M., Macente, A., Certini, D., Mastropaolo, E., Viola, I. M., and Nakayama, N. A separated vortex ring underlies the flight of the dandelion. *Nature*, 562(7727):414–418, 2018. doi: 10.1038/s41586-018-0604-2.
- Curry, A. Ecology. Deadly flights. *Science*, 325(5939):386–387, 2009. doi: 10.1126/science.325_386.
- de Langre, E. Effects of wind on plants. *Annual Review of Fluid Mechanics*, 40: 141–168, 2008. doi: 10.1146/annurev.fluid.40.111406.102135.
- de Langre, E. Plant vibrations at all scales: a review. *Journal of Experimental Botany*, 70(14):3521–3531, 2019. doi: 10.1093/jxb/erz209.
- de Langre, E., Gutierrez, A., and Cossé, J. On the scaling of drag reduction by reconfiguration in plants. *Comptes Rendus Mécanique*, 340(1-2):35–40, 2012. doi: 10.1016/j.crme.2011.11.005.
- de Langre, E., Penalver, O., Hemon, P., Frachisse, J.-M., Bogeat-Triboulot, M.-B., Niez, B., Badel, E., and Moulia, B. Nondestructive and fast vibration phenotyping of plants. *Plant Phenomics*, 2019:6379693, 2019. doi: 10.34133/2019/6379693.
- Der Loughian, C., Tadrist, L., Allain, J.-M., Diener, J., Moulia, B., and de Langre, E. Measuring local and global vibration modes in model plants. *Comptes Rendus Mécanique*, 342(1):1–7, 2014. doi: 10.1016/j.crme.2013.10.010.
- Derzaph, T. L. and Hamilton, H. J. Effects of wind on virtual plants in animation. *International Journal of Computer Games Technology*, 2013, 2013. doi: 10.1155/2013/674848.
- Diener, J., Rodriguez, M., Baboud, L., and Reveret, L. Wind projection basis for real-time animation of trees. In *Computer Graphics Forum*, volume 28, pages 533–540. Wiley Online Library, 2009. doi: 10.1111/j.1467-8659.2009.01393.x.
- Dixon, M. and Grace, J. Effect of wind on the transpiration of young trees. *Annals of Botany*, 53(6):811–819, 1984. doi: 10.1093/oxfordjournals.aob.a086751.

- Drake, B., Raschke, K., and Salisbury, F. Temperature and transpiration resistances of *Xanthium* leaves as affected by air temperature, humidity, and wind speed. *Plant Physiology*, 46(2):324–330, 1970. doi: 10.1104/pp.46.2.324.
- Dümmer, M., Forreiter, C., and Galland, P. Gravitropism in *Arabidopsis thaliana*: Root-specific action of the EHB gene and violation of the resultant law. *Journal of Plant Physiology*, 189:24–33, 2015. doi: 10.1016/j.jplph.2015.09.008.
- El-Makdah, A. M. and Oweis, G. F. The flow past a cactus-inspired grooved cylinder. *Experiments in Fluids*, 54(2):1464, 2013. doi: 10.1007/s00348-013-1464-z.
- Ennos, A. The mechanics of the flower stem of the sedge *Carex acutiformis*. *Annals of Botany*, 72(2):123–127, 1993. doi: 10.1006/anbo.1993.1089.
- Ennos, A. Wind as an ecological factor. *Trends in Ecology & Evolution*, 12(3):108–111, 1997. doi: 10.1016/S0169-5347(96)10066-5.
- Ennos, A., Spatz, H.-C., and Speck, T. The functional morphology of the petioles of the banana, *Musa textilis*. *Journal of Experimental Botany*, 51(353):2085–2093, 2000. doi: 10.1093/jexbot/51.353.2085.
- Etnier, S. A. and Vogel, S. Reorientation of daffodil (*Narcissus*: Amaryllidaceae) flowers in wind: drag reduction and torsional flexibility. *American Journal of Botany*, 87(1):29–32, 2000. doi: 10.2307/2656682.
- Evans, M. L. and Vesper, M. J. An improved method for detecting auxin-induced hydrogen ion efflux from corn coleoptile segments. *Plant Physiology*, 66(4):561–565, 1980. doi: 10.1104/pp.66.4.561.
- Evenson, R. E. and Gollin, D. Assessing the impact of the Green Revolution, 1960 to 2000. *Science*, 300(5620):758–762, 2003. doi: 10.1126/science.1078710.
- Faisal, T. R., Abad, E. M. K., Hristozov, N., and Pasini, D. The impact of tissue morphology, cross-section and turgor pressure on the mechanical properties of the leaf petiole in plants. *Journal of Bionic Engineering*, 7(4):S11–S23, 2010. doi: 10.1016/S1672-6529(09)60212-2.
- Falk, S., Hertz, C. H., and Virgin, H. I. On the relation between turgor pressure and tissue rigidity. I: Experiments on resonance frequency and tissue rigidity. *Physiologia Plantarum*, 11(4):802–817, 1958. doi: 0.1111/j.1399-3054.1958.tb08274.x.

- Finch-Savage, W. E. and Leubner-Metzger, G. Seed dormancy and the control of germination. *New Phytologist*, 171(3):501–523, 2006. doi: 10.1111/j.1469-8137.2006.01787.x.
- Fiorani, F. and Schurr, U. Future scenarios for plant phenotyping. *Annual Review of Plant Biology*, 64:267–291, 2013. doi: 10.1146/annurev-arplant-050312-120137.
- Fish, F. and Lauder, G. V. Passive and active flow control by swimming fishes and mammals. *Annual Review of Fluid Mechanics*, 38:193–224, 2006. doi: 10.1146/annurev.fluid.38.050304.092201.
- Fitt, B. D., Walklate, P., McCartney, H., Bainbridge, A., Creighton, N., Hirst, J., Lacey, M., and Legg, B. A rain tower and wind tunnel for studying the dispersal of plant pathogens by rain and wind. *Annals of Applied Biology*, 109(3):661–671, 1986. doi: 10.1111/j.1744-7348.1986.tb03224.x.
- Fukaki, H., Fujisawa, H., and Tasaka, M. Gravitropic response of inflorescence stems in *Arabidopsis thaliana*. *Plant Physiology*, 110(3):933–943, 1996a. doi: 10.1104/pp.110.3.933.
- Fukaki, H., Fujisawa, H., and Tasaka, M. SGR1, SGR2, and SGR3: novel genetic loci involved in shoot gravitropism in *Arabidopsis thaliana*. *Plant Physiology*, 110(3):945–955, 1996b. doi: 10.1104/pp.110.3.945.
- Gälweiler, L., Guan, C., Müller, A., Wisman, E., Mendgen, K., Yephremov, A., and Palme, K. Regulation of polar auxin transport by AtPIN1 in *Arabidopsis* vascular tissue. *Science*, 282(5397):2226–2230, 1998. doi: 10.1126/science.282.5397.2226.
- Gardiner, B., Schuck, A. R. T., Schelhaas, M.-J., Orazio, C., Blennow, K., and Nicoll, B. *Living with storm damage to forests*, volume 3. European Forest Institute Joensuu, 2013.
- Gardiner, B., Berry, P., and Moulia, B. Wind impacts on plant growth, mechanics and damage. *Plant Science*, 245:94–118, 2016. doi: 10.1016/j.plantsci.2016.01.006.
- Gardiner, B. A. and Quine, C. P. Management of forests to reduce the risk of abiotic damage—a review with particular reference to the effects of strong winds. *Forest Ecology and Management*, 135(1-3):261–277, 2000. doi: 10.1016/S0378-1127(00)00285-1.

- Garner, W. W. Comparative responses of long-day and short-day plants to relative length of day and night. *Plant Physiology*, 8(3):347–356, 1933. doi: 10.1104/pp.8.3.347.
- Gartner, B. L. Root biomechanics and whole-plant allocation patterns: responses of tomato plants to stem flexure. *Journal of Experimental Botany*, 45(11):1647–1654, 1994. doi: 10.1093/jxb/45.11.1647.
- Gastineau, G. and Soden, B. J. Model projected changes of extreme wind events in response to global warming. *Geophysical Research Letters*, 36(10), 2009. doi: 10.1029/2009GL037500.
- Geagea, L., Huber, L., Sache, I., Flura, D., McCartney, H., and Fitt, B. Influence of simulated rain on dispersal of rust spores from infected wheat seedlings. *Agricultural and Forest Meteorology*, 101(1):53–66, 2000. doi: 10.1016/S0168-1923(99)00155-0.
- Geer, G. A., Wold, M. P., Bo, B., Gamow, R. I., et al. Phycomyces: control of transpiration and the anemotropic reversal. *Experimental Mycology*, 14(3):268–273, 1990. doi: 10.1016/0147-5975(90)90024-N.
- Geitmann, A. and Ortega, J. K. Mechanics and modeling of plant cell growth. *Trends in Plant Science*, 14(9):467–478, 2009. doi: 10.1016/j.tplants.2009.07.006.
- Gillies, J., Nickling, W., and King, J. Drag coefficient and plant form response to wind speed in three plant species: Burning Bush (*Euonymus alatus*), Colorado Blue Spruce (*Picea pungens glauca.*), and Fountain Grass (*Pennisetum setaceum*). *Journal of Geophysical Research: Atmospheres*, 107(D24):ACL–10, 2002. doi: 10.1029/2001JD001259.
- Gladala-Kostarz, A., Doonan, J. H., and Bosch, M. Mechanical stimulation in *Brachypodium distachyon*: Implications for fitness, productivity, and cell wall properties. *Plant, Cell & Environment*, 43(5):1314–1330, 2020. doi: 10.1111/pce.13724.
- Goodman, A. and Ennos, A. A comparative study of the response of the roots and shoots of sunflower and maize to mechanical stimulation. *Journal of Experimental Botany*, 47(10):1499–1507, 1996. doi: 10.1093/jxb/47.10.1499.
- Gosselin, F. P. Mechanics of a plant in fluid flow. *Journal of Experimental Botany*, 70(14):3533–3548, 2019. doi: 10.1093/jxb/erz288.

- Goubet, F., Barton, C. J., Mortimer, J. C., Yu, X., Zhang, Z., Miles, G. P., Richens, J., Liepman, A. H., Seffen, K., and Dupree, P. Cell wall glucomanan in *Arabidopsis* is synthesised by CSLA glycosyltransferases, and influences the progression of embryogenesis. *The Plant Journal*, 60(3):527–538, 2009. doi: 10.1111/j.1365-313X.2009.03977.x.
- Grace, J. The effect of wind on grasses: 1. Cuticular and stomatal transpiration. *Journal of Experimental Botany*, 25(3):542–551, 1974. doi: 10.1093/jxb/25.3.542.
- Grace, J. and Wilson, J. The boundary layer over a *Populus* leaf. *Journal of Experimental Botany*, 27(2):231–241, 1976. doi: 10.1093/jxb/27.2.231.
- Grace, J., Malcolm, D., and Bradbury, I. K. The effect of wind and humidity on leaf diffusive resistance in Sitka spruce seedlings. *Journal of Applied Ecology*, 12(3):931–940, 1975. doi: 10.2307/2402099.
- Gratani, L. Plant phenotypic plasticity in response to environmental factors. *Advances in Botany*, 2014, 2014. doi: 10.1155/2014/208747.
- Green, R. B., Gillies, E. A., and Brown, R. E. The flow field around a rotor in axial descent. *Journal of Fluid Mechanics*, 534:237–261, 2005. doi: 10.1017/S0022112005004155.
- Greenberg, A. R., Mehling, A., Lee, M., and Bock, J. H. Tensile behaviour of grass. *Journal of Materials Science*, 24(7):2549–2554, 1989. doi: 10.1007/BF01174526.
- Grierson, C., Nielsen, E., Ketelaarc, T., and Schiefelbein, J. Root hairs. *The Arabidopsis Book/American Society of Plant Biologists*, 12, 2014. doi: 10.1199/tab.0172.
- Griggs, R. F. The timberlines of Northern America and their interpretation. *Ecology*, 27(4):275–289, 1946. doi: 10.2307/1933539.
- Hanke, W., Witte, M., Miersch, L., Brede, M., Oeffner, J., Michael, M., Hanke, F., Leder, A., and Dehnhardt, G. Harbor seal vibrissa morphology suppresses vortex-induced vibrations. *Journal of Experimental Biology*, 213(15):2665–2672, 2010. doi: 10.1242/jeb.043216.
- Harder, D. L., Speck, O., Hurd, C. L., and Speck, T. Reconfiguration as a prerequisite for survival in highly unstable flow-dominated habitats. *Journal of Plant Growth Regulation*, 23(2):98–107, 2004. doi: 10.1007/s00344-004-0043-1.

- He, G. S., Li, N., and Wang, J. J. Drag reduction of square cylinders with cut-corners at the front edges. *Experiments in Fluids*, 55(6):1745, 2014. doi: 0.1007/s00348-014-1745-1.
- Hedden, R., Fredericksen, T., and Williams, S. Modeling the effect of crown shedding and streamlining on the survival of loblolly pine exposed to acute wind. *Canadian Journal of Forest Research*, 25(5):704–712, 1995. doi: 10.1139/x95-078.
- Hepworth, D. and Vincent, J. The growth response of the stems of genetically modified tobacco plants (*Nicotiana tabacum* ‘Samsun’) to flexural stimulation. *Annals of Botany*, 83(1):39–43, 1999. doi: 10.1006/anbo.1998.0784.
- Hill, T. L., Cammarano, A., Neild, S. A., and Wagg, D. J. Out-of-unison resonance in weakly nonlinear coupled oscillators. *Proceedings of the Royal Society A: Mathematical, Physical and Engineering Sciences*, 471(2173):20140659, 2015. doi: 10.1098/rspa.2014.0659.
- Hoerner, S. F. *Fluid-dynamic drag: practical information on aerodynamic drag and hydrodynamic resistance*. Published by the author, 1965.
- Höfte, H., Peaucelle, A., and Braybrook, S. Cell wall mechanics and growth control in plants: the role of pectins revisited. *Frontiers in Plant Science*, 3:121, 2012. doi: 10.3389/fpls.2012.00121.
- Hosking, J. S., MacLeod, D., Phillips, T., Holmes, C., Watson, P., Shuckburgh, E., and Mitchell, D. Changes in European wind energy generation potential within a 1.5 C warmer world. *Environmental Research Letters*, 13(5):054032, 2018. doi: 10.1088/1748-9326/aabf78.
- Howe, H. F. and Smallwood, J. Ecology of seed dispersal. *Annual Review of Ecology and Systematics*, 13(1):201–228, 1982. doi: 10.1146/annurev.es.13.110182.001221.
- Hu, J., Zhou, Y., and Dalton, C. Effects of the corner radius on the near wake of a square prism. *Experiments in Fluids*, 40(1):106, 2006. doi: 10.1007/s00348-005-0052-2.
- Huang, R., Lin, B., and Yen, S. Time-averaged topological flow patterns and their influence on vortex shedding of a square cylinder in crossflow at incidence. *Journal of Fluids and Structures*, 26(3):406–429, 2010. doi: 10.1016/j.jfluidstructs.2010.01.003.

- Huang, S., Cerny, R. E., Bhat, D. S., and Brown, S. M. Cloning of an Arabidopsis patatin-like gene, STURDY, by activation T-DNA tagging. *Plant Physiology*, 125(2):573–584, 2001. doi: 10.1104/pp.125.2.573.
- Huberman, M. and Jaffe, M. Thigmotropism in organs of the bean plant (*Phaseolus vulgaris* L.). *Annals of Botany*, 57(2):133–137, 1986. doi: 10.1093/oxfordjournals.aob.a087099.
- Igarashi, T. Characteristics of the flow around a square prism. *Bulletin of JSME*, 27(231):1858–1865, 1984. doi: 10.1299/jsme1958.27.1858.
- Igarashi, T. Drag reduction of a square prism by flow control using a small rod. *Journal of Wind Engineering and Industrial Aerodynamics*, 69:141–153, 1997. doi: 10.1016/S0167-6105(97)00150-5.
- Iino, M. Toward understanding the ecological functions of tropisms: interactions among and effects of light on tropisms. *Current Opinion in Plant Biology*, 9(1): 89–93, 2006. doi: 10.1016/j.pbi.2005.11.012.
- Inman, D. J. *Engineering vibration*. Pearson, 2013.
- Iungo, G. V. and Buresti, G. Experimental investigation on the aerodynamic loads and wake flow features of low aspect-ratio triangular prisms at different wind directions. *Journal of Fluids and Structures*, 25(7):1119–1135, 2009. doi: 10.1016/j.jfluidstructs.2009.06.004.
- Jacobs, M. and Ray, P. M. Rapid auxin-induced decrease in free space pH and its relationship to auxin-induced growth in maize and pea. *Plant Physiology*, 58(2): 203–209, 1976. doi: 10.1104/pp.58.2.203.
- Jaffe, M. and Forbes, S. Thigmomorphogenesis: the effect of mechanical perturbation on plants. *Plant Growth Regulation*, 12(3):313–324, 1993. doi: doi.org/10.1007/BF00027213.
- Jaffe, M. J. Thigmomorphogenesis: the response of plant growth and development to mechanical stimulation. *Planta*, 114(2):143–157, 1973. doi: 10.1007/BF00387472.
- Jaffe, M. J., Telewski, F. W., and Cooke, P. W. Thigmomorphogenesis: on the mechanical properties of mechanically perturbed bean plants. *Physiologia Plantarum*, 62(1):73–78, 1984. doi: 10.1111/j.1399-3054.1984.tb05925.x.

- Jaffe, M. J., Leopold, A. C., and Staples, R. C. Thigmo responses in plants and fungi. *American Journal of Botany*, 89(3):375–382, 2002. doi: 10.3732/ajb.89.3.375.
- James, K. R., Haritos, N., and Ades, P. K. Mechanical stability of trees under dynamic loads. *American Journal of Botany*, 93(10):1522–1530, 2006. doi: 10.3732/ajb.93.10.1522.
- Jiang, L., Yang, S.-L., Xie, L.-F., San Puah, C., Zhang, X.-Q., Yang, W.-C., Sundaresan, V., and Ye, D. VANGUARD1 encodes a pectin methylesterase that enhances pollen tube growth in the Arabidopsis style and transmitting tract. *The Plant Cell*, 17(2):584–596, 2005. doi: 10.1105/tpc.104.027631.
- Jie, H. and Liu, Y. Z. Large eddy simulation of turbulent flow over a cactus-analogue grooved cylinder. *Journal of Visualization*, 19(1):61–782, 2016. doi: 10.1007/s12650-015-0294-x.
- Jones, H. G. *Plants and microclimate: a quantitative approach to environmental plant physiology*. Cambridge University Press, 2013.
- Jones, L., Ennos, A. R., and Turner, S. R. Cloning and characterization of irregular xylem4 (irx4): a severely lignin-deficient mutant of Arabidopsis. *The Plant Journal*, 26(2):205–216, 2001. doi: 10.1046/j.1365-313x.2001.01021.x.
- Joseph, G., Mohammadi, M., Sterling, M., Baker, C., Gillmeier, S., Soper, D., Jesson, M., Blackburn, G., Whyatt, J., Gullick, D., et al. Determination of crop dynamic and aerodynamic parameters for lodging prediction. *Journal of Wind Engineering and Industrial Aerodynamics*, 202:104169, 2020. doi: 10.1016/j.jweia.2020.104169.
- Ju, J., Bai, H., Zheng, Y., Zhao, T., Fang, R., and Jiang, L. A multi-structural and multi-functional integrated fog collection system in cactus. *Nature Communications*, 3(1):1–6, 2012. doi: 10.1038/ncomms2253.
- Kashiwagi, T. and Ishimaru, K. Identification and functional analysis of a locus for improvement of lodging resistance in rice. *Plant Physiology*, 134(2):676–683, 2004. doi: 10.1104/pp.103.029355.
- Kawall, J., Shokr, M., and Keffer, J. A digital technique for the simultaneous measurement of streamwise and lateral velocities in turbulent flows. *Journal of Fluid Mechanics*, 133:83–112, 1983. doi: 10.1017/S0022112083001809.

- Keller, E. and Steffen, K. L. Increased chilling tolerance and altered carbon metabolism in tomato leaves following application of mechanical stress. *Physiologia Plantarum*, 93(3):519–525, 1995. doi: 10.1111/j.1399-3054.1995.tb06852.x.
- Kern, K. A., Ewers, F. W., Telewski, F. W., and Koehler, L. Mechanical perturbation affects conductivity, mechanical properties and aboveground biomass of hybrid poplars. *Tree Physiology*, 25(10):1243–1251, 2005. doi: 10.1093/treephys/25.10.1243.
- King, L. V. XII. On the convection of heat from small cylinders in a stream of fluid: Determination of the convection constants of small platinum wires with applications to hot-wire anemometry. *Philosophical Transactions of the Royal Society of London. Series A, Containing Papers of a Mathematical or Physical Character*, 214(509-522):373–432, 1914. doi: 10.1098/rsta.1914.0023.
- Kiss, J. Z., Hertel, R., and Sack, F. D. Amyloplasts are necessary for full gravitropic sensitivity in roots of *Arabidopsis thaliana*. *Planta*, 177(2):198–206, 1989. doi: 10.1007/BF00392808.
- Knight, T. A. XI. Account of some experiments on the descent of the sap in trees. in a letter from Thomas Andrew Knight, Esq. to the Right Hon. Sir Joseph Banks, Bart. KBPR S. *Philosophical Transactions of the Royal Society of London*, (93): 277–289, 1803. doi: 10.1098/rstl.1803.0011.
- Ko, J.-H., Han, K.-H., Park, S., and Yang, J. Plant body weight-induced secondary growth in *Arabidopsis* and its transcription phenotype revealed by whole-transcriptome profiling. *Plant Physiology*, 135(2):1069–1083, 2004. doi: 10.1104/pp.104.038844.
- Koornneef, M. and Meinke, D. The development of *Arabidopsis* as a model plant. *The Plant Journal*, 61(6):909–921, 2010. doi: 10.1111/j.1365-313X.2009.04086.x.
- Lamesch, P., Berardini, T. Z., Li, D., Swarbreck, D., Wilks, C., Sasidharan, R., Muller, R., Dreher, K., Alexander, D. L., Garcia-Hernandez, M., et al. The *Arabidopsis* Information Resource (TAIR): improved gene annotation and new tools. *Nucleic Acids Research*, 40(D1):D1202–D1210, 2012. doi: 10.1093/nar/gkr1090.
- Latimer, J. G. Drought or mechanical stress affects broccoli transplant growth and

- establishment but not yield. *HortScience*, 25(10):1233–1235, 1990. doi: 10.21273/HORTSCI.25.10.1233.
- Lawton, R. O. Wind stress and elfin stature in a montane rain forest tree: an adaptive explanation. *American Journal of Botany*, 69(8):1224–1230, 1982. doi: 10.1002/j.1537-2197.1982.tb13367.x.
- Lee, B. The effect of turbulence on the surface pressure field of a square prism. *Journal of Fluid Mechanics*, 69(2):263–282, 1975. doi: 10.1017/S0022112075001437.
- Legris, M. and Boccaccini, A. Stem phototropism toward blue and ultraviolet light. *Physiologia Plantarum*, 2020. doi: 10.1111/ppl.13098.
- Letchford, C., Lander, D., Case, P., Dyson, A., and Amitay, M. Bio-mimicry inspired tall buildings: The response of cactus-like buildings to wind action at Reynolds number of 10^4 . *Journal of Wind Engineering and Industrial Aerodynamics*, 150: 22–30, 2016. doi: 10.1016/j.jweia.2016.01.001.
- Levy, B. and Liu, Y. The effects of cactus inspired spines on the aerodynamics of a cylinder. *Journal of Fluids and Structures*, 39:335–346, 2013. doi: 10.1016/j.jfluidstructs.2013.03.006.
- Lim, H.-C. and Lee, S.-J. Flow control of circular cylinders with longitudinal grooved surfaces. *AIAA Journal*, 40(10):2027–2036, 2002. doi: 10.2514/2.1535.
- Liscum, E. and Briggs, W. R. Mutations in the NPH1 locus of Arabidopsis disrupt the perception of phototropic stimuli. *The Plant Cell*, 7(4):473–485, 1995. doi: 10.1105/tpc.7.4.473.
- Liu, Y. Z., Shi, L. L., and Yu, J. TR-PIV measurement of the wake behind a grooved cylinder at low Reynolds number. *Journal of Fluids and Structures*, 27(3):394–407, 2011. doi: 10.1016/j.jfluidstructs.2010.11.013.
- Liu, Y., Schieving, F., Stuefer, J. F., and Anten, N. P. The effects of mechanical stress and spectral shading on the growth and allocation of ten genotypes of a stoloniferous plant. *Annals of Botany*, 99(1):121–130, 2007. doi: 10.1093/aob/mcl230.
- Lockheed Martin. Lockheed Martin unveils Samarai flyer at unmanned vehicle conference. <https://news.lockheedmartin.com/2011-08-16-Lockheed-Martin-Unveils-Samarai-Flyer-at-Unmanned-Vehicle-Conference>, 2011. Accessed: 15-01-2021.

- López, A., Molina-Aiz, F. D., Valera, D. L., and Peña, A. Wind tunnel analysis of the airflow through insect-proof screens and comparison of their effect when installed in a Mediterranean greenhouse. *Sensors*, 16(5):690, 2016. doi: 10.3390/s16050690.
- Lopez, D., Michelin, S., and de Langre, E. Flow-induced pruning of branched systems and brittle reconfiguration. *Journal of Theoretical Biology*, 284(1):117–124, 2011. doi: 10.1016/j.jtbi.2011.06.027.
- Lysenko, D. A., Ertesvåg, I. S., and Rian, K. E. Large-eddy simulation of the flow over a circular cylinder at Reynolds number 2×10^4 . *Flow, Turbulence and Combustion*, 92(3):673–698, 2014. doi: 10.1007/s10494-012-9405-0.
- Magnuson, K. Saguaro. <https://unsplash.com/photos/T2CJ4ZI7-hg>, 2018. Accessed: 25-11-2020.
- Mahner, M. and Kary, M. What exactly are genomes, genotypes and phenotypes? And what about phenomes? *Journal of Theoretical Biology*, 186(1):55–63, 1997. doi: 10.1006/jtbi.1996.0335.
- Malik, F., Clement, R., Gethin, D., Kiernan, M., Goral, T., Griffiths, P., Beynon, D., and Parker, A. Hierarchical structures of cactus spines that aid in the directional movement of dew droplets. *Philosophical Transactions of the Royal Society A: Mathematical, Physical and Engineering Sciences*, 374(2073):20160110, 2016. doi: 10.1098/rsta.2016.0110.
- Mann, J., Tatchell, G., Dupuch, M., Harrington, R., Clark, S., and McCartney, H. Movement of apterous *Sitobion avenae* (Homoptera: Aphididae) in response to leaf disturbances caused by wind and rain. *Annals of Applied Biology*, 126(3): 417–427, 1995. doi: 10.1111/j.1744-7348.1995.tb05376.x.
- Mannini, C., Šoda, A., and Schewe, G. Unsteady RANS modelling of flow past a rectangular cylinder: Investigation of Reynolds number effects. *Computers & Fluids*, 39(9):1609–1624, 2010. doi: 10.1016/j.compfluid.2010.05.014.
- Manwell, J. F., McGowan, J. G., and Rogers, A. L. *Wind energy explained: theory, design and application*. John Wiley & Sons, 2010.
- Martínez, A. L., Martínez, D. L. V., Aiz, F. D. M., Fernández, A. A. P., and Membrive, P. M. Microclimate evaluation of a new design of insect-proof screens in a Mediterranean greenhouse. *Spanish Journal of Agricultural Research*, (2):338–352, 2014.

- Martínez, D. L. V., Álvarez, A., and Molina, F. Aerodynamic analysis of several insect-proof screens used in greenhouses. *Spanish Journal of Agricultural Research*, (4):273–279, 2006.
- Massa, G. D. and Gilroy, S. Touch modulates gravity sensing to regulate the growth of primary roots of *Arabidopsis thaliana*. *The Plant Journal*, 33(3):435–445, 2003. doi: 10.1046/j.1365-313X.2003.01637.x.
- Mayhead, G. Some drag coefficients for British forest trees derived from wind tunnel studies. *Agricultural Meteorology*, 12:123–130, 1973. doi: 10.1016/0002-1571(73)90013-7.
- McCloskey, M. A., Mosher, C. L., and Henderson, E. R. Wind energy conversion by plant-inspired designs. *PloS One*, 12(1):e0170022, 2017. doi: 10.1371/journal.pone.0170022.
- McGhee, G. R. *Convergent evolution: limited forms most beautiful*. MIT Press, 2011.
- Mehta, R. D. and Bradshaw, P. Design rules for small low speed wind tunnels. *The Aeronautical Journal (1968)*, 83(827):443–453, 1979. doi: 10.1017/S0001924000031985.
- MetOffice. Where are the windiest parts of the UK? <https://www.metoffice.gov.uk/weather/learn-about/weather/types-of-weather/wind/windiest-place-in-uk>, 2020. Accessed 11-May-2020.
- Mitchell, S. Wind as a natural disturbance agent in forests: a synthesis. *Forestry: An International Journal of Forest Research*, 86(2):147–157, 2013. doi: doi.org/10.1093/forestry/cps058.
- Mitra, P. P. and Loqué, D. Histochemical staining of *Arabidopsis thaliana* secondary cell wall elements. *JoVE (Journal of Visualized Experiments)*, (87):e51381, 2014. doi: 10.3791/51381.
- Molina-Aiz, F., Valera, D., Alvarez, A., and Madueno, A. A wind tunnel study of air-flow through horticultural crops: determination of the drag coefficient. *Biosystems Engineering*, 93(4):447–457, 2006. doi: 10.1016/j.biosystemseng.2006.01.016.
- Monteith, J. L. Evaporation and environment. In *Symposia of the Society for Experimental Biology*, volume 19, pages 205–234. Cambridge University Press (CUP) Cambridge, 1965.

- Morita, M. T. Directional gravity sensing in gravitropism. *Annual Review of Plant Biology*, 61:705–720, 2010. doi: 10.1146/annurev.arplant.043008.092042.
- Moulia, B. and Fournier, M. The power and control of gravitropic movements in plants: a biomechanical and systems biology view. *Journal of Experimental Botany*, 60(2):461–486, 2009. doi: 10.1093/jxb/ern341.
- Nakagawa, T. Vortex shedding mechanism from a triangular prism in a subsonic flow. *Fluid Dynamics Research*, 5(2):69–81, 1989. doi: 10.1016/0169-5983(89)90012-9.
- Nakata, M. T., Takahara, M., Sakamoto, S., Yoshida, K., and Mitsuda, N. High-throughput analysis of Arabidopsis stem vibrations to identify mutants with altered mechanical properties. *Frontiers in Plant Science*, 9, 2018. doi: 10.3389/fpls.2018.00780.
- Naudascher, E., Weske, J., and Fey, B. Exploratory study on damping of galloping vibrations. *Journal of Wind Engineering and Industrial Aerodynamics*, 8(1-2): 211–222, 1981. doi: 10.1016/0167-6105(81)90020-9.
- Newcombe, F. C. The regulatory formation of mechanical tissue. *Botanical Gazette*, 20(10):441–448, 1895.
- Niez, B., Dlouha, J., Moulia, B., and Badel, E. Water-stressed or not, the mechanical acclimation is a priority requirement for trees. *Trees*, 33(1):279–291, 2019. doi: 10.1007/s00468-018-1776-y.
- Niez, B., Dlouha, J., Gril, J., Ruelle, J., Toussaint, E., Moulia, B., and Badel, E. Mechanical properties of “flexure wood”: compressive stresses in living trees improve the mechanical resilience of wood and its resistance to damage. *Annals of Forest Science*, 77(1):17, 2020. doi: 10.1007/s13595-020-0926-8.
- Niklas, K. J. The aerodynamics of wind pollination. *The Botanical Review*, 51(3): 328–386, 1985. doi: 10.1007/BF02861079.
- Niklas, K. J. *Plant biomechanics: an engineering approach to plant form and function*. University of Chicago press, 1992.
- Niklas, K. J. Influence of tissue density-specific mechanical properties on the scaling of plant height. *Annals of Botany*, 72(2):173–179, 1993. doi: 10.1006/anbo.1993.1096.

- Niklas, K. J. Mechanical properties of black locust (*Robinia pseudoacacia*) wood: Correlations among elastic and rupture moduli, proportional limit, and tissue density and specific gravity. *Annals of Botany*, 79(5):479–485, 1997. doi: 10.1006/anbo/79.5.479.
- Niklas, K. J. Effects of vibration on mechanical properties and biomass allocation pattern of *Capsella bursa-pastoris* (Cruciferae). *Annals of Botany*, 82(2):147–156, 1998. doi: 10.1006/anbo.1998.0658.
- Niklas, K. J. and Moon, F. C. Flexural stiffness and modulus of elasticity of flower stalks from *Allium sativum* as measured by multiple resonance frequency spectra. *American Journal of Botany*, 75(10):1517–1525, 1988. doi: 10.1002/j.1537-2197.1988.tb11225.x.
- Niklas, K. J. and Spatz, H.-C. Wind-induced stresses in cherry trees: evidence against the hypothesis of constant stress levels. *Trees*, 14(4):230–237, 2000. doi: 10.1007/s004680050008.
- Niklas, K., Molina-Freaner, F., and Tinoco-Ojanguren, C. Biomechanics of the columnar cactus *Pachycereus pringlei*. *American Journal of Botany*, 86(6):767–775, 1999. doi: 10.2307/2656697.
- Nobel, P. S. *Physicochemical & Environmental Plant Physiology*. Academic press, 2020.
- Nobel, P. Water relations and photosynthesis of a barrel cactus, *Ferocactus acanthodes*, in the Colorado Desert. *Oecologia*, 27(2):117–133, 1977.
- Nobel, P. Surface temperatures of cacti—influences of environmental and morphological factors. *Ecology*, 59(5):986–995, 1978. doi: 10.2307/1938550.
- Nobel, P. Wind as an ecological factor. In *Physiological Plant Ecology I*, pages 475–500. Springer, 1981. doi: 10.1007/978-3-642-68090-8_16.
- Nobel, P., Geller, G., Kee, S., and Zimmerman, A. Temperatures and thermal tolerances for cacti exposed to high temperatures near the soil surface. *Plant, Cell & Environment*, 9(4):279–287, 1986. doi: 10.1111/1365-3040.ep11611688.
- Noguchi, Y. Deformation of trees in Hawaii and its relation to wind. *The Journal of Ecology*, pages 611–628, 1979. doi: 10.2307/2259116.

- Norberg, C. Fluctuating lift on a circular cylinder: review and new measurements. *Journal of Fluids and Structures*, 17(1):57–96, 2003. doi: 10.1016/S0889-9746(02)00099-3.
- O’Brien, T., Feder, N., and McCully, M. E. Polychromatic staining of plant cell walls by toluidine blue O. *Protoplasma*, 59(2):368–373, 1964. doi: 10.1007/BF01248568.
- Oh, S., Han, H., Han, S., Lee, J., and Chun, W. Development of a tree-shaped wind power system using piezoelectric materials. *International Journal of Energy Research*, 34(5):431–437, 2010. doi: 10.1002/er.1644.
- Oka, S. and Ishihara, T. Numerical study of aerodynamic characteristics of a square prism in a uniform flow. *Journal of Wind Engineering and Industrial Aerodynamics*, 97(11):548–559, 2009. doi: 10.1016/j.jweia.2009.08.006.
- Owen, J. C., Bearman, P. W., and Szewczyk, A. A. Passive control of VIV with drag reduction. *Journal of Fluids and Structures*, 15(3-4):597–605, 2001. doi: 10.1006/jfls.2000.0358.
- Paul-Victor, C. and Rowe, N. Effect of mechanical perturbation on the biomechanics, primary growth and secondary tissue development of inflorescence stems of *Arabidopsis thaliana*. *Annals of Botany*, 107(2):209–218, 2011. doi: 10.1093/aob/mcq227.
- Perbal, G., Driss-Ecole, D., Tewinkel, M., and Volkmann, D. Statocyte polarity and gravisensitivity in seedling roots grown in microgravity. *Planta*, 203(1):S57–S62, 1997. doi: 10.1007/PL00008115.
- Pierson, E. A. and Turner, R. M. An 85-year study of saguaro (*Carnegiea gigantea*) demography. *Ecology*, 79(8):2676–2693, 1998. doi: 10.1890/0012-9658(1998)079[2676:AYSOSC]2.0.CO;2.
- Pigliucci, M. Touchy and bushy: phenotypic plasticity and integration in response to wind stimulation in *Arabidopsis thaliana*. *International Journal of Plant Sciences*, 163(3):399–408, 2002. doi: 10.1086/339158.
- Pineiro, M. and Coupland, G. The control of flowering time and floral identity in *Arabidopsis*. *Plant Physiology*, 117(1):1–8, 1998. doi: 10.1104/pp.117.1.1.
- Premalatha, M., Abbasi, T., and Abbasi, S. A. Wind energy: Increasing deployment, rising environmental concerns. *Renewable and Sustainable Energy Reviews*, 31: 270–288, 2014. doi: 10.1016/j.rser.2013.11.019.

- Pruyn, M. L., Ewers III, B. J., and Telewski, F. W. Thigmomorphogenesis: changes in the morphology and mechanical properties of two *Populus* hybrids in response to mechanical perturbation. *Tree Physiology*, 20(8):535–540, 2000. doi: 10.1093/treephys/20.8.535.
- Quine, C., Coutts, M., Gardiner, B., and Pyatt, G. Forests and wind: Management to minimise damage. *HMSO Forestry Commission Bulletin 114*, 114, 1995.
- Rédei, G. P. A heuristic glance at the past of *Arabidopsis* genetics. In Koncz, C., Chua, N.-H., and Schell, J., editors, *Methods in Arabidopsis Research*, pages 1–15. World Scientific Singapore, 1992.
- Rees, D. and Grace, J. The effects of wind on the extension growth of *Pinus contorta* Douglas. *Forestry: An International Journal of Forest Research*, 53(2):145–153, 1980. doi: 10.1093/forestry/53.2.145.
- Reis, G. S. M., Almeida, A.-A. F. d., Mangabeira, P. A. O., Santos, I. C. d., Pirovani, C. P., and Ahnert, D. Mechanical stress caused by wind on leaves of *Theobroma cacao*: Photosynthetic, molecular, antioxidative and ultrastructural responses. *PloS One*, 13(6):e0198274, 2018. doi: 10.1371/journal.pone.0198274.
- Richmond, T. d. A. and Mueller-Dombois, D. Coastline ecosystems on Oahu, Hawaii. *Vegetatio*, 25(1):367–400, 1972. doi: 10.1007/BF00452982.
- Rivero, L., Scholl, R., Holomuzki, N., Crist, D., Grotewold, E., and Brkljacic, J. Handling *Arabidopsis* plants: growth, preservation of seeds, transformation, and genetic crosses. In *Arabidopsis Protocols*, pages 3–25. Springer, 2014.
- Robertson, D. J., Smith, S. L., and Cook, D. D. On measuring the bending strength of septate grass stems. *American Journal of Botany*, 102(1):5–11, 2015. doi: 10.3732/ajb.1400183.
- Roshko, A. On the wake and drag of bluff bodies. *Journal of the Aeronautical Sciences*, 22(2):124–132, 1955. doi: 10.2514/8.3286.
- Roshko, A. Experiments on the flow past a circular cylinder at very high Reynolds number. *Journal of Fluid Mechanics*, 10(3):345–356, 1961. doi: 10.1017/S0022112061000950.
- Roshko, A. Perspectives on bluff body aerodynamics. *Journal of Wind Engineering and Industrial Aerodynamics*, 49(1-3):79–100, 1993. doi: 10.1016/0167-6105(93)90007-B.

- Rudnicki, M., Mitchell, S. J., and Novak, M. D. Wind tunnel measurements of crown streamlining and drag relationships for three conifer species. *Canadian Journal of Forest Research*, 34(3):666–676, 2004. doi: 10.1139/x03-233.
- Ruosteenoja, K., Vihma, T., and Venäläinen, A. Projected changes in European and North Atlantic seasonal wind climate derived from CMIP5 simulations. *Journal of Climate*, 32(19):6467–6490, 2019. doi: 10.1175/JCLI-D-19-0023.1.
- Russell, G. and Grace, J. The effect of windspeed on the growth of grasses. *Journal of Applied Ecology*, 16(2):507–514, 1979. doi: 10.2307/2402525.
- Ryden, P., Sugimoto-Shirasu, K., Smith, A. C., Findlay, K., Reiter, W.-D., and McCann, M. C. Tensile properties of Arabidopsis cell walls depend on both a xyloglucan cross-linked microfibrillar network and rhamnogalacturonan II-borate complexes. *Plant Physiology*, 132(2):1033–1040, 2003. doi: doi.org/10.1104/pp.103.021873.
- Sakai, T., Kagawa, T., Kasahara, M., Swartz, T. E., Christie, J. M., Briggs, W. R., Wada, M., and Okada, K. Arabidopsis *nph1* and *npl1*: blue light receptors that mediate both phototropism and chloroplast relocation. *Proceedings of the National Academy of Sciences*, 98(12):6969–6974, 2001. doi: 10.1073/pnas.101137598.
- Sanchez-Serrano, J. J. and Salinas, J. *Arabidopsis protocols*. Springer, 2014.
- Schelhaas, M.-J., Nabuurs, G.-J., and Schuck, A. Natural disturbances in the European forests in the 19th and 20th centuries. *Global Change Biology*, 9(11): 1620–1633, 2003. doi: 10.1046/j.1365-2486.2003.00684.x.
- Schneider, C. A., Rasband, W. S., and Eliceiri, K. W. NIH image to ImageJ: 25 years of image analysis. *Nature Methods*, 9(7):671, 2012. doi: 10.1038/nmeth.2089.
- Seyed-Aghazadeh, B., Carlson, D. W., and Modarres-Sadeghi, Y. Vortex-induced vibration and galloping of prisms with triangular cross-sections. *Journal of Fluid Mechanics*, 817:590–618, 2017. doi: 10.1017/jfm.2017.119.
- Shah, A. N., Tanveer, M., ur Rehman, A., Anjum, S. A., Iqbal, J., and Ahmad, R. Lodging stress in cereal—effects and management: an overview. *Environmental Science and Pollution Research*, 24(6):5222–5237, 2017a. doi: 10.1007/s11356-016-8237-1.

- Shah, D. U., Reynolds, T. P., and Ramage, M. H. The strength of plants: theory and experimental methods to measure the mechanical properties of stems. *Journal of Experimental Botany*, 68(16):4497–4516, 2017b. doi: 10.1093/jxb/erx245.
- Sherman, M., Hassanalian, M., and Bradley, S. Dandelion-inspired micro-rovers: Novel concept of extraterrestrial systems for mars exploration. In *AIAA Aviation 2020 Forum*, page 2935, 2020. doi: 10.2514/6.2020-2935.
- Siemens. Star-CCM+. <http://mdx.plm.automation.siemens.com/>, 2017. Accessed: 2017-05-15.
- Sims, R. E., Mabee, W., Saddler, J. N., and Taylor, M. An overview of second generation biofuel technologies. *Bioresource Technology*, 101(6):1570–1580, 2010. doi: 10.1016/j.biortech.2009.11.046.
- Smika, D. and Shawcroft, R. Preliminary study using a wind tunnel to determine the effect of hot wind on a wheat crop. *Field Crops Research*, 3:129–135, 1980. doi: 10.1016/0378-4290(80)90018-0.
- Smith, A. P. Notes on wind-related growth patterns of paramo plants in Venezuela. *Biotropica*, pages 10–16, 1972. doi: 10.2307/2989640.
- Smith, R. A., Schuetz, M., Roach, M., Mansfield, S. D., Ellis, B., and Samuels, L. Neighboring parenchyma cells contribute to Arabidopsis xylem lignification, while lignification of interfascicular fibers is cell autonomous. *The Plant Cell*, 25(10): 3988–3999, 2013. doi: 10.1105/tpc.113.117176.
- Smith, V. and Ennos, A. The effects of air flow and stem flexure on the mechanical and hydraulic properties of the stems of sunflowers *Helianthus annuus* L. *Journal of Experimental Botany*, 54(383):845–849, 2003. doi: 10.1093/jxb/erg068.
- Spatz, H.-C. and Speck, O. Oscillation frequencies of tapered plant stems. *American Journal of Botany*, 89(1):1–11, 2002. doi: 10.3732/ajb.89.1.1.
- Spatz, H.-C. and Theckes, B. Oscillation damping in trees. *Plant Science*, 207:66–71, 2013. doi: 10.1016/j.plantsci.2013.02.015.
- Spatz, H.-C., Brüchert, F., and Pfisterer, J. Multiple resonance damping or how do trees escape dangerously large oscillations? *American Journal of Botany*, 94(10): 1603–1611, 2007. doi: 10.3732/ajb.94.10.1603.

- Speck, O. Field measurements of wind speed and reconfiguration in *Arundo donax* (Poaceae) with estimates of drag forces. *American Journal of Botany*, 90(8): 1253–1256, 2003. doi: 10.3732/ajb.90.8.1253.
- Sterling, M., Baker, C., Berry, P., and Wade, A. An experimental investigation of the lodging of wheat. *Agricultural and Forest Meteorology*, 119(3-4):149–165, 2003. doi: 10.1016/S0168-1923(03)00140-0.
- Taddei, S., Manes, C., and Ganapathisubramani, B. Characterisation of drag and wake properties of canopy patches immersed in turbulent boundary layers. *Journal of Fluid Mechanics*, 798:27–49, 2016. doi: 10.1017/jfm.2016.312.
- Tadrist, L., Saudreau, M., Hémon, P., Amandolese, X., Marquier, A., Leclercq, T., and de Langre, E. Foliage motion under wind, from leaf flutter to branch buffeting. *Journal of The Royal Society Interface*, 15(142):20180010, 2018. doi: 10.1098/rsif.2018.0010.
- Takahashi, H. and Jaffe, M. J. Thigmotropism and the modulation of tropistic curvature by mechanical perturbation in cucumber hypocotyls. *Physiologia Plantarum*, 80(4):561–567, 1990. doi: 10.1111/j.1399-3054.1990.tb05679.x.
- Talley, S. and Mungal, G. Flow around cactus-shaped cylinders. *Center for Turbulence Research, Annual Research Briefs*, 2002:363–376, 2002.
- Talley, S., Iaccarino, G., Mungal, G., and Mansour, N. An experimental and computational investigation of flow past cacti. *Annual Research Briefs, Center for Turbulence Research, NASA Ames/Stanford University*, pages 51–63, 2001.
- Tamasi, E., Stokes, A., Lasserre, B., Danjon, F., Berthier, S., Fourcaud, T., and Chiatante, D. Influence of wind loading on root system development and architecture in oak (*Quercus robur* L.) seedlings. *Trees*, 19(4):374–384, 2005. doi: 10.1007/s00468-004-0396-x.
- Tamura, T. and Miyagi, T. The effect of turbulence on aerodynamic forces on a square cylinder with various corner shapes. *Journal of Wind Engineering and Industrial Aerodynamics*, 83(1-3):135–145, 1999. doi: 10.1016/S0167-6105(99)00067-7.
- Teboho, N., Mpholo, M., and Lennard, C. Long-term austral summer wind speed trends over southern Africa. *International Journal of Climatology*, 37:2850–2862, 2017. doi: 10.1002/joc.4883.

- Telewski, F. W. A unified hypothesis of mechanoperception in plants. *American Journal of Botany*, 93(10):1466–1476, 2006. doi: 10.3732/ajb.93.10.1466.
- Telewski, F. W. Is windswept tree growth negative thigmotropism? *Plant Science*, 184:20–28, 2012. doi: 10.1016/j.plantsci.2011.12.001.
- Telewski, F. W. Thigmomorphogenesis: The response of plants to mechanical perturbation. *Italus Hortus*, 23(1):1–16, 2016.
- Telewski, F. W. and Jaffe, M. J. Thigmomorphogenesis: field and laboratory studies of *Abies fraseri* in response to wind or mechanical perturbation. *Physiologia Plantarum*, 66(2):211–218, 1986a. doi: 10.1111/j.1399-3054.1986.tb02411.x.
- Telewski, F. W. and Jaffe, M. J. Thigmomorphogenesis: anatomical, morphological and mechanical analysis of genetically different sibs of *Pinus taeda* in response to mechanical perturbation. *Physiologia Plantarum*, 66(2):219–226, 1986b. doi: 10.1111/j.1399-3054.1986.tb02412.x.
- Telewski, F. W. and Pruyn, M. L. Thigmomorphogenesis: a dose response to flexing in *Ulmus americana* seedlings. *Tree Physiology*, 18(1):65–68, 1998. doi: 10.1093/treephys/18.1.65.
- Thom, A. The flow past circular cylinders at low speeds. *Proceedings of the Royal Society of London. Series A, Containing Papers of a Mathematical and Physical Character*, 141(845):651–669, 1933. doi: 10.1098/rspa.1933.0146.
- Thom, A. The exchange of momentum, mass, and heat between an artificial leaf and the airflow in a wind-tunnel. *Quarterly Journal of the Royal Meteorological Society*, 94(399):44–55, 1968. doi: 10.1002/qj.49709439906.
- Thompson, J. The effect of wind on grasses II. Mechanical damage in *Festuca arundinacea* Schreb. *Journal of Experimental Botany*, 25(5):965–972, 1974. doi: 10.1093/jxb/25.5.965.
- Tsutsui, T. and Igarashi, T. Drag reduction of a circular cylinder in an air-stream. *Journal of Wind Engineering and Industrial Aerodynamics*, 90(4-5):527–541, 2002. doi: 10.1016/S0167-6105(01)00199-4.
- Turner, S. R. and Somerville, C. R. Collapsed xylem phenotype of *Arabidopsis* identifies mutants deficient in cellulose deposition in the secondary cell wall. *The Plant Cell*, 9(5):689–701, 1997. doi: 10.1105/tpc.9.5.689.

- United Nations. The 17 goals. <https://sdgs.un.org/goals>, 2011. Accessed: 15-01-2021.
- Van Gardingen, P. and Grace, J. Plants and wind. In *Advances in Botanical Research*, volume 18, pages 189–253. Elsevier, 1991. doi: 10.1016/S0065-2296(08)60023-3.
- Van Gardingen, P., Grace, J., and Jeffree, C. Abrasive damage by wind to the needle surfaces of *Picea sitchensis* (Bong.) Carr. and *Pinus sylvestris* L. *Plant, Cell & Environment*, 14(2):185–193, 1991. doi: 10.1111/j.1365-3040.1991.tb01335.x.
- Verhertbruggen, Y., Marcus, S. E., Chen, J., and Knox, J. P. Cell wall pectic arabinans influence the mechanical properties of *Arabidopsis thaliana* inflorescence stems and their response to mechanical stress. *Plant and Cell Physiology*, 54(8):1278–1288, 2013. doi: 10.1093/pcp/pct074.
- Virgin, H. I. A new method for the determination of the turgor of plant tissues. *Physiologia Plantarum*, 8(4):954–962, 1955. doi: 10.1111/j.1399-3054.1955.tb07791.x.
- Vitasse, Y., Bresson, C. C., Kremer, A., Michalet, R., and Delzon, S. Quantifying phenological plasticity to temperature in two temperate tree species. *Functional Ecology*, 24(6):1211–1218, 2010. doi: 10.1111/j.1365-2435.2010.01748.x.
- Vogel, S. Drag and flexibility in sessile organisms. *American Zoologist*, 24(1):37–44, 1984. doi: 10.1093/icb/24.1.37.
- Vogel, S. Drag and reconfiguration of broad leaves in high winds. *Journal of Experimental Botany*, 40(8):941–948, 1989. doi: 10.1093/jxb/40.8.941.
- Vogel, S. *Life in moving fluids: the physical biology of flow*. Princeton University Press, 1994.
- Vollsinger, S., Mitchell, S. J., Byrne, K. E., Novak, M. D., and Rudnicki, M. Wind tunnel measurements of crown streamlining and drag relationships for several hardwood species. *Canadian Journal of Forest Research*, 35(5):1238–1249, 2005. doi: 10.1139/x05-051.
- Wadsworth, R. An optimum wind speed for plant growth. *Annals of Botany*, 23(1):195–199, 1959. doi: 10.1093/oxfordjournals.aob.a083639.

- Wadsworth, R. The effect of artificial wind on the growth-rate of plants in water culture: with plate and three figures in the text. *Annals of Botany*, 24(2):200–211, 1960. doi: 10.1093/oxfordjournals.aob.a083695.
- Wang, S. F., Liu, Y. Z., and Zhang, Q. S. Measurement of flow around a cactus-analogue grooved cylinder at $Re_D = 5.4 \times 10^4$: Wall-pressure fluctuations and flow pattern. *Journal of Fluids and Structures*, 50:120–136, 2014. doi: 10.1016/j.jfluidstructs.2014.06.019.
- Wang, S. and Liu, Y. Wake dynamics behind a seal-vibrissa-shaped cylinder: A comparative study by time-resolved particle velocimetry measurements. *Experiments in Fluids*, 57(3):32, 2016. doi: 10.1007/s00348-016-2117-9.
- Wang, W., He, X., Wang, X., Wang, M., and Xue, K. A bioinspired structure modification of piezoelectric wind energy harvester based on the prototype of leaf veins. *Sensors and Actuators A: Physical*, 279:467–473, 2018. doi: 10.1016/j.sna.2018.06.059.
- Wang, Y.-H., He, W.-M., Yu, F.-H., Zhang, L.-L., Cui, Q.-G., Chu, Y., and Dong, M. Brushing effects on the growth and mechanical properties of *Corispermum mongolicum* vary with water regime. *Plant Biology*, 11(5):694–700, 2009. doi: 10.1111/j.1438-8677.2008.00168.x.
- West, G. and Apelt, C. Measurements of fluctuating pressures and forces on a circular cylinder in the Reynolds number range 10^4 to 2.5×10^5 . *Journal of Fluids and Structures*, 7(3):227–244, 1993. doi: 10.1006/jfls.1993.1014.
- Western Regional Climate Center. RAWS USA Climate Archive. <https://raws.dri.edu>, 2020. Accessed: 15-01-2021.
- Whitehead, F. Experimental studies of the effect of wind on plant growth and anatomy. II. *Helianthus annuus*. *New Phytologist*, 61(1):59–62, 1962. doi: 10.1111/j.1469-8137.1962.tb06274.x.
- Whitehead, F. Experimental studies of the effect of wind on plant growth and anatomy. III. Soil moisture relations. *New Phytologist*, 62(1):80–85, 1963a. doi: 10.1111/j.1469-8137.1963.tb06315.x.
- Whitehead, F. Experimental studies of the effect of wind on plant growth and anatomy. IV. Growth substances and adaptative anatomical and morphological

- changes. *New Phytologist*, 62(1):86–90, 1963b. doi: 10.1111/j.1469-8137.1963.tb06316.x.
- Whitehead, F. and Luti, R. Experimental studies of the effect of wind on plant growth and anatomy. I. *Zea mays*. *New Phytologist*, 61(1):56–58, 1962. doi: 10.1111/j.1469-8137.1962.tb06273.x.
- Williamson, C. H. Vortex dynamics in the cylinder wake. *Annual Review of Fluid Mechanics*, 28(1):477–539, 1996. doi: 10.1146/annurev.fl.28.010196.002401.
- Xu, W., Purugganan, M. M., Polisensky, D. H., Antosiewicz, D. M., Fry, S. C., and Braam, J. Arabidopsis TCH4, regulated by hormones and the environment, encodes a xyloglucan endotransglycosylase. *The Plant Cell*, 7(10):1555–1567, 1995. doi: 10.1105/tpc.7.10.1555.
- Yagmur, S., Dogan, S., Aksoy, M. H., Goktepe, I., and Ozgoren, M. Comparison of flow characteristics around an equilateral triangular cylinder via PIV and Large Eddy Simulation methods. *Flow Measurement and Instrumentation*, 55:23–36, 2017. doi: 10.1016/j.flowmeasinst.2017.04.001.
- Yamagishi, Y. and Oki, M. Effect of groove shape on flow characteristics around a circular cylinder with grooves. *Journal of Visualization*, 7(3):209–216, 2004. doi: 10.1007/BF03181635.
- Yamagishi, Y. and Oki, M. Effect of the number of grooves on flow characteristics around a circular cylinder with triangular grooves. *Journal of Visualization*, 8(1): 57–64, 2005. doi: 10.1007/BF03181603.
- Zebrowski, J. The use of free vibrations to measure peduncle stiffness in Triticale. *Journal of Experimental Botany*, 42(9):1207–1212, 1991. doi: 10.1093/jxb/42.9.1207.
- Zhang, G., Azorin-Molina, C., Chen, D., Guijarro, J. A., Kong, F., Minola, L., McVicar, T. R., Son, S.-W., and Shi, P. Variability of daily maximum wind speed across China, 1975–2016: An examination of likely causes. *Journal of Climate*, 33(7):2793–2816, 2020. doi: 10.1175/JCLI-D-19-0603.1.
- Zhdanov, O. and Busse, A. Angle of attack dependence of flow past cactus-inspired cylinders with a low number of ribs. *European Journal of Mechanics-B/Fluids*, 75:244–257, 2019. doi: 10.1016/j.euromechflu.2018.09.008.

- Zhdanov, O., Blatt, M. R., Cammarano, A., Zare-Behtash, H., and Busse, A. A new perspective on mechanical characterisation of Arabidopsis stems through vibration tests. *Journal of the Mechanical Behavior of Biomedical Materials*, 112:104041, 2020. doi: 10.1016/j.jmbbm.2020.104041.
- Zhdanov, O., Blatt, M. R., Zare-Behtash, H., and Busse, A. Wind-evoked anemotropism affects the morphology and mechanical properties of Arabidopsis. *Journal of Experimental Botany*, 72(5):1906–1918, 2021. doi: 10.1093/jxb/eraa541.
- Zhou, B., Wang, X., Guo, W., Zheng, J., and Tan, S. K. Experimental measurements of the drag force and the near-wake flow patterns of a longitudinally grooved cylinder. *Journal of Wind Engineering and Industrial Aerodynamics*, 145:30–41, 2015. doi: 10.1016/j.jweia.2015.05.013.